

Continuous slow pyrolysis of wheat straw in a screw reactor and use of the char for water decontamination

Filipe António Henriques Rego

Doctor of Philosophy

Aston University

June 2021

© Filipe António Henriques Rego, 2021

Filipe António Henriques Rego asserts their moral right to be identified as the author of this thesis

This copy of the thesis has been supplied on condition that anyone who consults it is understood to recognise that its copyright belongs to its author and that no quotation from the thesis and no information derived from it may be published without appropriate permission or acknowledgment.

Continuous slow pyrolysis of wheat straw in a screw reactor and use of the char for water decontamination

Filipe António Henriques Rego
Doctor of Philosophy
June 2021

Thesis Summary

There is a need to replace fossil fuels and fossil fuel-derived products, and pyrolysis can contribute to both production of energy and production of useful bioproducts such as biofertilisers and bioadsorbents. At the same time, there is increasing demand for solutions to polluted air and water, due to population and consumption growth, and more stringent limits on pollutants. Adsorption is one of the main solutions for water decontamination, and activated carbon is the most used adsorbent due to its high performance and stability. However, production of activated carbon is usually time and resource-demanding, using high temperatures, coal or coconut shells as feedstock, and activating agents which can be strong acids and bases that can harm the environment. There is thus a need to develop novel adsorbents, with comparable performance to activated carbon, and be produced through more sustainable processes from greener and abundant feedstocks such as biowastes.

To address this, slow pyrolysis was used on a wheat straw feedstock to produce the solid product char and also the liquid and gaseous products. The char was tested as an adsorbent for water contaminants, using a cationic dye as model compound for organic pollutants. The liquid and gaseous products were characterised and useful to use as fuel. Both the feedstock and the slow pyrolysis process conditions were modified in order to evaluate how product properties and adsorption performance were affected.

The adsorption performance with the chars was evaluated mainly in terms of maximum removal of the dye, and comparable values to a commercial activated carbon ($\approx 99\%$ removal) were achieved. The adsorption capacity was also determined, and for the tested adsorption conditions a maximum of 98 mg/g was achieved, which was even higher than the commercial activated carbon.

The best performing chars were the ones produced at lower pyrolysis temperature (400 °C), and feedstock modifications such as increased moisture content, and impregnation with a diluted KOH solution allowed to improve the adsorption results. The chars were valuable for water decontamination even though the surface area was relatively low (maximum 8.8 m²/g), which signified that adsorption of the cationic dye with the chars occurred mainly due to interactions with the surface chemical functionalities of the chars. For the commercial activated carbon, on the other hand, the relatively high surface area (615 m²/g) was the main cause for its high adsorption performance.

The chars as bioadsorbents were produced in a continuous process, requiring relatively low temperature, and with additional treatment not being strictly necessary, although some improvements were verified when mild modifications were implemented on the feedstock or the process conditions. This contributes to the possibility of replacing or improving traditional activated carbon production processes, which are time- and resource-consuming. Furthermore, the feedstock used was wheat straw, which is a relatively abundant agricultural by-product frequently considered low value.

Keywords: biomass, slow pyrolysis, char, adsorption, water decontamination.

This project has received funding from the European Union's Horizon 2020 research and innovation programme under the Marie Skłodowska-Curie grant agreement No 721991.

Acknowledgments

The work during the PhD and for this thesis would not be possible without the people that surround me and who I contacted with during that time. It is difficult to account for everyone here, so my thanks go out to all of those people.

To my supervisors, Dr. Jiawei Wang and Prof. Tony Bridgwater, who provided very important guidance throughout this journey and have shared much of their extensive knowledge with me. To Dr. Yang Yang, who I also considered a guide and provided very valuable help with everything.

To Jorge, who was the project partner that everyone should have! Thanks for all the help, conversations, games, translations, everything! You're amazing and I hope this project can lead to many great things!! And to the rest of the GreenCarbon project team, it was great to be a part of such an amazing project with you, and to get to know all of you and share those experiences we had. Also, to those involved with the ERA consortium, it was great to be a part of that group and to be able to experience awesome events and hangouts!

To lecturers and staff at EBRI and Aston University, such as Katie, Paula, Marta, Amin, Jinesh, Scott, Ana, Clara, Daniel, Emma, Jude, Alfred, Vesna, Zoran, Rob, Konstantina, Qingchun, Patricia, Mirjam, Alanna, Martha, Catriona, Pippa, Irene, Tim, Vitor, was great to meet you and share good moments and conversations with you.

The work at EBRI and Aston University had the advantage of being shared with awesome students and researchers, always available to help, thank you for all the good times! Costanza, Regina, Mo, Chris, Michael, Sainab, Tom, Joe, Sarah, Lorena, Stelios, Ife, Carmen, Marta, Iram, Cristiane, Huan, Josephine, Özben, Cristina, Tian, Rima, Lucia, Mariano, Brunella, Charlotte, Helena, Ayesha, Arash, Kassam, Jai, Karthik, Elis, Moussa, among so many other great people.

In Birmingham I had the pleasure to befriend, meet and hang out or even share a home with awesome people such as Tiago, João, Patrícia, Alex, Sonia, Noelia, Sandra, Manju, António, Abdullah and the Mary Sturge crew, Krish and the Lakeside crew. Thank you for everything.

Para os de lá de casa! Mãe, pai, irmã, sempre me apoiaram e às minhas decisões, obrigado por isso e por tudo o resto. Aos meus amigos por sempre trazerem boa disposição e a ocasional festa quando eu regressava!

Para a minha namorada Diana, que sempre apoiou e cuidou, muito obrigado por estares comigo mesmo sem ser fisicamente, e por me visitares, foi um grande desafio mas conseguimos!!

List of Contents

List of Abbreviations and Acronyms	9
List of Figures	10
List of Tables	16
Chapter 1 – Introduction.....	20
1.1. Background and motivation	20
1.2. Work aims and objectives	25
1.3. Thesis structure	26
1.4. GreenCarbon Project.....	27
Chapter 2 – Literature review.....	29
2.1. Slow pyrolysis of biomass.....	29
2.1.1. Lignocellulosic biomass.....	29
2.1.1.1. Wheat straw feedstock	31
2.1.2. Biomass conversion processes into bioenergy and bioproducts.....	34
2.1.3. Types of pyrolysis processes and products.....	36
2.1.4. Pyrolysis reactions and mechanisms.....	39
2.1.5. Effect of pyrolysis conditions on product yields	43
2.1.5.1. Effect of operating temperature and heating rate	43
2.1.5.2. Effect of solid residence time	44
2.1.5.3. Effect of reaction environment (by gas injection) and vapour residence time.....	45
2.1.5.4. Effect of feedstock particle size.....	46
2.1.5.5. Effect of feedstock moisture content	47
2.1.5.6. Effect of operating pressure.....	47
2.2. Pyrolysis reactors	48
2.2.1. Fast pyrolysis reactors	48
2.2.2. Slow pyrolysis reactors	49
2.2.3. Screw reactors	50
2.3. Char from slow pyrolysis of biomass.....	55
2.3.1. Main properties and analysis techniques.....	55
2.3.2. Char applications	60
2.3.3. Activated carbon	66
2.4. Removal of contaminants from water.....	73
2.4.1. Water decontamination routes.....	74

2.4.2. Adsorption for water decontamination	75
2.4.3. New and sustainable carbonaceous adsorbents for organic contaminant removal from water.....	76
Chapter 3 – Methodologies and materials	80
3.1. Feedstock.....	80
3.2. Experimental set-up.....	81
3.2.1. Continuous screw reactor system	81
3.2.1.1. First screw reactor	82
3.2.1.2. Second screw reactor	84
3.2.2. Slow pyrolysis procedures.....	86
3.2.2.1. Continuous slow pyrolysis with as-received wheat straw	91
3.2.2.2. Continuous slow pyrolysis with varying feedstock moisture content.....	92
3.2.2.3. Continuous slow pyrolysis with CO ₂ as reaction atmosphere	94
3.2.2.4. Continuous slow pyrolysis with KOH-impregnated feedstock	95
3.2.2.5. Comparison between the two screw reactors.....	97
3.3. Analyses of feedstock and products	98
3.3.1. Feedstock and solid product analyses.....	98
3.3.1.1. Proximate analysis.....	98
3.3.1.2. Ultimate analysis.....	99
3.3.1.3. Inorganic contents	100
3.3.1.4. Heating value.....	100
3.3.1.5. pH (in H ₂ O).....	101
3.3.1.6. FTIR	101
3.3.1.7. N ₂ physisorption (77 K).....	101
3.3.1.8. Scanning Electron Microscopy (SEM).....	102
3.3.2. Liquid product analyses.....	102
3.3.2.1. Composition by GC-MS	102
3.3.2.2. Water content	103
3.3.2.3. pH.....	103
3.3.2.4. Ultimate analysis.....	104
3.3.2.5. Heating value.....	104
3.3.3. Gaseous product analyses	104
3.4. Study of adsorption from aqueous solution	105
3.4.1. Model compound selection.....	105

3.4.2. Adsorption procedures	107
3.4.3. Adsorption quantification	109
Chapter 4 – Slow pyrolysis of wheat straw biomass	111
4.1. Introduction.....	111
4.2. Feedstock characterisation	111
4.2.1. Proximate analysis and thermal degradation.....	111
4.2.2. Ultimate analysis and inorganic composition	114
4.2.3. pH and FTIR analysis.....	116
4.3. Product yields	117
4.3.1. Effect of process temperature and solid residence time	117
4.3.2. Comparison between the two lab-scale screw reactors	122
4.3.3. Effect of feedstock moisture content.....	124
4.4. Characterisation of solid products.....	132
4.4.1. TGA profiles and proximate analyses.....	133
4.4.2. Ultimate analyses and inorganic contents	141
4.4.3. Surface functional groups.....	145
4.4.4. pH (in H ₂ O)	148
4.4.5. Porosity and surface area	151
4.4.6. Microscopic analyses with SEM	155
4.5. Characterisation of gaseous products.....	157
4.6. Summary of Chapter 4.....	161
Chapter 5 – Slow pyrolysis with CO ₂ as reaction atmosphere	164
5.1. Introduction.....	164
5.2. Product yields	164
5.3. Characterisation of solid products.....	171
5.3.1. TGA profiles and proximate analyses.....	171
5.3.2. Ultimate analyses.....	174
5.3.3. Surface functional groups.....	175
5.3.4. pH (in H ₂ O)	177
5.3.5. Porosity and surface area	178
5.4. Summary of Chapter 5.....	181
Chapter 6 – Slow pyrolysis of KOH-impregnated feedstock	183
6.1. Introduction.....	183

6.2. Characterisation of KOH-impregnated feedstock	183
6.3. Product yields	184
6.4. Characterisation of solid products.....	189
6.4.1. TGA profiles and proximate analyses.....	191
6.4.2. Ultimate analyses and inorganic contents	196
6.4.3. Surface functional groups.....	198
6.4.4. pH (in H ₂ O)	200
6.4.5. Porosity and surface area	201
6.5. Summary of Chapter 6.....	204
Chapter 7 – Adsorption of an organic contaminant from water using chars	206
7.1. Introduction.....	206
7.2. Adsorption performances of chars with a cationic dye as model compound.....	207
7.2.1. Chars from slow pyrolysis of as-received wheat straw	207
7.2.2. Chars from slow pyrolysis of wheat straw with varying moisture content.....	213
7.2.3. Chars from slow pyrolysis with CO ₂ as reaction atmosphere.....	215
7.2.4. Chars from slow pyrolysis of KOH-impregnated feedstock.....	218
7.3. Potential mechanisms for MB adsorption with chars.....	220
7.4. Further adsorption studies	223
7.4.1. Varying adsorbent mass.....	223
7.4.2. Varying initial dye concentration.....	224
7.4.3. Adsorption of an acidic dye	226
7.4.4. Kinetics studies	228
7.5. Comparison of adsorption performance with the literature	230
7.6. Limitations of the adsorption studies.....	233
7.7. Summary of Chapter 7.....	234
Chapter 8 – Future work and recommendations.....	237
8.1. Reactor system.....	237
8.2. Slow pyrolysis process conditions and modifications	239
8.3. Char quality	240
8.4. Liquid and gas products from slow pyrolysis.....	240
8.5. Adsorption with char products.....	241
Chapter 9 – Conclusions.....	243
References	247

Appendices	279
Appendix A – Properties of gaseous species	279
Appendix B – Screw reactor operation.....	280
B.1. Feeding rate	280
B.2. Solid residence time	280
B.3. Vapour residence time	283
Appendix C – Char properties	285
C.1 – FTIR spectra for chars produced with varying slow pyrolysis temperature and SRT	285
C.2 – N ₂ physisorption (77 K) isotherms and pore size distribution for chars produced with varying slow pyrolysis temperature, SRT, and feedstock moisture content	285
C.3 – N ₂ physisorption (77 K) isotherms and pore size distribution for chars produced without injected gas in the second screw reactor	288
Appendix D – Liquid product analyses.....	289
D.1. Liquid products from varying slow pyrolysis temperature and solid residence time	289
D.1.1. Physical aspects.....	289
D.1.2. Water content and reaction water	291
D.1.3. pH of the liquid products	292
D.1.4. Elemental analyses and heating values	293
D.1.5. GC-MS	295
D.2. Liquid products from varying injected gas during slow pyrolysis (CO ₂ , N ₂ , and none)	300
D.3. Liquid products from varying KOH solution concentration (0.1 and 1 M KOH)	301
Appendix E - Characterisation of commercial activated carbon	304
E.1 – FTIR analysis.....	304
E.2 – N ₂ physisorption (77 K)	304
Appendix F – Correlations between maximum MB dye removal and char properties.....	305
Appendix G– Kinetics study of adsorption of methylene blue from water using the chars	310
Appendix H – Dissemination, outputs, and list of publications	313
References for Appendices	315

List of Abbreviations and Acronyms

A	Ash (content)
ASTM	American Society for Testing and Materials
BET	Brunauer-Emmett-Teller (theory)
C	Carbon (element)
FC	Fixed Carbon (content)
FTIR	Fourier Transform Infra-Red
GC	Gas Chromatography
H	Hydrogen (element)
HHV	High Heating Value
KOH	Potassium Hydroxide
M	Moisture (content) or Molarity/Molar concentration
MB	Methylene Blue
MO	Methyl Orange
N	Nitrogen (element)
O	Oxygen (element)
LHV	Lower Heating Value
S	Sulphur (element)
SEM	Scanning Electron Microscopy
SRT	Solid Residence Time (for the slow pyrolysis process)
T	Temperature (for the slow pyrolysis process)
TGA	Thermo-Gravimetric Analysis
UV-Vis	Ultraviolet-Visible (spectrophotometry)
VM	Volatile Matter (content)
VRT	Vapour Residence Time (for the slow pyrolysis process)

List of Figures

Figure 1.1: Temperature anomaly (median) compared to the 1961-1990 average, and average CO ₂ concentration in the atmosphere [2][4].	20
Figure 1.2: Schematic depiction of different forms of biomass (own artwork, based on [5][6]).	21
Figure 1.3: Depiction of the differences between char products (biochar, charcoal and activated carbon) according to their application.	23
Figure 2.1: Skeletal structural formulas (abbreviated) of the lignocellulosic groups: a) cellulose, b) hemicellulose, and c) lignin (with monophenol precursors in inset).	30
Figure 2.2: Wheat production per continent and in European countries (Mton, 2018 FAO data from [63]).	32
Figure 2.3: Thermochemical and biochemical processes employed to convert solid biomass into various products.	34
Figure 2.4: General representation of the biomass pyrolysis process.	36
Figure 2.5: Typical product distribution from different types of pyrolysis.	38
Figure 2.6: The Broido-Shafizadeh mechanism for cellulose thermal decomposition in inert atmosphere.	41
Figure 2.7: Simplified representation of a typical screw reactor.	50
Figure 2.8: Feedstock type frequency studied in screw reactors (own artwork and interpretation, based on data from [154]).	54
Figure 2.9: Picture of a wheat straw char produced in this work (500 °C, 3 min SRT).	55
Figure 2.10: Scheme depicting interactions between a char adsorbent particle and MB molecule in solution (own artwork).	78
Figure 3.1: A sample of the as-received wheat straw feedstock.	80
Figure 3.2: Representation of the bench-scale screw reactor system used for the slow pyrolysis experiments.	81
Figure 3.3: A representation of a section of the left-hand side of the screw.	83
Figure 3.4: Diagram of the positioning of the thermocouples in the screw reactor.	83
Figure 3.5: A picture of the second bench-scale screw reactor system.	85
Figure 3.6: The wheat straw feedstock after soaking with water.	93
Figure 3.7: Chemical structure representation of methylene blue (drawn on ChemDoodle software).	105
Figure 3.8: Chemical structure representation of methyl orange (drawn on ChemDoodle software).	107

Figure 4.1: Thermogram and derivative from the TGA (in nitrogen atmosphere) of the wheat straw feedstock.	112
Figure 4.2: FTIR spectrum of the wheat straw feedstock.....	117
Figure 4.3: Reactor temperature (inside, T1 and outside/wall, T2) during a slow pyrolysis experiment (600 °C, 10 min SRT) in the first screw reactor.	120
Figure 4.4: Temperature profile along the reactor tube (T1-T2-T3) in the second screw reactor during slow pyrolysis experiments with 10 min SRT (left: 400 °C; right: 600 °C).	122
Figure 4.5: Char yields (wt.%, dry feedstock basis) from slow pyrolysis experiments with varying feedstock moisture content and pyrolysis temperature.	128
Figure 4.6: Reactor temperature (inside, T1 and outside/wall, T2) during a slow pyrolysis experiment (600 °C, 10 min SRT, 50 wt.% M) in the first screw reactor.....	131
Figure 4.7: Samples of three of the produced chars (3 min SRT).	133
Figure 4.8: TGA profiles (N ₂ atmosphere) of chars produced in the screw reactor from wheat straw with varying temperature (10 min SRT).....	134
Figure 4.9: TGA profiles (N ₂ atmosphere) for chars produced at different pyrolysis temperatures and SRT.....	135
Figure 4.10: TGA profiles for chars produced at 400 and 600 °C (10 min SRT) in the first and second screw reactors.	136
Figure 4.11: TGA profiles (N ₂ atmosphere) of chars produced in the screw reactor from wheat straw with varying moisture content (10 min SRT).	137
Figure 4.12: FTIR spectra for the wheat straw feedstock and chars produced from slow pyrolysis with 10 minutes SRT and varying temperature and feedstock moisture content.	146
Figure 4.13: pH (in H ₂ O) of the produced chars with varying temperature and solid residence time.....	149
Figure 4.14: pH (in H ₂ O) of the produced chars with varying feedstock moisture content (“M”).	150
Figure 4.15: N ₂ adsorption-desorption isotherm (a) and pore size distribution (QS-DFT applied on adsorption branch) (b) for char produced from as-received feedstock at 600 °C, 10 min SRT.	151
Figure 4.16: SEM micrographs of chars produced at (a) 400, (b) 500 and (c) 600 °C in the screw reactor with 3 minutes SRT and no carrier gas. Zoomed-in areas highlighted in green rectangles are depicted on the right. The highlighted pore has ≈3.6 μm diameter.	156
Figure 4.17: SEM micrographs of chars produced at (a) 400 °C and feedstock with 50 wt.% M, (b) 400 °C and feedstock with 75 wt.% M, and (c) 600 °C and feedstock with 50 wt.% M (10 minutes SRT, no carrier gas).	157

Figure 5.1: Differences in char yield (wt.%) between experiments with different injected gases and experiments without injecting gas.....	166
Figure 5.2: TGA profiles (N ₂ atmosphere) for chars produced at 400 and 600 °C with N ₂ or CO ₂ as injected gases or without injected gas.....	172
Figure 5.3: FTIR spectra of chars produced at 400 and 600 °C and absence of injected gas or using N ₂ or CO ₂ as injected gas.	176
Figure 5.4: pH (in H ₂ O) of chars produced from slow pyrolysis without injected gas and using N ₂ or CO ₂ as injected gas.	177
Figure 5.5: N ₂ adsorption-desorption isotherms (a), and pore size distribution (QS-DFT applied on adsorption branch) (b), for chars produced from as-received feedstock at 400 °C with N ₂ (left-hand side) or CO ₂ (right-hand side) as injected gas.	178
Figure 5.6: N ₂ adsorption-desorption isotherms (a), and pore size distribution (QS-DFT applied on adsorption branch) (b), for chars produced from as-received feedstock at 600 °C with N ₂ (left-hand side) or CO ₂ (right-hand side) as injected gas.	179
Figure 6.1: Left picture – char produced at 600 °C from feedstock impregnated with 1 M KOH solution, with different-looking particles marked; right picture – char produced at 600 °C from soaked and dried feedstock (0 M KOH).	190
Figure 6.2: TGA profiles (N ₂ atmosphere) for chars produced at 400 °C (top) and 600 °C (bottom) with varying concentration of KOH in the impregnation solution.	192
Figure 6.3: Ratio between volatile matter and fixed carbon contents (dry ash-free basis) for chars produced with varying KOH concentration.....	194
Figure 6.4: Ashes from chars produced from feedstock impregnated with 1 M KOH solution and at 400 (left) and 600 °C (right).....	196
Figure 6.5: Potassium contents (wt.%, d.b.) in ash from chars produced from KOH-impregnated feedstock (bars, left axis) and increase (%) compared to chars from feedstock without KOH (dots, right axis).....	198
Figure 6.6: FTIR spectra of chars produced at 400 and 600 °C with varying KOH solution concentrations used for feedstock impregnation.	199
Figure 6.7: pH value (in H ₂ O) of chars produced with varying KOH solution concentration.	200
Figure 6.8: N ₂ adsorption-desorption isotherms (a), and pore size distribution (QS-DFT applied on adsorption branch) (b), for chars produced from KOH-impregnated feedstock at 400 °C with 0.1 M KOH solution (left-hand side) and 1 M KOH solution (right-hand side).....	202

Figure 6.9: N ₂ adsorption-desorption isotherms (a), and pore size distribution (QS-DFT applied on adsorption branch) (b), for chars produced from KOH-impregnated feedstock at 600 °C with 0.1 M KOH solution (left-hand side) and 1 M KOH solution (right-hand side).....	202
Figure 7.1: Calibration curve in UV-Visible spectrophotometry for the MB dye.	207
Figure 7.2: Samples of MB solutions with different concentrations (1, 3, 5, 10, and 90 mg/L).	207
Figure 7.3: MB dye removal from water (at equilibrium) using commercial activated carbon and produced chars from varying T (°C) and SRT (minutes).	208
Figure 7.4: Samples of MB solution after adsorption using a commercial activated carbon (left), and chars produced with 400 and 600 °C pyrolysis temperature (middle and right tubes, respectively).....	209
Figure 7.5: Correlations between MB removal from solution (% at equilibrium; vertical axis) and char properties (horizontal axis), for the whole collection of produced chars.	221
Figure 7.6: Removal of MB dye from water at equilibrium (bars; main vertical axis) and adsorption capacity (♦; secondary vertical axis) for selected chars using different adsorbent mass.	223
Figure 7.7: Maximum MB removal (% at equilibrium) for adsorption tests with varying initial dye concentration.....	225
Figure 7.8: Final MB concentration (mg/L, at equilibrium) for adsorption tests with varying initial dye concentration.....	225
Figure 7.9: Removal of methyl orange dye from water (at equilibrium) by produced chars and a commercial activated carbon.....	227
Figure 7.10: Evolution of MB dye removal from water with time (≤5 min) for selected chars and commercial activated carbon.....	229
Figure C.1: FTIR spectra for the wheat straw feedstock and chars produced from slow pyrolysis with 10 minutes SRT and varying temperature and feedstock moisture content.	285
Figure C.2: N ₂ adsorption-desorption isotherm for chars produced from as-received feedstock at 400, 500, and 600 °C, and 3, 6 and 10 min SRT.	286
Figure C.3: Pore size distribution (QS-DFT applied on N ₂ adsorption branch) for chars produced from as-received feedstock at 400, 500, and 600 °C, and 3, 6 and 10 min SRT.	287
Figure C.4: N ₂ adsorption-desorption isotherms (a), and pore size distribution (QS-DFT applied on adsorption branch) (b), for chars produced from as-received feedstock at 400 °C (left-hand side) and 600 °C (right-hand side) without injected gas.	288

Figure D.1: Pyrolysis liquids produced from wheat straw at temperatures of 500 and 600 °C and 6 minutes SRT (top: aqueous phases; bottom: organic phases).....	290
Figure D.2: Aqueous phases of pyrolysis liquids produced from wheat straw (400-600 °C and 10 min SRT); picture on the far right is an organic phase.....	291
Figure D.3: GC-MS chromatogram for the aqueous phase produced at 400 °C and 3 minutes SRT.	295
Figure D.4: GC-MS chromatograms for the aqueous (top) and organic (bottom) phases produced at 500 °C and 3 minutes SRT.....	296
Figure D.5: GC-MS chromatograms for the aqueous (top) and organic (bottom) phases produced at 600 °C and 3 minutes SRT.....	297
Figure D.6: First section of the cotton filter with accumulated condensate at the end of an experiment using gas injection during slow pyrolysis.	300
Figure D.7: Pyrolysis liquids produced with CO ₂ as injected gas at 400 °C (two left-hand side pictures) and 600 °C (two right-hand side pictures) (10 min SRT).....	301
Figure D.8: Examples of produced pyrolysis liquids with KOH-impregnated feedstock at 400 °C slow pyrolysis temperature.....	302
Figure D.9: Examples of produced pyrolysis liquids with KOH-impregnated feedstock at 600 °C slow pyrolysis temperature.....	302
Figure E.1: FTIR spectrum for the commercial activated carbon tested in this work.....	304
Figure E.2: N ₂ adsorption-desorption isotherm (a) and pore size distribution (QS-DFT applied on adsorption branch) (b) for the commercial activated carbon.....	304
Figure F.1: Correlations between MB removal from solution (% at equilibrium; vertical axis) and char properties (horizontal axis), for the chars produced with varying slow pyrolysis temperature and solid residence time.	306
Figure F.2: Correlations between MB removal from solution (% at equilibrium; vertical axis) and char properties (horizontal axis), for the chars produced with varying feedstock moisture content.....	307
Figure F.3: Correlations between MB removal from solution (% at equilibrium; vertical axis) and char properties (horizontal axis), for the chars produced with varying carrier gas.....	308
Figure F.4: Correlations between MB removal from solution (% at equilibrium; vertical axis) and char properties (horizontal axis), for the chars produced with KOH-impregnated feedstock.	309

Figure G.1: Adsorption of methylene blue dye from aqueous solution using selected chars and commercial activated carbon (0-180 minutes).....	310
Figure G.2: Linear fittings of MB adsorption to pseudo-first (a) and pseudo-second order (b) kinetics models, for a commercial activated carbon and char produced at 400 °C from as-received feedstock.	311
Figure G.3: Linear fittings of MB adsorption to pseudo-first (a) and pseudo-second order (b) kinetics models, for char produced from feedstock with 75 wt.% moisture content, and char from using CO ₂ as injected gas.	311
Figure G.4: Linear fittings of MB adsorption to pseudo-first (a) and pseudo-second order (b) kinetics models, for chars produced from feedstock impregnated with 0.1 M (left-hand side) and 1 M KOH solutions (right-hand side).....	312

List of Tables

Table 2.1: Physicochemical properties of wheat straw (examples from literature sources)..	33
Table 2.2: Types and typical main features of pyrolysis processes.	37
Table 2.3: Main char properties and respective most common methods of analysis.	56
Table 2.4: Summary of relevant research on slow and intermediate pyrolysis of wheat straw and other relevant biomass in screw reactors.	64
Table 2.5: Summary of results from CO ₂ activation of oak wood by Jung and Kim [263].	72
Table 2.6: Treatment stages in wastewater treatment.	74
Table 4.1: Results from proximate analysis of the wheat straw feedstock by TGA (number of experiments, n=3).	113
Table 4.2: Proximate analysis (wet basis) of wheat straw and rice straw from various literature sources.	113
Table 4.3: Results (n=3) and literature values from ultimate analysis of wheat straw, and ash contents.	114
Table 4.4: Experimental and calculated heating values of the feedstock (n=3).....	115
Table 4.5: Values of higher heating value for wheat straw from other research examples.	115
Table 4.6: Inorganic contents of the feedstock ashes performed by GreenCarbon project partners [332].....	116
Table 4.7: Mass balances from the slow pyrolysis experiments using as-received wheat straw with varying pyrolysis temperature and SRT (n=2).	118
Table 4.8: VRT values (calculated and from visual determination) for experiments with varying temperature and SRT (n=2).	121
Table 4.9: Values of VRT estimated from the visualisation of first vapours for the experiments comparing both screw reactors (n=2).	123
Table 4.10: Product yields from the second screw reactor and comparison with the first screw reactor (n=2).	124
Table 4.11: Mass balances from slow pyrolysis experiments using wheat straw with varying feedstock moisture content (n=2).	126
Table 4.12: Product yields from slow pyrolysis of oven-dry wheat straw (broken pellet form) at 600 °C and comparison with using as-received feedstock (first reactor; 10 min SRT).	126
Table 4.13: Values of VRT based on the visualisation of the first pyrolysis vapours for the slow pyrolysis experiments with varying feedstock moisture content (M) (n=2).	129
Table 4.14: Ash contents of the wheat straw feedstock for different feedstock moisture contents (n=3).	132

Table 4.15: Proximate analyses of chars produced from wheat straw slow pyrolysis at different pyrolysis temperature (T), solid residence time (SRT), and feedstock moisture content (M) (n=3).	139
Table 4.16: Ultimate analyses (wt.%, dry ash free basis) and calculated higher heating value (MJ/kg, dry basis) of the chars produced from slow pyrolysis of wheat straw with varying pyrolysis temperature (T), solid residence time (SRT), and feedstock moisture content (M) (n=3).	142
Table 4.17: Inorganic contents (wt.%, dry basis) in the ash from chars produced with varying process temperature (10 minutes SRT).....	144
Table 4.18: Surface area, total pore volume and pore diameter (mode) of chars produced from slow pyrolysis of wheat straw with varying pyrolysis temperature (T), solid residence time (SRT), and feedstock moisture content (M).	152
Table 4.19: Distribution of gaseous species (vol.%) and main calculated properties from slow pyrolysis experiments using as-received wheat straw with varying temperature and SRT (n=2).	158
Table 4.20: Gas products distribution (vol.%) and main calculated properties from the slow pyrolysis experiments using wheat straw with varying feedstock moisture content (n=2). .	160
Table 5.1: Product yields from slow pyrolysis experiments in the screw reactor without injecting gas or with N ₂ or CO ₂ as injected gases (number of experiments, n=2).	165
Table 5.2: VRT values for experiments without injected gas or with N ₂ or CO ₂ as injected gases (n=2).	166
Table 5.3: Gas products distribution (vol.%) and main calculated properties from slow pyrolysis experiments using N ₂ or CO ₂ as injected gases or not injecting gas (n=2).	168
Table 5.4: Proximate analysis (wt.%, dry basis) of the chars produced from slow pyrolysis without injected gas and using N ₂ or CO ₂ as injected gases (n=3).	173
Table 5.5: Elemental analysis (wt.%, dry ash-free) and HHV of chars produced from slow pyrolysis without injected gas and using N ₂ or CO ₂ as injected gas (n=3).	174
Table 5.6: Results from nitrogen physisorption at 77 K applied to chars produced using N ₂ or CO ₂ as injected gases or without injected gas.....	180
Table 6.1: Proximate analysis (wt.%, d.b.) of feedstock impregnated with different concentrations of KOH solution (number of experiments, n=3).....	184
Table 6.2: Ultimate analysis (wt.%, d.a.f.) and HHV (MJ/kg, d.b.) of feedstock impregnated with different concentrations of KOH solution (n=3).....	184

Table 6.3: Product yields (wt.%, dry and KOH-free feedstock basis) from experiments using KOH-impregnated feedstock in the second screw reactor (n=2).....	185
Table 6.4: Ratios between activating agent and char for experiments with KOH-impregnated wheat straw.....	186
Table 6.5: VRT values for experiments with varying KOH concentration obtained through visual and calculated methods (n=2).....	187
Table 6.6: Gaseous species distribution (vol.%), gas product density, molecular weight, and HHV for each slow pyrolysis experiment with KOH-impregnated feedstock (n=2).	188
Table 6.7: Proximate analyses (wt.%, dry basis) of the chars produced from experiments from feedstock with varying KOH solution concentrations (n=3).	194
Table 6.8: Ultimate analyses (wt.%, dry ash-free basis) and calculated higher heating value (MJ/kg, dry basis) of the chars produced from experiments with varying KOH concentration (n=3).	196
Table 6.9: Results from nitrogen physisorption at 77 K applied to chars produced from KOH-impregnated feedstock.....	203
Table 7.1: Results from N ₂ physisorption (77 K) analysed with QS-DFT model for commercial activated carbon.....	210
Table 7.2: Coefficients of determination for the linear relationship between char properties and MB removal for chars produced with varying temperature and SRT, and indication of positive (+) or negative (-) correlation.....	212
Table 7.3: Maximum MB removal from solution (at equilibrium) with feedstock and torrefied feedstock (300 °C).	212
Table 7.4: Removal of MB dye from water (at equilibrium) for chars produced from experiments with varying feedstock moisture content (“M”).	214
Table 7.5: Coefficients of determination for linear relationships between char properties and MB removal for chars from varying feedstock moisture content (M), and indication of positive (+) or negative (-) correlation.....	214
Table 7.6: Removal of MB dye from water (at equilibrium) for the chars produced from experiments with N ₂ or CO ₂ as injected gases, or using no injected gas.	216
Table 7.7: Coefficients of determination for linear correlations between char properties and MB removal for chars produced with varying injected gas, and indication of positive (+) or negative (-) correlation.	216
Table 7.8: Removal of MB dye from water (at equilibrium) for the chars produced from experiments with KOH-impregnated feedstock.....	218

Table 7.9: Coefficients of determination for linear correlations between char properties and MB removal for chars produced with varying KOH solution concentration, and indication of positive (+) or negative (-) correlation.....	219
Table 7.10: Coefficients of determination (R^2) for data fitting to pseudo-first and -second order kinetics models.	230
Table 7.11: Comparison of MB adsorption performance in this work with relevant literature examples.	231
Table A.1: Molecular weight, density and high heating value of individual gaseous species at normal temperature and pressure conditions (20 °C and 1 atm) [1].....	279
Table B.1: Values of solid residence time for the first screw reactor based on screw speed and on cold runs with wheat straw feedstock.	281
Table B.2: Selected solid residence times used for the slow pyrolysis experiments with wheat straw feedstock in the first screw reactor.....	282
Table B.3: Values of solid residence time for the second screw reactor based on screw speed and on cold runs with wheat straw feedstock.	283
Table B.4: VRT estimation for the first screw reactor for different assumed gas flow rates.....	283
Table D.1: Water contents of aqueous phases of pyrolysis liquids produced from wheat straw slow pyrolysis.....	291
Table D.2: pH value of the aqueous phase of the pyrolysis liquids produced from wheat straw.	292
Table D.3: Ultimate analyses of the organic phases of the liquids produced from wheat straw pyrolysis.....	293
Table D.4: Experimental and calculated HHV of the organic phases produced from wheat straw pyrolysis.	294
Table D.5: Most common compounds (ordered by retention time) found from GC-MS of the liquids produced from wheat straw pyrolysis at 400-600 °C and 3 minutes SRT.....	298

Chapter 1 – Introduction

1.1. Background and motivation

The dependency of mankind on fossil fuels and fossil fuel-derived products has been a reality since the nineteenth century. The use of fossil fuels leads to the removal of carbon from the soil and its release to the atmosphere, mainly as CO₂, which increases the concentration of greenhouse gases (GHG) in our atmosphere. GHG absorb and emit energy in the infrared range and cause a greenhouse effect, contributing to warming the planet's atmosphere and surface [1]. The increase in GHG has been significant in the last decades, e.g., CO₂ levels are now more than 400 ppm, increasing from 350 ppm in 1988 and 300 ppm in 1914 [2]. The accumulation of GHG from human sources has been connected to global warming and also increasing ocean acidity, which can be harmful for life on Earth [3]. Figure 1.1 shows the evolution since 1850 of the deviation of global surface temperature to the 1961-1990 average, and of the average CO₂ concentration (ppm) in the atmosphere [2][4].

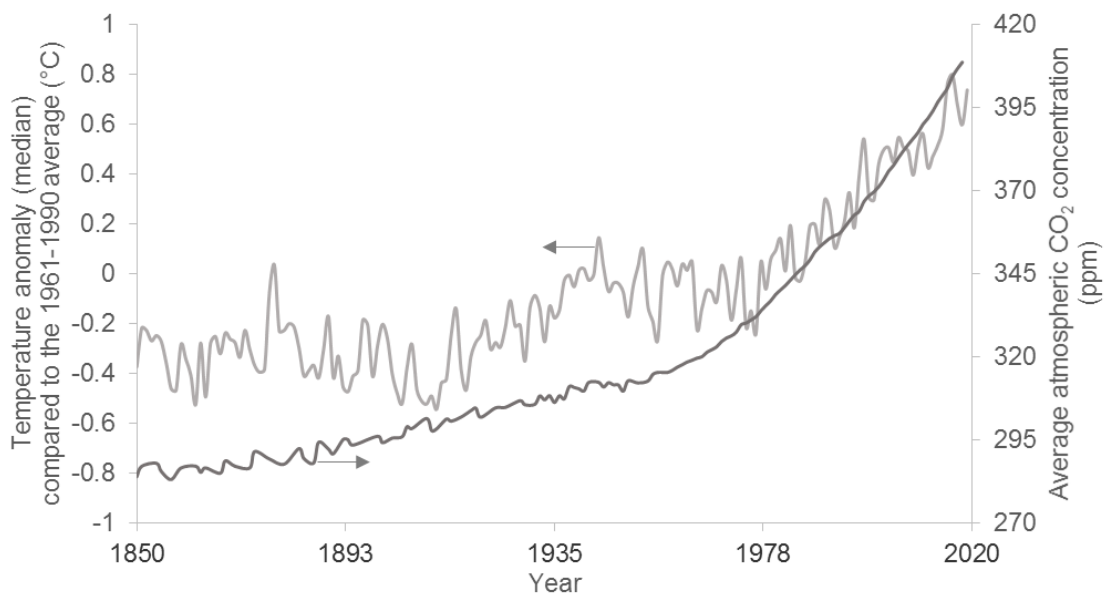


Figure 1.1: Temperature anomaly (median) compared to the 1961-1990 average, and average CO₂ concentration in the atmosphere [2][4].

In order to counter the underlying issues of fossil fuel consumption, mankind must divest from fossil fuels and invest in renewable forms of energy and products such as biomass (others are solar, wind, geothermal, hydropower). Biomass comes in a great variety of forms: wood and woody residues, agricultural residues, grasses, energy crops, algae, food waste, manure and other animal residues, sewage sludge, etc. [5][6]. Figure 1.2 indicates common biomass forms.

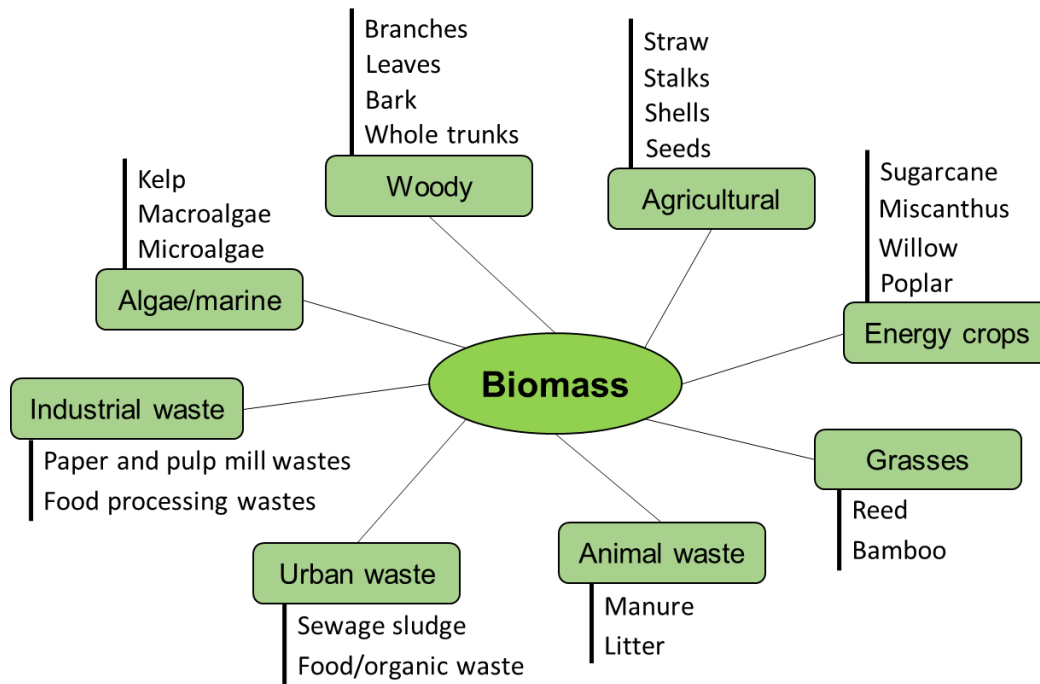


Figure 1.2: Schematic depiction of different forms of biomass (own artwork, based on [5][6]).

The use of bioenergy is referred to as being flexible enough to balance the intermittent production of energy from solar and wind sources [7]. Furthermore, bioenergy can promote energy access, independence, and resilience [7]. However, there are concerns with land use change, biodiversity and carbon balance [8][9][10], and the type of biomass that is used should also be considered when evaluating its benefit to society. When growing certain biomasses, there may be competition with food production, which must be avoided [11][12]. First generation biofuels (i.e., bioethanol and biodiesel) are produced from biomass that is sugar or oil-rich (e.g., maize, sugarcane, palm, rapeseed, etc.), while second generation biofuels derive from biomass which does not compete with food production, such as lignocellulosic biomass (e.g., wood, agricultural residues such as wheat straw) and animal and industrial waste [13][14]. Lignocellulosic biomass refers to biomass comprised mostly of polysaccharides (cellulose and hemicellulose) and lignin, and further details on this biomass type (the one used in this PhD work) are given in Chapter 2. The so-called third generation biofuels are produced from algal biomass, which usually have higher energy outputs [15].

Many biomass types are residues or wastes, with low value, which creates another advantage of using biomass for bioenergy and bioproducts, since this can help decrease the release of GHG such as CO₂ and CH₄ from waste accumulation and poor waste management. Especially in developing countries, part of the waste is disposed of in landfills or open dumps, and waste generation is increasing with population growth and industrial development [16]. Landfilling and dumping waste has issues such as depletion of useful land area for other

activities and pollution of air, water and soil, especially if poorly managed [17]. Transforming wastes into useful products helps tackle the waste accumulation problem more effectively.

Besides being an energy source, biomass can also provide products to replace those that are usually made from fossil fuels, e.g., plastics, fertilisers, adsorbents [5]. Examples of bioproducts being developed (i.e., products from biomass) are biofibres, bioplastics and biocomposites [18]. Bioadsorbents are also being produced from biomass and biomass-derived products, due to the increase in worldwide demand for decontamination of water and air, and to the relatively low cost of biomass [19]. Research to bring bioproducts to the market is on-going, with some of the main challenges being cost effectiveness and comparable performance to fossil fuel-based materials [18]. An economy based on utilising biomass and wastes to produce energy and replace existing unsustainable products – a bioeconomy, based on biorefineries – can also bring economic advantages for the regions in which it is implemented, through job and income creation [8][20].

The different processes that can process biomass into energy and other products are usually divided into biochemical and thermochemical processes. The biochemical processes typically rely on some kind of biological activity, e.g., microbes or enzymes, while thermochemical processes are based on heat and chemical reactions. Fermentation and anaerobic digestion are examples of biochemical processes, while combustion, gasification and pyrolysis are thermochemical processes.

Among the thermochemical processes, combustion consists of burning the material in excess oxygen and obtaining energy, and ash as a by-product. The energy from combustion can be used to produce steam and to run a turbine, producing heat and power at the same time. In the gasification process, the process atmosphere includes an oxidising agent such as air, O₂, CO₂ or steam, in low concentration (i.e., with 15-30% of the oxygen that would be used for combustion [21]), leading to partial oxidation of the feedstock. The main product from gasification is the gaseous product, usually used for energy purposes, and a residual solid product comprised mainly of inorganic compounds. Pyrolysis, on the other hand, exposes the feedstock to an atmosphere with zero or a very limited amount of oxygen (when air ingress occurs when feedstock is fed, or due to lack of air-tightness, usually in less developed systems), which thereby avoids burning and keeps most of the carbon in solid form [22][23][24]. In pyrolysis, the feedstock is thermally degraded, resulting in a carbonaceous solid product, and producing vapours which upon cooling separate into a liquid product and a gaseous product. The particular features of pyrolysis, addressed in more detail in Chapter 2, make it flexible to a large variety of feedstocks, and at the same time able to produce different useful products including energy-carriers, which is advantageous.

Among the three products obtained from pyrolysis, the solid product, called char, is a material comprised mostly of carbon and also hydrogen, nitrogen, oxygen, and inorganic

elements. Char is generally a porous material with pores of different sizes, that can originate from the original skeletal structure of the feedstock (especially if the feedstock is biomass), or pores can be created due to loss of material by devolatilisation during pyrolysis, especially at higher production temperatures [25]. Devolatilisation of biomass during pyrolysis also leads to greater energy density (by weight) than the original biomass, and increased stability [26]. The presence of heteroatoms can form functional groups on the surface, which promote interactions with the surroundings [27]. Details on composition and properties of char and how they are influenced by process conditions and feedstock choice are addressed in Chapter 2.

Char has a wide spectrum of applications, with accounts of more than 55 possible uses [28]. The use of char is not new, with evidence of its use for cave paintings in pre-history [29] and its use in smelting ores for bronze production being documented since ancient Egypt [30]. The ability of char to improve agricultural land has also been known for centuries [31]. Char applications range from energy production (in cooking and heating, with the char being referred to as charcoal), to improving soil conditions for agriculture (char referred to as biochar), to removing contaminants from air and water (mainly in the form of activated carbon after activation, but also as char, without activation), to uses in electrochemistry, as animal feed additive, and many others. Char properties can be tailored to different applications. For clarification of the differences between char and other nomenclature commonly used to refer to char in connection to its applications, see Figure 1.3. The application chosen to be studied in this work (water decontamination) is in bold.

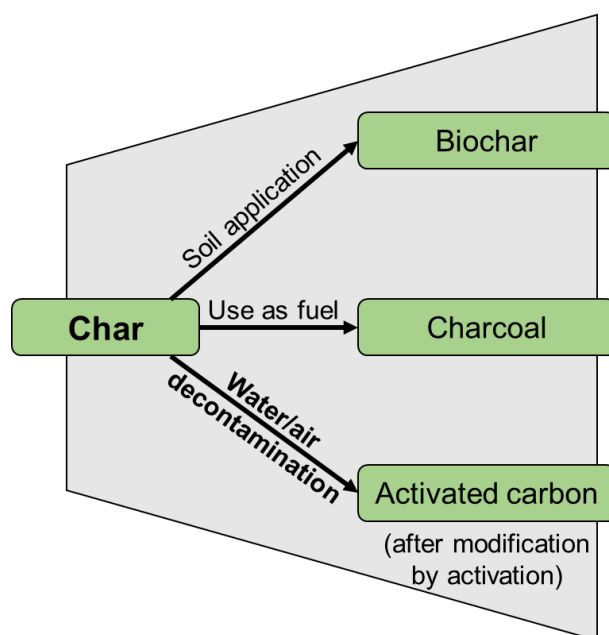


Figure 1.3: Depiction of the differences between char products (biochar, charcoal and activated carbon) according to their application.

Regarding the nomenclature used for the solid product, it should be noted that there are other classification methods, e.g., based on the feedstock used: if the feedstock is biomass or biobased, the char can be called biochar, while the term char can be used for the solid product from pyrolysis of non-biobased feedstocks, such as tires and plastics. In this work, since the feedstock used is solely biomass (wheat straw), the term biochar could be used, however it was chosen to use char as a general term, to avoid confusion between classification methods. The term char is used in this work to mean the solid product from slow pyrolysis, without taking into account the feedstock or the application.

Due to the large list of applications and environmental benefits, demand for char is increasing, and a lot of research is currently underway. Char and pyrolysis as its production technology can contribute to several of the UN's Sustainable Development Goals (SDGs), namely: zero hunger, affordable and clean energy, climate action, clean water, and sanitation, etc. [32][33].

The application of char as biochar is gaining much interest, due to its many advantages, with carbon storage being one of the most attractive. This is because of the relatively high carbon content and stability [26]. The IPCC has recognised biochar as one of the negative emission technologies that can help humanity reach the CO₂ reduction targets from the Paris Agreement [34][35].

One of the most promising applications of char is as an adsorbent of pollutants from air and water, to replace activated carbon which is the traditionally used and most popular adsorbent worldwide [19]. The feedstocks used to produce activated carbon vary, with the most common being coal, coconut shells and wood [36][37]. The use of fossil fuel coal as feedstock for activated carbon production, and also of coconut shells, which are not abundant worldwide, is one of the drivers for research into low-cost adsorbents such as char [36]. The production process for activated carbon is also often time and resource-consuming, due to the use of high temperatures and chemical agents for example, and there is a need to make the process more sustainable and affordable [19][38][39]. Furthermore, the demand for adsorbents is constantly increasing, due to the constant pollution of air and water by industries, and to the rise of stricter legislation regarding air and water quality [40]. Adsorption is one of the most effective techniques for water decontamination, and is increasingly used in wastewater treatment plants, especially for removing dissolved contaminants such as dyes, nutrients and heavy metals, and also pharmaceuticals and other micropollutants [41]. More details about the use of char and activated carbon in adsorption are given in Chapter 2.

Several companies produce activated carbon, including CPL Industries in the UK (which also produces charcoal) [42], and Calgon Carbon [43] and Cabot Corporation [44], both based in the US. Currently, char is being trialled in the US as a filter medium (blended with other natural materials) for removing contaminants from stormwater by the companies

Sunmark Environmental and Stormwater Biochar [45][46]. The company Glanris in the US is also commercialising a filtration media based on char, from rice hulls and produced without harsh chemical treatments, used mainly for removal of metals from water, but also for suspended solids and organic compounds [47][48].

In summary, char and char-related products have been known for a long time to have valuable properties and certain advantages over fossil fuel-based products such as activated carbon from coal and non-abundant biomass. However, to drive forward the investment required to bring the advantages of char application to reality, research and advancements are required on the fundamental science behind the product properties and integrating on a system-level of waste recycling and energy production [26][49]. This work intends to contribute to these objectives.

1.2. Work aims and objectives

The work in this PhD thesis had the main goal of producing char products from continuous slow pyrolysis of an agricultural residue, wheat straw, and testing them as bioadsorbents for water decontamination. Different strategies were employed, such as varying process parameters (temperature, solid residence time, reaction atmosphere) and pre-treating the feedstock (elevating moisture content, KOH-impregnation). The bioadsorbents were applied to significantly remove an organic cationic dye from water, with performance comparable to a commercial activated carbon, which is the most common traditional adsorbent with very high performance (>99% removal).

The underlying objectives were as follows:

- To study the influence and establish relationships between varying process/feedstock conditions (e.g., pyrolysis temperature, solid residence time, feedstock moisture content, injecting different gases to modify the reaction atmosphere, and feedstock pre-treatment), and the product yields and physico-chemical properties, with a focus on the solid product;
- To employ the chars produced from different conditions in the removal of an organic cationic dye from water, through batch tests;
- To investigate if it was possible to improve the quality and adsorptive performance of the produced chars by modifying the pyrolysis process/feedstock, either by injecting CO₂ (a physical activation agent) into the reactor, or by wet KOH-impregnation of the wheat straw feedstock to promote chemical activation;
- To find, based on the performances of the different employed chars, optimal process conditions to produce, from continuous slow pyrolysis of wheat straw, a

bioadsorbent to remove an organic cationic dye from water, and potentially other contaminants by extrapolation.

This work intends to further the knowledge on the impact of different process/feedstock conditions on the product yields and characteristics from continuous slow pyrolysis of biomass. Particularly, the feedstock moisture content, the reaction environment and a pre-treatment of the feedstock with KOH solution are conditions that have not been studied as deeply as others such as process temperature and solid residence time.

Due to arising stricter legislation regarding water quality, demand for adsorbents for water decontamination is rising, and this work has the objective of expanding the knowledge on the development of biobased adsorbents, to replace unsustainable and time- and resource-consuming traditional adsorbents such as activated carbon.

It is expected that the injection of a reactive gas (CO₂) into the reactor and pre-treating the feedstock by elevating its moisture content or impregnation with KOH will produce changes (i.e., activation) on the surface of the chars in terms of chemical functionalities, porosity, and surface area. These changes have the potential to benefit the application of the chars for the removal of contaminants from aqueous streams, and are traditionally produced by physical (e.g., with CO₂ or steam) and chemical (e.g., with KOH impregnation) activation. Physical activation is usually performed in a two-step process, with activation of char after a first carbonisation stage. Having the pyrolysis process occurring simultaneously with the activation process (*in situ*), which is the case in this work, has potential processual and economic benefits.

Using relatively low pyrolysis temperatures (400 to 600 °C) and short solid residence times (up to 10 minutes) compared to traditional industrial production of adsorbents (i.e., activated carbon) has advantages in terms of energy and time expenditure. Moreover, the use of a continuous reactor system can have benefits over using batch systems, and using a relatively abundant and low-value agricultural residue such as wheat straw is also beneficial. The employed conditions were optimised for the most appropriate properties and the best adsorption performance, with a compromise with char yield.

1.3. Thesis structure

The thesis has the following structure:

- 1) A comprehensive review of the literature on the subjects covered by this work:
 - a) Slow pyrolysis of biomass in screw reactors;
 - b) Modification of the pyrolysis process in order to produce a solid material for adsorption applications (e.g., activated carbon or modified/tailored char);

- c) Use of char or char-derived materials as adsorbents of organic pollutants from water, focusing on dyes.

In the literature review the fundamental knowledge of these subjects was covered and the most recent advances and current knowledge gaps were discussed.

2) A methodology chapter addressing the materials, methods and equipment used in the experimental work, including data treatment. The experimental work includes:

- a) Producing char products from slow pyrolysis and modified slow pyrolysis of a wheat straw feedstock in a screw reactor;
- b) Characterising the feedstock and the products from said processes, focusing on the solid products;
- c) Studying the use and performance of the solid products for the adsorption of an organic cationic dye from water.

3) Presentation and discussion of the experimental results from:

- a) The slow pyrolysis experiments with the wheat straw feedstock: influence of the studied parameters (temperature, solid residence time, feedstock moisture content) on the product yields and properties, with a focus on the char product;
- b) The slow pyrolysis experiments using CO₂ as reaction environment: influence of the CO₂ on the product yields and properties of the solid products, compared to using N₂ or not injecting gas into the reactor;
- c) The slow pyrolysis experiments using KOH-impregnated wheat straw: influence of KOH impregnation on product yields and solid product properties;
- d) The adsorption tests carried out using the produced solid products from slow pyrolysis and modified slow pyrolysis.

4) Discussion of the conclusions from the experimental work performed, and their implications for scientific knowledge.

5) Suggestions of future work to be performed, based on the findings of this work and on the knowledge gaps.

1.4. GreenCarbon Project

The research for this thesis is part of the GreenCarbon project, funded by the European Union in the framework of the H2020 Marie Skłodowska Curie Actions (Innovative Training Networks). The project (No. 721991) is entitled “Advanced Carbon Materials from Biowaste: Sustainable Pathways to Drive Innovative Green Technologies”.

The GreenCarbon project seeks to develop processes to produce tailor-made biomass-derived carbons, and using the carbon materials in advanced applications such as

heterogeneous catalysis and removal of pollutants, as well as for soil enhancement and CO₂ capture and sequestration. The project is comprised of eight different academic partners, and seven companies, and hosts 14 Early Career Researchers across the different partners. The experimental research programme is divided into four work packages:

WP4 – Pyrolysis conversion routes for dry feedstocks;

WP5 – Hydrothermal carbonisation (HTC) conversion routes for wet feedstocks;

WP6 – Refining of biomass-derived carbons and advanced applications;

WP7 – Sequential biochar systems.

The research topic covered in this thesis is included in WP4. Appendix H contains a summary of outputs and publications based on the work performed in this thesis and other work performed for the GreenCarbon project.

The GreenCarbon project also aims at providing the researchers with a connection with industry, through a secondment. The secondment for this work was with the company Biomass Power Projects, Ltd. (BPP), based in Oxford, UK. The company specialises in the development of energy production plants from biomass and wastes using advanced technologies such as gasification and pyrolysis.

With the secondment, several industrial facilities were visited, such as a materials recovery facility, a recycling centre, a waste to energy plant, a biomass-based combined heat and power plant, and a manufacturer of equipment for solids handling, transport, and processing. The industrial visits allowed to dialogue with industrial experts and have a connection to industrial solutions to different challenges in the area of waste management and energy production.

The secondment was a valuable way to connect with and have a sense of various aspects of industry, from feedstock sourcing to equipment design (e.g., reactors, boilers, conveyors, screws, feeders), to control and automation, and to product application.

Chapter 2 – Literature review

2.1. Slow pyrolysis of biomass

2.1.1. Lignocellulosic biomass

Among the different kinds of solid biomass, the focus of this work is wheat straw, an agricultural residue, which is a lignocellulosic biomass. Lignocellulosic biomass is comprised of three main groups of polymeric compounds, interconnected between themselves: cellulose, hemicellulose, and lignin. The first two groups (cellulose and hemicellulose) can also be collectively referred to as holocellulose, and consist of polysaccharides (chains of five and six-carbon sugars), while lignin is comprised of a network of different organic polymers mainly derived from phenol [50]. A representation of the three lignocellulosic groups and the monophenol precursors of lignin is present in Figure 2.1.

Different lignocellulosic biomasses have distinct proportions of the lignocellulosic groups, which usually vary in the ranges: 35-50 wt.% for cellulose, 20-35 wt.% for hemicellulose, and 10-25 wt.% for lignin [51]. There is significant variation in these values depending on the species of biomass, the soil and weather conditions, and other factors. Generally, herbaceous biomass such as wheat straw has lower cellulose content compared to woody biomass [50]. Apart from the lignocellulosic compounds, biomass also has an extractive fraction, called extractives, which consist of organic substances such as waxes, fatty acids, and phenols [53].

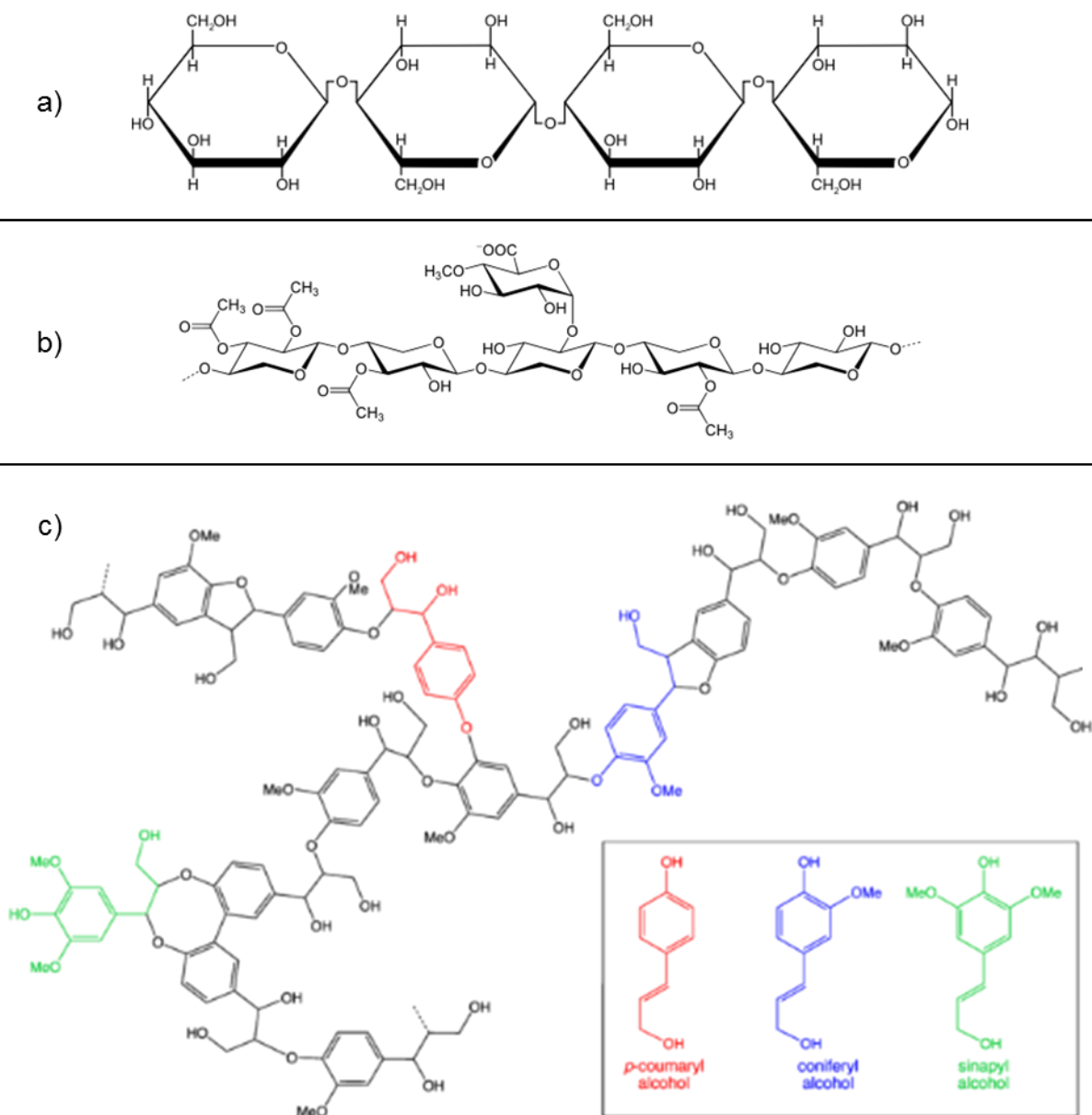


Figure 2.1: Skeletal structural formulas (abbreviated) of the lignocellulosic groups: a) cellulose, b) hemicellulose, and c) lignin (with monophenol precursors in inset).

Cellulose and hemicellulose images are public domain; lignin image is modified from [52].

While the lignocellulosic compounds and the extractives comprise the organic fraction of the biomass, there is also an inorganic fraction, which is converted into ash upon combustion. Numerous inorganic elements can be present in the inorganic fraction of biomass, such as Ca, K, Mg, Na, P, Cl, Si, S, Fe, Mn, and Al [54], in the form of oxides, and also carbonates, sulphates, oxalates, and other forms [55]. The fraction of inorganics in lignocellulosic biomass can vary from <2 wt.% to >15 wt.%, depending on the type and origin [56]. Inorganic contents are usually higher in herbaceous biomasses such as wheat straw, when compared to woody biomass for example [57]. When biomass is exposed to high

temperatures and non-inert/oxidative atmospheres (i.e. during combustion or gasification), the inorganic compounds can suffer chemical reactions between them to form other compounds, which can cause fouling, slagging and corrosion in boilers, heat exchangers, piping, and other equipment [58][59]. A relatively high inorganic/ash content can thus be a disadvantage in thermochemical processing of biomass through combustion and gasification. Besides this, the inorganic contents can also act as catalysts for cracking and other reactions, which can be beneficial in gasification and pyrolysis. This catalytic effect is discussed in subsection 2.1.4.

Solid biomass also has a certain moisture content, which can vary up to ≈ 60 wt.%, depending on collection, atmospheric, and storage conditions [60]. The moisture content is very important and can negatively affect transport, handling, and processes such as drying and conversion to energy. A relatively high moisture content reduces the value of the biomass due to having less dry weight, lowers its energy value, and can reduce the efficiency of a thermochemical process due to the amount of energy needed for drying. It is therefore usually more advantageous to dry biomass before transporting to a thermochemical plant, however, for mobile plants or plants using locally available biomass it could be more economically advantageous to avoid drying.

The composition of biomass (e.g., lignocellulosics, inorganics and moisture) governs its physicochemical properties, which are fundamental for the design and implementation of logistics (e.g., collection, transport), and pre-treatment and conversion processes [61].

2.1.1.1. Wheat straw feedstock

Wheat straw is the lignocellulosic biomass studied in this work (details on its selection in Chapter 3, subsection 3.1). Generated from the harvest of wheat, a cereal crop, it can be considered an agricultural residue, although it is more and more seen as a resource due to the possibility of obtaining bioenergy and bioproducts from it. Wheat straw is one of the most abundant agricultural residues in the world, along with rice straw and residues from maize and sugar cane [62].

Worldwide production of cereal crops (e.g., barley, rice, wheat, maize, rye) was estimated to be 2,700 Mton/year in the world, with maize being the most produced (1,150 Mton/year), followed by rice (782 Mton/year) and wheat (735 Mton/year) (2018 FAO data) [63]. The distribution of wheat production in the world, with over 75% in Europe and Asia, is pictured in Figure 2.2 [63]. In Europe, the top wheat producers in 2018 (in decreasing order) were Russia, France, Ukraine, Germany and the UK [63]. Although the UK produces a significant amount of wheat (13.6 Mton/year in 2018), it only accounted for around 6% of the wheat produced in Europe in 2018.

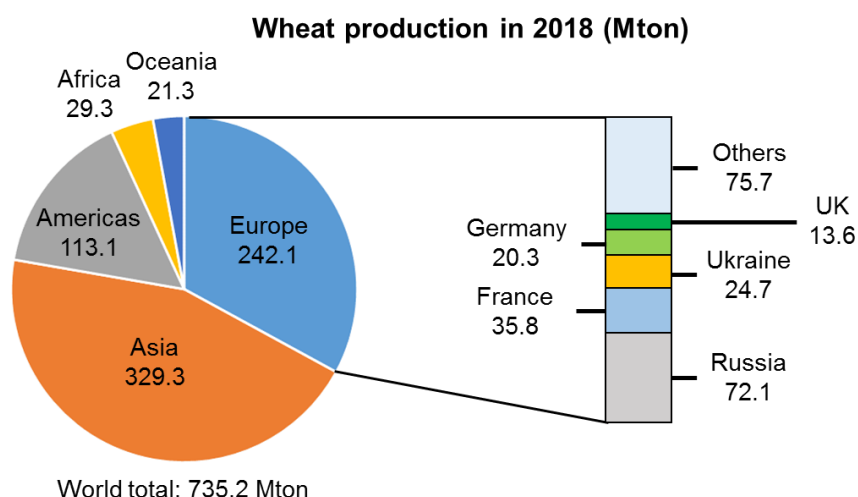


Figure 2.2: Wheat production per continent and in European countries (Mton, 2018 FAO data from [63]).

In the UK, wheat is the predominant straw generator (over 50 wt.%), and others are for example rapeseed, barley, and oat [64][65]. There is a lack of information regarding straw generation, and its estimation is challenging and depends on several factors [66]. Straw yield is usually estimated using the straw-to-grain/cereal ratio, which varies between 0.60 and 1.75 for wheat based on several EU sources [67]. Using these ratios and the 2018 FAO data in Figure 2.2, the range of produced wheat straw in the UK was calculated for this thesis as \approx 8-24 Mton. The proportion of straw that is recoverable from the field, due to removal efficiency <100%, is lower than the total produced straw.

In developing regions especially, in order to save time for the following crop season, the straw is left in the field to be integrated in the soil, or is burned, also often on the fields themselves [62]. Open-field burning is a very serious problem in developing countries such as India, due to the associated air pollution [68][69]. Integrating the straw into soil can allow for carbon and nutrients to be returned.

The livestock sector is the main user of straw in the UK, to be used in animal bedding and feed rations [65]. Other markets for wheat straw are for substrate in mushroom production and as fuel for heat and power generation [65]. Wheat straw is viewed as an important feedstock for a biobased economy in Europe, for example for bioethanol production [62][70]. Studies have been performed on the UK straw availability for biofuels production, for example by Glithero *et al.* [66]. There are concerns about depletion of carbon from soils if straw is removed for other uses, but competition with food production is considered low, allowing to consider wheat straw as a second generation lignocellulosic biomass [62].

Straw has a relatively low bulk density, which makes transport costs high [65]. An option is to densify straw through pelletising, subjecting the material to sequential cutting,

drying, milling/grinding, screening and compressing into a pellet with usually 0.6-1.2 cm diameter and up to 4 cm length [71]. The high pressure and consequent high temperature can lead to plasticisation of lignocellulosic components, which can act as a natural binder for the pellet [72]. An additive (natural or synthetic) can be added to the process to promote agglomeration and pellet resistance. Densifying biomass is useful for its transportation, handling, storage, and also combustion due to greater energy density. Pelletising also has the benefits of lowering the moisture content and increasing the homogeneity of biomass [73], but may decrease the efficiency of thermal conversion processes due to temperature gradients inside the particles [74]. Pelletising can improve biomass quality and decrease transport costs, however, the pelletising cost can be significant.

Physicochemical characteristics of wheat straw biomass are presented in Table 2.1.

Table 2.1: Physicochemical properties of wheat straw (examples from literature sources).

Property	Value(s)	Wheat straw characteristics	Reference(s)
Cellulose (wt.%)	35-39	N/A	[51]
Hemicellulose (wt.%)	23-30		
Lignin (wt.%)	12-16		
Volatile matter (wt.%, d.b.)	80.9 / 71.7 / 72.2 / 83.1	4 types: cut to \approx 1 cm / pelletised with epoxy binder / cut to below 0.15 mm / cut to 0.5-2.0 mm	[74][75][76]
Fixed carbon (wt.%, d.b.)	7.7 / 18.1 / 17.5 / 10.3		
Ash (wt.%, d.b.)	11.4 / 9.6 / 10.3 / 6.6		
C (wt.%, d.b.)	42.8 / 76.7	2 types: cut to \approx 1 cm / pelletised with epoxy binder	[74]
H (wt.%, d.b.)	7.1 / 4.3		
N (wt.%, d.b.)	0.6 / 2.3		
S (wt.%, d.b.)	0.2 / 0.3		
O (wt.%, d.b.)	37.8 / 6.8		
HHV (MJ/kg)	15.6 / 27.8 / 17.2 / 14.7	4 types: cut to \approx 1 cm / pelletised with epoxy binder / cut to below 0.15 mm / cut to 0.5-2.0 mm	[74][75][76]

From the values presented in Table 2.1 it is possible to observe that the pelletising with an epoxy binder led to an increase in the carbon and fixed carbon contents and decrease of oxygen contents, thereby increasing the heating value of the feedstock.

A relatively low proportion of nitrogen in wheat straw (compared to other biomasses) is an advantage for thermal conversion processes due to the lower production of NO_x , however, a higher proportion of inorganics can be detrimental due to slagging and corrosion. [62]. The inorganic content of herbaceous biomass such as wheat straw is generally higher than in woody biomass. Among the inorganic contents of wheat straw, compounds with potassium and silica are usually in greater proportion, with also calcium, phosphorous,

chlorine, and other inorganic elements [75][77][78]. The relatively low sulphur content leads to a diminished release of harmful sulphur compounds, which is a positive aspect.

2.1.2. Biomass conversion processes into bioenergy and bioproducts

Solid lignocellulosic biomass, such as wood and agricultural residues, can be converted into bioenergy and bioproducts through a variety of different processes, mainly divided into thermochemical and biochemical. Figure 2.3 represents the main pathways used for solid biomass conversion, along with the main products from each process.

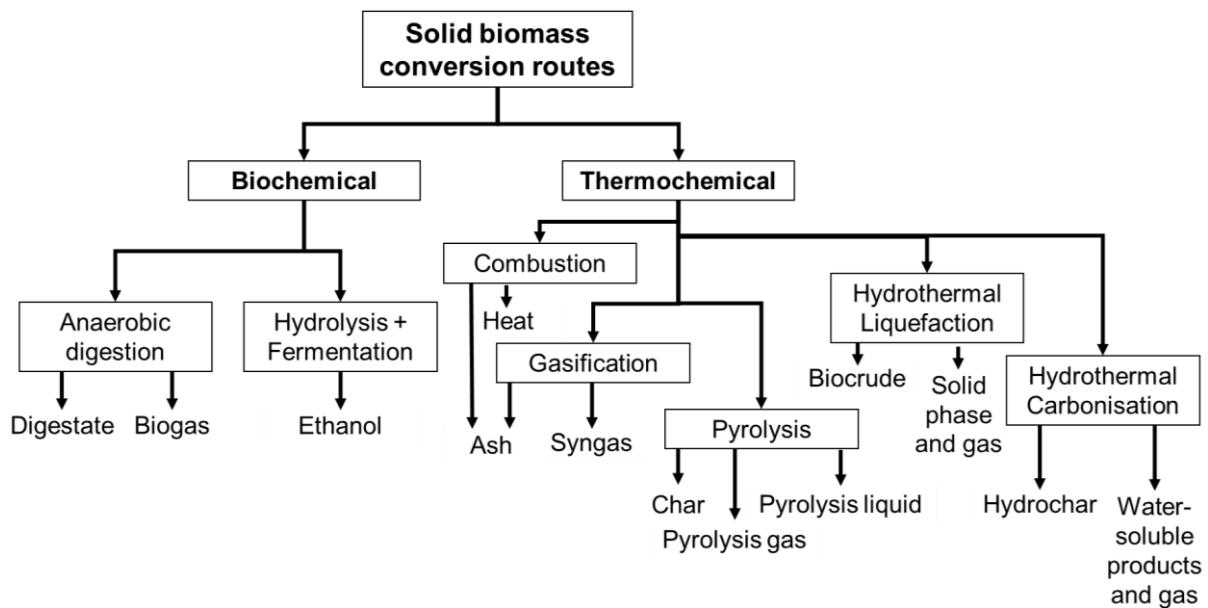


Figure 2.3: Thermochemical and biochemical processes employed to convert solid biomass into various products.

The biochemical processes utilise water and hence are more applicable to wet feedstocks, such as sewage sludge treated by anaerobic digestion. Among the thermochemical processes, some processes also utilise water or a water-containing solvent: hydrothermal liquefaction (HTL) and hydrothermal carbonisation (HTC). These processes are thermochemical because they also rely on the effect of temperature and are also more employed for wet feedstocks such as brewery waste or manures. These hydrothermal processes also develop considerable pressures inside the reactor system, up to 20 MPa or more [5]. HTL focuses more on obtaining a liquid product (biocrude), employing higher temperatures than HTC (typically 400 °C maximum), compared to the usual maximum of 250 °C for HTC, which is more focused on obtaining a solid product called hydrochar [79][80].

Among the thermochemical processes, combustion, gasification and pyrolysis are mostly used for relatively dry feedstocks. The factor that differentiates the three processes is

the proportion of oxygen in the reaction atmosphere: combustion occurs under an excess of oxygen, causing the feedstock to burn; gasification employs a low concentration of oxygen (15-30% of the oxygen that would be used in combustion [21]), allowing partial oxidation; and pyrolysis uses an oxygen-free or oxygen-limited atmosphere (from air ingress during feeding, or from leaks in the system), minimising oxidation [22][23][24]. There are also differences in terms of temperature: combustion and gasification usually occur above 700 °C, while pyrolysis can be operated as low as 400 °C [13]. The possibility of using lower temperatures in pyrolysis leads to less heating requirements and lower energy consumption, which is economically beneficial. Combustion has as main objective the generation of heat, with ash as by-product, while gasification maximises the production of the gaseous product (up to 85 wt.% yield), mainly comprised of CO, H₂, and CO₂ and CH₄, and also with ash as by-product [5][81]. Pyrolysis, on the other hand, obtains a liquid product, a solid product (not transformed into ash), and a gaseous product. Obtaining more products can be seen as an advantage, because the process can be tailored according to the product(s) of interest [13].

Pyrolysis is mainly used for dry feedstocks, however, it can be also used for wet feedstocks, and also soft and hard materials [13]. Besides different biomass, pyrolysis can also be used for wastes such as plastics and tyres, an area which has significant on-going research and also operational industrial-scale applications [82][83][84].

A thermochemical process which is used for biomass and however not present in Figure 2.3 is torrefaction, which is similar to pyrolysis, due to the use of temperature and an oxygen-limited or oxygen-free atmosphere. The difference is the temperature employed is lower than pyrolysis (<400 °C), and it does not reach full carbonisation due to the lignocellulosic composition of the biomass. Torrefaction is mainly used to increase the mass and energy density of the solid biomass, converting it into a torrefied material with lower oxygen content, producing some volatiles which are usually burned to obtain process heat. Other properties of the solid material are improved upon torrefaction, such as its hygroscopic (moisture absorption) nature, which is reduced [5].

In comparison, combustion is generally a more affordable process, due to its simplicity and the lower number of equipment used. In terms of efficiency, however, gasification and pyrolysis can be better than combustion, which compensates particularly at larger scales [13]. The emissions from gasification and pyrolysis are also usually less harmful than from combustion (e.g. low sulphur and NO_x), which reduces to some extent the need for stringent emission control [13]. Furthermore, due to the lower temperatures usually employed in pyrolysis compared to combustion and gasification, the risk of fouling, slagging and corrosion from inorganic species can be reduced.

2.1.3. Types of pyrolysis processes and products

The pyrolysis process causes the thermal degradation of a material, in anaerobic conditions (without oxygen, or in oxygen-limited conditions). In this way, the material suffers decomposition into smaller molecules, in the form of volatiles. The name *pyrolysis* is connected to this thermal degradation, since *pyro* originates from fire or heat, and *lysis* signifies breaking down, decomposition, or disintegration. Part of the evolved volatiles (in vapour form) can be condensed into a liquid product, with the other part comprising the gaseous product from pyrolysis. Char is the solid material resulting from the pyrolysis process. A general representation of the pyrolysis process is represented in Figure 2.4.

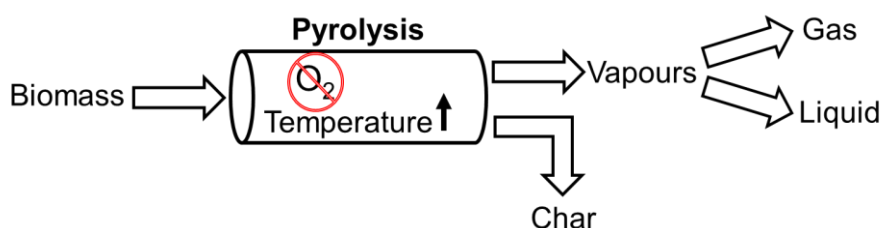


Figure 2.4: General representation of the biomass pyrolysis process.

The gases produced from pyrolysis are mainly comprised of CO, CO₂, CH₄, H₂ and light hydrocarbons (e.g., ethane, ethane, propane), with the proportions depending on the applied conditions. The energy value of the pyrolysis gas can be used to generate heat and power, through a turbine or engine [81], with the resulting energy being used for the pyrolysis process heating or feedstock drying [5]. However, the energy content is usually relatively low, of ≈5% of the original feedstock energy value, while the heat requirements in a pyrolysis process are usually higher (≈15% of the feedstock energy) [85]. Another heat source is in this case necessary for the pyrolysis process, which could come from burning other products or from electrical heating.

The liquid product from pyrolysis is comprised of organic compounds, e.g., water, sugars and sugar-derived compounds, acids, aldehydes, and esters [5][56]. Different compounds can be extracted from the liquid product, such as acetic acid, or substances which can be used for example in food flavouring, preservatives, resins and other applications [86][87]. The proportion of the compounds present in the liquid depends on the process conditions and the feedstock, and, due to the presence of water-soluble and water-insoluble compounds, it can be obtained in one single phase or in two distinct phases: an aqueous phase, of usually lighter colour, and an organic phase, with a darker colour and higher viscosity [88][89], which can be refined into a biofuel and used for power and heat generation [81]. The higher heating value (HHV) of the pyrolysis liquid product is typically between 16 and 19 MJ/kg, which is ≈40% of the HHV of hydrocarbon fuels such as diesel [86]. Due to the

relatively high density of 1.2 kg/L, by volume the HHV is $\approx 60\%$ of a hydrocarbon fuel [89]. The water content of the pyrolysis liquid product is variable, and can be as high as 50 wt.%, depending on production and collection methods [81]. The liquid product from pyrolysis has an acidic pH that can be as low as 2, due to the substantial presence of organic acids, resulting in corrosive properties [89]. It has a relatively high oxygen content of ≈ 40 wt.%, similar to the original biomass [81]. The high oxygen and water contents that can be present in the liquid product contribute to a relative instability, and possible reactions taking place, which can lead to changes in molecular weight, water content, viscosity, and even phase separation [81][89]. The aging and alterations of the liquid product with time can be favoured by the presence of inorganics [90].

The solid product from pyrolysis, called char, is usually of black colour and brittle, mostly comprised of carbon, and also oxygen, hydrogen, nitrogen, and some inorganics [29]. It has numerous applications, with the most popular being the use for heating and cooking (as charcoal) [29][91], the use as soil amendment (as biochar) [26], the use in animal bedding and feed [92], the use as a reductant in iron [93] and silicon making [94], and the use as activated carbon (requires post-treatment) for gas and water purification [40][80]. The characteristics and applications of the char product are explored in section 2.3 in this chapter.

Pyrolysis can be performed in different ways, depending on the main product of interest. The main product is mainly dependent on the operating temperature, heat transfer, and the residence time of solid and vapours. There is a distinction between types of pyrolysis based on heat transfer, which in turn relates to other parameters and governs for example the selection of a reactor, heating methods, and product collection. Table 2.2 (information based on [13][81][95][96]) summarises the different pyrolysis processes and the main features that differentiate them.

Table 2.2: Types and typical main features of pyrolysis processes.

	Heating rate (°C/s)	Operating temp. (°C)	Solid residence time	Vapour residence time
Fast pyrolysis	High (≥ 10)	500-600	Short (a few seconds or less)	Very short (0.5 to a few seconds)
Intermediate pyrolysis	Medium (1-10)	400-500	Long (minutes)	Medium (10 to 30 seconds)
Slow pyrolysis	Low (0.1-1)	400-600	Long or very long (minutes to days)	Long (over 1 minute)

Figure 2.5 indicates the typical product yields obtained from different types of pyrolysis processes, from wood and on a dry basis [86].

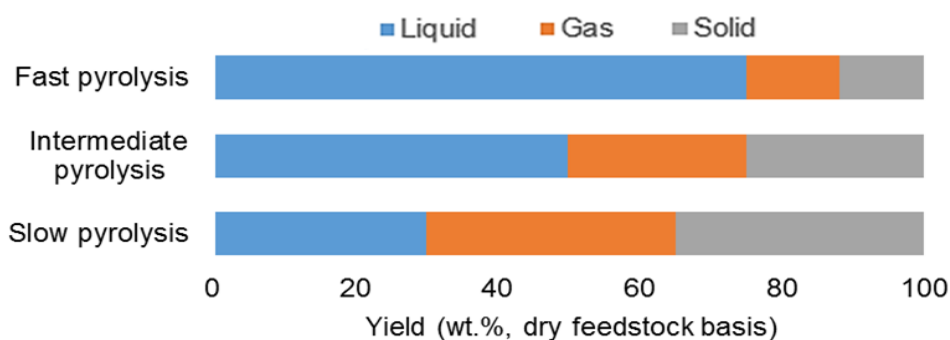


Figure 2.5: Typical product distribution from different types of pyrolysis.

Fast pyrolysis intends to maximise the liquid product recovery, based on the high temperature and high heating rates employed. High heating rates can be achieved by using a feedstock with very small particle size (order of magnitude of mm or μm) and very good mixing inside the reactor (e.g. using a fluidised bed) [81]. These conditions are used in order for the heat transfer to occur rapidly and efficiently within and across the biomass feedstock particles, which normally has a relatively low thermal conductivity [81]. To further improve mixing and heat transfer, in many cases it is possible to find the use of heat carriers, such as fine heated sand particles and heated steel shot [81]. Flash pyrolysis is also a type of pyrolysis process, where the heating rates and temperatures are even greater than in fast pyrolysis, possible for example through ablative pyrolysis [13].

Both flash and fast pyrolysis employ very short residence times, i.e., the extraction of solid and vapour products is very fast, and quenching of the vapours is also relatively fast, which allows to maximise liquid production and also its quality [97]. The use of short vapour and solid residence times (VRT and SRT, respectively) has the effect of reducing the contact time between the pyrolytic vapours and the solid product. Char is known to act as a catalyst, for example for cracking reactions, which increase the gas and solid products yield at the expense of the liquid product [85][98][99]. The presence of char in the liquid product also exacerbates aging and instability, and so the vapours usually go through a cyclone or hot vapour filtration, to try to minimise the solid content of the liquid product [85].

For pyrolysis processes, and especially for fast and flash pyrolysis, the feedstock is dried, typically to under 10 wt.% moisture content, in order to minimise water content in the liquid product, which can reduce its quality [86]. The feedstock's water content upon pyrolysis is vaporised, and the vapours are usually condensed and form the liquid product.

Fast pyrolysis obtains a liquid as its main product, also called bio-oil, which is usually dark brown and free flowing, with a smoky odour [86]. Due to the growing interest in its use as a fuel, and the consequent industrial production of fast pyrolysis bio-oil, quality standards have been produced, including by ASTM [100]. Fast pyrolysis bio-oil has been defined by the IEA Bioenergy Task 34 in 2014 as a single-phase liquid condensate recovered by thermal

treatment of lignocellulosic biomass, without oxygen, at short VRT, operating temperature between 450 and 600 °C, and at near or below atmospheric pressure [101].

The by-product char from fast pyrolysis is typically ≈15 wt.% of the products, while its energy content constitutes ≈25% of that of the original feedstock [85]. Due to this, in many commercial fast pyrolysis facilities the char product is burned to obtain process heat, since the pyrolysis process usually requires ≈15% of the feedstock energy value [85]. The char from fast pyrolysis has usually a relatively low particle size (e.g. powder) and is often pyrophoric (spontaneously oxidising even at ambient temperature) [85][87]. These properties require careful handling and storage.

Slow pyrolysis, on the other hand, usually employs lower temperatures and is therefore is focused on the solid product, char. Slow pyrolysis is typically known as the conventional type of pyrolysis, or carbonisation, used for centuries to obtain charcoal [5]. Intermediate pyrolysis is a much more recent term, developed with features between slow and fast pyrolysis, and said to be more flexible than fast pyrolysis in terms of feedstocks, to be able to minimise the formation of tars (high molecular weight compounds which can negatively affect product quality), and obtain pyrolysis products with high quality [102].

The fact that slow and intermediate pyrolysis obtain a more balanced production of all three products can be an advantage due to the value and possible applications of the different products [96]. Slow and intermediate pyrolysis processes are also more flexible to feedstock shapes and sizes than fast pyrolysis, which requires very small particle size [87]. The flexibility is also in terms of moisture content, since slow and intermediate pyrolysis can process a greater range of feedstock moisture contents than fast pyrolysis [56]. This is advantageous in terms of flexibility, but it can also have a negative effect because of the higher heat load on the process. A too high moisture content may prevent a feedstock from being carbonised due to heat transfer limitations. Due to the longer residence times, the liquid product from slow and intermediate pyrolysis is most often of lower quality and in two phases (aqueous and organic) [87].

Since slow and intermediate pyrolysis usually occur at a lower temperature than fast pyrolysis, there is a lower energy requirement, and there is also a reduced risk of formation of inorganic species that can lead to slagging, fouling and corrosion. These are technical and economic advantages.

2.1.4. Pyrolysis reactions and mechanisms

In a pyrolysis process, the feedstock undergoes a complex series of chemical reactions, according to the conditions employed and the feedstock composition [13][103]. All of the components of biomass, unless previously extracted, are subjected to the pyrolysis

process, and each type of component has different behaviours. The thermal decomposition of lignocellulosic biomass is often studied by analysing the individual behaviour of cellulose, hemicellulose, and lignin. Although there is interaction between the different components, the thermal degradation of lignocellulosic biomass can be approximated to a linear combination of the degradation profiles of the lignocellulosic constituents [104].

The thermal degradation of cellulose, hemicellulose and lignin in inert atmosphere was studied by Yang *et al.* [105] with thermogravimetry analysis (TGA). The study found that hemicellulose was the first lignocellulosic material to thermally degrade, in the range of 220 to 315 °C, while cellulose decomposed between \approx 315-400 °C. The thermal decomposition of lignin occurred over a wider temperature range, from around 160 °C and up to 900 °C. These temperature values are not universal, since the thermal degradation depends on what technique and starting material was used to obtain each lignocellulosic component. Furthermore, in biomass, the lignocellulosic compounds interact between themselves during thermal degradation. The highest final solid residue was obtained from lignin, with \approx 46 wt.%, while cellulose and hemicellulose obtained \approx 6.5 and \approx 20 wt.%, respectively [105]. This signifies that lignin is the lignocellulosic material that most contributes to forming char product in pyrolysis. This was also found in a study of whole woody biomasses, which also correlated (negatively) the char yield with hemicellulose contents [106]. In terms of gaseous products, it was found that cellulose has a higher contribution to the formation of CO, while hemicellulose yields more CO₂, and lignin yields more H₂ and CH₄ [105].

The mechanism for whole lignocellulosic biomass decomposition in pyrolysis has been debated for some time and is not yet entirely clear [107]. For cellulose, there is some consensus around the one formulated by Broido and Shafizadeh [108], represented in Figure 2.6 (based on [109]), and that can be extrapolated to biomass itself [90]. In the Broido-Shafizadeh mechanism, an unstable intermediate compound, active cellulose, undergoes chemical reactions that are dependent on temperature and heating rate. The first pathway, forming gases and char, is favoured by thermal treatments of lower intensity, while the second pathway is favoured by high intensity thermal treatments and forms gases, char and tars [109].

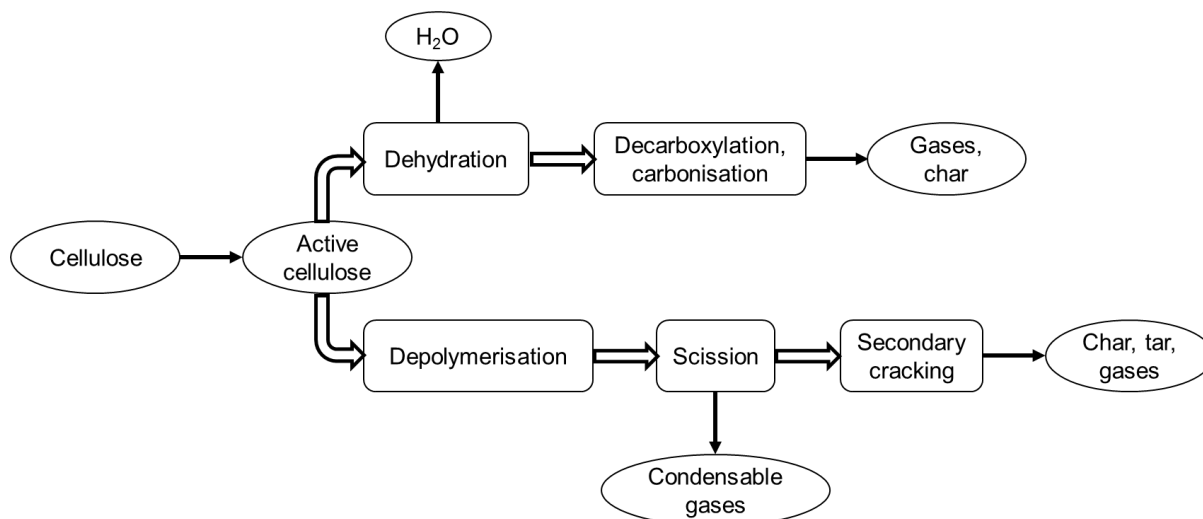


Figure 2.6: The Broido-Shafizadeh mechanism for cellulose thermal decomposition in inert atmosphere.

Using TGA data and applying the Distributed Activated Energy Model (DAEM), two studies found that the pyrolysis reactions could be divided into the ones that form volatiles (degradation reactions), and the ones that form char and gases (condensation reactions) [110][111]. Due to the branched structures of hemicellulose and lignin, their decomposition produces multiple fragments which can randomly polymerise to form char, and so the condensation reactions can have a greater importance than degradation reactions, when comparing with cellulose decomposition [107]. Hence, it has been observed that the simulation of thermal degradation of whole biomass during pyrolysis can be described with relatively high accuracy by three sets of reactions: the degradation reactions for cellulose, the degradation reactions for hemicellulose and lignin, and the condensation reactions for hemicellulose and lignin [112][113].

The different lignocellulosic materials (hemicellulose, cellulose, and lignin) yield different pyrolysis products, owing to their differences in composition and structure, although some products are common between them, such as permanent gases (e.g., CO, CO₂, CH₄, H₂), and carbonyls and alcohols [114][115]. Other products from hemicellulose and cellulose pyrolytic decomposition are heterocyclic compounds (e.g., furans) and sugars (e.g., levoglucosan, xylose), while lignin yields mainly phenolic compounds (e.g., phenols, guaiacols, syringols) [114][115]. Other compounds can be formed, such as single-ring aromatics (e.g., benzene, toluene, xylene) and multi-ring (i.e., polycyclic) aromatics, formed mainly from lignin, or through reactions between pyrolytic products from (any) lignocellulosic material [114][115]. The pyrolysis reactions also yield the solid product char, by concentration of the carbon from the lignocellulosic structures (mainly, aromatic) and also through repolymerisation, cracking and other reactions between pyrolysis products, such as furans,

aromatics and tars [115]. Some pyrolysis reactions, such as dehydration and condensation, form water as a product, called reaction water [89][90][104], adding to the water originating from the feedstock's moisture content.

The pyrolysis reactions can also be grouped into primary and secondary reactions [13]. In the primary reactions, the solid feedstock material is devolatilised by heat, with reactions such as dehydration (loss of H₂O), decarboxylation (loss of CO₂), decarbonylation (loss of CO), and dehydrogenation (loss of H₂) [13]. Primary reactions form vapours (condensable and non-condensable), and solid product [29][99]. Secondary reactions occur in gas phase and are favoured by high temperatures and long contact times between solid and vapour phases within the pyrolysis process [56][115]. The secondary reactions consist of cracking of volatile compounds, forming more char and gas products [13][116]. Recombination of molecules can also occur, e.g., through reactions involving free radicals [117]. Tars can be formed, which are a mixture of high molecular weight hydrocarbons (e.g., polycyclic aromatic hydrocarbons, PAH), usually viscous/glue-like, that are harmful if accumulated in equipment such as engines, boilers, and piping, diminishing efficiency [86]. Tars can be difficult to separate from the pyrolysis products [5], and can also provoke deactivation of catalysts during catalytic pyrolysis [98]. In cellulose pyrolysis, research indicates that char is formed mainly through secondary reactions, with primary reactions forming a relatively small char yield [118]. Despite the general acceptance of the existence of primary and secondary char, assessing between those types of char remains very challenging, and the pathways not fully understood [115].

The inorganic compounds in the biomass (or in the char during pyrolysis), especially the alkali and alkaline earth metals (AAEM), are known to act as catalysts for secondary reactions [77][90][99][108]. Potassium and sodium are regarded as the most active inorganic elements in terms of catalytic activity in pyrolysis [81], and potassium usually accounts for a large proportion of the biomass inorganic material. A study of agricultural residues and wood by Raveendran *et al.* [119] found that a higher mineral content in biomass leads to a decrease in thermal decomposition rates and in starting decomposition temperature. Furthermore, a greater biomass inorganic content yielded less volatile species, which led to a reduction in liquid production and an increase in char yield. Sekiguchi and Shafizadeh [120] also found increasing char and gas yields from biomass with greater inorganic contents. In a study comparing woody and herbaceous biomass, the higher ash content in miscanthus and wheat straw ($\approx 3\text{--}4$ wt.%, compared to ≈ 1 wt.% in woody biomass) was found to catalyse the decomposition of intermediates to char, low molecular weight compounds and gas, resulting in lower organic phase yield and higher char and water production [121]. This occurred even though the lignin content of the wheat straw was considerably lower (≈ 16 wt.%) than the woody biomasses ($\approx 23\text{--}28$ wt.%). On the other hand, impregnation of lignocellulosic feedstocks with

inorganic compounds such as potassium or zinc carbonates can cause a decrease in char yields [119], which relates to another process called activation, discussed in section 2.3.3.

Regarding the energy of the reactions involved in pyrolysis, the study by Yang *et al.* found that the main thermal decomposition process (containing the maximum weight loss rate) for cellulose was endothermic, while the main processes for hemicellulose and lignin decomposition were exothermic [105]. The exothermicity was connected to char-forming reactions, while the endothermicity found for cellulose was related to its faster and more complete devolatilisation (lower char residue). Overall, the pyrolysis process is considered endothermic [56], and the heat requirement for the pyrolysis of several agricultural and wood-based biomasses was reported to be between 207 and 434 kJ/kg [122].

2.1.5. Effect of pyrolysis conditions on product yields

A variety of process variables influence the pyrolysis process: the operating temperature, the residence times (of solid and vapours), the pressure, the heat transfer, the reactor design, the atmosphere, and the product collection systems. Different combinations of process conditions and feedstock properties influence the product distributions and qualities, and they can be tailored to obtain a higher yield and/or improved properties of a product of interest [123].

2.1.5.1. Effect of operating temperature and heating rate

Temperature is viewed as the main pyrolysis process variable contributing to changes in product yields, since it governs the degradation of the lignocellulosic compounds. In a study of 12 feedstocks (lignocellulosic and others), Zhao *et al.* found that for a wide range of temperatures (200-650 °C), operating temperature was the determinant parameter for char yield [123].

When pyrolysis is performed at relatively high temperatures (and heating rates), there is sufficient energy to rapidly and extensively break bonds in the lignocellulosic structure and form smaller and more volatile molecules, compared to when employing lower temperatures and heating rates [56][116]. This results in having a higher production of vapours when the operating temperature is high, and less char yield. If the high temperatures are coupled with a short residence time of the vapour products, allowing to quickly produce and quench the vapour phase, it will result in a higher liquid yield (fast pyrolysis conditions) [56][81][116]. On the other hand, if the contact time between pyrolysis vapours and solid products is extended, the high temperatures will favour secondary reactions and produce more gaseous products [56]. Secondary reactions can contribute to char yield, although the high temperatures cause the char yield to diminish.

Manyà *et al.* studied the pyrolysis of agricultural wastes (wheat straw, almond shells, olive stones and grape refuse) in a fixed bed and found a decrease in char yields for increased heating rates (5, 10, 15, 30 °C/min), but the change was not as significant as the change in gas and liquid yields [124]. The same study also found that at the highest heating rate the effect of the inorganics from the biomass in promoting secondary reactions was increased. This may be connected to a higher thermal lag within the particles due to the higher heating rate [125].

The composition and structure of the char also change with operating temperature, mainly due to the loss of volatiles from the lignocellulosic components and rearrangements of the char's aromatic structure. This will be detailed in section 2.3.

Therefore, for having higher char production, lower temperatures and heating rates are preferred [5][81][29], as is the case in slow and intermediate pyrolysis. There is however a compromise between char yield and quality (depending on the application), as will be further detailed in section 2.3.

2.1.5.2. Effect of solid residence time

The solid residence time (SRT) employed in pyrolysis depends on the product of interest: for maximising liquid production (fast pyrolysis), the SRT needs to be short, while for solid production (slow pyrolysis), the SRT can be extended. There is a certain minimum value of SRT to guarantee full carbonisation, but this depends on other parameters such as temperature and heating rate, reactor type, feeding rate, and particle size. In slow pyrolysis, the SRT can be up to hours depending on the reactor used [56][86][29]. Furthermore, the residence time of the products is related to the contact time between solid and vapour phases, which in turn affects the product distribution through cracking and other secondary reactions. Secondary reactions typically cause char and gas yields to increase, while liquid product yields decrease (see previous subsection 2.1.4).

A study of the effect of SRT on product yields and properties was done by Puy *et al.* with pine wood chips (up to 20 mm nominal size) in a screw reactor (up to 15 kg/h feed capacity) [126]. Using a pyrolysis temperature of 500 °C and 3.9 kg/h feedstock flow rate, the SRT was varied as 1.5, 2, 3 and 5 minutes. The product yields were significantly affected for the lower values of SRT: for 1.5 minutes, the char yield was 41.5 wt.%, and by increasing the SRT to 2 minutes, the char yield decreased almost one third, to 28.7 wt.%. Further increasing the SRT to 3 minutes led to a further decrease in char yield, although with relatively lower variation, of 2.7 wt.%. For 5 minutes SRT, the char yield was 26.4 wt.%, which is not a significant change to the yield at 3 minutes SRT (26.0 wt.%). These results were connected to a lower carbonisation degree occurring for shorter SRT, since the time was not sufficient

for the feedstock to be fully carbonised (torrefaction occurs instead). A minimum of 2 minutes was considered required for pyrolysis to be complete.

The work by Solar *et al.* [127] involved the pyrolysis of pine wood waste (0.5–2.0 mm sizes) in a screw reactor (39 g/h feeding rate). The studied pyrolysis temperatures were relatively high, 750 and 900 °C, due to the char product quality requirements (mainly, high fixed carbon contents, for the metallurgical industry as reducing agent), and the SRT was 32 or 64 minutes. The production of pyrolysis gas was seen to increase with SRT (and temperature), while liquid production decreased. This was justified with the favouring of secondary reactions, which decreased the molecular weight of the liquid compounds and raised the presence of CO and H₂ in the gas, while reducing CO₂.

2.1.5.3. Effect of reaction environment (by gas injection) and vapour residence time

Pyrolysis, especially in laboratory/industrial environments, often employs a carrier gas, which is most commonly nitrogen. The carrier gas firstly makes the system inert, removing the oxygen/air, and allows for the vapour products to be extracted quickly, which is crucial for fast pyrolysis. However, if quick extraction of the vapours is not required, i.e., the focus is on the solid product instead, the use of carrier gas during pyrolysis is not mandatory. Traditional slow pyrolysis processes producing charcoal, e.g., in developing regions, do not use carrier gas at all. Most modern systems use carrier gas at least before pyrolysis starts to have an inert atmosphere inside the system. More details on reactor systems can be found in section 2.2.

Carrier gas flow during pyrolysis correlates with the vapour residence time (VRT) of the produced volatiles. When the flow rate of carrier gas is low or null, the pyrolysis vapours have an increased contact time with the solid, which promotes secondary reactions and increases char yields [128]. Using carrier gas such as N₂ during pyrolysis makes the product gas become diluted [129], reducing its value for energy/heat generation when that is the case.

Using a CO₂ atmosphere or another non-inert atmosphere such as steam during pyrolysis is known to change product distribution and the surface of the char, both chemically and physically (in terms of surface chemistry, surface area and porosity), through a process called activation. A study that compared injecting N₂ or CO₂ into the reactor during slow pyrolysis (600 °C, 5 °C/min and 1 h SRT) of vine shoots in a fixed bed found however no significant difference on char yields [130]. Using CO₂ and steam during pyrolysis/activation is further analysed in section 2.4.

Another gas that is being investigated is hydrogen, leading to the term hydrolysis. The reducing H₂ atmosphere generates hydrogen radicals which react with the evolved volatiles and increase production of aromatics and other valuable hydrocarbons [131]. High selectivity for hydrocarbons can be achieved, and deactivation of the catalyst (commonly used in hydrolysis) can be minimised [131]. Disadvantages are the H₂ requirement and high

pressure, up to 30 bar or more [131]. The potential for commercialisation is high, however, further research is needed.

Despite several studies on the effect of injecting different gases into the reactor during pyrolysis, the effects depend on the feedstock, reactor and operating conditions, and therefore are still not clear. Therefore, further research is necessary to study the effect of injected gases on the product yields and properties.

2.1.5.4. Effect of feedstock particle size

In conventional slow pyrolysis, the biomass feedstock (most commonly wood) is often in a relatively large size, i.e. pellets, briquettes, whole logs [56]. In slow pyrolysis systems the char product can be obtained more or less in the same shape as the original feedstock [29].

The use of relatively large particles of biomass in slow pyrolysis generally contributes to a higher char yield [29], which can be advantageous due to avoiding energy intensive processes such as milling, grinding or crushing. This also allows the process to be more flexible, compared to fast pyrolysis for example, since slow pyrolysis can handle larger particle sizes. Wang *et al.* highlighted that systems that use a small particle size are not adequate to obtain high char yields [132].

When heating a particle, the temperature difference between the outside and the inside becomes greater as the particle size is increased. The temperature gradient increases the time it takes for carbonisation of the whole particle, resulting in higher char yields and decreasing volatile release. Furthermore, the diffusion rate of volatiles is decreased, which can promote secondary reactions and lead to further solid yield increase [124][133]. Secondary char-forming reactions are considered exothermic, and so the external heat demand of the process can be reduced when using larger particles [134].

There is however a dependency of the effect of particle size on other parameters such as feedstock type and the contact time between vapours and solid. A study of slow pyrolysis of different agricultural residues in a fixed bed found no significant effect when using relatively small wheat straw pellets (5 or 10 mm length, 5 mm outer diameter) or cut wheat straw [124]. Demirbas, on the other hand, found that char yields increased with particle size (ranging from <0.5 to >2.2 mm) for olive husks, corncob, and tea waste, pyrolysed in a cylindrical fixed bed at different temperatures (177-977 °C) [135]. Mani *et al.* [136] reported char yield increase when the particle size of wheat straw was increased from 0.250 to 0.475 mm, but no further increase when it was augmented to 1.350 mm. A contrasting effect was seen by Onay and Kockar [137], for rapeseed pyrolysis at 550 °C: char yields decreased when particle size was increased from 0.425 to 0.850 mm, and a further increase in particle size led to the opposite effect (higher char yields).

2.1.5.5. Effect of feedstock moisture content

When a feedstock with relatively high moisture content is pyrolysed, more heat is required for water evaporation (endothermic), which lowers the heating rate [138]. Several authors have observed that this leads to higher char yields, since the release of volatile matter takes longer time [138–140]. However, the effects seem to depend on the contact between vapours and solids, as reviewed by Antal *et al.* [29]. If pyrolysis was conducted in a sealed reactor, which could develop pressure from the evolved volatiles, high feedstock moisture contents led to higher char yields, related to increased pressure and higher contact between vapours and char [26][29][106]. In TGA studies with closed crucibles, the same results were found [29]. Furthermore, water has been considered a catalyst for char-forming reactions during high pressure pyrolysis [106][141]. At atmospheric pressure reactors, though, or open crucibles in TGA studies, the effect of feedstock moisture content seemed to be negligible [29].

A study of slow pyrolysis (450, 550, 700, 850 °C; 1 atm; 6 min SRT; 7-17 s VRT) of the organic fraction of MSW (mainly food and garden waste, paper) with different moisture contents (12.7, 22.8, 34.6, and 45.8 wt.%) was performed on the screw reactor used in this work, and found that char yields were not significantly affected by moisture content, only by pyrolysis temperature [142]. The effect of feedstock moisture content requires further research.

If feedstock moisture content correlates with greater char yields, it could be useful to artificially raise the moisture content by soaking with water. However, firstly there is the issue of a higher heat demand in the process, which involves higher costs. Secondly, the water soaking could alter the physical structure of the lignocellulosic materials [143], which will modify the behaviour of the feedstock in pyrolysis. Furthermore, the inorganic content of the feedstock may also suffer modifications and could even be removed to a certain extent, if excess water is removed, which will affect product distribution.

2.1.5.6. Effect of operating pressure

The effect of pressure on pyrolysis has received some attention, particularly due to the potential of improving char yields. Research on the effects of pressure have been extensively performed by Antal, Manyà, and their research groups. Increased pressure has been shown to decrease carbonisation time in batch systems [144]. It is known that increased partial pressure and residence time of the vapours favour secondary reactions and thus char and gas formation, due to the greater interactions between solid and vapours [26][29][145]. Furthermore, the saturation temperature and pressure of the liquid products are increased, which delays the transition to vapour phase [132]. The char yield increases with pressure were encountered especially when the reactor was sealed, which exacerbates the contact time

between vapours and char (high VRT) and therefore secondary reactions. However, when decoupling the effect of pressure from VRT, the results on product yields and properties differ. There is a need to continue researching the effect of pressure on slow pyrolysis.

A study from the GreenCarbon project of slow pyrolysis of wheat straw pellets (the same used in this work) in a fixed bed reactor found that pressure enhanced the release of gas products and decreased liquid yield, without affecting char yield [128].

The understanding of the influence of process conditions and feedstock-related conditions on the products of pyrolysis still needs improvement, as underlined in a review by Manyà [26]. Wang *et al.* also highlighted that for models to successfully simulate char formation and yield, it is necessary to consider a parametric dependence on variables such as particle size, pressure, and vapour residence time [132].

2.2. Pyrolysis reactors

2.2.1. Fast pyrolysis reactors

Although biomass pyrolysis was first developed with a focus on the solid product (mainly to be used as solid fuel), interest in the liquid product rose in the 1970s due to its potential to replace fossil fuels during the oil crisis [146]. Systems were thus developed that focused on obtaining the liquid product with high yields, through fast pyrolysis.

Fluidised bed (bubbling or circulating) reactors are the most popular in fast pyrolysis, with others being for example the rotating cone and the ablative system [147]. These types of reactors make it possible to have very short residence time of solids and vapours, in order to maximise the production of liquid [81][86]. For that purpose, relatively high flow rates of carrier gas are used, as well as heat carriers such as sand to promote heat transfer. In industrial-scale fast pyrolysis reactors, usually the char product is burned to obtain heat for biomass drying or the process itself [81].

To obtain the liquid product with high yield and quality, the vapour cooling and liquid collection systems must be very efficient. The vapours coming out of a fast pyrolysis reactor usually pass through a cyclone to remove solid particles (char, sand), and then are rapidly quenched to minimise secondary reactions and maximise liquid product [81]. Other methods of solid separation from the vapours such as hot vapour filtration are under research [86]. The vapour cooling and liquid collection can be done in different stages, usually with a condenser externally cooled by a low temperature medium (e.g., cold water), or a quencher and/or an electrostatic precipitator [81]. Quenching media usually employed are immiscible hydrocarbon solvents (e.g., isoparaffins/Isopar), or the pyrolysis liquid itself [86].

2.2.2. Slow pyrolysis reactors

Slow pyrolysis has been used for centuries to produce charcoal from wood [5]. The pyrolysis process is performed in batches, usually in the form of pits or earth-made mounds on the ground [148]. Biomass is used in the form of logs and other forms with large particle size, which are stacked on top of each other. Part of the biomass is used as fuel (burned) *in situ* to consume oxygen and provide heat for the rest of the material to be carbonised. The evolved vapours are also burned during the process [56]. This system is still widely used in developing countries and areas that rely on biomass for heating and cooking. Traditional charcoal-making systems can release a considerable amount of smoke and gases into the atmosphere, and the char product is mixed with ashes [149].

More modern batch systems were developed for slow pyrolysis such as kilns, in bricks, concrete or another material that can withstand the heat [148]. Kilns allow for better control of air flow, higher char yields than traditional systems, and lower ash contents in the char [149]. Some companies in Brazil use a type of kiln called the Brazilian kiln, and in the US the Missouri kiln is another example [148]. Kilns operate in batch, usually do not have heat recovery, and the processing time can be up to several days, including the cooling down period [148]. Part of the biomass is combusted, and the char yield is typically 20 wt.% [148], which is relatively low. Kilns have the advantage of being relatively cheap and simple to operate [148]. Other types of kilns were made from steel drums (e.g., oil containers), so they could be transportable and easy to handle [149].

Other systems were developed, which can be classified as semi-continuous, as the process can be running continuously, however the loading and discharged are performed in batches. Examples of these systems are the wagon retort and the twin retorts. The wagon retort consists of a tunnel where wagons loaded with biomass go through the sequential steps of drying, carbonisation, and cooling. Each cycle lasts between one and two days, and part of the vapours are removed and burned in a separate combustion chamber, with the resulting heat being used to dry and pyrolyse the biomass [148]. The twin retort consists of two retorts with distinct and interchangeable roles: in one retort, fresh feedstock is loaded to be dried and carbonised, using heat from a combustion chamber where the evolved vapours from a second retort, in which another batch of biomass is already under carbonisation or cooling [148]. The cooled char is removed and a new batch is loaded, to be carbonised using the heat produced from the vapours from the other retort, and so on. Industrially, several units of the twin retort can be used, with a 8 hours carbonisation residence time, and char yields up to 33 wt.% [148].

Continuous slow pyrolysis systems were developed with the purpose to improve the process economics, avoiding time spent switching batches. Continuous reactors are also usually more flexible in terms of particle size, processing sawdust, chips, and pellets. Wang *et al.* indicated that reactors that can process larger particle sizes are more adequate to

produce char more efficiently and with higher yields [132]. In a continuous reactor, the feedstock is transported along the reactor with rotation and inclination, in the case of rotary kilns, with paddles or similar means, or with a screw in the case of screw reactors [148].

In industrial-scale charcoal production, although in many cases the product vapours are burned to obtain energy, in other cases chemicals (e.g. methanol and acetic acid) are obtained from the by-product liquid and sold, adding another source of revenue to the process [150].

2.2.3. Screw reactors

Among the continuous systems, the screw or auger reactor (from here onwards referred to as screw reactor/system) has great potential for slow pyrolysis due to some of its advantages, mainly the flexibility for different feedstock shapes and sizes [81]. The feedstock is transported along the cylindrical tube reactor by means of a horizontal screw, and the solid product usually falls into a container by gravity. Heat is provided externally, with an electric furnace or an outer shell with hot flue gases, and heat carriers such as hot sand, steel particles or metal/ceramic spheres can be used [81]. Heat carriers can be collected with the char, be separated and recycled into the reactor. The formed vapours exit the reactor usually opposite the feeding side, or along outlets on the reactor tube. Figure 2.7 shows a simplified representation of a typical screw reactor.

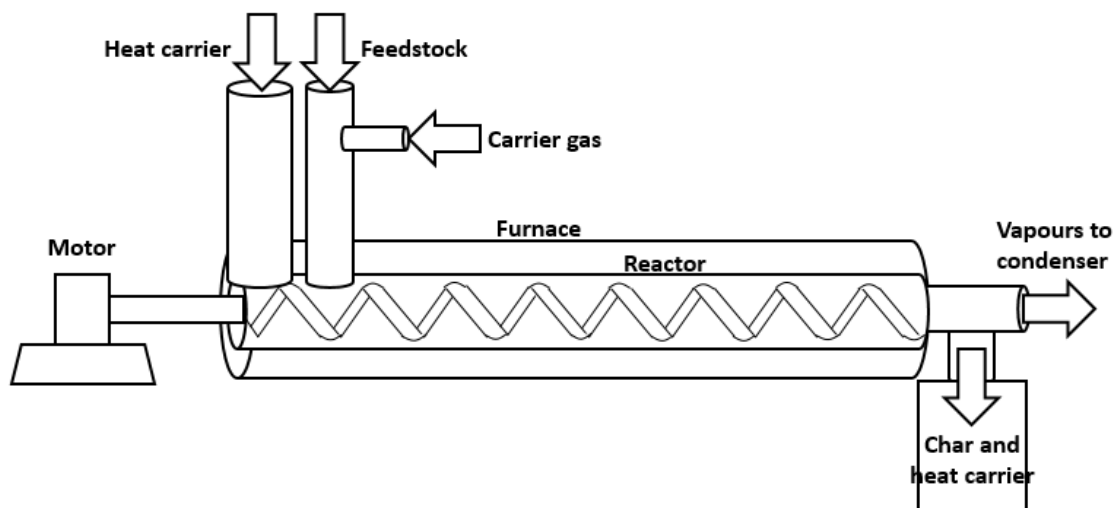


Figure 2.7: Simplified representation of a typical screw reactor.

Operation and handling are relatively simple in screw reactors [151], and the design is compact, allowing the possibility for modularity and transportation [126]. This allows to transport the reactor to where biomass is widely available, reducing transport costs, and producing char and energy in decentralised and/or remote areas [152]. A study with forestry

waste demonstrated that the design was robust for scaling-up, and that the economics of the process were improved by the avoidance of grinding/milling the feedstock [126]. Screw reactors are flexible to different feedstock types, shapes and sizes, and more adequate for heterogeneous materials than other reactors [81]. The screw is usually driven by an electric motor and it is possible to adjust its speed and thus control solid residence time, which is advantageous. The use of carrier gas is not strictly necessary [151][153], and the screw movement can provide good mixing and heat transfer inside the reactor.

Some reactors have been developed with two screws (commonly called twin screws), to improve mixing and heat transfer [154], and can be designed in different ways, including as co-axial (concentric) screws, allowing counter-rotation, and as intermeshing screws [155][156][157]. To improve mixing and depending on feedstock properties, the screw can have different flight designs (e.g. ribbon-like, cut, folded, in paddles), it can be shaftless (like a spring/coil), and the pitch (distance between adjacent flights) can be of different sizes [154].

Some disadvantages have however been verified for screw reactor use in pyrolysis: mechanical issues and construction material constraints due to hot moving parts inside the reactor; risk of blockage due to accumulation of biomass/products and consequent possible damage/destruction of the equipment; and difficulties in scaling-up in terms of heat transfer [129][153][154]. A screw reactor also requires careful design and material selection to avoid leakages and air ingress. The advantages and disadvantages of screw reactors comparing with others, and the best design practices, have been reviewed by Campuzano *et al.* [154].

Screw reactors have been used since the beginning of the XX century, e.g. for conveying, drying, and pyrolysis, firstly of coal [154]. The first known reference of screw reactor use for biomass pyrolysis was in 1969, using starch as feedstock [158]. Due to their flexibility and possibility of high heating rates using heat carriers, screw reactors were firstly used for fast pyrolysis research rather than for slow pyrolysis. Brassard *et al.* (2017) [159] and Campuzano *et al.* (2019) [154] have done literature reviews regarding the use of screw reactors for pyrolysis of biomass and wastes.

Research on pyrolysis in screw reactors has been conducted by universities and research institutes for example in the US (e.g. Mississippi State, Iowa State), in Germany (e.g. KIT), in the UK (Aston, Leeds, Birmingham) and in Spain (Instituto de Carboquímica (ICB-CSIC)) [154]. Commercial units were firstly developed for fast pyrolysis, for example by the company ABRI-Tech (Canada), at 1 (dry) ton/day scale, and by Renewable Oil International (US) with 200 kg/h scale [148][153].

The german company Pyreg developed since 2005 commercial twin screw reactors for slow pyrolysis, with units in Germany and Switzerland [160]. The product gases are burned in a combustor to obtain heat for the process and external applications [161]. One of the plant

models (Pyrec 500) can be delivered in a 20 ft. ISO container, and can process up to 180 kg/h (dry feedstock) [161].

In France, Biogreen/ETIA Group has developed the Spirajoule® system, a reactor with a single shaftless screw that is heated by the Joule effect (by means of a current flowing through a conductor material) [162]. The reactor system was developed for several applications including drying, torrefaction and pyrolysis, and has a range of scales up to 3,500 L/h [163].

Some screw reactors were developed for intermediate pyrolysis, in three generations: the Haloclean® system, the Pyroformer™, and the Thermo-Catalytic Reformer (TCR®). These systems were important because they allowed to optimise the screw reactor for biomass pyrolysis, for numerous feedstocks, and with a more balanced production of all three pyrolysis products, instead of focusing on one of them (commonly the liquid product).

Firstly, the Haloclean® system was developed by the company Sea Marconi (Italy) and the Forschungszentrum Karlsruhe (Germany), and patented in 2002 [164][165]. The purpose was to convert waste electronic and electrical equipment (WEEE) into fuels and to recover noble metals [166], and it was discovered afterwards that it was suitable for biomass pyrolysis [167]. The system was said to produce less tars, and have lower solids content and lower acidity in the liquid and gas products, compared to fast pyrolysis [167]. The first system was lab-scale (3 kg/h), and a pilot-scale system (100 kg/h) was also developed [164][168]. Heat carriers were employed (metal spheres), which could be separated from the char and recycled back to the system [168]. Various feedstocks were tested in the Haloclean® system, with particle sizes up to 5 cm, such as coconut and rapeseed residues, wheat straw (cut or pellets), olive stones, rice husk [164]. SRT was typically 4-8 min, and char yields were up to 35 wt.% and liquid yields 45 wt.% [169].

The Pyroformer™ is a pilot-scale system (20 and 100 kg/h scales) developed at Aston University and patented in 2009 [170]. A distinguishing feature of this reactor is its two co-axial screws, which can be moved independently and forwards and backwards. This feature is for internal char recycling, due to slots in the screws which allow material to pass from one screw to another. Char can be processed backwards and mixed with fresh feedstock, acting as heat carrier and catalyst for secondary reactions [102]. The vapour treatment system consists of two hot gas filter candles to remove solids, and a shell and tube heat exchanger where liquid condensation occurs, for collection into a container [171]. The non-condensable gases pass through an electrostatic precipitator (ESP) to remove aerosols, while the char product is collected in a char pot at the bottom of the reactor when both screws are driven forward [172]. Typically, from biomass, the Pyroformer™ system yields 40-60 wt.% liquid product, 15-25 wt.% char, and 20-30 wt.% gas [156]. SRT is usually 2-10 min and VRT a few seconds [169].

More recently (2013/2014), the Thermo-Catalytic Reformer (TCR®) system was developed in Germany (Fraunhofer UMSICHT). There are TCR® units installed at Fraunhofer UMSICHT (2, 30, and 300 kg/h), in Tyseley Energy Park in Birmingham, UK (30 kg/h), and other units being implemented. The heat supply for the largest scale is from flue gases from a combustion chamber, while the smaller scale systems are electrically heated [169]. The TCR® system is comprised of a screw reactor combined with a post-reforming reactor (vertical fixed bed). The feed is transported through the first reactor, where the pyrolysis process occurs, and the products are directed into the second reactor. In this second reactor, the char acts as a catalyst to upgrade the quality of the product vapours, before they go through a condensation system to be separated into the liquid and gaseous products [173]. The pyrolysis reactor operates usually at 400-500 °C, while the post-reforming reactor operates at 500-750 °C. Typical SRT is 5-15 min, and VRT is in the range of seconds [174]. The system is said to be considerably flexible to various feedstocks and to high ash and moisture contents, producing high quality and stable products [96]. The process can deal with a feedstock moisture content of technically up to 70 wt.%, although a maximum moisture content of 20 wt.% is suggested for economic reasons [96].

Besides the examples of intermediate pyrolysis, most of the research with screw reactors focused on liquid production and thus used fast pyrolysis process conditions: high temperature, small feedstock particle size (mm scale or lower), and heat carriers, besides carrier gas flow, to minimise the contact between vapours and solid and secondary char-forming reactions. However, depending on scale, it can be difficult to keep SRT relatively low, as is normally required in fast pyrolysis, and VRT in screw reactors can be >30 seconds depending on design and reactor size [81]. Due to the relatively high residence time of solid and vapours in screw reactors compared to other reactors, secondary reactions can have a more significant impact on product yields and quality, and this should be further addressed [154]. Catalysts have also been added to the pyrolysis process in screw reactor, mainly to evaluate the effect on the liquid product yield and quality [127][175].

Research using screw reactors for biomass pyrolysis has focused on a limited number of parameters, especially temperature and feedstock type, and also SRT and feedstock flow rate. Some process conditions have been scarcely studied in screw reactors, or not at all, such as VRT, feedstock moisture content and pre-treatment, and reaction environment/atmosphere (by injecting gas into the reactor, inert or not). Figure 2.8 shows the frequency of different feedstock groups studied in screw reactors, based on the 30 research groups reviewed by Campuzano *et al.* (2019) [154].

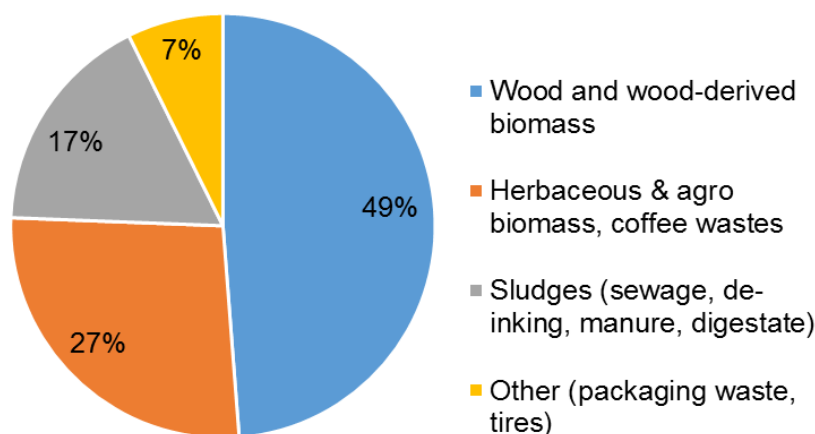


Figure 2.8: Feedstock type frequency studied in screw reactors (own artwork and interpretation, based on data from [154]).

The main feedstocks studied in screw reactors are woody biomass, mostly pine [126][127][172][176], and also beech [177]. Typical char yields from woody biomass pyrolysis in screw reactors were reported between 17 and 30 wt.% [148]. There also some accounts of herbaceous/agricultural biomasses: wheat straw (pellets) [164], barley straw (pellets) [172], rice husk and corn stalk [178], switchgrass [179], rice husk and bran [164], and rapeseed [164]. Examples of other wastes pyrolysed in screw reactors: sewage sludge (from wastewater treatment) [173][180][181], de-inking sludge (from paper production) [156][182], digestate from AD processes [96][173][183], brewing wastes [102], and organic fractions of MSW [142][184]. Non-biomass feedstocks have also been studied in screw reactors, e.g. spent tyres [83] and WEEE [166]. Research using agricultural biomass and other waste/residual biomass (e.g., from coffee) should be expanded, since pyrolysis is one of the most valuable ways to convert these materials into value-added products and energy, avoiding landfill disposal and GHG emissions, e.g., from combustion.

Most of the feedstocks were studied in relatively small particle size (i.e. powder form or very small chips), although some were in pellet form: wheat straw [164], pine wood residues and barley straw [172], de-inking sludge and sewage sludge [156][182], paper sludge [173], and AD digestate [96][173]. The 2017 review by Brassard *et al.* [159] found that studied feedstocks had particle sizes between 0.2 and 20 mm, although only five studies were reported using particle size >5 mm. The effect of different feedstock particle sizes on char yields and properties should be further addressed.

Fassinou *et al.* [176] studied pine wood pyrolysis in a screw reactor and found that operating temperature was the parameter with greatest effect on product yields. The feedstock flow rate and the SRT did not have a significant impact.

Different research groups have reported that when using screw reactors there can be a significant thermal gradient between the reactor wall and its interior ($>100\text{ }^{\circ}\text{C}$) [175][185]. With temperature being fundamental to determining product yields and quality, it is critical to have accurate temperature measurements inside the reactor, which can be challenging [159].

Continuous screw reactors can effectively produce chars with valuable uses, and there is a need for further correlations between process conditions and product yields and properties. The effect of variables such as vapour residence time and reaction atmosphere (by injecting gas into the reactor, e.g., N_2 or CO_2), and feedstock moisture, must be studied more in-depth.

2.3. Char from slow pyrolysis of biomass

2.3.1. Main properties and analysis techniques

Char is the solid carbon-rich product from pyrolysis. It is usually black in colour, dry, and often brittle (i.e., breaks up rather easily), depending on the feedstock [29]. Figure 2.9 presents a char produced in this PhD work from wheat straw with a screw reactor, at $500\text{ }^{\circ}\text{C}$ and with 3 minutes SRT.



Figure 2.9: Picture of a wheat straw char produced in this work ($500\text{ }^{\circ}\text{C}$, 3 min SRT).

Table 2.3 indicates the main char properties that usually serve to characterise a char, and the respective analysis method(s). The specific methods used to characterise the chars produced in this PhD work are further detailed in Chapter 3.

Table 2.3: Main char properties and respective most common methods of analysis.

Property	Analysis method	Property	Analysis method
Moisture content (M)	Oven at 105 °C (ASTM D1762) or TGA (ASTM E1131)	Functional groups	FTIR (surface), Boehm titration, XPS (surface)
Volatile Matter content (VM)	Oven at 950 °C in covered crucible (ASTM D1762) or TGA under N ₂ (ASTM E1131)	pH (in H ₂ O suspension)	pH meter
Ash content (A)	Oven at 750 °C (ASTM D1762) or TGA under O ₂ (ASTM E1131)	Surface area, pore size distribution	N ₂ , Ar and/or CO ₂ physisorption
Fixed Carbon content (FC)	Calculated by difference (FC=100-(M+VM+A))	Surface texture and morphology	SEM, TEM
Ultimate analysis (CHNSO)	Elemental analyser; oxygen by difference (O=100-(C+H+N+S+A))	Bulk density	Measuring mass up to a certain volume in a graduated cylinder
High Heating Value (and LHV by calculation)	Bomb calorimetry or calculated using CHNSO and A (Equation 3.3)	Carbon bonds (e.g., aromaticity)	Solid-state ¹³ C NMR
Inorganic elements analysis	ICP-OES, AAS, AES, SEM-EDX, XRF	Crystallinity and crystalline phases	XRD

When biomass is converted into char, it becomes more stable, due to the loss of volatile matter during devolatilisation [29]. As devolatilisation proceeds, the fixed carbon fraction of the solid product increases [26][29][123][144][186]. There has been, however, experimental evidence that the fixed carbon contents in char can be decreased for higher temperatures when the ash content in the biomass is relatively high (≥ 20 wt.%) [186]. There is therefore a dependence of the char's fixed carbon content on feedstock properties. This effect was seen for both fixed carbon and ash contents in char, by Zhao *et al.* in a study of 12 feedstocks (lignocellulosic and others) under a wide temperature range (200–650 °C) [123]. The same study found that operating temperature was the main factor influencing fixed carbon and volatile matter contents in the char. Furthermore, Wang *et al.* found that increased feedstock particle size led to an increased fixed carbon yield [132].

The fixed carbon yield (the FC content of the char multiplied by the char yield, in dry ash-free basis) is often used to measure the efficiency of a slow pyrolysis process [29][104][144]. This parameter is more advantageous than using just char yield or another parameter, since it takes both yield and quality into account [26]. Fixed carbon yield correlates positively with thermal stability, which is relevant for combustion, and recalcitrance and carbon sequestration potential.

The volatile compounds in biomass have relatively high oxygen and hydrogen proportions, which leads to elemental carbon being concentrated in the solid product, asymptotically due to the increase in inorganic fraction [29][178]. The decrease in oxygen and

hydrogen proportions in the char has the consequence of decreasing the H:C and O:C atomic ratios, which are a measure of the heating value, often visualised in a Van Krevelen diagram [186]. Char (depending on other properties such as ash content) can have a heating value of ≈ 30 MJ/kg [29], which is comparable to bituminous coals [187]. For non-lignocellulosic feedstocks, the change in the char's carbon content can also be highly dependent on the type of feedstock [123]. Nitrogen and sulphur proportions in the char are also reduced compared to the original biomass, based on partial devolatilisation to vapour phase during pyrolysis [104][107].

The devolatilisation of biomass with increasing temperature leads to inorganics becoming concentrated in the char product, due to their relative stability [104][107][149]. Although the inorganic compounds mostly remain in the solid product as temperature rises, part of them may be devolatilised to the vapour phase, as is the case of chlorine [188], which can have detrimental effects on gas post-treatment and conversion. Chlorine can be problematic in thermochemical processing due to corrosion and pollution. Contrarily to most inorganic elements, chlorine is assessed in chars through Scanning Electron Microscopy couple with Energy Dispersive X-ray analysis (SEM-EDX), and not Inductively Coupled Plasma (ICP).

Due to the loss of volatiles with hydrogen and oxygen, functional groups present on the surface of the char suffer modifications and/or are removed with increasing pyrolysis temperature [189][190]. Acidic functional groups exist in char for example in the form of phenols, carboxylic acids, lactones, and lactols, while basic functional groups can be for example of pyrone type [191][192]. It is possible to determine the concentration of acid and basic functional groups through Boehm titration [191][192], although this method can be challenging for chars due for example to interactions between reactants and the char inorganic contents [193]. There have been attempts to improve the method for char analysis [194].

Fourier Transform Infra-Red (FTIR) is commonly used to detect a variety of surface functional groups, while X-ray Photoelectron Spectroscopy (XPS) is more commonly used to evaluate carbon-oxygen bonds, by determining variations in binding energy [192]. Usually, acidic functional groups decrease with increasing pyrolysis temperatures [190][195]. A consequence of the loss of volatile matter and functional groups with temperature is an increased hydrophobicity and decreased polarity [196][197], which impacts interactions with the surroundings, e.g., by decreasing the attraction between the char surface and polar compounds in water or soil (depending on application).

The surface functional groups contribute to the pH value measured from a char suspension in water, and also to the cation exchange capacity (CEC), which relates to the amount of exchangeable cations in soils (e.g. Ca^{2+} , Mg^{2+} , K^+ , Na^+) [193]. Usually, the presence of negatively-charged functional groups leads to a relatively high CEC [193]. The loss of

functionalities leads to an increase in pH and a decrease in CEC [189][198]. These features are important for char applications in soils and for adsorption, which will be discussed in subsection 2.3.2 and 2.4.

The pH value of a char can be measured in a suspension of the solid in water. Zhao *et al.* in a study of 12 feedstocks (lignocellulosic and others) under a wide temperature range (200-650 °C) showed that pH was predominantly dependent on the operating temperature [123]. A char is usually alkaline, while the original biomass feedstock can have pH <7 [199]. The pH value of chars has been related to the feedstock's ash contents: a manure with high ash content (>32 wt.%) produced char with pH >10, while chars with pH <7.5 were only obtained from woody biomass which had <1.5 wt.% ash contents [186]. Besides pH, the electrical conductivity (EC) of a char can also be measured, a property related to electron transfer capability, relevant for soil applications (e.g. water uptake by plants) [199].

Due to the loss of volatiles and breaking down of the lignocellulosic structure, char gains surface area and porosity with increasing production temperature [196]. Char density is typically lower than feedstock density due to material loss and increased porosity.

The surface area and pore size distributions of char can be assessed using N₂ and/or CO₂ physisorption. The porosity domains, of micro-, meso-, and macroporosity, correspond to pore widths of <2 nm, between 2 and 50 nm, and >50 nm, respectively, according to IUPAC definitions [200][201]. N₂ physisorption (77 K) is commonly used to determine surface area and micro- and mesoporosity, although it is recommended that CO₂ physisorption (273 K) is also applied, especially for narrow micropores (ultramicroporosity, <0.7 nm). Operating at higher temperatures allows for the CO₂ molecules to have higher kinetic energy to minimise diffusion issues and access smaller pores which can be relevant in carbonaceous solids such as chars [202][203][204]. Furthermore, deviations to linearity occur for the lower range of relative pressures in N₂ adsorption at 77 K, and with CO₂ adsorption at 273 K these deviations are avoided [203]. Porosity and surface area are relevant properties for a char, relating to its exchange and sorption capacities in soil and adsorption applications [25][199].

Scanning Electron Microscopy (SEM) and Transmitting Electron Microscopy (TEM) can be used to evaluate particle shape and sizes, as well as porous structure [193]. SEM is often combined with EDX and can be used to map a certain sample area for chemical elements. High-Resolution TEM can observe char at a nanometric level [193].

The proportion of the carbon in the char that is arranged in an aromatic structure (i.e., in multi-ring or polycyclic form) increases with pyrolysis temperature, making it more condensed and graphite-like [95][120][123]. This is due to the lower stability of the aliphatic compounds in the biomass, which contain paraffinic, carbonyl and carboxyl functionalities [120]. When using feedstock with a high ash content, however, the increase in aromatic carbon may not occur [186].

The degree of aromatic condensation (cluster size and purity) of a char and the distribution of carbon bond types (ketones, amide/carboxyl, phenolic, aromatic, alkyl-substituted, di-O-alkyl, O-alkyl, N-alkyl/methoxyl, methylene and methyl) in the char structure can be evaluated using solid state Nuclear Magnetic Resonance (NMR), usually ^{13}C [205]. A char with higher proportions of aromatic carbon is considered to be more stable than chars with lower proportions [206]. Usually the NMR technique applied in chars suffers from overlapping peaks/bands and poor resolution, due to the complex structure of char [193]. 2D NMR (e.g., ^{13}C allied to ^1H NMR) and ^{31}P NMR have also been used to analyse char [193].

X-Ray Diffraction (XRD) can be applied on char to evaluate crystalline and amorphous regions. Ma *et al.* [207] studied chars from manure at different temperatures and found that crystallinity from cellulose was found at 300 °C, with those peaks decreasing with pyrolysis temperature. From 600 °C onwards, the crystalline structure had disappeared, and amorphous carbon regions were formed, and at 1,000 °C a new peak was attributed to regions of aromatic carbon rings (graphitisation).

Other techniques that have been used to analyse char are Raman spectroscopy, near-edge X-ray absorption fine structure (NEXAFS) spectroscopy and electron paramagnetic resonance (EPR) or electron spin resonance (ESR). Raman and NEXAFS can be used to complement information such as structure disorder and aromatisation/graphitisation from other techniques, while EPR and ESR can be used to detect radicals [193].

Volatile organic compounds (VOCs) can be present in the char due to condensation during the pyrolysis process or adsorption after production [208]. Some VOCs are known to be toxic and can pollute water sources, hence these compounds need special attention in terms of their potential harm to the environment and living organisms [208][209]. This is of special importance for soil and adsorption applications, in which the compounds can potentially leach into the soil and water streams nearby the soil in which the char is applied, or into the water that the char is decontaminating. A study of 77 chars from different origins found that over 140 VOCs were desorbed by some chars, with HTC and fast pyrolysis chars overall having the greatest number of VOCs [208]. Slow pyrolysis chars had a more variable number of VOCs, however it was found that production temperatures <350 °C had more aldehydes, furans, and ketones, while temperatures >350 °C produced more aromatic compounds and longer chain hydrocarbons. It was also found that production conditions seemed to play a more significant role than the feedstock type on char VOC contents, and that post-production handling/processing also plays an important role [208].

Other potentially harmful compounds that can be found on char are polycyclic aromatic hydrocarbons (PAH), made up of carbon and hydrogen in interconnected aromatic rings (e.g.,

naphthalene, phenanthrene, pyrene, benzopyrene). These compounds can be formed during pyrolysis and be found on char, and are known for their toxicity [210].

Research has shown that the PAH and VOC contents of char can be reduced if a CO₂ atmosphere is used during pyrolysis [211]. Decreasing those compounds increases the char's quality, since they are in general detrimental for char applications (e.g., in soil, contaminant removal), mainly due to the release or decomposition of those substances into the environment [208][209][210].

2.3.2. Char applications

Historically, char has been widely used as a solid fuel for heating and cooking (as charcoal), as well as a reducing agent in the metallurgical industry (iron and silicon making) [29][93][94]. However, char has been a part of Human development for much longer: the use of charcoal for cave paintings was discovered to date back at least 38,000 years [29], and the first documented use of charcoal in smelting ores for bronze-making was almost 6,000 years ago in ancient Egypt [30].

A char that is meant to be used for domestic heating or cooking typically has a volatile matter content of 20-30 wt.% (40 wt.% is acceptable), whereas for metallurgical applications it should be <15 wt.% [29]. A char for these applications has typically 0.5-5.0 wt.% ash content, resulting in 28-33 MJ/kg heating value [29]. Industrially, char could be used for example to replace coal in power stations [212]. The inorganic contents of char can be detrimental for certain applications, such as energy generation through combustion, due to potential fouling and corrosion [58][59]. Other applications such as gasification can benefit from the inorganic contents of char due its role as a catalyst in cracking reactions [99][213].

Advantages of converting biomass to charcoal are for example: higher resistance to rain/moisture and natural decay; increased volumetric energy and mass density (requires less space to store); and less smoke produced during its combustion [214].

A char application that is gaining worldwide interest is as soil amendment (as biochar). Investigations made on soils in the Amazon area found that soil fertility was enhanced by charcoal, perhaps inadvertently through the deposition of remains from cooking fires. Since the soils remained fertile for a long time (hundreds or thousands of years), the potential of char for soil enhancement and carbon sequestration was (re)discovered and its exploration grew. Research is on-going, and results are usually positive, although depending on the soil and char production conditions the applied biochar can have a negative effect.

Soils worldwide have suffered negative effects from intensive agriculture, mining, and climate change, such as acidification and loss of carbon and microbial diversity. Char can be used as a sustainable material to restore carbon to the soils, intercept contaminants and improve plant growth [199]. Inorganic fertiliser use, which poses environmental problems, can

be reduced by replacement with biochar [149]. Due to the potential for long-term carbon sequestration, biochar application can make pyrolysis a carbon negative process [215].

A biochar with favourable qualities for soil applications usually has high carbon content and proportions of aromatic (stable) carbon, low density, high porosity and surface area, and high CEC [198]. However, the effect of char application depends on soil properties and needs, which must be assessed beforehand, and not all soils benefit from char application [216].

The fixed carbon and the aromatic carbon fractions, as well as the H:C and O:C atomic ratios, are seen by several researchers to be adequately related to the char's stability and degradation resistance, e.g., in soil applications and carbon sequestration [186][189]. The (decrease in) volatile matter has also been used as a proxy for stability, with its use allowing to distinguish between chars from high-ash or low-ash feedstocks [186]. The resistance of the char to degradation is referred to as its recalcitrance, and char usually becomes more recalcitrant with increasing pyrolysis temperature.

There is therefore a compromise on operating temperature, between char yield and stability, a characteristic which is relevant for all applications overall, and especially for soil applications, metallurgic uses, and the use as fuel.

Char can be used to increase the pH of acidic soils (liming), although it depends on the ability of the char to retain its pH (buffer capacity) [199]. Char pH and buffer capacity contribute to control nutrient retention and mobility in a soil [190]. Usually, higher temperature chars have higher pH and will thus be beneficial when the purpose is to reduce the acidity of a soil [190].

Applying biochar is beneficial in terms of returning plant nutrients present in the char structure (e.g., K, Ca, P, N) [149][217]. Manures usually have higher nutrient content than herbaceous or woody biomass, so char from manure has higher potential for soil nutrient enrichment [206]. Nevertheless, the inorganic composition must be assessed to check for harmful elements such as heavy metals, which can pollute soil and water. Biochars also have the potential to reduce the phytotoxicity of heavy metals by minimising their bioavailability through immobilisation [218].

The porosity present in chars can lead to better aeration, drainage capacity, and water and nutrient holding capacity [198]. Soil density can also be improved (lowered) by adding biochar, when the soil is too dense and compact, and microorganisms can use the porous structure to develop [198]. Adding biochar to soils has been seen to reduce GHG emissions such as CH₄ and N₂O, possibly through better aeration and stability [219]. Furthermore, biochar can prevent leaching of nitrates, phosphates and other valuable ionic solutes, due to its adsorption capability [219][220].

A char's water retention capacity depends not only on porosity but also on water affinity (hydrophobicity/hydrophilicity). There have been studies on clarifying the role of these two

characteristics, which showed for example that lower temperature chars can have lower water retention compared to higher temperature chars, due to greater hydrophobicity instead of low porosity [221].

As was already mentioned, not all soils benefit from char application. Biochar is more likely to be beneficial when soils have low nutrient or water holding capacity, and it can have further environmental benefits when char can intercept effluent runoff or groundwater laden with nutrients or other contaminants (e.g. pharmaceuticals from animal manures) [216].

In agriculture, char has also been used as an additive for cattle/poultry feed, and for animal bedding material [92][222]. Research has shown that char has the potential to reduce GHG emissions produced by cattle and poultry [92].

Other uses that are being investigated for char are for example as a material for electrodes in electrochemical applications (e.g. supercapacitors) [223][224], as a precursor for activated carbon [40][80][225][226], and as an adsorbent itself [13][196][227]. Char is said to have at least 55 possible uses [28]. Some more novel applications under investigation are in removal of tars in pyrolysis and vapour product upgrading [98][228], in composite materials for packaging/other uses [229][230], and as a humidity sensor [231]. A review of the recent advances in char utilisation was conducted by Qian *et al.* (2014) [232].

As mentioned, char can be converted into another carbonaceous material called activated carbon. Activated carbon functions as an adsorbent for substances in a fluid (gas or liquid), through the process of adsorption, favoured by porosity and usually large surface area. In commercial activated carbons, surface area can be as high as 3,000 m²/g [38]. The micropores (<2 nm) are useful for small molecules, particularly in gas phase [233], while macropores (>50 nm) have relatively small adsorption capacity, but are important in defining adsorption kinetics, providing paths for molecules to diffuse into smaller pores [234]. Larger micropores or mesopores (2-50 nm) are most useful for adsorption of organic molecules such as pharmaceuticals, herbicides, and dyes [235]. Further details on activated carbon and the activation process are in subsection 2.3.3.

The decontamination of air and water has had growing demand, and there is a search for inexpensive, sustainable and environmentally-friendly materials for adsorbent production, such as biomass and biomass-derived products. This has led to plenty of research on using char or char-derived products for adsorption, which is detailed in section 2.4.

It would be ideal to produce tailored chars with specific characteristics for each application, however the methods have not been fully mastered. The understanding of the impact of different feedstocks and process conditions on the char properties and consequently its applications must be improved to maximise value. A better knowledge of the physico-chemical characteristics of char, and how they are influenced by the char's origins, is needed to optimise the process for specific purposes.

A summary of research on slow and intermediate pyrolysis of wheat straw and other relevant biomass in screw reactors is made in Table 2.4. The table includes char yields (dry feedstock basis) and main conclusions regarding product yields and char quality.

Table 2.4: Summary of relevant research on slow and intermediate pyrolysis of wheat straw and other relevant biomass in screw reactors.

Feedstocks	Reactor system	Varied parameters	Other process conditions	Char yields (wt.%, dry basis)	Main conclusions and comments	Reference
Straw (finely ground)	Haloclean® (max. 3 kg/h) with steel spheres as heat carriers; no carrier gas	Temperature	1.4 kg/h feeding rate; 4 min SRT; 2 s VRT	325 °C: 73.0	Pilot-scale reactor ran continuously for 6 weeks with pelletised straw; Char HHV from pilot scale was 26 MJ/kg and carbon contents 63 wt.%; Other char analyses not reported	Hornung <i>et al.</i> (2005) [168] ¹
				350 °C: 48.0		
375 °C: 38.2						
400 °C: 36.2						
Straw (pellets, 8 mm diameter)	Haloclean® (max. 100 kg/h) with steel spheres as heat carriers; no carrier gas	Reactor scale (lab vs pilot)	2.4 kg/h feeding rate; 4 min SRT; 60 s VRT	375 °C: 45.0		
				385 °C: 39.0		
				400 °C: 35.0		
				450 °C: 28.3		
				500 °C: 35.0		
			25 kg/h feeding rate; 450 °C; 7.5 min SRT; 0.3 s VRT	35.0		
Pine wood (powder form, max. 0.85 mm particle size)	Single screw (max. 20 kg/h)	Temperature	5 kg/h feeding rate; 0.5 min SRT; N ₂ flow	450 °C: 28.8	Ash contents in switchgrass chars (13-22 wt.%) were greater than pine wood chars (1-5 wt.%) due to higher ash content in the herbaceous feedstock; Concentration of inorganic elements in switchgrass chars was 2-10 times higher; pH (in H ₂ O) and degree of aromaticity were higher in switchgrass chars	Kim <i>et al.</i> (2011) [236] ²
Switchgrass (4 mm max. particle size)				600 °C: 16.4		
		800 °C: 10.3				
	450 °C: 33.8					
	600 °C: 18.3					
	800 °C: 12.3					
Brewers spent grain (oven-dry and milled)	Pyroformer™ (max. 20 kg/h)	N/A (testing catalytic post-reforming)	450 °C; 1-4 min SRT; N ₂ flow	31.5	Char carbon content of ≈62 wt.% (d.a.f.) was ≈15% higher than the feedstock; Char HHV was ≈26-28 MJ/kg	Mahmood <i>et al.</i> (2013) [102]

¹ Product yields reported in wet basis, and feedstock moisture content not reported

² Pyrolysis referred to as fast (use of small feedstock particle size, relatively short SRT, carrier gas flow)

Table 2.4 (cont.): Summary of relevant research on slow and intermediate pyrolysis of wheat straw and other relevant biomass in screw reactors.

Feedstocks	Reactor system	Varied parameters	Other process conditions	Char yields (wt.%, dry basis)	Main conclusions and comments	Reference
Pine wood residue (pellets)	Pyroformer™ (max. 20 kg/h)	Feedstock type (same particle size: 15-25 mm length, 6 mm diameter)	5-6 kg/h feeding rate; 450 °C; 1.5 min SRT; no carrier gas	30.6	Prolonged SRT led to favoured secondary reactions, char formation and higher char carbon content (≈75 wt.%); Chars had HHV of 30-33 MJ/kg, which was an energy yield of ≈50% (total product energy yield was ≈75%)	Yang <i>et al.</i> (2014) [172]
Barley straw (pellets)				34.2		
Rice straw (2 mm max. particle size)	Single screw (max. 6 kg/h)	Reactor type	500 °C; In screw reactor: 0.6 kg/h feeding rate; 20-25 min SRT; N ₂ flow; In fluidised bed: 1.6 s resid. time	49.4	Char yield in fluidised bed was ≈50% of the ones in batch and screw reactors due to very fast heating rate in the fluidised bed; Screw reactor produced char with highest ash and lowest elemental and fixed carbon contents; Screw reactor had the lowest energy product yield (≈65%), with 72-75% for other reactors	Nam <i>et al.</i> (2015) [237]
	Batch (250 g; 4 °C/min)			52.5		
	Fluidised bed (5 g/min)			26.8		
Rice husk (<10 mm particle size; air dried)	Single screw (max. 300 g/h; same as used for this PhD work)	Temperature; feedstock type	0.12 kg/h feeding rate; 1 min SRT; 5 s VRT	350 °C: 46.2	Rice husk had higher char yields than corn stalk; Maximum liquid yield was obtained at 500 °C; Volatile matter and H:C and O:C atomic ratios decreased with temperature; Maximum char HHV (600 °C) was 21.3 and 26.1 MJ/kg for rice husk and corn stalk, respectively; Higher ash contents in rice husk (13.3 wt.%, w.b.) compared to corn stalk (8.2 wt.%, w.b.) contributed to the higher char yields and lower HHV in chars from rice husk	Yu <i>et al.</i> (2016) [178]
Corn stalk (<10 mm particle size; air dried)				400 °C: 43.9		
				450 °C: 39.4		
				500 °C: 34.3		
				550 °C: 32.3		
				600 °C: 31.1		
				350 °C: 38.0		
				400 °C: 33.4		
				450 °C: 30.6		
				500 °C: 28.6		
550 °C: 28.8						
600 °C: 27.0						
Wheat husk (pellets of 20 mm length and 6 mm diameter)	TCR® (max. 2 kg/h)	N/A	1.4 kg/h feeding rate; 430 °C pyrolysis and 600 °C post-reforming; 3-5 min SRT	23.3	Prolonged SRT favoured secondary reactions; Total energy yield was 77.2%; Char had 76.5 wt.% carbon content, 11.8 wt.% ash content and HHV of 28.4 MJ/kg (≈45% of energy yield)	Santos <i>et al.</i> (2019) [238]

2.3.3. Activated carbon

Char can be transformed into a material with high surface area and porosity, called activated carbon, in order to increase its efficiency in applications such as air and water decontamination by adsorption [40]. This is an increasingly attractive application for the solid product from pyrolysis, due to the rise of stricter air and water quality standards, sustainability concerns, and promising research results [40]. The char (or its precursor) goes through a process called activation, which can be of different types according to the conditions used. The activation process, besides increasing surface area, can also "tailor" the pore hierarchy, by for example favouring mesopore (2-50 nm) creation instead of micro (<2 nm) or macropores (>50 nm). Some chemical groups can also be added into the char's structure by using certain activation conditions.

Activated carbon is a largely amorphous structure, and mainly composed of aromatic configurations of carbon atoms, with random cross-linkages. Sheets or groups of atoms are stacked unevenly in a relatively disorganised manner (unlike graphite), the degree of order being based on the starting material and treatment (carbonisation and activation) sequence and conditions [234].

Activated carbon can also possess functional groups on the surface, which can be concentrated upon activation, by using certain chemical agents such as H₂O₂ or compounds containing sulphur or nitrogen [239]. The surface chemical functionalities play an important role in interactions of the solid material with the surroundings.

To produce activated carbon, a carbonaceous material undergoes thermal treatment (usually at >600 °C) to increase surface area and porosity by different activation techniques [37][202][240]. The process can be done after pyrolysis (2-step activation) or in 1-step (combined carbonisation and activation), and it can be classified into physical or chemical activation. Physical activation is typically a 2-step process, while chemical activation is often 1-step.

In physical activation, the carbonaceous material experiences heat (600-1,200 °C) and partial oxidation with a gas phase [240]. The oxidant used is typically steam, CO₂, or oxygen/air. The term "physical" originates from the initial misconception about steam activation, in that steam would only volatilise and remove condensed material, without chemical reactions, but the water is in fact an oxidising agent for the carbonaceous material, especially at temperatures >750 °C [22]. Physical activation works in two stages: firstly, tar is oxidised and clogged pores are opened; secondly, part of the carbon structure is also oxidised. The second stage, besides creating new pores, or interconnections between pores, can also change the chemical functionalities on the aromatic surface of the solid product [195].

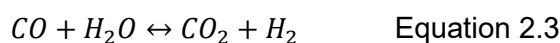
CO₂ can be introduced in the system by injection on its own, or could be sourced from flue gas produced from pyrolysis vapours/gases combustion, which can bring economic

advantages [130][241]. Steam, on the other hand, can be introduced into the reactor in different ways [242]: an inert carrier gas such as nitrogen can be saturated in water before injecting it into the reactor; or water can be vaporised inside the reactor, either by injecting liquid water on its own, or by feeding a feedstock with elevated moisture content.

When using CO₂, the main chemical reaction contributing to activation is the Boudouard reaction (a reduction reaction), shown in Equation 2.1. With steam, the steam reforming reaction is favoured, shown in Equation 2.2. The rate of the steam reaction is faster than the CO₂ reaction, allowing steam activation to occur in shorter times [239]. Both reactions consume part of the solid material (char), forming or expanding porosity.



Other reactions that can occur during physical activation with steam are Equation 2.3 (water gas shift) and Equation 2.4 (steam methane reforming) [243]:



During steam activation the main mechanism is a widening of existing pores, while with CO₂ both pore widening and creation contribute to increasing surface area [40][244]. As a consequence, a broader pore size distribution is created during steam activation, with meso and macroporosity being significantly developed, while CO₂ activation develops higher microporosity [244]. This means the pore hierarchy can be “tailored” by selecting the appropriate activating agent.

In terms of surface functional groups, a study with rice husks found that steam activation at 750 °C led to the disappearance of lactone and phenolic/hydroxyl groups, also decreased carboxyl functionalities, and overall led to a decrease in acidic functional groups [195]. The pH was found to be further increased upon activation, from 6.40 in the feedstock, to 8.75 in the char (produced at 550 °C) and 9.70 in the activated product [195].

Chemical activation, differently to physical activation, is done by first mixing a chemical agent with the precursor, i.e., impregnation, and then the mixture is thermally treated. The most common chemical agents are phosphoric acid (H₃PO₄), sulphuric acid (H₂SO₄), zinc chloride (ZnCl₂), and potassium or sodium hydroxides (KOH or NaOH), with various salts also being researched [37]. The precursor is most commonly the biomass itself, but chemical activation can also be performed on the carbonised biomass (char), with the precursor-to-

agent ratios being typically between 1:0.5 and 1:3 based on dry precursor weight [22]. The impregnation ratio, between the precursor and the chemical agent, is seen as a crucial parameter in activation, with its effect also depending on the chemical agent and the precursor themselves [239].

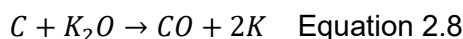
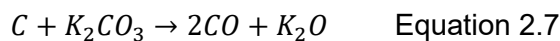
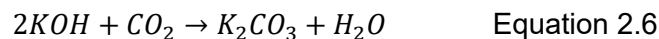
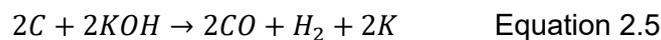
Mixing can be performed dry (with the chemical agent as a solid), or wet, using a solution of the chemical agent. The wet mixing method is said to better distribute the chemical agent into the precursor, and can sometimes be performed at temperatures higher than ambient (e.g., 50 °C) to improve mixing [239]. A comparison between dry and wet mixing found that the latter led to greater surface area and microporous volume [245]. However, the wet mixing method usually requires a drying step to concentrate the chemical agent [239]. The drying step can also influence the activation process: for example, a nitrogen flow led to a narrower pore size distribution compared to air drying [246]. When using char as the precursor, wet mixing can be challenging due to potential char hydrophobicity.

The mechanism of chemical activation varies according to the activation agent, but the following principles are common [22]: chemical bonds in the precursor structure start to break during mixing, and ions from the activation agent bind to the surface and occupy voids, defining the porosity created in the subsequent activation. During activation, the chemical agent avoids tar formation in the pores [22], and its interaction with the precursor facilitates devolatilisation, lowering the thermal degradation temperatures [37]. The pores become available post-activation, usually after washing the material to remove the activation agent [22]. Washing, usually done with a dilute acidic/basic solution and/or water, also serves to moderate the pH if the chemical agent is too basic/acidic. This leads to a disadvantage of chemical activation which is the creation of liquid waste streams. The reactions occurring during chemical activation depend on several variables, e.g. temperature, chemical agent and precursor, and have not yet been fully understood [247].

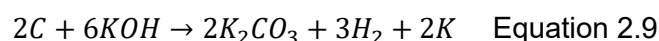
When performing ZnCl_2 activation, the impregnation step causes separation of cellulose fibres and partial depolymerisation of hemicellulose and lignin in the biomass, due to the agent's Brønsted acidity [248]. This reduces mechanical resistance and causes swelling, making the precursor more susceptible to activation. During activation, the ZnCl_2 promotes dehydration reactions and pore development due to devolatilisation, however, porosity can go through a maximum due to structure collapse at relatively high activation temperature and time and impregnation ratios [248].

For KOH activation, Otowa *et al.* witnessed formation of metallic K, from K_2O reacting with H_2 , producing also water [249]. The mechanism for KOH activation [249][250] starts with KOH reacting with the carbon matrix, imbedding metallic K in the carbon structure and releasing CO and H_2 (Equation 2.5) [250]. Other produced gases (e.g., CO_2) can react with KOH to generate K_2CO_3 (Equation 2.6), and this carbonate can cause further gasification

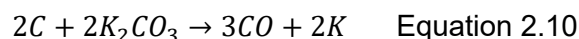
reactions (Equation 2.7 and Equation 2.8). Washing can remove imbedded K species and free the pores.



A study by Lillo-Rodenas *et al.* improved the understanding of the chemical reactions behind activation with KOH and NaOH, although it was performed on anthracite [251]. The following global chemical reaction (Equation 2.9) for KOH activation was proposed (analogous for NaOH):



A study of chemical activation of lignin found that K_2CO_3 can be reduced in an inert atmosphere (Equation 2.10), at temperatures >600 °C, reducing char yield and increasing porosity [252]:



Comparing KOH and NaOH, the latter has the advantages of being more affordable (produced from NaCl) and less corrosive [247]. However, in a study of coal activation, KOH was found to produce higher surface areas and porosity than NaOH [247]. Nitrogen flow and the ratio agent:precursor were found to be the most important factors influencing porosity in coal activation [247].

A study comparing KOH and NaOH activation on anthracite found that the starting temperatures of activation were lower using KOH (400 °C) compared to NaOH (570 °C) [251]. The same study found that higher carrier gas flows enhance porosity, especially for lower KOH:char ratios, which was explained by the removal of products and equilibrium displacement towards the products. A study of coal pitch activation found evidence that KOH can develop a narrower pore size distribution compared to NaOH [253].

The agent-to-precursor ratio can be used to control pore hierarchy, with the effect however depending on the chosen agent, precursor, temperature and other process conditions [254]. One study found that a 4:1 ratio (agent:precursor, by weight) was optimum for KOH activation of rice straw, achieving the highest surface area and pore volumes [255].

This was found, however, for two-stage chemical activation, with carbonisation at 700 °C and subsequent KOH activation at 900 °C. Another two-stage study using agricultural wastes (including wheat straw) found that the effect of ZnCl₂ impregnation ratio (2:1-5:1 by weight) depended on activation temperature: the effect on microporosity became insignificant or even negative for the highest temperatures applied (600-800 °C), while it was positive for 400-600 °C [248].

To avoid the corrosive nature of hydroxides, several researchers have investigated the use of K₂CO₃ or Na₂CO₃ instead. Due to the less hazardous nature of the carbonates, the washing step can be performed using only water [239]. However, the use of sodium carbonate instead of the hydroxide has been found to hinder activation [251]. A study comparing CO₂ physical activation and K₂CO₃ chemical activation found that the chemical activation produced lower surface areas (291 m²/g) compared to CO₂ activation (351-440 m²/g) [228]. Physical activation was performed at 800 °C, with N₂ atmosphere during heating, switching to CO₂ at maximum temperature, and with activation times of 30, 45 and 60 min, to yield different burn-off of 15, 30 and 40%. Chemical impregnation occurred using a 2.0 M K₂CO₃ solution and wet mixing with 1:1 char:K₂CO₃ ratio, with activation at 700 °C for 1 hour in N₂ atmosphere. Maximum temperature of 700 °C was selected to avoid vaporisation of metallic K, which can occur at >760 °C [256].

Comparing the hydroxides and carbonates with other chemical agents such as H₃PO₄ and ZnCl₂, the former usually yield higher pore volumes and surface area [245][252]. However, the maximum surface areas with hydroxides and carbonates have been found to occur only >700 °C, while for H₃PO₄ and ZnCl₂ the maximum was at 600 °C [252].

In chemical methods, activation time is usually 1-3 hours, with its influence depending on the employed agent [254]: for KOH and H₃PO₄, porosity increased with activation time [245][257][258], while for ZnCl₂ it was found to decrease [245]. A study of ZnCl₂ activation of several agricultural wastes including wheat straw found that when activation time was higher than 3 hours, microporosity started to decrease. This was explained by a loss of rigidity of the solid products (thermoplastic behaviour) and structure collapse, blocking micropores [248].

Researchers have experimented with pre-treatments prior to activation, such as removing inorganic matter, and a study found that demineralisation (by precipitation with H₂SO₄ and washing with distilled water) was detrimental for the activation process of a lignin with H₃PO₄ [259]. Hydrothermal carbonisation has also been studied as pre-treatment, and the solid product becomes more reactive during activation, due to a lower aromatisation degree, higher oxygen content and more surface chemical functionalities [260][261].

Other chemical treatments exist that are not usually referred to as activation, which are meant to functionalise a carbonaceous material such as char, adding certain chemical

functionalities to the surface. Chemical functionalisation is done for example with H_2O_2 to add O-containing groups such as hydroxyls or carboxyls, with H_2SO_4 to add sulphonic groups, with HNO_3 , and with amines [239].

In both chemical and physical activation, chemical reactions occur, with loss of solid material, called burn-off, and typically ranging 30-55 wt.% of the carbonised material [26]. Besides product yields, activation also decreases fixed carbon yield, affecting the potential for carbon sequestration [26].

In general, the temperatures used for chemical activation are lower (as low as 400 °C) than in physical activation [38][251]. Usually porosity and surface area increase at higher temperatures, activation times and activating agent doses, up to a certain point, because links/holes formed between pores can cause their collapse, reducing surface area when those values are too high [254].

The use of lower temperatures in chemical activation is an advantage compared to physical activation, and this also causes lower levels of burn-off (higher product yields) [37][248][251]. The porosity created by physical activation is usually narrower than in chemical activation [37]. The pore size distribution can be tailored according to the activating agent used and the process conditions. The surface areas obtained in chemical activation are usually higher than in physical activation [251], and can be $>3,000 \text{ m}^2/\text{g}$ [249][256]. However, performing of the post-treatment step of washing after chemical activation is a disadvantage, creating waste streams that can be polluting and require adequate disposal [248][251]. Design and material restrictions can also be greater in chemical activation due to the corrosive/hazardous nature of some chemical agents used [248][251].

Due to normally occurring in two steps, physical activation has higher energy consumption than chemical activation, and more equipment may be required. Furthermore, if the carbonised material is cooled down between the carbonisation and activation steps, it could adsorb volatiles/tars from the surrounding atmosphere (if not successfully purged), reducing its quality for adsorption due to pore blocking.

There is an interest in performing physical activation in 1-step, in order to decrease processing times and thus improve the economics of the process. Different research groups are investigating this. For example, Azuara *et al.* used CO_2 (from flue gases) in slow pyrolysis of vine shoots (fixed bed; 600 °C; 5 °C/min; 1 hour SRT) and achieved almost 200 m^2/g surface area, mostly microporous [130]. There was however a contribution of operating pressure: compared to slow pyrolysis with N_2 as carrier gas, the surface area increase occurred at 1.1 MPa, while there was a decrease in surface area at atmospheric pressure.

Another example of 1-step physical activation was performed on coconut shells with steam at 800 °C in a small-scale rotary kiln (scale of tens of grams/hour) [262]. Using a rotary

kiln allows for the process to be performed continuously, which is economically advantageous. Steam was employed at H₂O:feedstock weight ratios varying from 0.5:1 to 5:1, and it was observed that the solid product's surface area increased with this parameter, to a maximum of $\approx 1,400$ m²/g. Air or nitrogen were tested as carrier gas, co-currently to the steam, and no effect on surface area was found. When comparing with activating pre-carbonised coconut shells (2-step activation), it was found that the final activated carbon yield was greater in the case of 1-step activation. Micropores, especially <1 nm, were found to be the main contributor to surface area, with also some macropores, which resembled the skeletal structure of the original feedstock.

Jung and Kim studied different physical activation methods to produce activated carbon from oak wood (<1 mm particle size) in a fixed bed reactor [263]. Two methods, with carbonisation with N₂ atmosphere, and then CO₂ atmosphere for activation (with and without cooling in between carbonisation and activation), were compared to carbonisation and activation with CO₂ atmosphere (without cooling). Carbonisation was done at 500 °C, and activation at 800 or 900 °C, with activation times of 60, 120, and 180 min. Table 2.5 presents a summary of the obtained results.

Table 2.5: Summary of results from CO₂ activation of oak wood by Jung and Kim [263].

Atmospheres	Cooling?	Activation T (°C)	Activation time (min)	Burn-off (%)	BET Surface Area (m ² /g)
N ₂ (500 °C)	---	---	---	Reference	107
N ₂ (800 °C)	---	---	---	None	249
N ₂ /CO ₂	Yes	900	60	47.9	724
N ₂ /CO ₂	No	800	60	30.0	716
N ₂ /CO ₂	No	900	60	73.1	1,126
N ₂ /CO ₂	No	900	120	81.8	2
CO ₂ /CO ₂	No	800	60	27.0	786
CO ₂ /CO ₂	No	900	60	67.1	807

Activation with CO₂ atmosphere yielded much higher surface area than pyrolysis alone. An exception was the case with 120 min activation time, which consumed more material and produced almost no surface area. The experiment with 180 min activation time had the same result. Activation temperature increased surface area, especially after carbonisation with N₂ as carrier gas and when the cooling step between carbonisation and activation was avoided. However, comparing with the experiments with carbonisation with CO₂, the latter achieved lower burn-off (higher product yield) and comparable surface areas.

David and Kopac [211] studied the activation of chars from a pelletised mixture of rapeseed oil cake and walnut shells. Pyrolysis was performed in a vertical fixed bed reactor, at 400-750 °C, 5 °C/min heating rate and 60 minutes at peak temperature. Activation was then performed with CO₂ atmosphere, with the same temperature range (400-750 °C) and 0.5-3.5 h

activation time. It was found that surface area and porosity of the activated carbons depended mainly on activation temperature and time. The materials produced at 750 °C and 3 h activation time had the highest surface area (BET) of up to 1,000 m²/g, while the ones from 600 °C had 300-500 m²/g, and the 400 and 500 °C products yielded relatively small surface area.

In terms of chemical activation, Ma *et al.* [264] compared ZnCl₂ with KOH in activation of wheat straw (1:1 ratio; 700 °C and 1 hour activation time) and found that ZnCl₂ resulted in higher surface area (907 compared to 552 m²/g) and microporosity than using KOH. Overall, the porosity from KOH was more mesoporous than using ZnCl₂, and the surface analysed by SEM was less uniform. The differences were attributed to the activation mechanism, which was influenced by an uneven distribution of the KOH in the feedstock matrix. The chars were also tested in adsorption of methylene blue, which is analysed in subsection 2.4.3.

As discussed, activation can be performed in several different manners, depending on desired product properties and application, and on the feedstock and conditions employed. All activation procedures however usually have in common a long processing time (i.e., from the activation process itself, from when it is made in 2-steps, and from possible cooling down between those 2-steps), which is a point to improve with potential economic benefits. Besides time-consuming, activation procedures are also in general resource-consuming (e.g., injected gases, chemical agents, at times with high concentration and agent:precursor ratio). Furthermore, activation is also usually energy-intensive, with physical activation commonly requiring temperatures >600 °C. Production costs could be lowered if activated carbon (or an alternative bioadsorbent with comparable performance) was produced from less resource and energy-intensive processes.

2.4. Removal of contaminants from water

As society developed, pollution of air, soil, and water has become an increasingly threatening issue, as evidenced by health issues in highly polluted regions. Pollution reduction has been a pressing matter, and as regulations become more stringent, a need for better and more efficient decontamination methods arises [265]. Simultaneously, sustainability concerns have led to research around eco-friendly contaminant removal methods, and also the need for affordable production and application, since decontamination is required worldwide, both in developed and under-developed regions.

Contamination of water sources can occur in various ways, e.g., by contaminant runoff from fields and soils and due to poor efficiency of decontamination methods. Examples of water contaminants with impacts in health, even in low concentrations, are heavy metals (e.g., As, Cd, Cr, Pb, Hg), pesticides, pharmaceuticals, and other chemical substances [266].

2.4.1. Water decontamination routes

Wastewater has a variety of different contaminants present in it (e.g., solids, organic matter, heavy metals, nutrients, pharmaceuticals, pathogens), and different physical, chemical, and biological techniques can be used in wastewater treatment plants to treat/remove them so that the water can be safely returned to the water cycle. Table 2.6 lists the possible treatment stages in an industrial wastewater treatment plant [266].

Table 2.6: Treatment stages in wastewater treatment.

Treatment	Typical techniques	Main contaminants typically addressed
Preliminary	Screening, filtration, settling, degritting	Large solids, trash, inerts, grit
Primary	Clarifiers, settling, skimming, coagulation, flocculation	Suspended solids, oils, grease, biochemical oxygen demand (BOD) ¹
Secondary	Digestion with aerobic bacteria in biological contactors or biofilters, activated sludge processes	BOD, dissolved and colloidal organic matter
Tertiary/advanced (optional)	Denitrification (biological); phosphorous removal (biological or chemically precipitated); disinfection by ozonation, chlorine treatment, UV light treatment; adsorption with activated carbon; membrane separation (ultrafiltration)	Nutrients (e.g., N, P), dissolved contaminants (e.g., colour, heavy metals), pharmaceuticals, pathogens, bacteria, micropollutants

Recently, more stringent regulations in disposal practices regarding water quality have led to the need for improved wastewater treatment [265]. However, some contaminants are more challenging to remove, and removal becomes more challenging when the contaminant concentration is relatively low (micropollutants). Micropollutants are a diverse array of human-made and natural substances with quantities below $\mu\text{g/L}$ (or ppb), originating for example from pesticides, surfactants, pharmaceuticals and cosmetics [41].

The most common wastewater treatments (primary and secondary treatments) are often not efficient for micropollutants, and the control and removal of specific compounds is often unregulated [41][267]. Micropollutants have been found in wastewater, as well as in drinking water sources (rivers, lakes, groundwater) [41]. Research on the topic of micropollutants is of great importance and on-going, due to hazardous effects on health [267].

¹ Biochemical oxygen demand (BOD) is the amount of dissolved oxygen required by aerobic microorganisms to break down organic matter, and is thus a measure of biodegradable organic matter.

Despite being optional, the tertiary/advanced treatments have become more and more utilised in wastewater treatment facilities due to relatively high efficiency. These kinds of treatments, although being more efficient even at low contaminant concentrations, are more costly than the primary and secondary ones [41].

2.4.2. Adsorption for water decontamination

Adsorption is one of the most efficient techniques for the removal of contaminants from water, including micropollutants, and has thus been frequently adopted in wastewater treatment [41]. Advantages of adsorption over other advanced contaminant removal techniques such as ozonation are: greater versatility to different pollutants, affordability, and avoiding the creation of toxic by-products [39]. There is, however, the issue of recyclability/regeneration of the adsorbent, addressed in subsection 2.4.3.

Adsorption is in contrast with absorption, with the latter occurring through accumulation of a substance in the bulk of the adsorbent, and the former occurring through concentration in the interfacial layer between the adsorbent surface and the bulk fluid. Adsorption can be called physisorption when the process is governed by intermolecular forces of attraction and repulsion (van der Waals forces, e.g., dipole moments, dispersive attractive London forces) [268]. In contrast, chemisorption occurs through formation of chemical bonds. Due to this, chemisorption is often irreversible, while physisorption is reversible.

Activated carbon is the principal adsorbent used worldwide, due to its high adsorption capacities and stability, with other adsorbents being silica gel, activated alumina, zeolites (molecular sieves), polymers/resins and clay [269]. Many wastewater treatment plants apply activated carbon as a treatment, on its own or in conjunction with secondary biological treatments [41][267]. It has been found, however, that the efficacy of activated carbon in removing contaminants from wastewater can be significantly lowered by the presence of organic matter, due to competition with binding sites which can block porosity [41].

The main adsorbent properties which influence adsorption performance are surface area, pore volume and pore size distribution [268]. Surface chemistry also plays an important role [38]. The activated carbon properties depend on starting material and activation conditions, e.g., temperature and exposure time, activating agent and proportion (discussed in subsection 2.3.3.) [38][40].

Pyrolysis temperature is overall the parameter with greatest influence on most char or activated carbon properties, and consequently is a great influence on adsorption performance. With higher pyrolysis temperatures, due to the loss of volatile matter and functional groups from the surface, the solid becomes more hydrophobic and has less polarity, which does not favour interactions with polar compounds in water [196]. On the other hand, surface area can

be increased with higher pyrolysis temperatures, and this could benefit adsorption of compounds (if pore sizes are higher than the size of the adsorbate molecule) [233][235][270].

Surface functionalities of an adsorbent can be tuned by incorporation of heteroatoms such as oxygen, nitrogen, boron, sulphur, and phosphorous [271]. These heteroatoms can change the electrochemistry (i.e., electron density) of the surface, which can improve interactions with adsorbates. For example, oxygen and nitrogen heteroatoms are negatively charged, which can improve interaction with cationic molecules, while boron and phosphorous are positively charged and thus interact more with negatively charged (i.e., anionic) molecules [267][271]. Synergistic effects between different heteroatoms could also be achieved. The addition of heteroatoms could be used in adsorption in both liquid and gas phase.

The type and amount of functional groups on an adsorbent's surface are responsible for providing a negative or positive surface charge when the material is in aqueous solution [27]. This is very relevant for the mechanisms of adsorption and is commonly evaluated by the pH at the point of zero charge. The pH value at the point of zero charge, pH_{pzc} , is the pH value at which the net overall surface charge of a material (e.g., char or activated carbon) is zero [27]. The pH_{pzc} , equivalent to the isoelectric point of a molecule, mediates the zeta potential around the adsorbent and thus adsorption capacity. When solution pH is higher than the pH_{pzc} , the surface becomes negatively charged, attracting cations from solution, while for pH values lower than pH_{pzc} , the positively charged surface attracts anions [27][272][273].

2.4.3. New and sustainable carbonaceous adsorbents for organic contaminant removal from water

Although the use of activated carbon for contaminant removal from water has become very popular, the following downsides exist: relatively high production costs, coal or non-abundant biomass such as coconut shells are the main feedstocks, and separation from aqueous phase and subsequent regeneration can be challenging [38][39][274].

Research has been very active in using biomass and biomass-derived materials, including char, as adsorbents to replace activated carbon [39][274]. Char was applied for the first time as a potentially low-cost alternative adsorbent in wastewater treatment in 2009 [275].

As with any other adsorbent, the adsorption capacity of char depends mainly on surface area, pore size distribution and surface charge, i.e., the char's morphology and chemistry [92][190]. The surface charge depends on existing surface functional groups.

Similarly to activated carbon (previous subsection 2.4.2), char functionalisation by adding certain surface chemical groups or other features can also be performed in order to favour certain interactions with the surroundings. For example, treating char hydrothermally with H_2O_2 was found to increase its affinity to remove heavy metals from aqueous solutions, due to the insertion of oxygen-containing functional groups [276].

In section 2.3.1, it was stated that char can possess VOCs, PAHs and other potentially harmful compounds in its structure, and ways to avoid their formation were discussed. For the mentioned compounds to be harmful, they need to be released into aqueous phase, and normally the char itself prevents this from happening due to its binding/adsorption properties. The bioavailability of these compounds is reported to be lowered to 1-10% of the total content in the char [277]. Overall, however, research has shown that the probability that these compounds will leach into water in concentrations comparable to legislation limits is very low, due to the binding ability of the chars [277]. Nevertheless, those compounds are likely blocking sites available for adsorption and therefore decrease adsorption performance.

Examples of organic contaminants are organic solvents, PAHs, herbicides, pharmaceuticals, dyes, and dioxins, while heavy metals, salts, nitrates, and fluorides are examples of inorganic contaminants.

Synthetic dyes are organic compounds that are widely used to colour final products in several industries, e.g., textile, leather, paper, plastic manufacturing [39]. Health issues can arise upon contact with effluents with dyes, such as carcinogenicity, irritation, allergies [39].

Dyes are commonly used to test the capacity of adsorbents to remove contaminants from water, because they allow the operator to visually check the adsorption performance (preliminarily) and have relatively simple, accessible and affordable techniques such as UV-Vis spectrophotometry to determine their concentration.

Methylene blue (MB) is commonly used as a proxy for other organic contaminants in water, and is the most popular dye to test adsorption [278]. MB can assess mesoporosity or large micropores, with the molecule being able to access pores larger than 1.5 nm [254][279]. Iodine (not a dye) is also frequently used to test adsorbents in the same manner as methylene blue, accessing pores >1 nm [254].

Microporosity may not serve for adsorption of larger and higher molecular weight compounds such as pharmaceuticals, dyes, pesticides, and dioxins [235]. Meso and macroporosity are desirable for adsorption of those compounds and can be obtained by adjusting the pyrolysis parameters, without strictly requiring activation procedures [92]. In general, mesoporosity is increased at pyrolysis temperatures >600 °C [280].

Several mechanisms of adsorption of MB molecules to bioadsorbents such as char have been reported, such as electrostatic interactions, ion-dipole interactions, pore filling, partition onto surface, and van der Waals forces, i.e., dispersion (London forces, between temporary and induced dipoles), dipole-dipole (between polar molecules), and hydrogen bonding [196][281][282][283]. Multilayer adsorption of MB has also been reported [282]. Figure 2.10 illustrates the surface of a char particle and the potential main mechanisms contributing to MB adsorption.

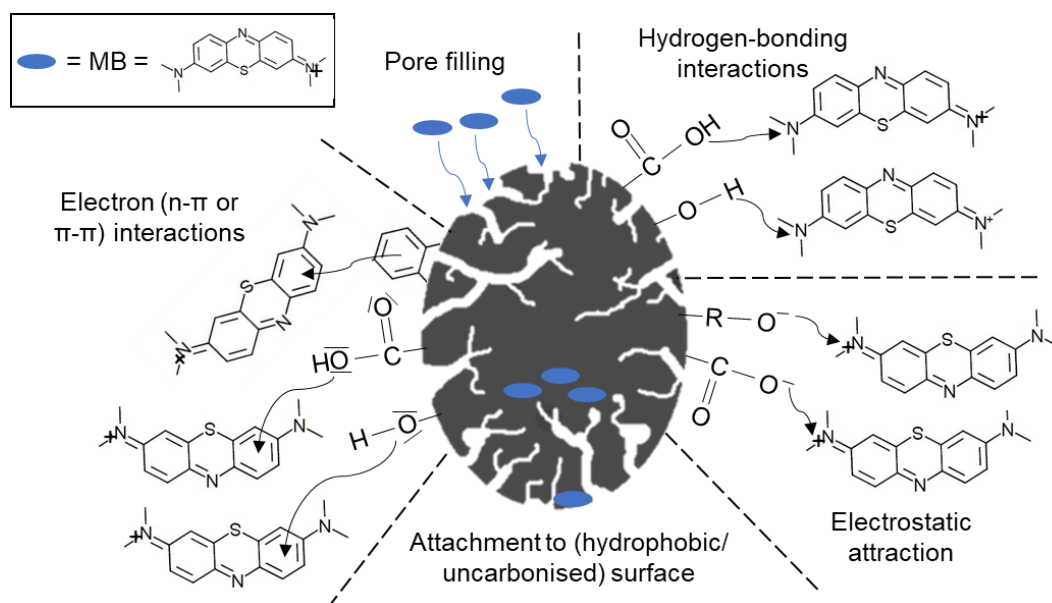


Figure 2.10: Scheme depicting interactions between a char adsorbent particle and MB molecule in solution (own artwork).

The adsorption mechanisms are influenced by adsorption parameters such as initial dye concentration, adsorbent load, temperature, and pH. Electrostatic interactions, for example, depend on the charge of the adsorbent particles, which is mainly governed by solution pH [282]. Ionic strength is another parameter that can influence adsorption, although some researchers found that it did not significantly influence dye adsorption [39][284]. In those studies, pH also did not significantly influence adsorption.

Ma *et al.* [264] compared chars activated with ZnCl_2 and KOH ($700\text{ }^\circ\text{C}$) in MB adsorption, and found that the ZnCl_2 one had greater adsorption capacity, 266 mg/g compared to 147 mg/g . This was attributed to the differences in porosity, with the char from ZnCl_2 having higher surface area, although microporosity was also greater, which does not contribute significantly to MB adsorption (mesoporosity does). Surface functionalities analysed by FTIR were similar between chars, with significant differences only in C=C bond manifestation, due to the more developed aromatic structure from ZnCl_2 char.

Char can have similar properties to activated carbon, depending on its production method, and can achieve comparable adsorption performance. Nevertheless, char is usually a more heterogeneous material and its behaviour in adsorption is more complex [281]. So far, the development of char-based wastewater treatments has been mostly limited to laboratory experiments, compared to activated carbon as a mature technology, although there have been some examples of pilot/industrial implementation, e.g., in sand filters and biofilters [281]. The usual limitations of using char/biochar for water purification are: a) low removal performance; b) slow removal rate (12-24 h); and c) poor recyclability [285].

One example called N-E-W Tech™ from the University of Idaho tested a char-based adsorbent in real wastewater treatment systems in the US, England, and South Korea [286]. The system efficiently removes phosphorous and other mineral contaminants, and when saturated the material can be used as fertiliser, making it more cost-effective.

Other trials are being performed in the US with char as a filter medium (blended with other natural materials) to remove contaminants from stormwater, by Sunmark Environmental [45] and Stormwater Biochar [46]. The company Glanris commercialises a char-based filtration media for removal of metals, suspended solids, organic compounds and other pollutants from water, produced from rice hulls and without harsh chemical treatments [47][48].

In the use of chars as adsorbents, research efforts are ongoing to reduce production costs and to allow easy separation and regeneration after use [287]. One option for simpler separation is having a magnetic element within the adsorbent, e.g., by impregnating it with an iron salt [287][288]. Although experimental separation and regeneration of spent adsorbent was not performed in this work, it is important to be aware of its importance for the economic viability of large-scale usage of a carbonaceous adsorbent.

Adsorption leads to the accumulation of contaminants on the adsorbent, and therefore the adsorbent loses adsorption capacity with time and needs replacement [41]. When spent, the adsorbent can be incinerated, disposed of in landfill, or regenerated [289]. For the two former options, new material can be produced and used to replace the exhausted one, but economically this is usually a disadvantage. Incineration can however be the most cost-effective method when using low-cost adsorbents from abundant local feedstocks [196][290].

Regeneration of activated carbon has been increasingly interesting for companies due to the potential of resource savings, reduction of disposal costs and lower CO₂ footprint [265][291]. Due to the research on using chars and biomass for adsorption being more recent than using activated carbon, research regarding their regeneration is scarcer, but increasingly popular. Although adsorption capacity drops with each regeneration cycle, sufficient capacity is usually maintained [292]. The decrease in adsorption capacity can be due to less available adsorption sites by blockage, and to repulsion by irreversibly sorbed contaminants [292].

Regeneration options are most commonly thermal treatment (inert or oxygen-limited atmosphere, to remove the contaminants and keep most of the adsorbent in its original configuration) [293], or chemical treatment (with a solvent with affinity for the adsorbate) [294]. Other options being researched are using HTC, ultrasonic processes, microwaves, microbiological, electrochemical treatments, and combinations of these [289][292][295][296].

Chapter 3 – Methodologies and materials

3.1. Feedstock

For the slow pyrolysis experiments performed in this work, wheat straw was used as feedstock. This feedstock was supplied by Agrodieren, an agricultural company near Ghent in Belgium, through the University of Ghent, one of the host institutions of the GreenCarbon project. The wheat straw was chosen as one of the common feedstocks for the Work Package 4 (WP4) of the project, to be used across several institutions and universities. For feedstock selection, the project partners included in WP4 compared several feedstock hypothesis, taking into account the sustainability of its production and collection, and also potential uses for products arising from its treatment [297]. For wheat straw, it is often kept on the fields from where it is collected, and its removal may lead to depletion of soil organic carbon and nutrients and an increased risk of erosion. It was, nevertheless, considered that these risks can be mitigated, by limiting the amount of straw that is removed from the fields and also returning straw-derived biochar to the soils.

The supplied wheat straw was in the form of broken-up pellets, ranging from small pieces under 0.5 cm, to larger pieces shaped like a cylinder, with 0.8 cm diameter and up to 1.6 cm length. A sample is displayed in Figure 3.1. The supplier indicated that no binder was used for production of the wheat straw pellets, which was also a criterion for their selection for the project.



Figure 3.1: A sample of the as-received wheat straw feedstock.

3.2. Experimental set-up

3.2.1. Continuous screw reactor system

The slow pyrolysis experiments were performed at an EBRI laboratory with a bench-scale screw/auger reactor system, with a maximum capacity of ≈ 300 g/h. The system consists basically of the reactor and furnace, a motor to rotate the screw, a feeding tube, and the product collection system. A representation of the screw reactor system is shown in Figure 3.2. Screw reactor is the nomenclature used for the reactor in this thesis, although “auger” is also used by other researchers.

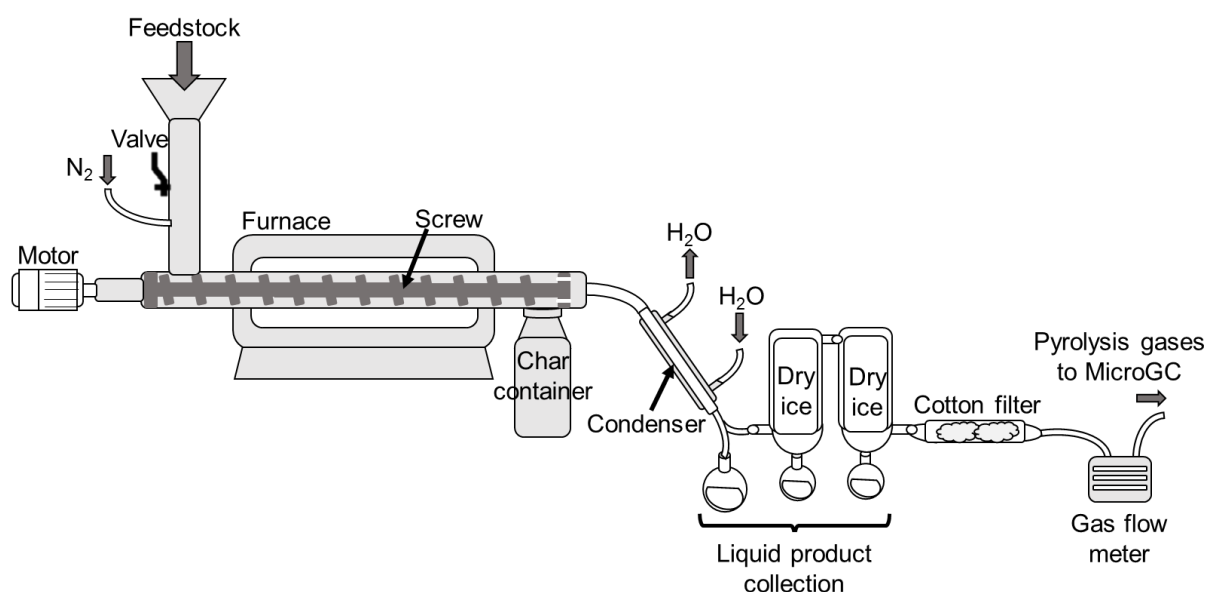


Figure 3.2: Representation of the bench-scale screw reactor system used for the slow pyrolysis experiments.

A horizontal electrical furnace (Carbolite VST 12/400, 2 kV of power capacity) encases the reactor tube to provide external heat. The heated length of the reactor tube is ≈ 40.0 cm. On the ends of the heated length of the tube, a thermal insulation material (fiber mat, BCTEX fleece) is placed, to minimise heat loss to the surroundings. Other parts of the system are also insulated, such as the right-hand side of the reactor tube and the collection vessel for the char. This is to prevent a temperature drop and possible condensation of vapours inside the metal parts of the system.

Gases that are passing through the reactor tube exit from the right-hand side, through a metal outlet that is narrower (diameter ≈ 1 cm) than the reactor tube. After the reactor outlet, the gases move into a cooling system made up of different parts of glassware. The cooling system consists firstly of a water-cooled jacketed condenser, which is able to condense most of the condensable vapours from pyrolysis. The cooling water is usually at 5 to 10 °C

(controlled by a Huber cooling bath circulator), and the condensed product liquids are collected in a 100 mL round flask at one end of a 3-way connection after the condenser. The remaining gases are directed from the 3-way into two cold traps, in series, in which dry-ice is kept. These cold traps can reach temperatures as low as $-78.5\text{ }^{\circ}\text{C}$ (dry ice sublimation temperature) [298], to ensure condensable vapours are condensed before leaving the system. Each of the cold traps has its own 25 mL round flask to collect liquids that have condensed in them.

The non-condensable gases after the cold traps pass through a horizontal cotton filter, with the aim to retain remaining particles and aerosols. After the cotton filter, the gases are transported through a gas meter (steel case diaphragm-type) that measures the volume of the gas passing through it. From the outlet of the gas meter, a fraction is sent to online analysis (MicroGC), while the majority of the non-condensable gases are directed to a vent for safe extraction. More details on the gas analyser are in subsection 3.3.3.

Three extractors are available to use if there are leaks or another circumstance occurs that requires safe extraction of gases. One of the extractors is the one at the outlet of the gas meter, while the other two are usually positioned above the inlet tube of the reactor and above the reactor outlet.

As for the reactor, two screw reactors were used for the slow pyrolysis experiments, with common basic design features represented by Figure 3.2 above. Extraction, liquid product cooling and collection system, furnace and inlet for carrier/injected gas are common to both reactors. Specific features that are different between the two reactors are explained in each corresponding subsection.

3.2.1.1. First screw reactor

The reactor is a horizontal pipe which contains a screw that can rotate with the help of an electrical motor. The motor has controllable rotational speed (0-600 rpm), which in turn controls the rotation of the screw and thus the movement of solid material inside the reactor.

The reactor pipe and screw were made by an external contractor, using stainless steel. The pipe has an internal diameter of 1" (2.54 cm), while the diameter of the screw is ≈ 2.20 cm. The clearance (space between the screw and the reactor tube wall) is therefore 0.17 cm. Due to the relatively small clearance, it is possible that during pyrolysis the reactor wall develops a thin layer of carbonised material, which serves as a lubricant for the screw movement. The screw has a shaft only on the left-hand side (the start/inlet side), with the remainder of the screw being hollow, with a coil/spring-like design. The screw is therefore free on the right-hand side, and can even "sit" on the bottom of the reactor tube, which poses issues in terms of physical rigidity and stability. A section of the left-hand side of the screw is represented in Figure 3.3. As indicated in Figure 3.3, the pitch length of the screw is 2.0 cm, while flight thickness is 0.5 cm.

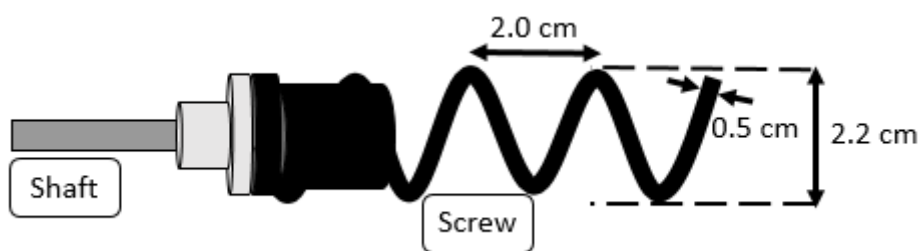


Figure 3.3: A representation of a section of the left-hand side of the screw.

The length of the screw is 85.0 cm (including the shaft), while the reactor pipe has a total length of 83.5 cm, including the inlet and outlet junctions. The reactor pipe itself, without the junctions, has ≈ 61.0 cm length. The start of the screw is positioned at the start of the inlet junction of the reactor tube, and it ends at the middle of the outlet junction, which is a T-junction, for the separated exit of solids and gases from the reactor.

For pyrolysis, temperature is a critical parameter and thus requires proper monitoring and control. There are four K-type thermocouples placed along the system, connected to a data logger for temperature recording. The positioning of the thermocouples is as indicated in Figure 3.4.

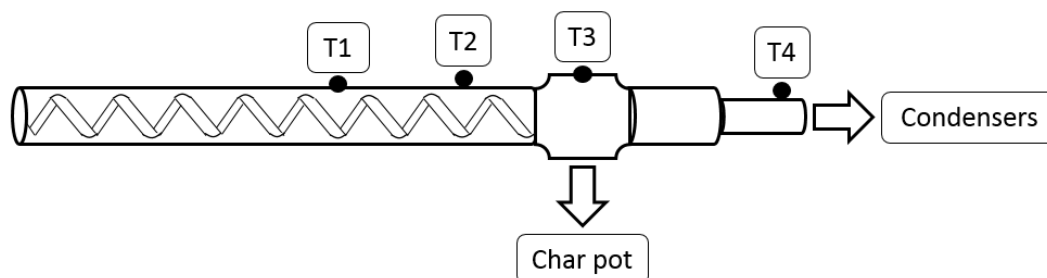


Figure 3.4: Diagram of the positioning of the thermocouples in the screw reactor.

The first thermocouple (T1) has its ending inside the reactor (not touching the screw), giving a measure of the temperature inside the middle section of the reactor. This temperature is comparable to the process temperature to which the material inside is subjected to. The second thermocouple (T2) measures temperature on the outer wall of the reactor, which is comparable to the furnace temperature. The third thermocouple (T3) has its ending inside the right-hand side T-shaped junction of the reactor tube, where the solid materials separate from the gases to leave the reactor. This thermocouple gives an approximate temperature of the materials exiting the reactor tube. The fourth thermocouple (T4) is placed around the last metal section, giving an approximate temperature of the reactor outlet.

A vertical stainless steel pipe attached to the left-hand side junction of the reactor tube allows to feed the biomass into the reactor tube. The vertical pipe has 1" (2.54 cm) internal diameter, a small hopper on top, and a ball valve in the middle to close the system. It also has a gas inlet for gas injection into the reactor system. Gas flow can be controlled with a rotameter.

The material that is fed into the reactor is transported by the movement of the screw along the horizontal tube. Upon reaching the right-hand side exit of the tube, it falls by gravity into a collection vessel (char pot) through a 1" inlet with a thread connection. The collection vessel is made of stainless steel, with ≈ 33 cm height and ≈ 9 cm outer diameter.

The outlet of the reactor tube and the char pot are heated using a heating tape (Omega Engineering Ltd., Samox heavy insulated tape, model STH101-040) and a ceramic band heater, respectively. The thermocouple used for the control of the heating tape is the fourth thermocouple (T4) in the system described above. It is connected to a control box to which the heat tape is also connected. The ceramic band heater is controlled by a fifth thermocouple connected to the same control box. These two temperatures can be controlled independently but are usually kept at the same temperature. By having these sections of the system heated (300 to 400 °C), cold spots are minimised, and thus also possible condensation of the vapours produced during slow pyrolysis. Condensation in these sections can lead to blockages and even to an early stop in operation and damage to equipment.

3.2.1.2. Second screw reactor

In order to improve the control, monitoring, performance and robustness of the screw reactor, the drawbacks and weaknesses of the equipment were analysed and a new system was designed. The new system was meant to keep most of the physical features of the existing one, without drastic changes to dimensions, but with improved characteristics. Dr Yang Yang (Aston University lecturer) was the main responsible for the design of the new screw reactor, in partnership with me and my supervisors, and an external contractor which was responsible for the manufacture of the new system. A picture of the second screw reactor system is shown in Figure 3.5.

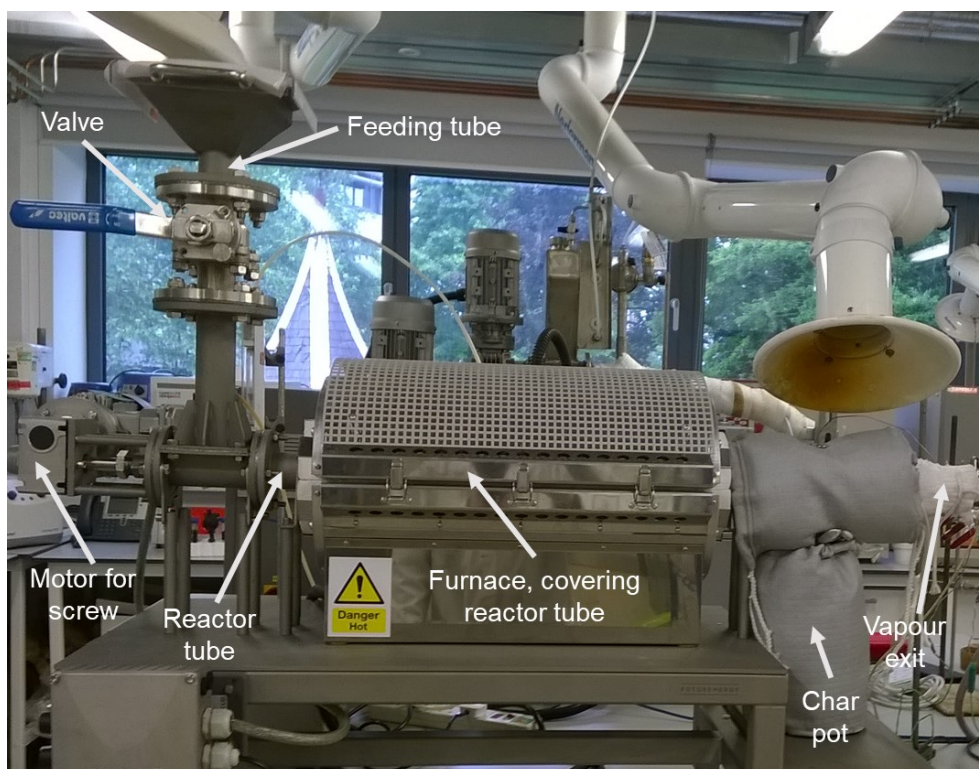


Figure 3.5: A picture of the second bench-scale screw reactor system.

The first step was to change the capacity of the system, allowing to process more feedstock and increase production. This was achieved mainly by slightly increasing the dimensions of the reactor diameter and of the char collection vessel. The opening of the char pot had been identified as a problematic point in the system due to the relatively small width, which at times leads to accumulation of product and potential blockages. The internal diameter of the reactor tube and feeding tube were increased from 1" (2.54 cm) to 1.5" (3.81 cm), with the same occurring with the char pot opening. The char pot connection was modified into a tri-clip coupling, which improved tightness and ease of assembly and disassembly. The heated length of the tube was kept the same because it is determined by the length of the furnace, which was maintained. The furnace also limited the increase in the reactor tube diameter. The outer diameter of the char vessel increased from 9 to 10 cm.

Another important change was to have a solid shaft across the entire screw, and support it on both ends, to improve its stability and robustness and to reduce damage made on the equipment in each operation. It was considered that this change could also enhance heat transfer, due to a higher solid surface area to conduct heat. The existence of a shaft along the screw could however decrease the capacity of the system, by diminishing the free space inside the reactor tube. This capacity decrease was countered by having a relatively low shaft diameter (1.6 cm). The clearance was decreased from 0.17 cm to 0.10 cm.

Process temperature is a crucial parameter for pyrolysis, and thus it must be monitored efficiently in the reactor. Due to the reactor design as a relatively long horizontal tube, and also because it is not completely covered by the furnace, the temperature is not the same along the whole reactor tube, e.g., there is a temperature profile inside. For this reason, it was decided that the reactor should have three temperature measurements inside and along the length, instead of just one as in the previous system. One of the thermocouples was positioned in the middle of the heated zone of the reactor, and the other two were positioned equally distant from the middle one (≈ 15 cm), and near the edges of the heated zone of the reactor tube. Measuring the temperature profile along the reactor provides better monitoring of the heating efficiency and of the pyrolysis process itself.

Due to the increase in the diameter of the char pot, the ceramic band heater had to be replaced by a heating tape, controlled by the same thermocouple as the heating tape for the reactor tube outlet. The insulation of the reactor system was also improved by having insulation jackets for both the char collection vessel and the reactor outlet section. The motor for turning the screw was also changed, for a more robust one, with reversible drive and reduction gearbox.

3.2.2. Slow pyrolysis procedures

This section indicates the procedures made before, during, and after the slow pyrolysis experiments, regardless of process conditions and of reactor. These procedures are thus common to all experiments, with any differences stated in the corresponding subsection, after this section. A risk assessment and a safe operating procedure have been developed for the reactor systems and the slow pyrolysis experiments.

The slow pyrolysis experiments indicated in subsections 3.2.2.1 and 3.2.2.2 were performed in the first screw reactor, whereas the subsequent experiments (subsections 3.2.2.3, and 3.2.2.4) were done with the second screw reactor.

For the wheat straw feedstock, and whenever a new feedstock is processed in the screw reactor, the solid residence time (SRT) needs to be determined, e.g., the time it takes for the material to be transported from the inlet to the outlet of the reactor. An appropriate feeding rate is also determined. These parameters are different for every reactor, and for the screw reactor they depend mainly on the dimensions and shape of the feedstock and on the speed of the screw, which is determined by the motor speed. Each motor level corresponds to different rotational speeds of the screw, and these in turn correspond to different solid residence times. As the motor level and rotational speed increase, the SRT decreases. The tests for the determination of these parameters are performed without operating the heating elements (e.g., under room temperature conditions), since it is not possible to visualise the movement of solids inside the reactor while it is operating at high temperatures. There is some

degree of difference between room temperature conditions and operating (i.e., hot) conditions, due to different physical properties of the solid material and to the evolving volatile matter inside the reactor. The hot conditions are expected to decrease the SRT when compared to cold conditions, however, not to a significant degree, because the dimensions of the reactor and screw do not change significantly when hot, and most of the solid material also keeps its shape and size. Changes in feedstock moisture content will also affect SRT, likely increasing the average SRT value due to greater adhesion of particles to the screw and reactor walls. However, in this work, the increase in moisture content leads to the disintegration of the feedstock in broken pellet form, decreasing particle size which likely counteracts the increase in SRT (tested in cold conditions, see Appendix B). The presence of injected gas flow can also change the solid material distribution inside the reactor, and thus changing SRT. However, this effect can be considered negligible if the gas flow is kept to relatively low levels, and because it will mainly affect smaller sized particles, which do not exist in large proportion in the wheat straw feedstock. Nevertheless, the determined SRT values are taken as an approximation, not as entirely accurate and realistic values. The results of feeding rate and solid residence time determination are presented in Appendix B.

Before assembling the system for an experiment, the char collection vessel and all the empty glassware in the cooling system are weighed. The thermocouples are inserted in place and the glassware and char pot are assembled, along with the heating elements for the reactor outlet and char pot. The ends of the reactor tube and the char collection vessel are insulated. Once everything is in place and the system is closed, the system can be tested for leaks using nitrogen flow. The flow of injected gas selected with the inlet rotameter can be checked against the volume measured by the gas meter at the other end of the system, to ensure they are matching. The gas flow coming through the meter is calculated by timing the measured volume. If the flows do not match, the connections in the system are checked for leaks using a soap solution spray to identify where the leak comes from. Once that connection is corrected and/or tightened, the flows are checked again until they match up and there are no leaks in the system.

Before a slow pyrolysis experiment starts, the system is purged with an inert gas, nitrogen (≈ 2 L/min), to drive off oxygen that is present inside, maintaining a desired inert atmosphere. The reactor furnace is gradually heated up to the target operating temperature, observing the temperatures registered by the thermocouples and giving time for temperatures to stabilise. The heating elements for the reactor outlet and char pot are also heated up gradually, to a temperature of 300 to 400 °C, depending on process temperature. During the heating up, the motor for the screw is turned on and set to the desired motor level, corresponding to the target screw rotational speed and thus solid residence time. The cooling

water is turned on and set to 5-10 °C, and dry-ice is placed in the cold traps. The system is once again checked for leaks.

If a static atmosphere (comprised of the pyrolysis vapours only) is to be used in the reactor, the nitrogen flow is turned off before the biomass feeding starts. This was the case for most of the slow pyrolysis experiments, except the ones in subsection 3.2.2.4, corresponding to the experimental set employing CO₂ as reaction atmosphere, with N₂ also tested as reaction atmosphere.

An inert carrier gas is commonly used in industrial-scale modern slow pyrolysis systems, in order to maintain an oxygen-free system, to push pyrolysis vapours away from the reactor, and also to promote heat transfer. However, the continuous use of a carrier gas can have a considerable economic cost, and it also dilutes the pyrolysis gas product, lowering its calorific value which is relevant if it will be used to obtain energy by combustion. Therefore, and since the configuration of the reactor system allows for the pyrolysis vapours to be pushed in the desired exit direction (due to the screw movement, to extraction at the end of the gas meter and to pumping from the MicroGC), the use of carrier gas during operation is dispensable. Experience with the reactor also showed that relatively high gas flow rates could cause a greater burden on the condensing system, due to the vapours reaching the condensation system at a higher temperature. In an extreme case, not all condensable products get condensed in the cooling/condensing system, and this can lead to damage on downstream lines/equipment (e.g., the gas meter) upon condensation there. High gas flow rate can also cause transport of solids with vapours, increasing the chances of a blockage, and decreasing the quality of the liquid product. Research has also shown (see Chapter 2, subsection 2.1.5.3.) that the absence of carrier gas allows a greater contact time between vapours and solids, due to higher vapour residence times (VRT), and that can promote more secondary reactions and lead to greater char yields. Another advantage of not using carrier gas is a simpler estimation of the produced gas volume during an experiment, by checking the value of the gas meter before and after the experiment (for the mass balance, explained ahead in this subsection). The absence of carrier gas can however represent a higher danger for laboratory users, due to flammability and potential toxicity of pyrolysis vapours. The risks were minimised through leak tests and adequate extraction.

As for the gas analysis system (MicroGC), it is left in conditioning mode (180 °C) usually the night before, and set to the desired analysis method when heating up the reactor. Once the analysis method is ready (temperatures and pressures at the set-point and stabilised), a sample list is created, and the automatic periodic sample injections are started.

Once reactor temperature is stabilised, feeding can commence, at a rate of ≈5 g/min, and the experiment is performed until a significant amount of solid and liquid products is obtained (usually 30-60 minutes), in order to perform product analyses.

The vapour production and gas coming through the gas meter are monitored to check if the pyrolysis reactions are taking place. If feedstock has been fed and vapours are not seen or gas is not coming through, it is likely that there is a blockage in the system, commonly in the inlet feeding tube. The inlet tube can be checked for blockages visually or using a stainless steel rod, which also helps pushing down blocked feedstock if necessary.

The VRT inside the screw reactor can be estimated visually, by checking at what time the first vapours appear in the reactor outlet after feeding started, or by checking when the gas meter first changes value. The first option has delay comparing with the gas meter option, since part of the gases passing through the system will not be visible. VRT values for different slow pyrolysis experiments are shown and discussed in Chapter 4.

The VRT can also be calculated using the volume of gas measured by the gas meter during operation time. With the volume and time, it is possible to estimate a flow rate, and by knowing the volume of free space inside the reactor it is possible to calculate the time it takes for the vapours to go through the reactor. To obtain the value of free space volume in the reactor, one needs to subtract the volume of the screw from the volume of the reactor tube. The volume of the reactor tube (a cylinder, without the screw) is given by its radius (1/2" or 1.27 cm) and length (61.0 cm heated length), and equals $\approx 309.1 \text{ cm}^3$ for the first screw reactor. The volume of the screw was possible to obtain due to having a small section ($\approx 4.0 \text{ cm}$) of the screw from a cutting that was made. By water displacement using that small section ($\approx 3 \text{ cm}^3$), the volume for the total screw inside the reactor tube was determined to be $\approx 45.8 \text{ cm}^3$. The free space volume in the reactor is obtained by difference: 263.3 cm^3 . These calculations were not performed for the second reactor due to the screw volume being unknown. Values of VRT calculated through this method for different slow pyrolysis experiments with the first screw reactor are shown and discussed in Chapter 4.

The peak process temperature and the solid residence time are kept constant throughout each slow pyrolysis experiment. If necessary, the temperature of the furnace is corrected so as to keep the process temperature (given by the thermocouple located inside the middle section of the reactor tube) as close as possible to the target value.

At the end of the operation time, the heaters are turned off and the system is left to cool down naturally. The water cooler is turned off and the screw is turned off after some time, once the system is at lower temperatures (usually from $\approx 200\text{-}300 \text{ }^\circ\text{C}$). Inert carrier gas flow (i.e., nitrogen) is turned on to remove leftover vapours and to keep the system inert and safe. The MicroGC is turned off once the pyrolysis vapours are not being detected.

When the system has cooled down, the glassware and char pot are removed and weighed. The liquid products are collected from the collection glassware into glass flasks, and the solid product is collected from the char pot. The glassware is cleaned with acetone and rinsed with hot water, and then dried in an oven at least overnight before re-use.

The char product is collected in a sealable plastic bag, while the liquid products in glass flasks are kept in glass flasks in a fridge at ≈ 4 °C. Usually the liquid product is only collected from the first collection flask, because the other two flasks do not have sufficient product for collection. However, in some experiments it was possible to collect liquid product from the second and third flasks (stored separately), and even from the condenser (stored together with the liquid from the first flask). A portion of the product liquid (usually part of the organic phase) can get stuck in the condenser and 3-way connection, due to its relatively high viscosity. If necessary, this product can be collected by providing heat to the glassware, with hot water or a hot air gun.

For every slow pyrolysis experiment, a mass balance was calculated for both wet feedstock basis and dry feedstock basis. For the mass balance, the weights of the products are required: the solid product is simply weighed after collection from the char pot; the liquid product total weight is the sum of the liquids in the collection flasks and also in the other glassware (obtained by difference to the empty glassware); and the gaseous product weight is calculated.

For the calculation of the gas product yield, the analysis of the MicroGC results was required, to determine the distribution of the different gas species in the total produced gas (details in subsection 3.3.3). With those proportions and knowing the density of the individual gases (from normal temperature and pressure conditions of 20 °C and 1 atm, in Appendix A), the density of the total product gas was calculated. With the volume of gas measured by the gas meter, the mass of gas produced can be obtained using Equation 3.1.

$$m = \rho \times V \quad (\text{Equation 3.1})$$

The yield of each product was then calculated dividing the obtained weight by the weight of the pyrolysed feedstock, either in a wet basis or in a dry basis (discounting the moisture content from the total feedstock weight used for the experiment). For the liquid product however, since the feedstock moisture ends up in the liquid product, the weight of feedstock moisture was subtracted from the total liquid product weight for the dry feedstock basis mass balance.

Each slow pyrolysis experiment was performed in duplicate to obtain standard deviation and to check repeatability, unless stated otherwise. The mass balances of the performed slow pyrolysis experiments are presented (in Chapters 4, 5, and 6) on a dry feedstock basis, unless stated otherwise.

3.2.2.1. Continuous slow pyrolysis with as-received wheat straw

Continuous slow pyrolysis was performed in the screw reactor using the wheat straw feedstock, to study the effect of temperature and solid residence time on the product yields and quality, with a focus on the char. These experiments were performed in the first screw reactor system described in section 3.2.1, and the wheat straw pellets were used as received.

The choice of the pyrolysis temperatures to study was based on the decomposition of lignocellulosic material, which is known to start ≈ 220 °C and have a maximum at ≈ 355 °C, corresponding mainly to cellulose decomposition [105]. After 400 °C, most of the hemicellulose and cellulose have been degraded, and lignin is still decomposing. Using temperatures lower than ≈ 350 °C, the solid product is considered to be torrefied instead of carbonised. As temperature increases and lignocellulosic decomposition occurs, the solid product proportion decreases, and the proportion of gas and liquid products increases. Although the yield of char is decreasing, its quality changes, mainly through increasing carbon and fixed carbon contents, rising porosity, and decreasing functional groups on the surface (see Chapter 2, subsections 2.1.5.1. and 2.3.1.). Depending on the application, it is thus necessary to have a compromise between the amount of solid product obtained and its quality, according to which temperatures are chosen for its production. Hence, the temperatures chosen for slow pyrolysis were 400, 500, and 600 °C, so as to study the changing properties of the material during carbonisation.

The solid residence time depends on the motor used in the system, which has limitations on the rotational speed it can operate at. After initial tests with cold feedstock, it was established that the fastest that the motor could be operating at, and ensuring safe operation, was corresponding to 3 minutes SRT (results in Appendix B). This level was thus chosen as the lowest SRT. After the initial slow pyrolysis experiments, it was seen that this SRT was sufficient to ensure carbonisation of the feedstock (checked visually from the colour of the solid product), so this value was kept. For slow rotation speeds, the motor could keep the biomass inside the reaction area for not much longer than 10 minutes, so this value was chosen as the maximum SRT. In order to have a third value to better establish the trends of product yield and quality with SRT, 6 minutes was also used. A value closer to the lowest SRT was seen as more useful than one closer to the highest SRT, in order to better check for possible fluctuations in the char quality.

Each slow pyrolysis experiment with varying process temperature and solid residence time was performed in duplicate, with the average value presented. The exception for this were the experiments using 500 and 600 °C pyrolysis temperature and SRT of 3 minutes, because the motor for the screw had to be changed, and the new motor did not allow a SRT lower than 5 minutes.

3.2.2.2. Continuous slow pyrolysis with varying feedstock moisture content

For testing the effect of feedstock moisture content, two pyrolysis temperatures were selected, 400 and 600 °C, and the solid residence time was fixed at 10 minutes.

The use of elevated feedstock moisture content had the purpose of verifying if this could have a similar effect to physical activation with steam, while occurring at the same time as slow pyrolysis, in 1-step. If char properties such as porosity can be improved by an integrated 1-step process instead of the traditional 2-step physical activation (see Chapter 2, subsection 2.3.3.), this would benefit the process economics. Additionally, other changes in char properties, such as creation and/or modification of functional surface groups, are of interest to this work, due to their influence in adsorptive capacity, and it is likely that the evolved steam during slow pyrolysis will influence these properties.

For physical activation, the process temperatures are usually >600 °C [240], however, it was chosen to reduce the process temperature in order to benefit the sustainability and economics of the process due to lower energy consumption. Furthermore, using 400 and 600 °C it was possible to compare with the results from experiments with as-received feedstock.

The solid residence time was chosen to allow for comparisons with the other slow pyrolysis experiments and to ensure carbonisation. Traditionally, the solid product is exposed to the activation conditions for longer time (e.g., >1 hour), to maximise contact time between the produced vapours and the solid product. However, with the screw reactor system it was not possible to obtain sufficiently slow motor speed and thus greater SRT. The maximum achievable SRT was \approx 15 minutes (see Appendix B), so 10 minutes was selected to be able to do direct comparisons with other experiments in this work. Furthermore, if a suitable solid product is produced using lower SRT, this signifies a less time and resource-consuming process, which is advantageous.

The moisture content of the as-received wheat straw was \approx 8 wt.% (wet basis), determined by oven-drying overnight at 105 °C. It was desired that this value was increased to study the impact of higher feedstock moisture content on the slow pyrolysis process. To increase the moisture content, the feedstock was simply soaked in distilled water and left to absorb the water. Different ratios of water to feedstock were used so as to yield different moisture contents. A 50 wt.% moisture content was achieved by soaking with a weight ratio of 1:1, and a 75 wt.% moisture content was achieved through soaking with a weight ratio of 3:1 (water to feedstock). The resulting moisture content was evaluated through oven-drying at 105 °C overnight.

For soaking, a portion of wheat straw feedstock (usually \approx 100 g) was placed on a large pyrex container and water was added with the appropriate ratio. Weight was constantly

measured, and since it did not decrease significantly (<0.1 g), it was considered that the water was absorbed by the feedstock, which was confirmed visually. Mixing with a spoon was done to ensure a more even absorption of water through all the feedstock particles. In the case of the 3:1 ratio mixture, excess water had to be removed from the container, since it was too much for the feedstock to absorb.

Water absorption, at first, led to swelling of the broken pellets, and then to disintegration, e.g., the feedstock particles crumble. After this, the pieces of feedstock had smaller sizes: more than 90% (by weight) had a particle size below 0.1 cm, tested by sieving. However, a portion of the particles still had larger sizes, up to a maximum of 1.2 cm in length, with a needle-like shape. Figure 3.6 presents the wheat straw feedstock after soaking with water.



Figure 3.6: The wheat straw feedstock after soaking with water.

The feedstock with increased moisture content was ready to be fed to the reactor once there was no visible loose water in the container. Before and after a slow pyrolysis experiment with elevated moisture feedstock, a sample was analysed for moisture content (105 °C oven) to confirm the value of this property. The experiments using feedstock with elevated moisture content were performed in the first screw reactor.

To study the impact of particle size/shape separately from the feedstock moisture content, slow pyrolysis experiments were performed on the wheat straw feedstock with a similar particle size, however, without the elevated moisture content. This was achieved by soaking the feedstock in water (1:1 ratio), and, after water absorption, oven-drying the wheat straw, at 105 °C and for at least 24 hours. This allowed to obtain feedstock with reduced moisture content (≈ 0.1 wt.%, wet basis), with the same particle size/shape as the feedstock

with elevated moisture content. Slow pyrolysis experiments with the soaked and dried feedstock were performed under the same conditions as the experiments with elevated moisture feedstock: 400 and 600 °C, and 10 minutes SRT. The moisture content of the soaked and dried wheat straw feedstock was also checked before and after each experiment (by 105 °C oven-drying overnight), to verify its reduction. These slow experiments had to be performed in the second screw reactor due to the decommissioning of the first one.

An additional slow pyrolysis experiment was performed (in the first screw reactor) using a temperature of 600 °C and with oven-dry (105 °C) wheat straw feedstock in its original broken pellet form. This experiment was performed to compare with the experiments with as-received feedstock, to help distinguish between the effects of feedstock moisture and of particle size on product yields.

3.2.2.3. Continuous slow pyrolysis with CO₂ as reaction atmosphere

To potentially increase the surface area and porosity of the solid products, as well as producing other changes in char properties such as surface functionality, slow pyrolysis was performed using CO₂ as reaction atmosphere (by injecting it into the reactor).

The injection of CO₂ into the slow pyrolysis process was intended to be similar to slow pyrolysis integrated with physical activation in 1-step in the screw reactor. Physical activation using CO₂ is widely used industrially to develop high surface area activated carbons, in a 2-step process: pyrolysis is first performed, and then the chars are separately activated in a second process (see Chapter 2, subsection 2.3.3.). The possibility of performing both pyrolysis and activation in 1-step would decrease production time and potentially benefit the process economically. The activation step with CO₂ is most frequently done at relatively high temperatures of >700 °C. It was also an objective to reduce this temperature and to verify if activation or benefits for adsorption applications can still occur at lower temperatures. Although surface area may not be increased due to relatively low temperatures, chemical functionalities on the surface are likely to be affected by the CO₂ atmosphere even at lower temperatures.

The selected processing temperatures were 400 and 600 °C, and the solid residence time was 10 minutes, which allows for comparisons with the other slow pyrolysis experiments. The choice of SRT is due to the limitations of the motor speed discussed in the previous subsection. The experiments were performed in the second screw reactor system described in subsection 3.2.1.2. Slow pyrolysis experiments using nitrogen as carrier gas were also performed for comparison purposes.

It was possible to feed either nitrogen or carbon dioxide, or even a mixture of both, because the flow of the two gases passed through a common t-joint. The nitrogen was coming

from the laboratory's gas line, and the CO₂ was from a small cylinder (from BOC, with vapour withdrawal, 200 bar (when full) and >99.9 vol.% purity) installed in the laboratory for these experiments.

For experiments using CO₂, the gas was only inserted into the system when the process of slow pyrolysis started, after feeding the first portion of feedstock. As with the other slow pyrolysis experiments, the atmosphere inside the system had been made inert with nitrogen flow. While feeding, due to having to manually open the inlet valve, the CO₂ flow was cut-off, for safety reasons, since the inlet for the gas was in the feeding tube. The flow was re-established when the valve was closed after feeding, and the amount of time the CO₂ flow was off was relatively short (<10 seconds). The same was applied to experiments with N₂ carrier gas. However, this procedure made the determination of VRT more difficult, both for the visual and the calculated methods. VRT calculation had greater error because of the changes in gas meter values from stopping the flow for some time, and the visual method was affected because at the start of the experiment the injected gas flow was started some time after feeding, in a similar way for both temperatures and injected gases tested, which made the timing of vapours appearing at the reactor outlet similar between experiments.

The volumetric flow of injected gas through the experimental rig during the pyrolysis experiment was chosen as 1 L/min. A higher flow would be expected to have a greater impact on the process, but it could lead to solid particles being elutriated and transported to the vapour outlet, potentially leading to a blockage and forcing the operation to stop. A higher flow would also keep the produced vapours at a high temperature in the cooling system, which can be an issue. Even with 1 L/min flow, it was seen that the vapours would still be considerably hot after the water cooler, allowing for a part of the liquid product to condense in the gas filter, which did not happen when gas was not injected during the pyrolysis process. High injected gas flow can also lead to liquid product contamination with solid particles, which is undesirable for liquid product quality. When the operation needed to be stopped at the end of the experiment, the injected gas flow was left on for some minutes to ensure contact with the last solid products being formed and to make sure all the pyrolysis vapours were removed from the reactor. After some time, for the experiments with CO₂, the flow was changed to nitrogen, removing the CO₂ from the system for opening safely.

3.2.2.4. Continuous slow pyrolysis with KOH-impregnated feedstock

To attempt to increase the adsorption capabilities of the produced chars, experiments were designed to incorporate chemical activation with the slow pyrolysis process inside the screw reactor.

Chemical activation can be performed by impregnation of the feedstock with different chemical agents, such as H₂SO₄, H₃PO₄, ZnCl₂, KOH and NaOH. (see Chapter 2, subsection

2.3.3.). As discussed in Chapter 2, the chemical agents used industrially are strong acids or bases and therefore present risks to the environment and health. There is a need to make the chemical activation process more sustainable and safe, and using less harmful chemical agents is a way to contribute to this. For example, KOH and NaOH have been used as less harmful chemical agents to replace H_3PO_4 and ZnCl_2 in activation, and the use of the hydroxides has been found to produce higher porosity than using the acids, although higher temperatures were required to achieve maximum surface area [245][252]. Less harmful compounds have been used such as carbonates (K_2CO_3), however, in general it was found that surface areas are lower compared to using other activation agents [251][228].

Several studies have found that KOH develops more surface area than NaOH during activation, and a study by Lillo-Ródenas *et al.* [251] on chemical activation of coal concluded that the temperatures at which activation starts are lowered when using KOH (400 °C) instead of NaOH (570 °C). More details can be found in Chapter 2. Due to the potential to create greater porosity and at lower temperatures, KOH was selected as the chemical agent for the experiments.

Impregnation of the feedstock with the chemical agent can be performed in two ways: wet impregnation, by mixing the feedstock with a solution of the chemical agent, and dry impregnation, through mixing the feedstock with the chemical agent in a solid form. As discussed in Chapter 2, wet impregnation is considered to provide improved mixing [239], and achieve greater surface area and microporous volume [245], although with the disadvantage of requiring a drying step [239]. Since a relatively large amount of feedstock was processed in the screw reactor in this work, it was important to achieve a homogeneous distribution of the chemical agent across the feedstock, through appropriate mixing. The wet impregnation method was thus selected for mixing the chemical agent with the feedstock before slow pyrolysis.

To prepare the impregnated feedstock, the KOH solution was firstly prepared, by dissolving an appropriate amount of KOH in distilled water. The KOH was supplied in pellet form by Sigma-Aldrich and with a >85 wt.% purity (technical grade) [299]. The chosen KOH concentrations were 0.1 M and 1.0 M, to minimise potential damage to the reactor material by corrosion that can occur from contact with concentrated acids or bases [248]. Furthermore, if more KOH was necessary, operational costs would increase, and it was desired that the process was made more affordable. The mixing of the KOH solution with the feedstock was done in a 1:1 weight ratio, and the amount of feedstock used was usually 300 g. The ratio was chosen based on the soaking tests described in subsection 3.2.2.2: ratios higher than 1:1 would lead to not all the water being absorbed by the feedstock, which could lead to the KOH not being fully incorporated into the feedstock. For the 0.1 M solution, ≈ 1.980 g of KOH was

required, while for the 1.0 M solution, ≈ 19.802 g of KOH were used. Considering an average char yield of 30 wt.%, weight ratios between KOH and char were calculated to be 0.019 and 0.187, respectively, for the 0.1 and 1.0 M solutions.

The mixing of the solution with the feedstock was performed in the same way as the soaking with water in section 3.2.2.2: the feedstock was spread on a pyrex container and then the solution was added (1:1 weight ratio). The solution was absorbed by the wheat straw feedstock. After absorption, the feedstock was oven-dried at 105 °C for at least 1 day to remove moisture and was then ready to be fed to the reactor (after removing from oven and cooling to room temperature).

The experiments using KOH-impregnated wheat straw feedstock were performed in the second screw reactor system (described in subsection 3.2.1.2.), without carrier/injected gas. The selected slow pyrolysis temperatures for the experiments with KOH were 400 and 600 °C, and a 10 minutes SRT. These conditions were chosen so as to allow for comparisons with the other experiments and due to the reasons given in the previous subsection.

Furthermore, the temperature selection was based on two main reasons: 1) to allow for comparisons with the experiments performed without chemical agent, and 2) because previous studies found that activation using KOH could start at relatively low temperatures (400 °C) compared to other activation agents [251]. Additionally, a study found that metallic potassium vaporisation can occur at >760 °C [256], and the lower temperatures employed would prevent that from occurring.

In terms of the solid products from the KOH experiments, it was chosen not to perform the washing step, which is usually done on chemically activated carbons to remove inorganic material and neutralise pH, since the use of strong acids or bases can lead to the solid product having significantly low or high pH values (for acids or bases, respectively) that can be detrimental for subsequent applications and even for analysis equipment. The removal of inorganic material with the washing step also liberates pores which can have trapped inorganic compounds during the activation process. The choice of not doing the washing step had two reasons: 1) the KOH:char ratios obtained are significantly lower than the ones usually employed, which will lead to a lower impact on the pH of the solid product and thus its harmfulness, and 2) the washing step uses resources and creates a liquid waste stream, which is an economic disadvantage.

3.2.2.5. Comparison between the two screw reactors

Since the slow pyrolysis experiments in this work were performed using two screw reactors, a comparison was made between them. The conditions chosen for the comparison were 400 and 600 °C operating temperature and 10 minutes SRT, since these were the

conditions chosen for the other experimental sets. The experiments were performed without carrier/injected gas and using as-received wheat straw feedstock (broken pellets).

3.3. Analyses of feedstock and products

3.3.1. Feedstock and solid product analyses

The wheat straw feedstock, for the following analyses, was firstly milled in a cutting mill (Retsch SM) equipped with a sieve with 0.5 cm square mesh, and then further milled with a coffee grinder. As for the solid products from slow pyrolysis, they were ground with mortar and pestle, and sieved to particle sizes under 425 μm , as indicated in section 3.2.2.

3.3.1.1. Proximate analysis

Proximate analysis is the determination of the contents of moisture, volatile matter, fixed carbon and ash in a sample, and it was performed on the feedstock and on the solid products from the slow pyrolysis experiments. This analysis was performed with thermogravimetric analysis (TGA), in which a sample is exposed to a pre-determined temperature programme, under a selected atmosphere (inert or oxidizing). The weight of the sample is continuously measured and plotted (in absolute values or in percentage) against the elapsed time or the programmed temperature.

To determine moisture and volatile matter, the sample was exposed to an inert atmosphere (nitrogen, flow rate of 30 mL/min), and to the following temperature programme:

- 1) Holding at 50 °C for 5 minutes.
- 2) Heating to 105 °C at a heating rate of 5 °C/min, and hold for 5 minutes.
- 3) Heating to 900 °C at a heating rate of 10 °C/min, and hold for 15 minutes.
- 4) Cool down.

The procedure was based on ASTM method E1131 [300]. The moisture content (M) was determined from the weight difference of the sample at the end of step 2, and the released volatile matter (VM) from the sample weight difference at the end of step 3.

To obtain the ash content (A) in the samples, the sample was exposed to an oxidizing atmosphere (oxygen, flow rate of 20 mL/min) and to the temperature programme:

- 1) Holding at 50 °C for 5 minutes.
- 2) Heating to 105 °C at a heating rate of 10 °C/min, and hold for 5 minutes.
- 3) Heating to 750 °C at a heating rate of 5 °C/min, and hold for 5 minutes.
- 4) Cool down.

The procedure was based on ASTM method D1762 [301], with the ash being the sample at the end of the temperature programme. The oxygen atmosphere was mixed with nitrogen (10 mL/min), and a protective nitrogen flow (30 mL/min) was present in both

described procedures. The fixed carbon content (FC) was obtained by difference to 100% using the other determined parcels (Equation 3.2):

$$FC \text{ (wt. \%)} = 100 - M \text{ (wt. \%)} - VM \text{ (wt. \%)} - A \text{ (wt. \%)} \quad (\text{Equation 3.2})$$

The equipment used for TGA was a Perkin Elmer Pyris 1 TGA, with Pyris software. Sample weight used for the analyses was between 5 and 10 mg, and the crucibles were of ceramic. Averages were calculated from triplicates of each temperature programme for each sample. A blank measurement was performed in order to subtract the buoyancy effect.

The moisture and ash contents of the as-received feedstock and the solid products from slow pyrolysis were also determined by use of a furnace and based on ASTM methods D1762 [301] for moisture, and E1755 for biomass ash [302] and D1762 for char ash [301]. For moisture content, ≈ 5 g of a sample were heated up to 105 ± 3 °C in a furnace and left overnight. Moisture was determined by difference between initial and final weights. The moisture content determined with the 105 °C oven-drying method was the one used for the dry feedstock basis calculations on the slow pyrolysis product yields. Ash contents were determined from the final weight of an oven-dried sample (≈ 0.5 g) in a furnace at 575 ± 25 °C for >6 hours, to ensure constant weight. For the char products, the final temperature was instead 750 ± 5 °C [301]. Ceramic crucibles were used, and the furnace for moisture content evaluation was from LTE Scientific Ltd., Swallow oven model, while the one for ash content evaluation was a Carbolite model AAF1100.

3.3.1.2. Ultimate analysis

The determination of the main elemental constituents of the samples (carbon, hydrogen, nitrogen, sulphur, and oxygen, obtained by difference), was done for the feedstock and the solid products from the slow pyrolysis experiments. This analysis was carried out by combustion of the sample and analysis of the evolved gases by Gas Chromatography (GC), with a CHNS/O Flash 2000 Organic Elemental Analyser (Thermo Fisher Scientific). This equipment allows to obtain the concentration of organic carbon (C), hydrogen (H), nitrogen (N), and sulphur (S). The oxygen fraction was calculated by difference to 100 (if in percentage) from the sum of the other elements and ash. Approximately 2-5 mg of sample was added to a tin crucible, along with ≈ 5 mg of vanadium pentoxide (oxidant, to assist complete sample conversion). Sulphanilamide was used as the standard for the analyses. The analysis of each sample was performed in triplicate and average values were taken.

3.3.1.3. Inorganic contents

Chars from the three tested slow pyrolysis temperatures were analysed for K, Ca, Si and P contents, by an external laboratory, which used ICP. The selected chars were produced with 10 minutes SRT, to be comparable with the chars from KOH-impregnated feedstock, which were also analysed, however only for K content.

The four inorganic elements were selected based on XRF analyses on the same wheat straw feedstock made by other GreenCarbon project researchers at the University of Zaragoza [128]. Potassium oxide was the most prevalent inorganic compound (≈ 53 wt.% of feedstock ash), followed by oxides of Ca (≈ 17 wt.%), Si (≈ 17 wt.%) and P (≈ 5 wt.%). Other inorganic compounds found had less significant proportions (< 2 wt.%): oxides of Al, Mg, and Fe, and also inorganic forms of Cl and S.

3.3.1.4. Heating value

To calculate the higher heating value (HHV) of the feedstock and solid products from slow pyrolysis, the proximate and elemental analyses were used, using the Channiwala and Parikh correlation for solid, liquid and gaseous fuels [303] (Equation 3.3). The variables C, H, S, O, N and A correspond to the contents, in wt.% units, of carbon, hydrogen, sulphur, oxygen, nitrogen, and ash, respectively.

$$HHV (MJ/kg) = 0.3491 \times C + 1.1783 \times H + 0.1005 \times S - 0.1034 \times O - 0.0151 \times N - 0.0211 \times A \quad (\text{Equation 3.3})$$

Using HHV and the moisture content, it is possible to calculate the lower heating value (LHV), which considers that the water produced in combustion is not condensed. The calculation used is in Equation 3.4, where M is the moisture content in the material (in weight fraction), and H_{vap} is the latent heat of vaporization of water at 25 °C (2.440 MJ/kg) [304]. This means that for the LHV, part of the heat was used to vaporize the water, and is not counted as useful heat from the combustion of the material.

$$LHV (MJ/kg) = HHV - M \times H_{vap} \quad (\text{Equation 3.4})$$

The heating value was also determined experimentally, using an IKA C1 Compact bomb calorimeter. This equipment, however, suffered a technical issue and thus was only used for the feedstock and solid products that were produced in the first experiments. Cotton string was used as ignition source, with its heating value (50 J per cotton string) being subtracted from the obtained result to get the heating value of the sample.

3.3.1.5. pH (in H₂O)

For testing pH, a Sartorius PB-11 pH meter was used. Before usage, the pH meter was calibrated with pH standards (pH 4, 7, and 10). Measurements for each sample were performed at least in triplicate and at a temperature of 20 (\pm 1) °C. The solid products were tested for pH in a suspension, because it was only possible to test the pH in the water in contact with those materials. Different methods are used in literature for measuring char pH in water, with increasing usage of this analysis method due to the growing popularity of char soil applications.

A method recommended for biochars [305] uses char to water ratio of 1:10, however, it was experimentally found that this could lead to poor mixing due to the relatively small amount of water used, and to char hydrophobicity. The weight ratio of solid sample to water employed in this work was 1:100 (i.e., 0.5 g char in 50 g water), based on Lima *et al.* [306].

Furthermore, some methods use a relatively short mixing time of \leq 1 hour [305][307][308], and it was considered that this could lead to not reaching equilibrium. The method by Lima *et al.* [306] used 72 hours mixing time, however the mixing time used in this work was \approx 24 hours (stirring overnight with a magnetic stirrer plate at 500 rpm), which was considered to be enough to achieve equilibrium.

Finally, most methods measure pH without mixing or after some resting time, and this was considered to yield potentially erroneous pH measurements due to changes in equilibrium. Measurement of pH in this work was thus performed under stirring conditions to avoid settling of the char and changes in equilibrium.

3.3.1.6. FTIR

Fourier Transform Infra-Red (FTIR) was used to analyse the feedstock and the chars for chemical bonds and functionalities, qualitatively. The equipment was a Perkin Elmer Frontier FT-IR Spectrometer, with PIKE Technologies GladiATR (Attenuated Total Reflectance) and Spectrum software. The scanned wavelength was from 4000 to 400 cm⁻¹, with 4 cm⁻¹ resolution, using 16 scans and at least in triplicate.

3.3.1.7. N₂ physisorption (77 K)

Nitrogen physisorption (-196 °C or 77 K) was used to determine surface area, pore volume and size distributions on the solid products. The equipment was a Quantasorb Nova 4000e porosimeter with Quantachrome Novawin 11.0 software. Oven-dry samples were degassed in vacuum overnight to remove possible adsorbed gases and volatiles. However, different degassing temperatures were used to minimise volatile matter loss from the sample,

which can cause the sample bulb to become stained upon recondensation, and analysis interference. If the chars were produced at 400 °C, the degassing was at 200 °C, and if the samples were pyrolysed at 500 or 600 °C, degassing was at 300 °C. Using 300 °C for the 400 °C chars would sometimes cause volatiles to condense on the sample bulb and interfere with the analysis.

The adsorption branch of the isotherms was analysed with Quenched Solid Density Functional Theory (QS-DFT), a non-local pore-specific model, to obtain surface area and pore size distribution, as recommended for carbonaceous materials with micro and mesoporosity, including chars [309][310][311].

3.3.1.8. Scanning Electron Microscopy (SEM)

A selected number of char products were analysed by Scanning Electronic Microscopy (SEM), with a JEOL 7800 series equipment. This allowed to analyse the surface of the solids in terms of microscopic structure and morphology. However, due to limited equipment availability, it was not possible to evaluate all produced chars, and so the analysis was only performed on chars from varying temperature and feedstock moisture content.

3.3.2. Liquid product analyses

After each slow pyrolysis experiment, the liquid product was collected in glass flasks and stored refrigerated (4 °C). If possible (due to phase separation), it was collected and stored as two separate phases (aqueous and organic). Often, this phase separation did not occur easily and thus storage occurred as a single liquid product, with later separation of the phases that were present for their analyses.

Since the main work objective was related to the solid product, only a selected number of liquid products from the first set of slow pyrolysis experiments were analysed with the techniques described ahead. The selected products were produced with operating temperatures of 400, 500 and 600 °C, and 3 minutes SRT. The liquid product analyses are shown in Appendix D.

3.3.2.1. Composition by GC-MS

The chemical composition of selected liquid pyrolysis products was analysed by coupled Gas Chromatography, Mass Spectroscopy and Flame Ionisation Detector (GC-MS-FID). The equipment used was a Varian 450-GC and Varian 220-MS, and the software was Star Chromatography Workstation.

Both phases of the liquid products were analysed, and they were firstly filtered using a 0.2 µm HPLC filter and then mixed with acetone (GC-grade). The use of acetone was to lower

the viscosity of the sample and to function as a solvent. The aqueous phase was mixed with acetone in a weight ratio of 1:3 (sample to acetone), and the organic phase was in a weight ratio of 1:5 (sample to acetone), due to its higher viscosity.

For each analysis, 0.5 μL of sample was injected into the GC column, and the injection port was kept at 250 °C. Helium was used as the carrier gas, with a 1:20 split ratio (sample to helium). The GC oven was held at 45 °C for 2.5 min, then heated at 5 °C/min to 260 °C, and held at this temperature for 7.5 min. A Column Elite-1701 was used to separate the components (30 m, 0.25 mm internal diameter, 0.25 μm film thickness, 14% cyanopropylphenyl/ 86% dimethyl-polysiloxane stationary phase). The FID was kept at a temperature of 50 °C, and the mass spectra were obtained for a range of 45–300 (m/z).

Peak assignments were performed on the mass spectra using the NIST05 MS library and from assignments found in the literature. A threshold of 100,000 counts in the chromatogram peaks was used to select which peaks were identified or not (those with lower counts were not identified). This was due to the large number of peaks present, especially in the organic phases, which was considered normal since the pyrolysis liquid product is a complex mixture of compounds. The selection of the compound belonging to the peak was based on the percentage of each match and on the likelihood of that compound being present in the sample. For example, multi-ringed compounds or compounds with a high presence of chlorine or sulphur were regarded as not likely to be present in the liquid products, due to a low chance of multi-ring compounds being formed during pyrolysis and due to the low amount of chlorine and sulphur present in the feedstock (see Chapter 4 for feedstock analyses).

3.3.2.2. Water content

The aqueous phase of selected liquid products were tested for water content through Karl Fischer titration, with standard method ASTM E203 [312]. The equipment used was a Mettler Toledo V20 Volumetric Karl Fischer Titrator, with working medium Hydranal K, and titrant Hydranal Composite 5K. The tested samples were diluted with acetone to reduce the water content due to the high sensitivity of the equipment and to decrease the analysis time. The result obtained was corrected to the weight of the original samples accounting for the acetone. Water content analyses were performed at least in triplicate and average values were taken. Using the water content in the liquid product and knowing the feedstock moisture content it was possible to calculate the reaction water (produced during slow pyrolysis).

3.3.2.3. pH

For testing pH, a Sartorius PB-11 pH meter was used calibrated with pH standards before usage. For the liquid products from slow pyrolysis, the standards used had pH 2, 4, and 7, due to an expected acidic character of these liquids. Only the aqueous phases were

tested for pH, due to the high viscosity of the organic phase. Measurements for each sample were performed at least in triplicate and at a registered temperature of 19 to 21 °C.

3.3.2.4. Ultimate analysis

The organic phases from the selected slow pyrolysis experiments were analysed for elements C, H, N, S, and O (by difference), by an external laboratory.

3.3.2.5. Heating value

The heating value of the liquid products was determined experimentally using an IKA C1 Compact bomb calorimeter. Paraffin strips were used as ignition source, with its heating value (737 J per paraffin strip) being subtracted from the obtained result to get the heating value of the sample.

The higher heating value (HHV) of the organic phases from the liquid products was also calculated with the Channiwala and Parikh correlation for solid, liquid and gaseous fuels [303] (Equation 3.3). Ash contents were assumed as 0 wt.%.

3.3.3. Gaseous product analyses

During the slow pyrolysis experiments, it was possible to determine the gaseous species present in the gas product, with direct inline sampling from the outlet of the gas meter. The equipment used was a Varian CP-4900 Micro GC, with a thermal conductivity detector (TCD) and two columns: Varian CP-5Å Molsieve for H₂, O₂, and CO, and Varian CP-PortalPLOT for N₂, CO₂, and light hydrocarbons as in methane (CH₄), ethane (C₂H₆), ethylene (C₂H₄), propane (C₃H₈), propylene (C₃H₆), and n-butane (C₄H₁₀). Helium was used as carrier gas, and the injection of gas samples occurred every 150 seconds and lasted for 20 seconds.

The equipment was calibrated beforehand using gas mixtures with different concentrations of 3 and 7 vol.% each (balanced with N₂ or CO₂). Using the calibration data, it was possible to convert the experimental peak areas for each experiment into volumetric fractions and thus know how much of each gas species was produced during slow pyrolysis. Due to the proportion of unidentified or undetected gaseous species being quite variable between experiments, the obtained volumetric fractions were normalised to 1 (or 100%). With the proportions of gaseous species and using the individual densities of each gas, the average density of the total gas product was calculated, which was used to determine the gas product mass yield for each experiment (using Equation 3.1 in subsection 3.2.2.).

In the case of the experiments using CO₂ as reaction atmosphere, it was necessary to subtract the peak area corresponding to the injected gas from the CO₂ total peak area determined by the MicroGC during slow pyrolysis. The injected gas peak area was the CO₂

peak area registered just before or after the operation time (during gas product formation) for each slow pyrolysis experiment.

The heating value of the product gas was also determined, using the volumetric proportions of each gaseous species and the individual heating values (or heat of combustion) of the combustible components (see Equation 3.5 for HHV calculation). All the gaseous components in the pyrolysis gas are considered combustible, except for carbon dioxide. The values used for the individual heating values (in Appendix A) were in normal conditions (1 atm, 25 °C) [304].

$$HHV (MJ/Nm^3) = [CO] \times HHV_{CO} + [CH_4] \times HHV_{CH_4} + [H_2] \times HHV_{H_2} + \sum [C_nH_m] \times HHV_{C_nH_m}$$

(Equation 3.5)

3.4. Study of adsorption from aqueous solution

3.4.1. Model compound selection

To test the adsorption performance of the solid products from slow pyrolysis, it was necessary to select one compound (or more) to adsorb from aqueous solution.

Dyes are commonly used for testing the adsorption performance of adsorbent materials. Among the dyes used, methylene blue (MB) was identified as the most commonly employed to estimate adsorption capacity, being commonly used as a proxy for other organic contaminants in water [278]. MB can be used to estimate mesoporosity or large micropores (>1.5 nm) in certain materials [254][279].

Methylene blue is known as a basic (i.e., alkaline, or cationic) synthetic dye, and has the chemical formula $C_{16}H_{18}ClN_3S$, structured as represented in Figure 3.7. MB is a thiazine dye, known by other names such as basic blue 9, tetramethylthionine chloride, and CI 52015 (colour index) [278]. The methylene blue used for the adsorption tests was supplied by Sigma-Aldrich, with >82% purity [313].

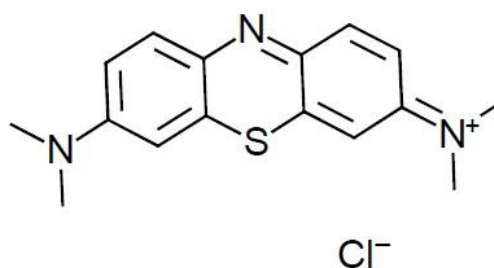


Figure 3.7: Chemical structure representation of methylene blue (drawn on ChemDoodle software).

In its solid form, MB is a dark green powder, and dissociates into the MB cation and chlorine anion in aqueous solution, with a dark blue colour [278]. Besides the textile industry, MB has also widespread use in medicine, e.g., for biological staining and as a treatment for the uncommon condition of methemoglobinemia [314]. The presence of MB in wastewater is toxic and can cause several health impacts such as nausea, vomiting, eye injury, and methemoglobinemia [315]. Relevant physico-chemical properties of MB are indicated in Table 3.1.

Table 3.1: Physicochemical properties of the dye methylene blue.

Property [units]	Value	References
Molecular weight (anhydrous) [g/mol]	319.85	[313]
Molecular volume [cm ³ /mol]	241.9	[316]
Molecular diameter [nm]	0.8	[316]
Solubility in water [g/L]	1.0	[313]
Wavelength for maximum absorption [nm]	660-670	[25][248][317][272]

MB has relatively high solubility in water, while some dyes have very low solubility in water, and are instead soluble in alcohols and other similar solvents [318]. Apart from its common use for assessing the adsorption performance of activated carbons and other carbon-based adsorbents, relatively high solubility was another reason to select MB as model compound for adsorption tests in this work. Furthermore, MB quantification in aqueous solution is relatively simple, by means of UV-Vis spectrophotometry, which is a simple and accessible method of analysis.

For testing hypothesis regarding adsorption mechanisms and explaining the results obtained with methylene blue, the adsorption of another compound of similar composition but different chemical groups was performed. A dye was also targeted in order to have a similar composition, but with an acidic character instead of a basic character which methylene blue has. Since sufficient solubility in water was necessary, the dye methyl orange was chosen, because other available acid dyes (e.g., methyl red, Sudan blue) had very low or negligible solubility in water [318–320]. Methyl orange is an acid azo dye with ≈ 5 mg/mL solubility in water (at 20 °C) [321], the chemical formula $C_{14}H_{14}N_3NaO_3S$, and is represented in Figure 3.8. The molecular weight of methyl orange is 327.34 g/mol [321], similar to methylene blue, and it is commonly used as a pH indicator in acid titration [322].

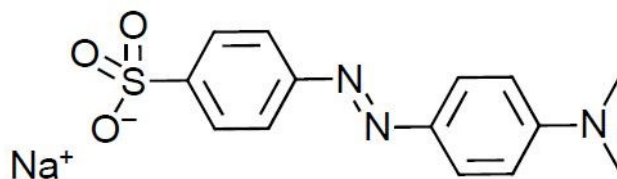


Figure 3.8: Chemical structure representation of methyl orange (drawn on ChemDoodle software).

UV-Vis spectrophotometry can also be used as detection method, and the wavelength at which maximum absorption occurs is ≈ 460 nm [323]. The methyl orange used in this work was supplied by Sigma-Aldrich and had $>85\%$ purity [321].

3.4.2. Adsorption procedures

A stock solution (1 L) of methylene blue was prepared with a concentration of 100 mg/L in distilled water. A stock solution of methyl orange was also prepared with 100 mg/L concentration.

Besides the chars, a commercial activated carbon was also tested as adsorbent and used as control for comparison. The activated carbon, with commercial purpose to remove impurities from water, was supplied by Sigma-Aldrich [324], produced from lignite, in granular form (≈ 1 mm size), type Darco 12x20, from Norit (now Cabot Corp.).

The general procedure for the adsorption tests was as follows: a certain amount of oven-dry adsorbent (char or activated carbon) was weighed and placed in a 15 mL PE tube; 10 mL of the adsorbate solution (with the desired initial concentration) was pipetted into the PE tube; and mixing was performed for the desired contact time for adsorption. A first batch of tests was performed in order to determine the adequate amount of adsorbent to use and other parameters such as mixing time and mixing method. Another parameter that is usually very important in adsorption is pH, however, this parameter was not studied due to the preliminary nature of the adsorption tests carried out for this work. The pH value during adsorption was therefore not controlled.

In terms of mixing, initially, tests were made using a small magnetic stirrer inside the PE tubes and a stirrer plate, but the results from using this type of mixing resulted in significant differences when using the same conditions (low repeatability). An ultrasonic bath for sonication (Fischer Sci FB15061 series) was tested, and it was seen that this type of mixing would provide more consistent results between replicates. Furthermore, sonication led to better adsorption performances, which suggested that this mixing method promoted an improved, likely more uniform, particle dispersion. Other researchers have verified that sonication can be more effective for particle dispersion in solution and other applications, with particle agglomeration potentially occurring with magnetic stirring [325][326]. Sonication was

thus chosen as mixing method and used for the subsequent tests with the solid products from slow pyrolysis. With the ultrasonic bath there was also the advantage of testing more samples at the same time, comparing to magnetic stirring, which was limited by the size of the stirring plate. There was however a disadvantage with the sonication, which was a temperature increase in the bath due to the vibration, which could cause differences in the adsorption process. This increase in temperature was seen to stabilise at ≈ 50 °C, and so this temperature was selected for the adsorption tests. The sonicator was pre-heated up to that temperature before the samples were inserted for mixing, and temperature was monitored during adsorption. Although sonication can be used for mixing, it is acknowledged that for larger scale applications this method would have to be custom-made and not very affordable, so it is not the most suitable [327]. Furthermore, the very efficient mixing is likely to lead to over-estimation of the adsorption capacity, when compared to a “real world” situation, in which water decontamination by adsorption is commonly performed in continuous columns or filters packed with the adsorbent material through which the contaminated water flows through. For the small scale batch tests performed, however, sonication was considered to be a better option to magnetic stirring, and due to being simpler and faster, was chosen in detriment of a continuous process.

After the desired contact time for adsorption, the sonicator was stopped and the sample tubes were removed from the bath. The tubes were centrifuged at 3000 rpm for >2 hours, in an Eppendorf 5702 centrifuge. Centrifugation allows to separate the solid particles from solution, which minimises errors during analysis of the final solution concentration. After this process, the sample was ready to be tested by UV-Vis spectrophotometry, as described in the following section 3.4.3.

Initial adsorption tests with methylene blue solution were performed in order to establish which conditions were adequate to test the solid products from slow pyrolysis of wheat straw. The conditions to establish were: initial dye concentration, contact time (tested 15-240 minutes), and adsorbent mass (tested 2, 5, 10, and 25 mg).

At first, the stock solution concentration (100 mg/L) was used for tests with commercial activated carbon and some of the produced chars. For that initial concentration and using 25 mg of adsorbent, the commercial activated carbon achieved very high dye removal ($\approx 99\%$), while some chars also obtained relatively high removal ($>90\%$). Maximum removal was achieved for the chars at 180 minutes, while for the commercial activated carbon equilibrium was achieved significantly faster (≈ 60 min). The appropriate test conditions were thus established for the subsequent adsorption tests to perform on all the solid products from slow pyrolysis: initial dye concentration of 100 mg/L, adsorbent mass of 25 mg, and total adsorption time of 180 min (3 hours). These conditions were used for both the methylene blue and the

methyl orange dyes. In general, at least two adsorption tests were performed for each char produced from different slow pyrolysis conditions, since each slow pyrolysis experiment was repeated at least once (exceptions were the experiments with 3 minutes SRT at 500 and 600 °C, as explained in subsection 3.2.2.1, page 90). For the initial adsorption tests, the percentages of MB removed through adsorption and the values of adsorption capacity presented in the adsorption results chapter (Chapter 7) are thus averaged from at least two tests (chars produced with the same feedstock and process conditions), with the mentioned exceptions.

After performing adsorption tests with the established conditions on all produced chars, some of the best performing chars were selected for other tests in which the adsorption conditions were varied. Chars were selected based on achieving high removal of methylene blue dye, of >90%. The commercial activated carbon was also tested.

Tests were performed with different adsorbent mass (10 mg), to test if the adsorption capacity could be increased. The initial dye concentration was also varied (20 and 60 mg/L) to observe differences in adsorption performance and check their fitting to isothermal models.

The adsorption kinetics were also studied for some of the best performing chars and the commercial activated carbon, with samples being taken and analysed at certain time intervals: 1, 3, 5 and 10 minutes, then in 10-minute intervals until 1 hour, then every 20 minutes until 2 hours, and finally every 30 minutes until 3 hours. Kinetics models were fitted to the results to assess adsorption mechanisms.

Results from adsorption tests are presented and discussed in Chapter 7.

3.4.3. Adsorption quantification

To quantify the presence of adsorbate in solution, UV-Visible spectrophotometry was selected as analysis method, since it is sensitive to the presence of the dye methylene blue, at a wavelength of $\approx 660\text{-}670$ nm [25,248,272,317]. UV-Visible spectrophotometry was the method selected for quantification of methylene blue concentration in all the literature analysed (see Chapter 2, subsection 2.4.3.). Methyl orange is also detectable by UV-Vis spectrophotometry, at a wavelength of ≈ 460 nm [323].

The equipment used for UV-Visible spectrophotometry was a Thermo Scientific Evolution 220, and the cuvettes were from Apollo Scientific Ltd., type 1 Standard cell, made of quartz, with 10 mm pathlength (3.5 mL volume).

A calibration curve was created for the methylene blue solution, by analysing different dye concentrations (1, 3, 5, and 10-100 mg/L with 10 mg/L increments). From the preliminary tests described in section 3.4.2, an initial concentration of 100 mg/L was selected, and it was seen that the absorbance of UV-Vis for this concentration would reach values higher than 2 units. It is recommended that when using UV-Vis spectrophotometry, the absorbance should

remain below a value of 2 units (preferably <1), at which it starts to deviate from the Beer-Lambert law and lead to erroneous results. Therefore, a dilution had to be performed, considering the available volume of the cuvette for the sample (≈ 3.5 mL), and the absorbance levels. The selected dilution was 0.3 mL of sample in 3 mL of distilled water (1:10 ratio), which resulted in absorbance values within the desired range, i.e., <2 units. This dilution was used for every analysed sample. A calibration curve was also created for methyl orange, and every measurement was made using the same dilution as for methylene blue. With the calibration curve, an unknown value of concentration can be calculated from the correlation between concentration and values of absorbance. Calibration curves for both dyes are presented in Chapter 7 (adsorption results chapter).

Distilled water was used as background for the analyses, which the equipment subtracts automatically from the subsequent sample spectra. The range of scanned wavelengths was 200-800 nm, with 1 nm bandwidth, 0.1 seconds of integration time, and 1 nm data intervals. UV-Vis spectrophotometry is temperature-sensitive, and so the samples, after centrifuging and before analysing, rest for time enough to be thermostatic during analysis and to be analysed at the same (laboratory room) temperature.

Chapter 4 – Slow pyrolysis of wheat straw biomass

4.1. Introduction

This chapter contains the results from the slow pyrolysis experiments in a bench-scale screw reactor using wheat straw feedstock. The experiments were designed to study the influence of process variables on the product distribution and properties, with a focus on the char product. The variables pyrolysis temperature and solid residence time were studied using the feedstock in its as-received form (broken pellets).

The impact of elevated feedstock moisture content was also studied, by processing the feedstock after soaking it with water, at different sample-to-water ratios. Due to absorbing the water, the feedstock particles disintegrate and become smaller particles shaped like flakes. The release of this elevated feedstock moisture content during the slow pyrolysis process creates a steam atmosphere in the reactor, which was studied as a potential form of physical activation, however in 1-step instead of the traditional 2-step activation process (carbonisation first, followed by activation). Changes in product yields and char properties were evaluated.

The slow pyrolysis solid products were analysed in terms of their composition and other relevant properties: proximate and ultimate analyses, inorganic composition, heating value, surface chemical functionalities with FTIR, pH value (in H₂O), nitrogen physisorption (77 K), and SEM (results in subsection 4.4). Selected liquid products were analysed in terms of their water content, elemental composition, heating value, GC-MS, and pH (results in Appendix D). The gas product from the slow pyrolysis experiments was characterised in terms of gaseous species proportions (CO₂, CO, CH₄ and other light hydrocarbons, and H₂) and heating value (based on composition), with results in subsection 4.5.

4.2. Feedstock characterisation

4.2.1. Proximate analysis and thermal degradation

The wheat straw feedstock was analysed by proximate analysis using TGA, with the method described in Chapter 3. The thermogram obtained under inert nitrogen atmosphere and its derivative (DTG) are displayed in Figure 4.1.

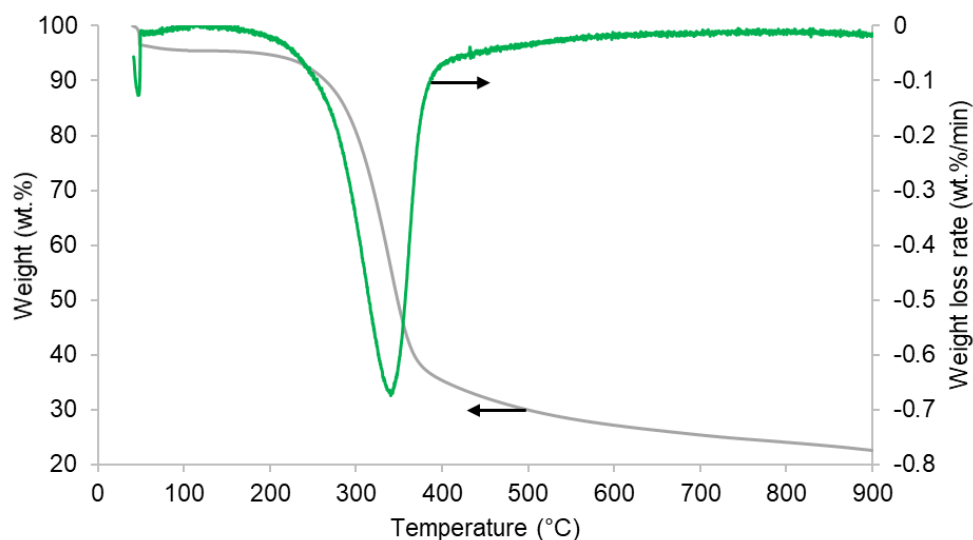


Figure 4.1: Thermogram and derivative from the TGA (in nitrogen atmosphere) of the wheat straw feedstock.

There is a relatively small moisture (and light volatiles) release at the beginning of the temperature programme (until 100 °C). From ≈ 200 °C, the main weight loss process begins, with a peak of the rate of weight loss at ≈ 340 °C. After the main process ends (≈ 375 °C), there is still some weight loss, but at a relatively low rate, without any peak. The rate of weight loss keeps decreasing, until it reaches approximately zero, and the sample weight remains constant.

Based on information reported in literature on biomass thermal degradation in an inert atmosphere, the main weight loss process is due to the decomposition of hemicellulose and cellulose, and to a smaller extent to the decomposition of lignin [105]. Hemicellulose is said to decompose in the range 220–315 °C and cellulose in the range 315–400 °C [105]. The thermal degradation of lignin occurs over a wider temperature range, which can be 180–900 °C [105]. The peak of weight loss rate can be corresponded to cellulose decomposition, which according to the literature has a maximum at ≈ 355 °C [105]. Depending on the proportions of the lignocellulosic components, there can be a shoulder before the main peak, which corresponds to hemicellulose degradation [104]. This shoulder was not observed for the wheat straw feedstock, and other differences for example in the maximum decomposition temperature (340 °C instead of 355 °C as indicated in literature) can be due to changes in the proportions of the lignocellulosic compounds, from pelletising for example. The pelletising process, involving thermal and mechanical treatments, probably modified the lignocellulosic structures and could even remove some compounds (mainly hemicelluloses), making the biomass more thermally stable.

The contents of moisture (M), volatile matter (VM) and ash (A) in the biomass were determined from the TGA results, and the fixed carbon (FC) content was obtained by difference. The averaged results of proximate analysis (in wet and dry basis) are indicated in Table 4.1.

Table 4.1: Results from proximate analysis of the wheat straw feedstock by TGA (number of experiments, n=3).

Basis (wt.%)	M	VM	A	FC
Wet	4.8 ± 0.3	75.5 ± 1.8	4.1 ± 0.3	15.5 ± 2.2
Dry	-----	79.4 ± 2.1	4.3 ± 0.3	16.3 ± 2.3

The volatile content is relatively high, and the moisture content is relatively low, which brings advantages in terms of using the biomass for energy production. If a fuel has more water content, it requires more energy to drive that moisture away, which can be a large burden in terms of heating requirements if the content is significantly high. Fresh biomass can have moisture contents up to 60 wt.% (wet basis) [60]. The relatively low moisture content can be explained by the fact that the feedstocks were in pellet form (thus subjected to thermal treatment), and that they were ground for the TGA analysis, which also subjects the sample to heat and loss of moisture. The proportion of ash is relatively low comparing with other herbaceous biomasses, however woody biomass usually has even lower ash contents, e.g., ≤1 wt.% (dry basis) [328]. The inorganic content can be detrimental in terms of energy production (e.g., causing fouling, corrosion, etc.) [58], but in pyrolysis it can be advantageous, due to catalysing secondary reactions that form char [77][90][99][108][213]. To compare with examples from literature, values from proximate analysis of several examples of wheat straw and one example of rice straw are shown in Table 4.2.

Table 4.2: Proximate analysis (wet basis) of wheat straw and rice straw from various literature sources.

	M (wt.%)	VM (wt.%)	A (wt.%)	FC (wt.%)	Reference
Wheat straw (≤150 μm)	6.7	67.4	9.6	16.3	[75]
Wheat straw (≈1 cm)	7.3	75.0	10.5	7.1	[74]
Wheat straw pellets, with epoxy binder	4.0	68.9	9.2	17.4	
Wheat straw (0.5-2.0 mm)	12.8	83.1	6.6	10.3	[76]
Rice straw (0.5-2.0 mm)	11.7	78.1	15.0	6.9	

The moisture content can vary significantly depending on the source, and a pelletised form usually has lower moisture, similarly to the value for the wheat straw analysed. It should be noted, however, that according to the supplier the wheat straw pellets tested in this work have not been produced with a binder or any additive. Comparing between the two different straws, it can be noticed that the ash content is significantly higher in the rice straw, a biomass which is known to have a high inorganic content [62]. The harvesting method plays an important role in the inorganic content of the biomass, since soil and debris from the ground can be incorporated in the biomass during that stage [329]. A lower ash content in wheat straw is an advantage in terms of energy production and is less hazardous in terms of slagging and fouling due to high temperatures [58].

4.2.2. Ultimate analysis and inorganic composition

The wheat straw was tested for elemental (ultimate) composition (C, H, N, S, and O by difference), with the results and literature comparisons in Table 4.3. Since the method of elemental analysis is based on the organic matter of the samples, the ash contents are shown as well, allowing to add the values up to 100 %.

Table 4.3: Results (n=3) and literature values from ultimate analysis of wheat straw, and ash contents.

Wheat straw type/basis	C (wt.%)	H (wt.%)	N (wt.%)	S (wt.%)	O (wt.%, by difference)	Ash (wt.%)	Ref.
Wet basis	44.9 ± 1.1	6.1 ± 0.0	0.8 ± 0.0	0.1 ± 0.0	48.1 ± 1.1	4.1 ± 0.3	This work
Dry basis	47.2 ± 1.1	6.4 ± 0.0	0.8 ± 0.0	0.1 ± 0.0	41.1 ± 1.1	4.3 ± 0.3	
Dry ash-free basis	49.3 ± 1.2	6.7 ± 0.0	0.9 ± 0.0	0.1 ± 0.0	43.0 ± 1.2	-----	
Raw, wet basis	39.7	6.6	0.6	0.2	52.9	10.5	[74]
Pellets with epoxy binder, wet basis	73.7	4.1	2.2	0.3	19.7	9.2	

Comparing with the raw straw material, when using an epoxy as binder for producing wheat straw pellets, a significant effect can be verified in the elemental analysis, mainly: carbon content increases, and oxygen content decreases, with the latter decreasing to less than half the value of the raw wheat straw. These changes lead to an increase in energy content. The epoxy binder is reported to have 70.6 wt.% of carbon, and 17.2 wt.% of oxygen [74], which can explain the changes, along with the thermal treatment during pelletising. This highlights the usefulness of pelletising in increasing feedstock quality, besides an increase in density. It would be interesting to know the elemental analysis of the wheat straw prior to pelletising (without artificial binder), which is unknown. The pellets' binding ability can be

achieved through the thermal treatment and the modification of lignocellulosic material, with lignin-based compounds probably acting as binding agents [330].

For the wheat straw used in this work, the calculated atomic H:C and O:C ratios (dry ash-free basis) were, respectively, 1.63 ± 0.03 and 0.65 ± 0.03 . The feedstock, as well as most biomasses, has higher H:C and O:C ratios than another solid fuel, coal, which typically has a H:C ratio ≤ 1.0 and a O:C ratio ≤ 0.3 [331]. This relates to the higher volatile matter and oxygen content in biomass, resulting in less value for use as solid fuel compared to coal.

The energy content of the feedstock was determined by bomb calorimeter and also calculated with a correlation using elemental analysis results. The correlation used to calculate the higher heating value (HHV) was developed by Channiwala and Parikh for fuels [303] (Equation 3.3 in Chapter 3). To obtain the lower heating value (LHV), Equation 3.4 in Chapter 3 was used. Table 4.4 shows the results of experimental and calculated heating values of the wheat straw feedstock.

Table 4.4: Experimental and calculated heating values of the feedstock (n=3).

	HHV _{exp} (MJ/kg)	HHV _{calc} (MJ/kg)	LHV _{calc} (MJ/kg)
Wheat straw	16.6 ± 0.1	18.3 ± 0.5	18.1

A difference of 1.7 MJ/kg was verified between the experimental value obtained with bomb calorimeter and the calculated value, which may suggest that the chosen correlation may not have been the most adequate choice. Values of higher heating values of several materials taken from literature examples are indicated in Table 4.5.

Table 4.5: Values of higher heating value for wheat straw from other research examples.

Wheat straw type/size	HHV (MJ/kg)	Reference
0.5-2.0 mm	14.7	[76]
$\leq 150 \mu\text{m}$	17.2	[75]
$\approx 1 \text{ cm}$	15.6	[74]
Pellets, with epoxy binder	27.8	

The obtained heating value for the wheat straw feedstock is comparable to literature values indicated for wheat straw. The wheat straw pellets with epoxy binder have a higher value, due to the effect of the binder, which is reported to have a HHV of 34 MJ/kg [74]. The wheat straw pellets used in this research, according to the supplier, do not possess binder compounds.

An analysis of the inorganic elements in the wheat straw feedstock by X-Ray Fluorescence spectroscopy was performed by partners from the GreenCarbon project at the University of Zaragoza. Results are indicated in Table 4.6 [332].

Table 4.6: Inorganic contents of the feedstock ashes performed by GreenCarbon project partners [332].

	K ₂ O	CaO	SiO ₂	P ₂ O ₅	Al ₂ O ₃	Cl	MgO	S	Fe ₂ O ₃
Inorganic contents in ashes (wt.%)	53.2	17.4	16.9	4.46	1.66	1.53	1.46	1.31	1.14

The presence of elements such as K, Ca, P, and Mg in the wheat straw can be explained by its agricultural (plant) origin. Some of the elements (in particular Si) may originate from soil particles that were collected with the wheat straw during harvest. There is a significant proportion of potassium and calcium, which are both Alkali and Alkaline Earth Metals (AAEMs), known to be catalysts for reactions that occur during thermal decomposition [77][90][99][108][213]. It has been reported that inorganic elements, especially potassium and also phosphorous, have significant impact in terms of catalysing secondary reactions during pyrolysis, modifying product yields and quality [90]. Part of the inorganic elements may become devolatilised during slow pyrolysis, however, it is expected, due to the relatively low temperatures employed, that most remain in the solid product [104][107]. During pyrolysis, inorganic compounds could block porosity and prevent surface area from being developed, which can negatively impact applications such as adsorption [307]. If the feedstock is a relatively clean biomass and harmful elements such as heavy metals are not present, the inorganic compounds have generally positive impacts when remaining in the char product, especially for soil applications, where they can act as nutrients for plants [149][217]. For use as solid fuel, however, inorganics can have a negative impact due to the formation of mineral species (e.g., with K, Si) with relatively low ash melting point and lead to slagging, fouling and corrosion upon combustion [58].

4.2.3. pH and FTIR analysis

The wheat straw feedstock was analysed for its pH value (in H₂O) as described in Chapter 3. The obtained value was 7.31 (± 0.04), slightly alkaline, with this value being expected to increase when the feedstock is pyrolysed (char becomes more alkaline with increasing pyrolysis temperature), as indicated by trends found in literature [307]. The pyrolysis process removes volatiles and certain chemical functionalities, many of acidic nature (-OH, -COOH, etc.), and thus the char usually becomes more alkaline, with pH increasing with increasing pyrolysis temperature.

The feedstock was analysed for its chemical surface functionalities, through FTIR, as indicated in Chapter 3. The spectrum resulting from this analysis is presented in Figure 4.2, and attribution of chemical features was done based on other research examples [333–336].

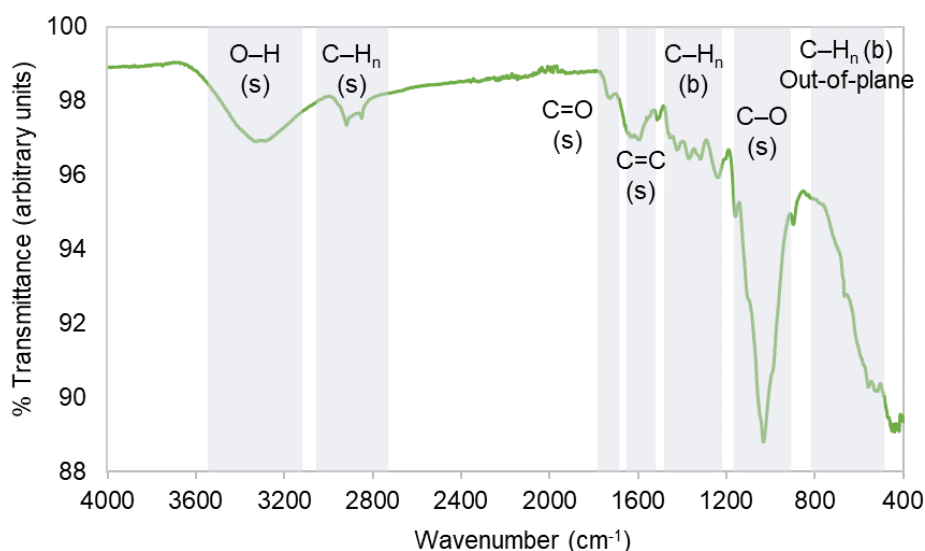


Figure 4.2: FTIR spectrum of the wheat straw feedstock.

The most prominent features detected by FTIR on the surface of the feedstock correspond to the vibration of O-H stretching bonds ($3600\text{--}3000\text{ cm}^{-1}$), C-H_n stretching vibration ($2950\text{--}2850\text{ cm}^{-1}$), and the stretching vibration of C-O bonds ($1150\text{--}1000\text{ cm}^{-1}$).

The first band of O-H bond vibration can be related to the presence of moisture, alcohols and phenols. The C-O bond vibrations can be attributed to carboxylic and ester groups, and also to aromatic rings, while the aliphatic C-H_n bonds originate from the lignocellulosic biopolymers and fatty acids in the feedstock [335,337]. Another region of the spectrum that manifests in FTIR with significant intensity is $1650\text{--}1550\text{ cm}^{-1}$, which corresponds to vibrating C=C bonds, indicating the presence of aromatics and alkenes. The region of wavenumbers $900\text{--}700\text{ cm}^{-1}$ (weak-medium peaks) corresponds mainly to the vibration of C-H bonds from aromatic compounds.

4.3. Product yields

4.3.1. Effect of process temperature and solid residence time

Slow pyrolysis experiments were performed in the first screw reactor described in Chapter 3 using the as-received wheat straw feedstock. Process conditions that were studied initially were pyrolysis temperature (400, 500 and 600 °C), and solid residence time (3, 6 and 10 minutes). Mass balances were calculated for each experiment, and a closure of $\geq 95\text{ wt.}\%$ (dry feedstock basis) was obtained in all cases. The mass yields of the pyrolysis products corresponding to the mentioned experiments, in a dry feedstock basis, can be visualised in Table 4.7. Standard deviation is based on two experiments for each pair of conditions (temperature and SRT) tested.

Table 4.7: Mass balances from the slow pyrolysis experiments using as-received wheat straw with varying pyrolysis temperature and SRT (n=2).

T (°C)	400			500			600		
SRT (min)	3	6	10	3 ^{a)}	6	10	3 ^{a)}	6	10
Char	34.6 ± 0.2	35.5 ± 0.3	35.1 ± 0.6	28.2 ± 0.0	29.5 ± 0.0	30.8 ± 0.2	26.4 ± 0.0	26.8 ± 0.1	26.7 ± 0.1
Total liquid product	46.0 ± 0.3	46.1 ± 0.9	42.9 ± 0.9	49.5 ± 0.0	47.0 ± 0.5	43.9 ± 0.5	46.8 ± 0.0	41.1 ± 1.0	39.3 ± 0.4
Aqueous phase	40.7 ± 0.9	42.8 ± 0.4	34.4 ± 1.9	40.0 ± 0.0	37.8 ± 1.3	35.2 ± 0.2	35.4 ± 0.0	32.7 ± 1.2	31.1 ± 0.4
Organic phase	5.3 ± 1.3	3.3 ± 0.5	8.5 ± 1.0	9.6 ± 0.0	9.2 ± 0.8	8.7 ± 0.6	11.4 ± 0.0	8.3 ± 0.1	8.2 ± 0.0
Gas product	17.3 ± 0.3	16.1 ± 3.6	19.8 ± 1.0	17.3 ± 0.0	22.4 ± 1.1	24.2 ± 2.2	24.2 ± 0.0	34.9 ± 2.6	36.5 ± 0.4
Losses	2.0 ± 0.2	2.3 ± 4.8	2.1 ± 1.3	4.9 ± 0.0	1.2 ± 1.6	1.0 ± 2.0	2.6 ± 0.0	0.0 ± 1.5	0.0 ± 0.1

Notes: a) Only one experiment was performed for these conditions, so the standard deviation is zero.

With increasing pyrolysis temperature, the solid yield decreased (35.1 to 26.7 wt.%, averaged for all three SRT), while gas yield increased (17.8 to 31.9 wt.%). At a slow pyrolysis temperature of 600 °C, the gas yields surpassed the yields of the solid product (except for the experiments with SRT of 3 minutes). Similar trends were found by Yu *et al.* using rice husk and corn stalk in the same reactor for pyrolysis temperatures between 350 and 600 °C [178]. For rice husk, solid product yields (wet basis) dropped from 46 to 31 wt.%, and from 38 to 27 wt.% for corn stalk. The higher char yields from the rice husk compared with the ones from corn stalk were explained by the higher ash and lignin content, and lower volatile matter content on the rice husks. The char yields are also higher when comparing to the ones obtained from the wheat straw feedstock used in this work, probably also due to the lower ash content in the wheat straw, which is approximately half of the one from the corn stalk feedstock (8.2 wt.%, wet basis), and to the higher volatile matter content (only 56.0 and 61.7 wt.% in rice husks and corn stalks, respectively) [178]. Although the wheat straw feedstock studied in this work obtained less char product, the lower ash content is an advantage comparing to the other chars from rice husks and corn stalks, e.g., in terms of energy production. The inorganic content in the ash may lead to corrosion, slagging and fouling in combustion equipment [58].

The liquid product yield had a maximum of 46.8 ± 2.8 wt.% (dry feedstock basis, averaged for the three SRT values) at a temperature of 500 °C. This maximum of liquid product yield at ≈500 °C from biomass pyrolysis has been recognised in the literature [81]. In terms of the aqueous and organic fractions of the pyrolysis liquid, the trend was that the aqueous phase decreases with temperature (39.3 to 33.1 wt.%), while the organic phase increases (5.7 to

9.3 wt.%). This trend can be connected to the greater decomposition of lignin for higher temperatures, since its thermal degradation occurs at a wider temperature interval and until higher temperatures compared to cellulose and hemicellulose [105]. Lignin has a more complex structure, and its degradation yields mainly phenolics and other compounds (e.g., acids) with greater molecular weight than the ones from cellulose and hemicellulose degradation, which are also mostly water-soluble (e.g., sugars and their derivatives, ketones) [338]. Furthermore, reforming reactions can be promoted at temperatures ≥ 450 °C, reducing the yield of reaction water and thus aqueous phase [339]. This was however contrary to what was observed for wood waste pyrolysis in a lab-scale screw reactor by Solar *et al.*, which can be due to the higher temperatures employed in that work (750 and 900 °C) [127].

Unlike pyrolysis temperature, the effect of SRT on char yields was much smaller, and this parameter is reported to have a lower influence on product distribution, being often dominated by other factors such as operating temperature and heating rate [13]. A relatively small increase in char yields was found, however, the standard deviation of the averages across the three different SRT was 0.4, 1.3, and 0.2 wt.% (dry feedstock basis), respectively for 400, 500, and 600 °C. The relatively small variation, along with a relative standard deviation (RSD) of ≤ 5 % can be considered to be within experimental error. Other SRT values would need to be tested to better assess the impact of this parameter.

The small impact of SRT on char yields can be an indicator that carbonisation is completed at the shortest SRT of 3 minutes. Puy *et al.* reported a minimum of 2 minutes for complete devolatilisation of pine wood chips at 500 °C in a screw reactor [126].

An indicator for completion of the carbonisation process is the temperature profile along the reactor. For the first screw reactor, there was only one measurement of temperature inside the reactor (in the middle), and this temperature value was used to check if the furnace temperature needed to be increased or decreased in order to maintain the desired process temperature (400, 500 or 600 °C). Figure 4.3 represents an example (600 °C and 10 min SRT) of the evolution of temperature during a slow pyrolysis experiment with as-received wheat straw feedstock, for the thermocouple inside the reactor (T1) and outside the reactor (on the reactor wall; T2).

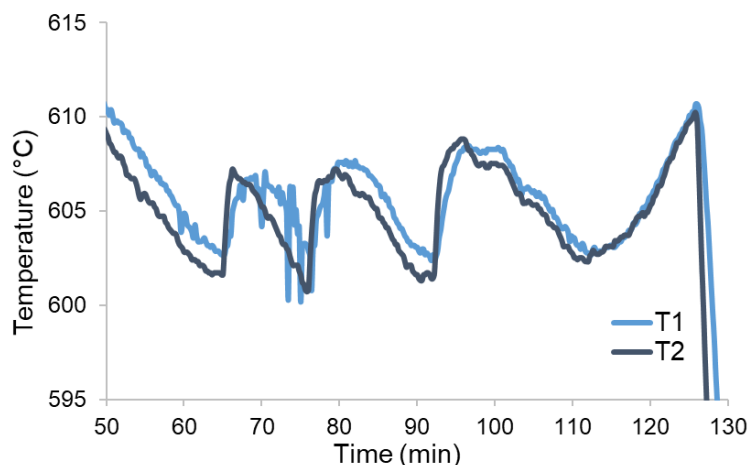


Figure 4.3: Reactor temperature (inside, T1 and outside/wall, T2) during a slow pyrolysis experiment (600 °C, 10 min SRT) in the first screw reactor.

Both thermocouples mimicked each other's motions with time, with the periodical temperature drops pertaining to feedstock being processed after feeding. The variations are not very significant, and the temperature inside was kept slightly above the desired pyrolysis temperature, to make sure the pyrolysed material reaches that temperature.

The second screw reactor, on the other hand and as explained in Chapter 3, was fitted with three thermocouples, which allowed to have three temperature measurements along the reactor tube and thus create a temperature profile. The temperature profiles are shown in subsection 4.3.3 in this Chapter for the experimental sets that used the second screw reactor (soaked and dry feedstock, 400 and 600 °C, 10 min SRT).

For the liquid and gaseous products, with varying SRT, the standard deviation of the yields is higher than for char, and the trend is that liquid yield decreases with SRT, while gas yield increases. It can thus be said that, with increasing SRT, more gas product was produced at the expense of the liquid product, which has been reported by other researchers using screw reactors [127]. Longer SRT can lead to favoured secondary reactions due to greater exposure time between solids and product vapours, if VRT is maintained. Secondary reactions (e.g., cracking of organic vapours) can produce higher gas yields and lower liquids yields, as well as secondary char, increasing char yield [13][29][116]. The impact of SRT was greater with increasing pyrolysis temperature, which can be related to the fact that secondary reactions are favoured by higher temperatures [56]. In terms of the yields of aqueous and organic phases, no clear trend with SRT was observed.

As discussed in Chapter 2 (subsection 2.1.5.3, page 43) and Appendix B, vapour residence time (VRT) is a relevant process parameter, influenced by process temperature, SRT, carrier/injected gas flow and other factors such as reactor design. Longer VRT values are likely to favour secondary reactions [29]. VRT calculated using experimental gas flow rates

(calculated from produced gas volume and experiment duration) from experiments in the first screw reactor can be visualised in Table 4.8. Another method of VRT estimation is by assuming it corresponds to the time of appearance of the first pyrolysis vapours in the reactor outlet. Values of estimated VRT using the visual method for the first screw reactor are also shown in Table 4.8. The values for this method were not registered for the experiments at 500 and 600 °C with 3 minutes SRT.

Table 4.8: VRT values (calculated and from visual determination) for experiments with varying temperature and SRT (n=2).

T (°C)	SRT (min)	Gas flow rate (L/min)	VRT, calculated		VRT, visual	
			(min)	(s)	(min)	(s)
400	3	0.42 ± 0.15	0.67 ± 0.23	40 ± 14	1.0 ± 0.0	62 ± 3
	6	0.41 ± 0.22	0.76 ± 0.41	46 ± 25	1.3 ± 0.1	80 ± 7
	10	0.45 ± 0.08	0.59 ± 0.11	36 ± 7	2.4 ± 0.1	145 ± 9
500	3	0.56 ± 0.00	0.47 ± 0.00	28 ± 0	N/A	N/A
	6	0.62 ± 0.03	0.42 ± 0.02	25 ± 1	1.5 ± 0.0	90 ± 0
	10	0.49 ± 0.07	0.54 ± 0.08	32 ± 5	1.7 ± 0.3	100 ± 17
600	3	0.84 ± 0.00	0.31 ± 0.00	19 ± 0	N/A	N/A
	6	0.87 ± 0.17	0.31 ± 0.06	19 ± 4	1.0 ± 0.0	60 ± 0
	10	0.92 ± 0.05	0.29 ± 0.02	17 ± 1	1.5 ± 0.0	90 ± 0

It can be verified that VRT resulting from visual confirmation is significantly higher than VRT estimated using gas flow rate. This is mainly because of a delay in visual confirmation, due to the lack of colour of part of the gases formed, which pass through without being visually detected (but are detected by the MicroGC). The VRT estimation method with experimental gas flow rates has greater experimental errors compared to the visual estimation method, due to uncertainty associated with the gas meter and when defining total processing time.

The overall trend with pyrolysis temperature is a decrease in VRT, caused by a higher vapour production during pyrolysis, since more lignocellulosic material is decomposed. VRT was also affected by SRT, however the effect is more difficult to ascertain due to relatively high standard deviations. Based on the visual method, which has lower standard deviations, VRT increased with increasing SRT. This can be explained by two factors: biomass takes longer time at the start of the reactor, which is colder, and thus devolatilisation and vapour release occur more slowly than at higher SRT, and part of the produced vapours stays inside the reactor for longer time due to the screw not moving as fast. The trend of VRT with SRT from the method with experimental gas flow rates was not as clear and sometimes was contrary to the visual method, due to greater standard deviation. Increasing VRT with SRT can be correlated to the trend of product yields that was verified with SRT: production of more gas product at the expense of liquid and solid products, favoured secondary reactions.

4.3.2. Comparison between the two lab-scale screw reactors

Since some slow pyrolysis experiments exploring the effect of feedstock moisture content (the ones using 0.1 wt.% M) were performed in the second screw reactor, it was necessary to do a comparison between the two reactors to check reproducibility. The comparison was made with the following process conditions: as-received wheat straw feedstock (broken pellets), 400 and 600 °C, 10 minutes SRT, and no carrier/injected gas during operation. The choice of temperature and SRT conditions were because they were common to most experimental sets. Experiments were performed in duplicate.

A design difference between the two reactors was that three thermocouples were installed in the second reactor tube, instead of just one in the case of the first reactor. In this way it was possible to obtain a temperature profile along the reactor for each experiment. Temperature profiles for experiments at 400 and 600 °C in the second reactor are shown in Figure 4.4. T1 is the first thermocouple on the left-hand side of the reactor tube, T2 is in the middle of the tube, and T3 is on the right-hand side of the tube.

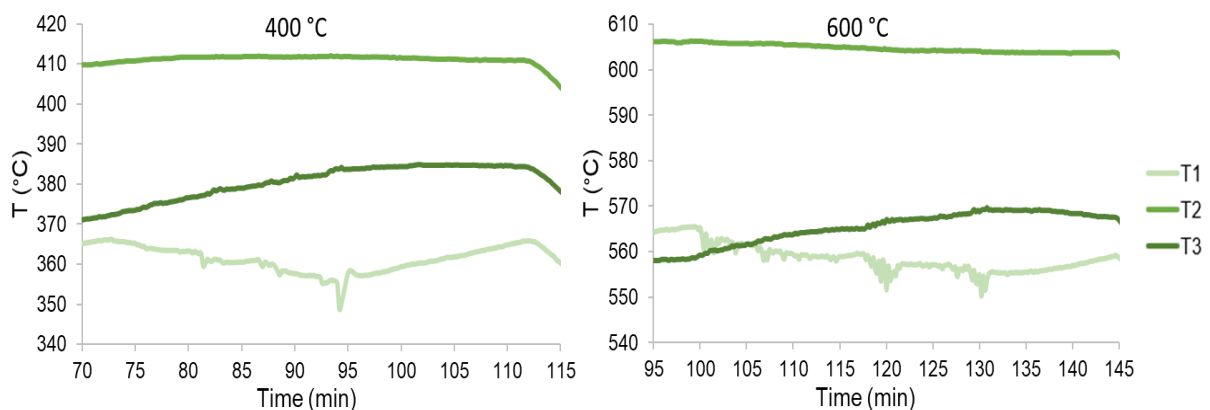


Figure 4.4: Temperature profile along the reactor tube (T1-T2-T3) in the second screw reactor during slow pyrolysis experiments with 10 min SRT (left: 400 °C; right: 600 °C).

The temperature in the middle of the reactor (T2) was used as reference for the processing temperature and was kept slightly higher than the desired slow pyrolysis temperature to make sure carbonisation occurred. Sometimes T2 dropped slightly, which was attributed to endothermic pyrolysis reactions, or the tube cooling down, so the furnace set-point was slightly increased (≈ 2 °C) when this happened. T1 and T3 had lower values due to being located closer to the outside of the reactor and thus more exposed to the surrounding lower ambient temperature. This signifies that the material inside the reactor was not exposed to the peak temperature for the full SRT, which may lead to carbonisation not occurring at the desired temperature but at a lower value.

With T1 it was possible to see the impact of feeding, which caused noticeable drops in measured temperature. T3 is closer to the reactor exit, and this temperature did not drop during operation, suggesting carbonisation was complete. T3 keeps increasing during operation due to conduction, since the reactor tube next to it is at higher temperature (T2), heated by the furnace. Since significant temperature drops were not noticed during operation on T2 and T3, this suggests carbonisation was complete from the middle of the reactor onwards, which means, considering 10 minutes SRT, that carbonisation was complete at ≈ 5 minutes (middle of the reactor where T2 is located). However, due to the temperature gradient between T2 and the other temperature measurements, carbonisation may be occurring at a lower temperature than desired.

During the reactor heating up phase, it was noticed that the temperatures inside the second reactor would take longer to reach the desired temperature than the first reactor, which was connected to design changes such as increased internal diameter, tube thickness, and existence of a shaft along the screw (described in Chapter 3). This probably contributed to the temperature gradients between the three thermocouples (Figure 4.4) and reduced the reactor length which was at the target pyrolysis temperature, and thus the time of exposure of the feed materials to that temperature. This has the potential to alter feedstock thermal degradation during slow pyrolysis and product properties.

The experimental VRT values (estimated visually) for the experiments at 400 and 600 °C with as-received feedstock for both reactors are presented in Table 4.9.

Table 4.9: Values of VRT estimated from the visualisation of first vapours for the experiments comparing both screw reactors (n=2).

T (°C)	SRT (min)	Reactor	VRT (min)	VRT (s)
400	10	First	2.4 ± 0.1	145 ± 9
		Second	3.1 ± 0.2	188 ± 11
First		1.5 ± 0.0	90 ± 0	
Second		1.9 ± 0.2	113 ± 11	

The experiments performed in the second reactor had slightly higher VRT values. Design changes such as having a middle shaft and reduced clearance could contribute to longer dwell time of vapours inside the second reactor since there is less free space available for vapours to travel along the reactor. Another factor that could contribute to the VRT differences is the temperature gradients inside the reactor tube seen in Figure 4.4. A reduction in exposure time of the materials inside the reactor to the maximum temperature can lead to a reduction in thermal degradation and thus produce less vapour, which reduces the flow rate and thus extends VRT. Greater VRT values may favour secondary reactions.

Table 4.10 presents the product yields (averaged from duplicate experiments, with standard deviation) from experiments with the second screw reactor in the conditions described above, and a comparison with the first screw reactor results (absolute difference to the yields from the first reactor, standard deviation (SD) and relative standard deviation (RSD)).

Table 4.10: Product yields from the second screw reactor and comparison with the first screw reactor (n=2).

	400 °C (wt.%, dry feed basis)				600 °C (wt.%, dry feed basis)			
	Yield	Difference	SD	RSD (%)	Yield	Difference	SD	RSD (%)
Char	36.8 ± 1.0	+2.0	1.4	3.9	28.3 ± 1.5	+1.6	1.1	4.1
Total liquid product	40.4 ± 0.8	-3.1	2.2	5.1	36.2 ± 3.9	-3.1	2.2	5.7
Gas product	20.2 ± 0.8	+0.2	0.2	0.9	29.7 ± 5.0 ^{a)}	-6.8	4.8	14.5

Notes: a) For one of the experiments the MicroGC did not produce data and so the gas yield was calculated using data from the other experiment performed under the same conditions.

The product yields suggest that overall, compared to the first screw reactor, the second screw reactor generates a slightly higher char yield and lower liquid product yield. Nevertheless, the relatively small RSD ($\leq 5\%$) suggests that char yields can be considered reproducible between the two screw reactors. For liquid and gaseous products, it is more difficult to guarantee reproducibility due to higher RSD. The greater RSD for gas yields at 600 °C can be due to using different calculation methods for that product.

The increased VRT and thus contact time between solids and vapours can lead to favouring of secondary reactions and higher char and gas yields and reduced liquid yields [13][29][116]. However, the results, especially at 600 °C, do not corroborate the occurrence of secondary reactions, due to lower gas yields from the second reactor. This suggests that the differences were alternatively due to carbonisation occurring to a lesser extent in the second reactor, due to temperature gradients inside the reactor tube. The temperature profiles and VRT values support this hypothesis.

The differences in reactor design and in operational features such as VRT may also impact char properties. The main properties (proximate and ultimate analyses) of chars produced in both reactors with the same process conditions are compared in the char characterisation subsection 4.4.

4.3.3. Effect of feedstock moisture content

The wheat straw feedstock was prepared with elevated moisture contents of 50 and 75 wt.% (wet basis), to evaluate the effect of this parameter on the slow pyrolysis process and

char properties. The pyrolysis temperatures were 400 and 600 °C, and 10 minutes SRT. As described in Chapter 3, the feedstock was soaked in water to obtain the elevated moisture contents. Due to disintegration of the wheat straw broken pellet particles, there was also a need to study the effect of the particle disintegration, without the moisture content effect. Therefore, slow pyrolysis experiments were also performed on the feedstock after soaking and then drying in an oven at 105 °C, which allowed to obtain a feedstock moisture content of ≈ 0.1 wt.% (wet basis). These experiments with soaked and dried feedstock were performed on the second screw reactor, while all others were on the first one.

The mass balances from the experiments using wheat straw with varying feedstock moisture content (M , in wet basis) are indicated in Table 4.11. Standard deviation is presented and based on two experiments for each tested condition.

For some of the experiments using feedstock with elevated moisture content (50 or 75 wt.%, wet basis), the liquid product yields possess a relatively high standard deviation or could not be obtained at all, due to the presence of water (moisture) from leftover feedstock inside the reactor between experiments, which ended up collected and mixed with the pyrolysis liquid. Furthermore, it was not possible to calculate gas product yields from those experiments due to a gas meter technical issue, which did not correctly record the volumes of gas produced. For these experiments, gas yields were estimated by difference to 100 wt.%, and thus the losses are null. The experiments using feedstock with 50 wt.% M at 600 °C do not possess these issues.

Something that was common during experiments using feedstock with elevated moisture content was feedstock becoming stuck in the inlet tube or at the bottom of it (at the start of the screw reactor), and thus not going through the reactor tube. Since the start of the reactor tube was relatively hot, some devolatilisation of the stuck material would occur, but not completely. This led to higher errors in product yields and mass balances.

Table 4.11: Mass balances from slow pyrolysis experiments using wheat straw with varying feedstock moisture content (n=2).

T (°C)	400			600		
Feedstock M (wt.%, w.b.)	0.1	50 ^{a)}	75 ^{a) b)}	0.1	50	75 ^{a)}
Char	36.8 ± 0.2	35.0 ± 0.7	30.4 ± 0.5	29.8 ± 0.5	26.6 ± 0.3	22.0 ± 2.5
Total liquid product	42.1 ± 2.0	19.9 ± 5.8	5.9	34.2 ± 1.2	26.1 ± 3.3	9.9 ± 8.6
Aqueous phase	33.6 ± 1.8	18.5 ± 4.9	5.7	27.1 ± 0.9	24.3 ± 3.1	9.3 ± 8.0
Organic phase	8.6 ± 0.2	1.4 ± 0.9	0.2	7.1 ± 0.3	1.8 ± 0.2	0.6 ± 0.6
Gas product	20.2 ± 0.8	45.1 ± 6.6	64.1	34.1 ± 0.1	42.1 ± 0.1	68.1 ± 11.1
Losses	0.9 ± 2.5	N/A	N/A	1.8 ± 1.6	5.3 ± 3.0	N/A

Notes: a) Gas yields obtained by difference to 100 wt.% (null losses).

b) Liquid yield only obtained for one of the replicates (null standard deviation).

Using soaked and dried feedstock (0.1 wt.% M), comparing with using as-received feedstock (in the same second reactor; Table 4.10), product yields were not significantly modified (differences within experimental error), especially for char. Besides the varying moisture content, the particle size/shape was also different between those experiments because of particle disintegration when soaking with water. The lack of effect could be from those variables not having significant influence, or from contrasting effects.

To investigate the influence of feedstock moisture content and particle size/shape, a slow pyrolysis experiment was performed in the first screw reactor with oven-dry wheat straw in broken pellet form, at 600 °C and with 10 min SRT. The oven-dry wheat straw was obtained by oven-drying the as-received feedstock at 105 °C for ≥24 hours, with resulting moisture of ≈0.1 wt.% (wet basis). This allowed to analyse the effect of feedstock moisture content without changes in particle size/shape. The product yields for this experiment and a comparison with using as-received feedstock are in Table 4.12 (absolute difference, standard deviation (SD) and relative standard deviation (RSD)). The gas yield was obtained by difference to 100% due to a malfunction of the MicroGC equipment.

Table 4.12: Product yields from slow pyrolysis of oven-dry wheat straw (broken pellet form) at 600 °C and comparison with using as-received feedstock (first reactor; 10 min SRT).

	Yield (wt.%, dry feedstock basis)	Difference	SD	RSD (%)
Char	27.4	+0.7	0.5	1.8
Total liquid product	38.1	-1.2	0.8	2.2
Gas product (by diff.)	34.5	-2.0	1.4	3.8

The standard deviations were comparable to or even lower than the ones obtained from replicates of slow pyrolysis experiments in Table 4.7 (varying T and SRT in the first reactor), and RSD is relatively low ($\leq 5\%$). This suggests that between 0.1 and 4.8 wt.% M and all other conditions being equal, product yields were not significantly modified, and so feedstock moisture content did not play an important role. Considering this would be valid for both screw reactors, and that the same would occur in the previous case of using soaked and dried feedstock, then the feedstock particle disintegration also did not affect the product yields.

The influence of feedstock particle size on product yields has been studied, however, it is still not completely understood [13]. The feedstock particle size is known to influence char yields due to secondary reactions being promoted for sufficiently large particles [26,29]. The larger distance between the particle centre and the periphery leads to decreased diffusion rate of the produced volatiles, increasing the contact time between solid and vapour. Furthermore, heat transfer limitations also occur, leading to temperature gradients inside larger particles and consequently higher char yields [104].

In the present work, when char yields from as-received feedstock (broken pellet form) were compared with the ones from soaked and dry feedstock (disintegrated form), it was considered that the decrease in particle size did not significantly affect product yields, based on the conclusion that the feedstock moisture content also did not play a significant role in that range of conditions.

In some research, changes in particle size sometimes do not affect product yields or affect it in contrast with what was expected based on heat and mass transfer limitations. Mani *et al.* [136] found that char yields increased when wheat straw particle size was increased from 0.250 to 0.475 mm (as expected), but there was no change when particle size was further augmented to 1.350 mm. Onay and Kockar studied the pyrolysis of rapeseed at 550 °C and found a contrasting effect: when particle size was increased from 0.425 to 0.850 mm, char yields decreased, and a further increase in particle size led to the opposite effect, of higher char yields [137]. The effect of feedstock particle size therefore seems to depend on selected particle sizes and on feedstock.

For better visualisation of solid product yields, Figure 4.5 graphically represents char yields for slow pyrolysis experiments with varying feedstock moisture content (M). Error bars represent standard deviation from two experiments.

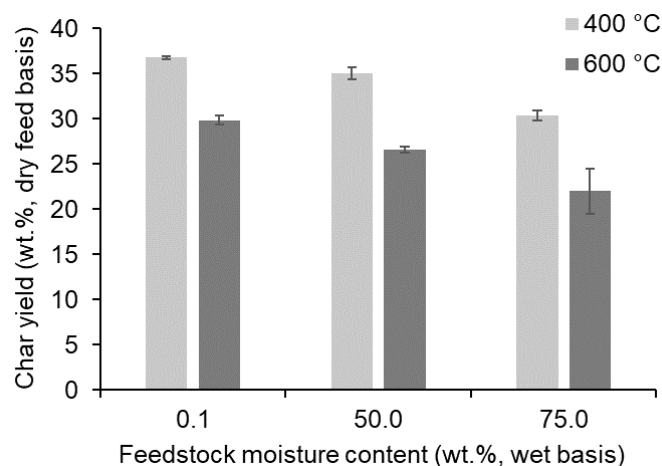


Figure 4.5: Char yields (wt.%, dry feedstock basis) from slow pyrolysis experiments with varying feedstock moisture content and pyrolysis temperature.

The difference in char yields between experiments with 0.1 and 50 wt.% M was relatively small: 1.7 and 3.3 wt.%, for 400 and 600 °C, respectively. This difference, besides being comparable to standard deviation, was also overestimated because the experiments with 0.1 wt.% M were performed in the second reactor, which yields slightly higher char yields compared to the first reactor (comparison in Table 4.10). This suggests there was no significant difference between char yields comparing experiments with soaked and dry feedstock with feedstock with 50 wt.% M. This suggests that the same proportion of char (in dry feedstock basis) can be obtained when performing slow pyrolysis of wheat straw in dry conditions or with moisture content up to 50 wt.%, in the screw reactor. This is relevant for the slow pyrolysis industry, since it allows the use of feedstock with elevated moisture content, without the need to pre-dry it, obtaining the same char yield compared to when feedstock is dried. Avoiding the feedstock drying step leads to reduced production costs.

In terms of liquid and gas yields (Table 4.11), for experiments using 50 wt.% M, compared to experiments with soaked and dried feedstock, liquid yields were significantly lower, while gas yields were higher. It should be noted, however, that gas yields for most experiments using feedstock with elevated M were obtained by difference to 100%, leading to overestimation. For experiments at 600 °C with 50 wt.% M, gas yield was calculated with MicroGC results, however, the gas product probably contains some moisture, the proportion of which was not possible to determine with the MicroGC. Although occurring for all experiments, this was more important in the case of processing feedstock with elevated moisture content, and indeed the proportion of unidentified/undetected species in the MicroGC results was greater for those experiments (50 and 75 wt.% M). This contributed to overestimated gas yields. Liquid yields were also affected by errors mentioned in the introduction to Table 4.11.

The same occurred comparing experiments with 50 and 75 wt.% M: the highest M led to lower liquid yields, and higher gas yields. The elevated M and the associated errors in the determination of liquid and gas yields contributed to this, as already discussed. However, even taking account standard deviation, the results suggested liquid yields did decrease when M was increased. For gas yields it was not possible to confirm the trend due to estimation by difference.

Comparing experiments with 50 and 75 wt.% M, the highest value led to a decrease in char yield, for both temperatures studied. The decrease in char yield was 4.6 and 4.5 wt.%, for 400 and 600 °C, respectively (dry feedstock basis). This was a significantly greater difference compared to 0.1 wt.% M, which did not significantly change char yields compared to 50 wt.% M.

Secondary reactions could cause increased char yields and liquid yields to decrease, due to reactions such as cracking of volatile vapour species, which can also increase gas yields [13][29][116]. The creation of greater proportion of vapours inside the reactor due to the elevated feedstock moisture content would favour secondary reactions, however, it could also lead to shorter VRT, which reduces vapour-solid contact and thus secondary reactions.

VRT values for slow pyrolysis experiments with varying M are presented in Table 4.13, estimated from the visualisation of the first pyrolysis vapours. VRT values calculated from experimental gas flow rates are not shown because it was possible to obtain them for the experiments with varying moisture content due to MicroGC technical issues. The experiments with wheat straw with 0.1 wt.% M were performed in the second screw reactor, while all the others were with the first screw reactor.

Table 4.13: Values of VRT based on the visualisation of the first pyrolysis vapours for the slow pyrolysis experiments with varying feedstock moisture content (M) (n=2).

T (°C)	M (wt.%, wet basis)	VRT (min)	VRT (s)
400	0.1	4.2 ± 0.0	255 ± 0
	50	1.2 ± 0.3	75 ± 21
	75	1.2 ± 0.0	75 ± 0
600	0.1	2.5 ± 0.0	150 ± 0
	50	1.2 ± 0.0	75 ± 0
	75	0.7 ± 0.3	45 ± 21

The studied parameter M represented significant influence on VRT, mainly because of the large amount of water vapour evolved from the feedstock with 50 and 75 wt.% M. The highest temperature of 600 °C and the highest M of 75 wt.% combined to produce the lowest VRT of 45 seconds. The relatively high values of VRT for experiments using soaked and dry wheat straw feedstock (\approx 0.1 wt.% M) were due to a lower proportion of vapours produced, but

also because the second reactor was used. This reactor, unlike the first one, has a shaft along the length of the whole screw, which decreases the available space inside the reactor. This leads to vapours staying for longer time inside the reactor as was verified from Table 4.9 comparing VRT between reactors. On the contrary, in the case of using elevated M, the VRT was lower, mainly due to the greater vapour proportion produced, and to being from the first reactor. This does not favour secondary reactions, and suggests those reactions were not the cause for decreased char yields for elevated M.

In biomass slow pyrolysis, literature shows a dependency of the role of feedstock moisture content (M) on the reactor and on the conditions applied. Antal *et al.* [29] and Manya [26] pointed out that high M can lead to higher char yields for slow pyrolysis under pressurised conditions. This was, however, not the case with the continuous screw reactor.

An increase in char yields caused by relatively high M values has been observed by different research groups. Gray *et al.* [139] verified that char yields in a fixed bed reactor increased ≈ 5 wt.% for wood waste pyrolysis (0.15–0.25 mm particle size, up to 28 wt.% M, demineralised), and Westerhof *et al.* [138] also noticed an increase in char yields with M for pine wood fast pyrolysis in a fluidised bed at 480 °C (feedstock with maximum 2 mm particle size; silica sand with 250 μm mean diameter as bed material). A study of wheat straw pyrolysis (475–575 °C, in a centrifugal reactor, with spherical feedstock particles of 1.4 mm maximum size) by Ibrahim *et al.* [140] showed that 15 wt.% M only affected the char yield (dry ash-free basis) at the lowest studied temperature of 475 °C, increasing it from 41 to 51 wt.%, respectively for dry feedstock and for 15 wt.% M. The increase in char yields was explained by a lower heating rate across feedstock particles, due to moisture evaporation, which is an endothermic process. The temperature gradient caused by the lower heating rate prevents (or delays) heat from reaching the centre of the particles, leading to less (or slower) thermal degradation. When comparing with literature, however, it should be noted that most other research used different pyrolysis reactors and employed carrier gas.

A study of the organic fraction of MSW in the same (first) screw reactor used in this work with varying moisture contents (12.7 to 45.8 wt.%; 450–850 °C; no carrier gas) found no significant influence of feedstock moisture content on char yields [142]. The feedstock moisture content did however modify the ratio between aqueous and organic phases in the liquid product, increasing aqueous phase and reducing organic phase yield for higher M.

For the experiments with wheat straw with elevated M and according to other research examples, it was expected that carbonisation would take longer time to occur, due to the endothermic nature of moisture evaporation. An indication of endothermicity during slow pyrolysis of a feedstock with elevated moisture content would be a temperature drop inside the reactor. This can happen during an experiment independently of moisture content (see Figure 4.3 and Figure 4.4), especially at the start of the experiment, since feedstock at room

temperature is being inserted into the reactor, but also due to possible endothermic reactions during pyrolysis (e.g., tar formation) [104]. When a drop in temperature inside the reactor occurred (monitored for the first screw reactor with one thermocouple only), the furnace temperature was raised slightly to maintain the desired pyrolysis temperature. This was performed for all experiments discussed in this chapter and it was not necessary, for experiments with elevated feedstock moisture, to increase the furnace set point more than what was done for other experiments. This suggests that there was not a significantly higher heat requirement inside the reactor to evaporate moisture and that carbonisation of feedstock with elevated moisture content was performed similarly to other experiments. Figure 4.6 presents an example of reactor temperatures during an experiment with feedstock with elevated M.

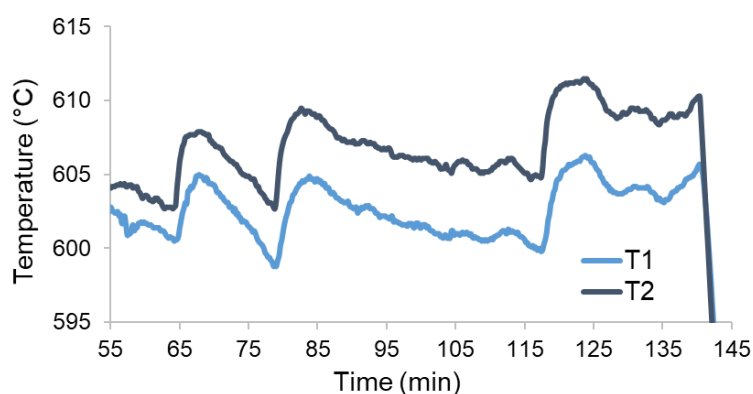


Figure 4.6: Reactor temperature (inside, T1 and outside/wall, T2) during a slow pyrolysis experiment (600 °C, 10 min SRT, 50 wt.% M) in the first screw reactor.

Other reactions that can occur due the presence of steam and cause decreased char yields are gasification reactions, e.g., $C + H_2O \leftrightarrow CO + H_2$ [340]. The process of char activation with steam is based on this gasification reaction, causing loss of solid material (burn-off), and consequent formation and expansion of pores [244]. One of the consequences of gasification is an increase in gas product yield, which in fact occurred for experiments with elevated feedstock moisture content, despite some uncertainty for gaseous product yields (see Table 4.11).

Despite product yields suggesting gasification reaction might have occurred, some operational factors did not favour those reactions. Firstly, the employed temperature was relatively low compared to traditional activation, which is usually >600 °C [225][240]. Secondly, steam is usually contacted with the solid material for longer, i.e., ≥ 30 minutes and typically 1-2 hours, and steam injection is employed instead of using feedstock with elevated moisture content [225]. Furthermore, reactor design and the consequent relatively prolonged VRT lead to longer contact time between vapours and solid materials, and while this could promote

gasification reactions, it also promotes secondary reactions, which are known to increase char production [13][29][116]. The increase in char yield can be from deposition of volatiles and other compounds on the char surface and pores, which can prevent porosity from being developed. Char porosity was analysed to investigate this effect (char analyses section 4.4).

Another factor that could contribute to the reduction in char yields for the experiments with 75 wt.% feedstock moisture content was a potential removal of soluble inorganic material from the feedstock, when excess water was removed from the soaked feedstock. The removed water had a yellow coloration. However, under the reasonable assumption that not all the feedstock inorganic content was water-soluble, and that the ashes were 4.3 wt.% of the feedstock (Table 4.1), the removal of excess water on its own could not account for the decreased char yield. The yellow colour in the removed water could be due to the solubilisation of the natural binder in the feedstock, produced during the pelletising process from part of the lignocellulosic material that composes the wheat straw. Furthermore, the wheat straw feedstock with different moisture contents was tested for moisture and ash contents, and it was verified that the ash contents were not significantly modified when the feedstock had elevated moisture content (Table 4.14).

Table 4.14: Ash contents of the wheat straw feedstock for different feedstock moisture contents (n=3).

Feedstock moisture content (wt.%, wet basis)	Ash content (wt.%, dry basis)
4.8 (as-received feedstock)	4.3 ± 0.3
0.1	4.0 ± 0.4
50	4.6 ± 0.1
75	3.8 ± 0.3

Along with possible solubilisation of inorganic material from the feedstock, the lignocellulosic compounds could be altered upon soaking with water [143], leading to potential effects on thermal decomposition, however, it was not possible to test this.

The different process and feedstock conditions likely affected not only the yields but also char properties, and will impact its performance in the desired applications. Analyses performed on char and other products are discussed in the following sections and will help investigate the effect of the different conditions employed.

4.4. Characterisation of solid products

The solid products produced in the bench-scale screw reactor had a black coloration and were mostly in broken pellet form. Figure 4.7 displays samples of three produced chars (400-600 °C, 3 minutes SRT). Other chars produced by slow pyrolysis experiments depicted in this Chapter did not possess visible physical differences.

A relatively small fraction of the produced char was in the form of powder, due to the temperature inside the reactor and the friction between the solid biomass material and the reactor walls and screw. Hence, processing the wheat straw feedstock inside the reactor did not change the solid particles' shape significantly, allowing it to mostly retain the original form. This was also verified during cold runs to test SRT, with only a small fraction of the feedstock being crushed to smaller pieces. Regardless of particle size, homogeneous black colour was seen all the way to the centre of all char particles, suggesting all particles were fully pyrolysed and not partially torrefied.



Figure 4.7: Samples of three of the produced chars (3 min SRT).

An interesting observation regarding the chars was their electrostatic properties, causing them to stick to plastic and other surfaces (e.g., gloves), which can make handling difficult, especially when the char is in powder form. This property was less significant for chars produced at higher temperature, which can be connected to loss of chemical functionalities, which can decrease interactions between the char surface and other materials.

During the weighing of char samples for analysis, it was verified that the weights would keep increasing (slightly) for most of the chars. This was usually more noticeable for chars produced at lower temperatures. The increase in weight is likely due to a certain degree of hydrophilicity and hygroscopicity, especially for the lower temperature chars, which may have more ability to sorb moisture from air due to a higher presence of favourable surface chemical functionalities [341]. Higher temperature chars typically become more hydrophobic due to loss of chemical functionalities [342].

4.4.1. TGA profiles and proximate analyses

The solid products obtained from the slow pyrolysis experiments, after being ground and sieved to particle sizes $\leq 425 \mu\text{m}$, were firstly characterised by proximate analysis using TGA with the temperature programmes described in Chapter 3. TGA profiles (under nitrogen

atmosphere) of char products produced at different pyrolysis temperatures (and 10 minutes SRT) are displayed in Figure 4.8.

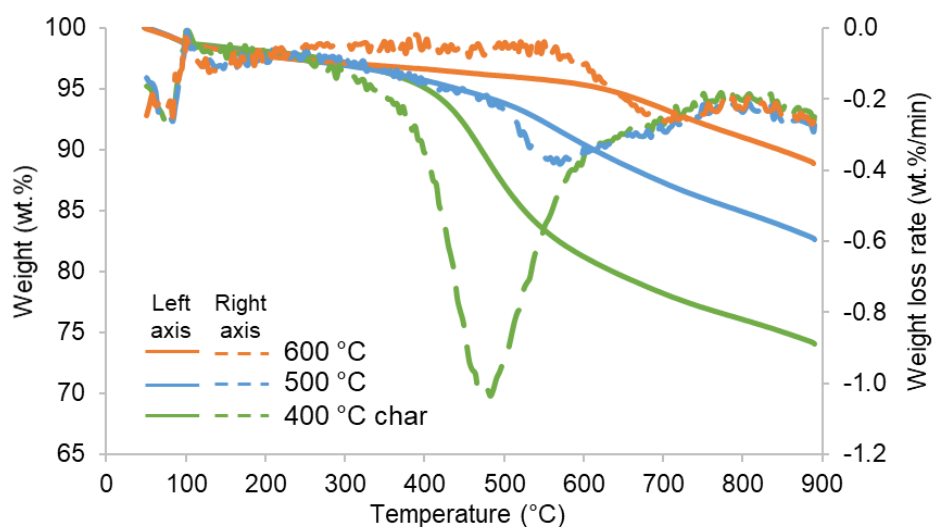


Figure 4.8: TGA profiles (N₂ atmosphere) of chars produced in the screw reactor from wheat straw with varying temperature (10 min SRT).

Comparing the TGA profiles of the chars with the one from the feedstock (Figure 4.1), the final residue under nitrogen atmosphere is much greater for the chars (≥ 65 wt.%) than for the wheat straw (≈ 20 wt.%). This is connected to the loss of volatile matter that occurred during the pyrolysis process, caused by the thermal degradation of a large proportion of the lignocellulosic material that composed the biomass feedstock.

With increasing pyrolysis temperature, it is possible to see that the peak of the DTG is shifted towards higher temperatures, and that it gets lowered. This is explained by the thermal degradation at different pyrolysis temperatures that the different chars went through, which removed more lignocellulosic material when processing temperature was increased. The chars produced at 600 °C, for example, only suffered significant thermal degradation in inert atmosphere at ≥ 600 °C, indicating that some lignin remained in the solid structure, and that cellulose and hemicellulose have been virtually completely removed.

The variation of the TGA profiles with SRT for each temperature is presented in Figure 4.9.

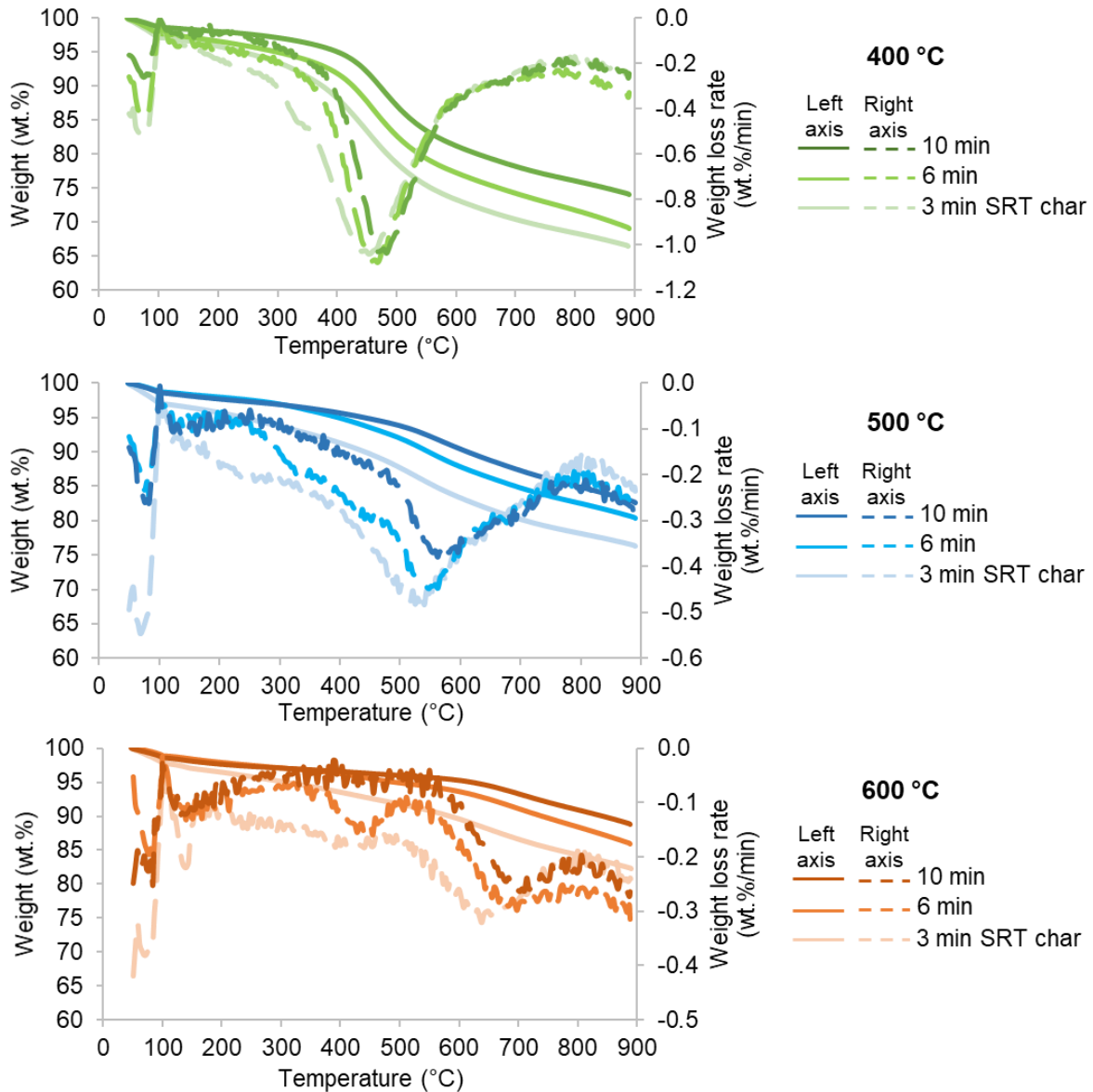


Figure 4.9: TGA profiles (N_2 atmosphere) for chars produced at different pyrolysis temperatures and SRT.

Regarding the effect of solid residence time, it was verified that chars produced using higher SRT had DTG peaks moved to higher temperatures, and also decreased, as had happened for increasing pyrolysis temperatures. This was verified for the three pyrolysis temperatures employed. These differences suggest that as the solids residence time inside the reactor is extended, volatile matter (probably from lignocellulosic material) is still being removed, making chars from higher SRT more stable and less prone to weight loss during the TGA programme.

Since the experiments with soaked and dried feedstock (0.1 wt.% moisture content) were done in the second screw reactor, it was necessary to compare the thermal degradation

of chars produced in both reactors in the same conditions. Figure 4.10 shows TGA profiles of chars produced at 400 and 600 °C with 10 minutes SRT from as-received feedstock.

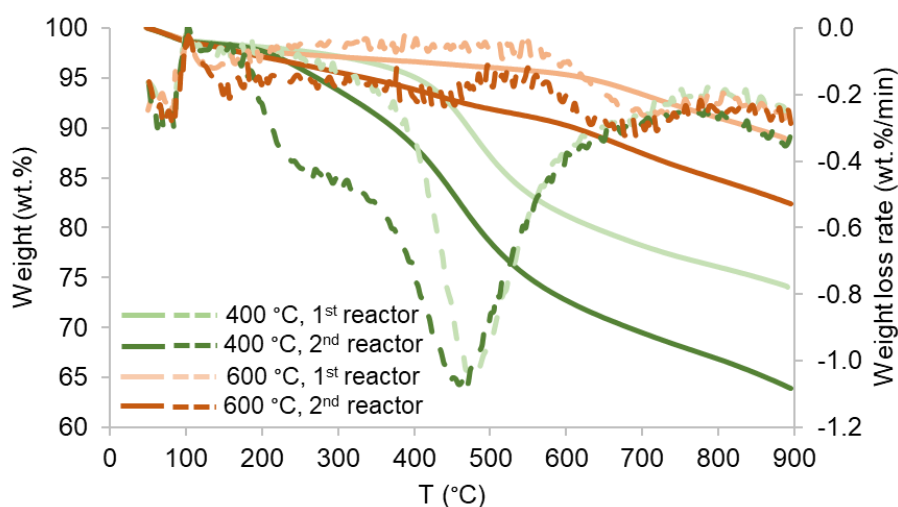


Figure 4.10: TGA profiles for chars produced at 400 and 600 °C (10 min SRT) in the first and second screw reactors.

Some differences were verified between TGA profiles of the chars produced in the two reactors. The main difference was that the chars produced in the second reactor had significantly greater weight loss. This was caused by more significant weight loss at lower temperatures compared to the chars produced in the first reactor. For 400 °C char from the second reactor, a pronounced weight loss started at ≈ 200 °C, then continued at a slower rate until ≈ 350 °C, and then the rate increased again until ≈ 450 °C, decreasing from then onwards similarly to the char produced in the first reactor. The char from the first reactor only had a main weight loss region, peaking at ≈ 480 °C. For 600 °C chars, the one from the first reactor also has one main weight loss region, peaking at ≈ 700 °C, while the one from the second reactor has significant weight loss in a region peaking at ≈ 450 °C. The weight loss starting at 200 °C for the 400 °C char from the second reactor could be attributed to volatiles trapped by the char during the slow pyrolysis process. If this was the case, then the char produced at 600 °C in the same reactor would also have similar weight loss, and since this was not verified, it does not seem to be the cause for the weight loss. Another reason for the different TGA profile could be due to secondary char, which was postulated to be favoured in the second reactor due to design differences leading to higher VRT and contact time between solids and vapours. The weight losses at lower temperature could also be due to carbonisation occurring to a lower extent in the second reactor, leaving more volatile matter in the char product compared to chars from the first reactor. This suggests carbonisation control in the second reactor is more challenging and that the measured temperatures may not be enough for that

control. The reasons for the different behaviours from the chars produced in the two reactors can be investigated by further analyses (proximate and ultimate analyses).

Figure 4.11 shows TGA profiles of chars with varying feedstock moisture content, for both 400 and 600 °C.

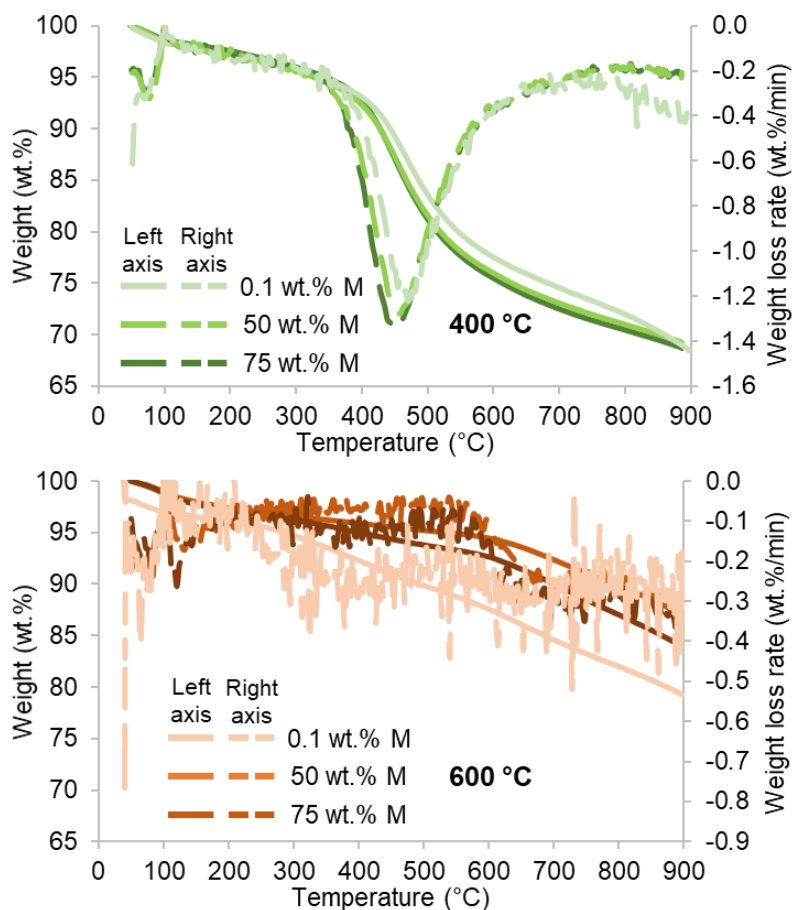


Figure 4.11: TGA profiles (N₂ atmosphere) of chars produced in the screw reactor from wheat straw with varying moisture content (10 min SRT).

Comparing the chars from 0.1 wt.% M feedstock to the ones with elevated moisture content, the thermal decomposition profiles were similar, especially at 400 °C. For 600 °C, the chars from 0.1 wt.% M feedstock had slightly higher weight loss. This could be related to the different reactor design (first reactor for elevated M chars; second one for 0.1 wt.% M chars), which was suggested to lead to lesser carbonisation extent in the second reactor (leaving more volatile matter in the solid product). The design differences may also lead to higher VRT in the second reactor, which can favour secondary char formation with different properties.

The 600 °C char produced from feedstock with 0.1 wt.% M had similar TGA profile to the one produced at 600 °C from as-received feedstock (Figure 4.10), with two weight loss regions around ≈ 400 and ≈ 650 °C. For 400 °C, however, the TGA profiles between those chars

were different, in that the weight loss in the region 200-350 °C is missing from the char from 0.1 wt.% M feedstock produced with the second screw reactor. This may be due to the difference in feedstock particle size/shape, which could facilitate thermal decomposition during slow pyrolysis.

Comparing with using as-received feedstock, using elevated feedstock moisture content resulted in chars with similar TGA (N₂) profiles, especially similar to chars produced with lower SRT (3 and 6 min) than chars from 10 min SRT. This can be related to the decrease in carbonisation time for feedstock with elevated M content, due to the need to evaporate more moisture.

Comparing between feedstock moisture contents ("M") of 50 and 75 wt.%, for 400 °C pyrolysis temperature there were no significant differences, unlike for 600 °C. This suggests different thermal degradation mechanisms occurring between different pyrolysis temperatures. The chars produced at 600 °C with 75 wt.% M had a slightly higher rate of weight loss than the ones from 50 wt.% M, and the total weight loss was ≈3 wt.% higher. This was probably due to the need to evaporate more water from the feedstock particles, which slowed heat transfer across particles. For the chars produced at 400 °C this effect did not occur due to the lower temperature, which the particles can reach in a shorter amount of time than 600 °C (and thus be exposed to that temperature for longer).

With TGA data, proximate analysis of the chars was performed, with the results indicated in Table 4.15. The chars in the table without an assigned feedstock moisture content are from wheat straw in as-received form (broken pellets, 4.8 wt.% M). Results pertaining to chars produced at 400 and 600 °C with 10 minutes SRT in the second screw reactor are also included, to compare with the chars produced in the first reactor under the same conditions. This is because the chars from feedstock with 0.1 wt.% moisture content were produced in the second screw reactor.

Table 4.15: Proximate analyses of chars produced from wheat straw slow pyrolysis at different pyrolysis temperature (T), solid residence time (SRT), and feedstock moisture content (M) (n=3).

T (°C)	SRT (min)	M (wt.%, wet basis)	Volatile Matter (wt.%, dry basis)	Ash (wt.%, d.b.)	Fixed Carbon (wt.%, d.b.)
400	3	4.8 ^{b)}	33.4 ± 1.8	13.9 ± 0.5	52.7 ± 1.5
	6	4.8	32.9 ± 1.0	15.0 ± 0.2	52.5 ± 0.8
	10	4.8	30.0 ± 3.5	12.9 ± 1.7	57.1 ± 1.9
	10 ^{a)}	4.8	39.8 ± 1.0	10.9 ± 0.1	49.9 ± 2.2
	10 ^{a)}	0.1	34.0 ± 1.4	13.4 ± 0.6	52.6 ± 2.5
	10	50	32.6 ± 1.0	14.2 ± 1.7	53.2 ± 0.7
	10	75	33.7 ± 2.6	14.7 ± 1.1	51.6 ± 3.8
500	3	4.8	23.6 ± 0.2	13.9 ± 0.8	62.5 ± 0.2
	6	4.8	21.5 ± 0.9	16.8 ± 0.2	61.7 ± 1.0
	10	4.8	20.4 ± 2.1	14.4 ± 1.1	65.2 ± 1.0
600	3	4.8	17.5 ± 0.7	15.0 ± 0.4	67.5 ± 0.7
	6	4.8	15.7 ± 0.2	17.5 ± 0.1	66.8 ± 0.3
	10	4.8	12.9 ± 0.2	17.4 ± 0.1	69.7 ± 0.1
	10 ^{a)}	4.8	22.6 ± 3.8	14.5 ± 0.8	65.0 ± 0.3
	10 ^{a)}	0.1	21.6 ± 0.6	18.0 ± 0.3	60.3 ± 0.7
	10	50	15.6 ± 0.2	18.9 ± 0.1	65.5 ± 0.3
	10	75	16.3 ± 0.3	17.0 ± 0.1	66.8 ± 0.2

Notes: a) Experiments performed in the second screw reactor.

b) Feedstock with 4.8 wt.% M was in as-received form (broken pellets).

The proximate analyses of the chars allowed to verify that an increase in pyrolysis temperature led to decreased volatile matter, and increased fixed carbon proportion, since thermal degradation (devolatilisation) keeps occurring when temperature is increased. This indicates that higher pyrolysis temperatures produce chars that are probably more appropriate for carbon storage in a soil application, due to higher fixed carbon content, correlated with higher char recalcitrance and stability [26][343]. Ash proportions in the chars also increased with pyrolysis temperature, since virtually all the inorganic matter remained in the solid product as volatile matter is lost [104][107]. The change in ash proportions was nevertheless not as significant as the changes in VM and FC with temperature. Since the wheat straw feedstock had a relatively low ash content (4.3 wt.%, dry basis), the resulting chars also had lower ash contents when compared with chars from other feedstocks. For example, chars produced from corn stalk and rice husk had ash contents between 20–33 wt.%, and 30–44 wt.%, respectively, because the feedstocks had an ash content of ≈10 and 16 wt.% (dry basis), respectively for corn stalk and rice husk [178]. A higher ash content is connected to a higher risk of fouling and corrosion when the char is applied for energy production through combustion [58]. The ash fraction and its contents also influence the char's potential soil applications [343].

For all three pyrolysis temperatures tested, an increase in SRT provoked a decrease in the volatile matter and increased fixed carbon content in the chars. This effect was also reported by Puy *et al.* for slow pyrolysis of forestry wastes in a screw reactor, using SRT between 1.5 and 5 minutes [126]. The authors in that study related this effect to continuing devolatilization reactions, supported by decreased char yields with SRT. The char yields stabilised from 2-3 minutes SRT onwards, and the authors mention this SRT as the minimum for complete devolatilization. In this work, char yields were not seen to decrease with SRT, on the contrary, a small increase was verified, although variation was low and comparable to standard deviation. In this work, decreased VM content and increased FC content, allied with similar or even increasing char yields suggests both devolatilisation reactions and secondary char-forming reactions can occur. The effect of SRT on ash proportion appeared to be an increase, but this trend was more difficult to ascertain, due to relatively low or contrasting variations.

Comparing chars produced in the same conditions in the two screw reactors, differences in proximate analysis were verified, most importantly: the second reactor produced chars with significantly higher VM fraction and lower FC.

Relating to the higher char yield obtained in the second reactor, this suggests the additional char produced contributed to volatile matter, instead of fixed carbon. This could be due to the previous suggestion that carbonisation occurred to a lesser extent in the second reactor compared to the first reactor. Secondary charring reactions may also be related to this and were suggested to be favoured in the second reactor in the previous subsection 4.3.2 (comparison of product yields between reactors). Solid product formed from secondary reactions (e.g., cracking and deposition of volatiles, tars and other compounds) has different characteristics compared to primary char [29]. A higher volatile matter content could result from volatiles and other compounds being deposited on the surface of the char, which would then be released during thermal degradation in TGA analyses.

From chars produced in the second reactor, the main difference was that volatile matter content in chars from 0.1 wt.% M feedstock was lower than in chars from as-received feedstock, although the associated standard deviations were relatively high. The differences can be attributed to the particle disintegration due to water soaking, which can improve heat transfer during slow pyrolysis. Despite the differences, the proximate analysis of chars produced in the second reactor were more similar between themselves than compared to chars produced under (supposedly) the same conditions in the first reactor. The differences suggest the two reactors can give repeatable results in terms of char yields, which were relatively similar, however char properties can be significantly different.

Regarding the effect of elevated feedstock moisture content ("M"), this parameter did not have a very significant effect on the proximate analysis of the chars, since the results were

within the range of results from the as-received feedstock. It was verified, however, that the volatile matter for chars from high M was closer to the higher-end of the values of volatile matter for the chars from as-received feedstock, which correspond to lower SRT (3 and 6 minutes). This can be explained by the fact that higher M increases the time required for carbonisation, because more energy is needed to remove the moisture from the solid, and the evaporation process is endothermic.

Connecting to the causes of the relatively lower char yields for the experiments with elevated moisture content, the proximate analyses give indications that the removal of excess water (for 75 wt.% M) was not the cause: the chars produced from wheat straw with elevated moisture content have ash proportion within the range of results from the as-received feedstock (because the feedstock ash content was not significantly modified, see Table 4.14). This confirms that, for the experiments with 75 wt.% M, where excess water was removed, the inorganic content was not significantly removed and thus did not cause the decreased char yields.

4.4.2. Ultimate analyses and inorganic contents

The char products were characterised by ultimate analysis, with the results shown in Table 4.16, along with atomic H:C and O:C ratios. The calculated higher heating values (HHV) using the correlation from Channiwala and Parikh (Equation 3.3 in Chapter 3) [303] are also included in Table 4.16. The sulphur content of the chars was ≤ 0.1 wt.%, so it is not shown. The chars without an assigned feedstock moisture content are from wheat straw in as-received form (broken pellets, 4.8 wt.% M). Results from chars produced in the second screw reactor are also included, to compare with the chars produced in the first reactor with 10 minutes SRT and at 400 and 600 °C. This is because the chars from feedstock with 0.1 wt.% moisture content were produced in the second screw reactor.

Table 4.16: Ultimate analyses (wt.%, dry ash free basis) and calculated higher heating value (MJ/kg, dry basis) of the chars produced from slow pyrolysis of wheat straw with varying pyrolysis temperature (T), solid residence time (SRT), and feedstock moisture content (M) (n=3).

T (°C)	SRT (min)	M (wt.%, wet basis)	C	H	N	O (by diff.)	H:C	O:C	HHV
400	3	4.8 ^{b)}	77.6 ± 0.3	5.0 ± 0.1	1.7 ± 0.0	15.6	0.77	0.15	26.9
	6	4.8	76.8 ± 0.0	4.5 ± 0.1	1.3 ± 0.0	17.1	0.72	0.17	25.7
	10	4.8	78.5 ± 0.2	4.6 ± 0.1	1.3 ± 0.1	15.5	0.70	0.15	26.6
	10 ^{a)}	4.8	75.1 ± 1.0	4.4 ± 0.1	1.6 ± 0.0	18.8	0.70	0.19	26.0
	10 ^{a)}	0.1	74.7 ± 1.9	4.2 ± 0.2	1.7 ± 0.1	19.3	0.66	0.19	24.8
	10	50	71.5 ± 0.0	3.7 ± 0.0	1.3 ± 0.1	23.4	0.62	0.25	23.2
	10	75	72.9 ± 0.1	4.0 ± 0.0	1.2 ± 0.0	21.8	0.66	0.22	23.8
500	3	4.8	82.5 ± 0.2	4.1 ± 0.1	1.5 ± 0.0	11.7	0.59	0.11	27.5
	6	4.8	82.9 ± 0.1	4.2 ± 0.0	1.2 ± 0.0	11.6	0.60	0.10	26.9
	10	4.8	83.2 ± 0.3	3.8 ± 0.1	1.2 ± 0.0	11.7	0.55	0.11	27.1
600	3	4.8	87.0 ± 1.3	3.4 ± 0.0	1.4 ± 0.1	8.2	0.46	0.07	28.1
	6	4.8	87.1 ± 0.0	3.3 ± 0.0	1.3 ± 0.0	8.1	0.45	0.07	27.3
	10	4.8	89.7 ± 0.2	3.1 ± 0.1	1.1 ± 0.0	6.0	0.42	0.05	28.0
	10 ^{a)}	4.8	84.2 ± 3.9	3.1 ± 0.0	1.3 ± 0.1	11.3	0.44	0.10	27.2
	10 ^{a)}	0.1	89.0 ± 1.3	3.0 ± 0.1	1.5 ± 0.0	6.5	0.40	0.05	27.5
	10	50	88.0 ± 0.3	3.2 ± 0.1	1.2 ± 0.0	7.5	0.43	0.06	27.0
	10	75	88.1 ± 0.3	2.7 ± 0.0	1.1 ± 0.0	8.0	0.37	0.07	27.2

Notes: a) Experiments performed in the second screw reactor.

b) Feedstock with 4.8 wt.% M was in as-received form (broken pellets).

The carbon proportion in the chars increased with pyrolysis temperature, while hydrogen decreased. As a result of this and along with oxygen fraction decreasing, the char heating value increased, although the ash content suffered an increase, but it was not as significant as the effects on the element proportions. The increase in carbon proportion and decrease in hydrogen and oxygen relates to the reactions happening during the pyrolysis process, e.g., dehydration (removal of hydroxyl groups) and decarboxylation and decarbonylation (removal of carboxyl and carbonyl groups) [344]. The trends of elemental composition with pyrolysis temperature indicate that the char is increasing its aromaticity (lower H:C ratio) and its resistance to degradation (lower O:C ratio) [345].

Although solid residence time did not have such a noticeable effect on elemental distribution of chars, in general (with some exceptions), the carbon proportion increased, while the hydrogen and oxygen fractions decreased, which can be correlated to the volatile matter content decrease (and fixed carbon increase), attributed to devolatilisation reactions still occurring for greater SRT. Secondary reactions due to extended contact time between vapours and solids could also be occurring, based on increasing char and gas yields and decreased liquid yields.

Comparing the chars with the wheat straw feedstock (18.3 MJ/kg, in Table 4.4), slow pyrolysis significantly increased the heating value, to an average for all chars of 26.5 (± 1.5) MJ/kg. The slow pyrolysis process has thus created a solid product significantly more valuable for energy generation (e.g., through combustion), mainly by decreasing the oxygen content. The results are comparable with the ones obtained from fixed bed slow pyrolysis of straw pellets by Ronsse *et al.* [307]. In that study, for chars produced at 450 and 600 °C, the HHV was 25–26 MJ/kg. In a study performed with the same screw reactor as in this work [178], corn stalk and rice husk chars (350–600 °C) had overall lower HHV than the wheat straw chars in this present work, especially the rice husk chars (17.1–21.3 MJ/kg). This can be explained mainly by the higher ash content that was present in these feedstocks (≈ 10 and 16 wt.%, dry basis, respectively for corn stalks and rice husk) [178]. This shows the greater value that the wheat straw feedstock possesses for energy generation, comparing with other herbaceous feedstocks. Furthermore, the obtained char HHV are comparable to or even higher than the HHV of some types of coals [346]. The chars produced at higher pyrolysis temperatures have a greater heating value than the ones from lower temperatures, although the effect is not very significant. The solid residence time did not produce a clear trend on the HHV of the chars. In terms of energy yields, based on char HHV and feedstock HHV (Table 4.4, page 144, subsection 4.2.2 in this Chapter 4), the char represented 40–51% of the feedstock energy. The energy yield decreased with temperature since the char HHV did not increase as much as the char mass yield decreased. The obtained results were comparable to the ones obtained by Park *et al.* for slow pyrolysis of rice straw (40–50% energy yield between 400 and 600 °C) [347].

Comparing the chars produced under the same conditions but in different reactors, there were significant differences, mainly, carbon content was lower from the second reactor, and oxygen content was higher. The difference was higher than comparing between chars with different SRT in the same reactor. This suggests low reproducibility of char properties between reactors, similarly to what was found with proximate analysis.

The chars produced in the second reactor from either as-received or soaked and dry feedstock, had similar elemental distribution, however, only at 400 °C. For 600 °C, the chars from soaked and dry feedstock were more similar to the other chars produced in the first reactor. This suggests different reactions occurred for different pyrolysis temperatures, although the same trend did not occur with proximate analysis, and that at 600 °C the difference in particle size had a more significant effect than at 400 °C. This was probably due to heat transfer: at 600 °C the particles in broken pellet (as-received) form take longer time to get heated up to pyrolysis temperature, compared to particles from soaked and dry (disintegrated) feedstock.

The increased feedstock moisture content only affected the elemental make-up of the chars produced at 400 °C pyrolysis temperature, since for 600 °C the results were in the same range as the chars from the experiments with as-received wheat straw (in the first reactor). For chars produced at 400 °C, the oxygen fraction suffered a significant increase (≈ 7.1 wt.%) with increased M, while carbon fraction decreased (≈ 6.2 wt.%). On the other hand, the nitrogen fraction did not suffer significant changes, and the hydrogen fraction decreased (≈ 0.7 wt.%), closer to the value of 500 °C chars from slow pyrolysis (higher carbonisation degree). The increase in oxygen proportion and decrease in carbon was an indication that the carbonisation process was occurring to a lesser extent, however the hydrogen fraction is instead decreasing. This suggests that the increased moisture and subsequent interaction of the evolved steam with the solid product changed the degradation mechanism, increasing the proportion of hydrogen released in vapour products, and lowering the proportions of oxygen and carbon. When analysing the gas product distribution from the 400 °C experiments (section 4.5), there was in fact an increase in H₂ fraction with increasing M, however with only a relatively small decrease for CO yields, and no change on CO₂ yields. The oxygenated compounds in the pyrolysis vapours could, nonetheless, have taken part of liquid product instead of the gas product.

The observed changes in elemental composition of the chars from using feedstock with elevated moisture content could have positive influence on the adsorption of organic contaminants from water. For example, a study of 21 types of chars found that higher O:C ratio correlated with higher cation exchange capacity, which improves adsorption [348].

The chars produced in the first screw reactor at the three tested temperatures and 10 minutes SRT were externally analysed for K, Si, Ca and P contents. The distribution of these inorganic elements in the char ashes, both in elemental and oxide forms, is presented in Table 4.17.

Table 4.17: Inorganic contents (wt.%, dry basis) in the ash from chars produced with varying process temperature (10 minutes SRT).

T (°C)	K	Si	Ca	P	K ₂ O	SiO ₂	CaO	P ₂ O ₅
400	18.6	14.0	7.4	1.8	22.3	29.9	10.3	4.2
500	14.5	11.6	5.6	1.5	17.5	24.7	7.8	3.5
600	14.9	14.6	5.9	1.5	18.0	31.2	8.2	3.4

In the wheat straw feedstock (Table 4.6), K₂O had a dominant proportion, whereas SiO₂ had highest concentration for the chars. This suggests K₂O suffered significant devolatilization during slow pyrolysis, and that SiO₂ is more resistant to degradation. It should be nevertheless noted that the inorganic contents of the feedstock were determined with XRF [332], and the chars with ICP, which can affect the detection of each element. Furthermore,

some of the inorganic composition could be in other forms besides oxide form, for example, in carbonate form, especially K_2CO_3 and $CaCO_3$, which increases the error in the mathematical conversion between elemental and oxide form.

As for the influence of pyrolysis temperature, overall, K, Ca and P contents decreased, suggesting part of these inorganic elements were devolatilised and contributed to vapour product. This has been verified in other instances from literature [188]. On the other hand, Si, although decreasing between 400 and 500 °C, its concentration for 600 °C char was greater than for 400 °C, suggesting this element devolatilised to a lower extent compared to other elements. This can be related to the relatively high melting and boiling points of Si and Si-containing compounds such as SiO_2 .

The inorganic elements present in the chars can be useful for soil applications, especially K and P that are important nutrients for plants [149][217]. For use as solid fuel, however, the char inorganic content may contribute to formation of slagging, fouling and corrosion upon combustion, especially from K and Si species with relatively low ash melting point [58]. For other applications such as adsorption, interactions with adsorbates may be negatively impacted by inorganic compounds which may be blocking pores and reducing surface area [307].

4.4.3. Surface functional groups

The solid products from slow pyrolysis of the wheat straw feedstock were analysed using FTIR to assess the presence of surface chemical functionalities. Figure 4.12 presents the spectra for the chars, as well as the feedstock's spectrum for comparison. The spectra for the different solid products are from chars produced with 10 minutes SRT. Since IR manifestation of the char materials was not significant for the region of wavenumbers 4000–2000 cm^{-1} , the spectra shown here only have the region of 2000–400 cm^{-1} wavenumbers. The full spectra can be visualised in Appendix C. The peaks/bands present in the spectra were assigned to surface chemical functionalities based on [333,334,336,349].

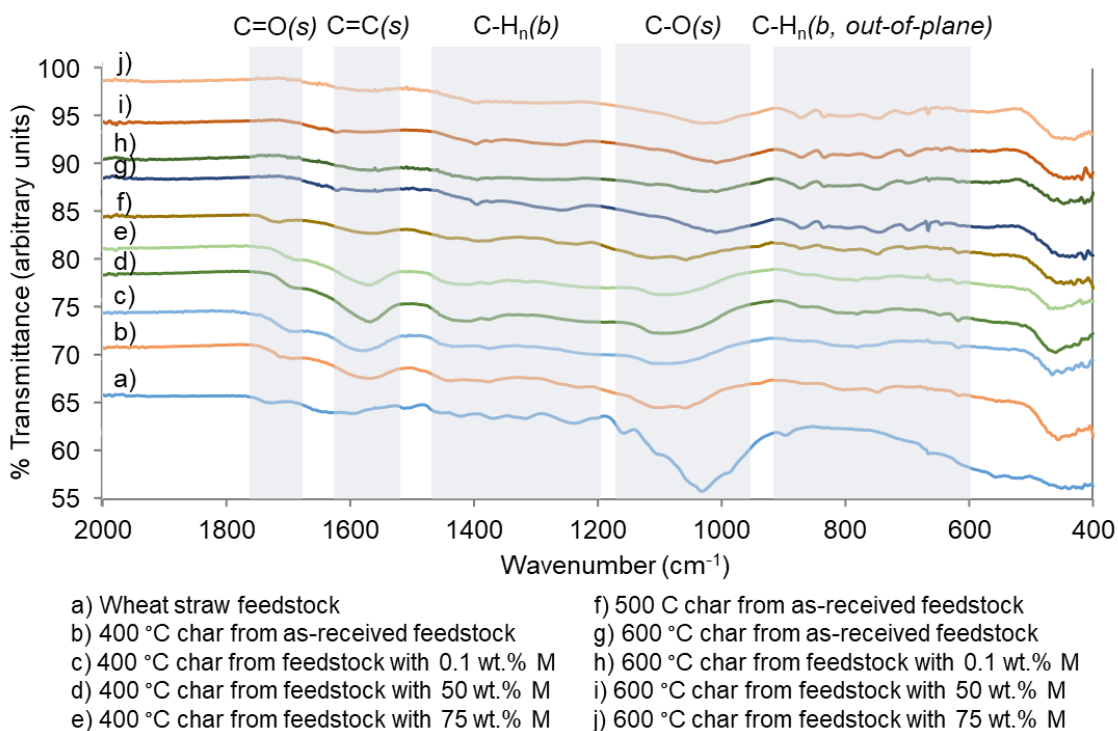


Figure 4.12: FTIR spectra for the wheat straw feedstock and chars produced from slow pyrolysis with 10 minutes SRT and varying temperature and feedstock moisture content.

The impact of solid residence time is not shown here since there were no significant feature changes with different SRT. Temperature was therefore the only parameter that significantly affected IR manifestation of the slow pyrolysis chars produced from the as-received wheat straw feedstock. The lack of effect of SRT on the surface functional groups can be correlated to the fact that this parameter was verified to not significantly change the elemental composition of the produced chars (Table 4.16).

Overall, for the slow pyrolysis chars, the spectra had only relevant IR manifestation for wavenumbers in the region 1800–400 cm^{-1} . The reduction in chemical functionalities is connected to a loss of surface chemical compounds in the form of volatiles, and to the development of an aromatic structure on the char product's surface when it is exposed to higher temperatures under pyrolysis conditions [334,350].

When comparing the FTIR spectra of the wheat straw feedstock with the chars, a considerable difference in IR manifestation was found, especially in the regions corresponding to O-H (band centered at $\approx 3300 \text{ cm}^{-1}$), aliphatic C-H_n (3000–2850 and 1200–1500 cm^{-1}), and C-O (1150–1050 cm^{-1}) bond vibrations.

The first band of O-H bond vibration was connected to the presence of moisture, alcohols and phenols, and in the char spectra this band practically disappears.

The presence of peaks in the region 2850-2950 cm^{-1} correspond to the stretching vibration of C-H_n bonds and indicate the presence of aliphatic compounds. This region in the

infra-red spectrum of the chars does not show significant manifestation, especially for 600 °C chars, indicating the loss of most linear hydrocarbons such as (low-molecular weight) paraffins [351]. This is also indicated by the lower intensity peaks in the region of 1350-1480 cm^{-1} (bending vibration of C-H), mainly found in the wheat straw spectrum.

The IR manifestation of C–O bonds present in the feedstock and significantly reduced in the chars was attributed to carboxylic and ester groups, and also to aromatic rings, while the aliphatic C–H_n bonds originated from the feedstock lignocellulosic biopolymers and fatty acids [335,337]. The region of wavenumbers 900–700 cm^{-1} corresponded mainly to the vibration of out-of-plane C–H_n bonds from aromatic compounds, and its manifestation increased with pyrolysis temperature. This was connected to an increase in aromatisation degree on the chars' surface, as a consequence of the increasing pyrolysis temperature [334]. In the work of Tag *et al.*, the FTIR spectra for the chars produced from agricultural residues at the highest studied temperature of 600 °C were considered to be similar to that of graphite, which has practically no IR manifestation [352]. Fu *et al.* considered this graphitisation to occur only at pyrolysis temperatures ≥ 800 °C for chars from agricultural residues [353]. The increasing upwards drift in the region 1200–400 cm^{-1} for the char produced at 600 °C was a baseline drift, which has been identified by other authors and attributed to an increase in carbonisation degree from high temperature [333].

A noticeable change with pyrolysis temperature is the absence of IR manifestation in the wavenumber region 1750–1650 cm^{-1} , corresponding to carbonyl (C=O) stretching bond vibrations, in the spectra of the chars produced at 600 °C, regardless of the feedstock moisture content. This peak was present for both the feedstock and the chars produced at 400 and 500 °C. This effect was found by Chen *et al.* for chars produced from pine needles when the employed pyrolysis temperature was higher than 500 °C [336].

Regarding the effect of feedstock moisture, it was verified that the chars from soaked and dried feedstock had no significant differences to the chars from as-received feedstock, which indicates that the particle size reduction due to soaking and posterior oven-drying of the feedstock did not impact the char's chemical functionalities analysed by FTIR. When the feedstock moisture was increased to 50 and 75 wt.%, however, this parameter produced noticeable changes in the FTIR spectra, however only for the chars produced at 400 °C pyrolysis temperature. There were increases in IR manifestation for the 400 °C chars produced from the wheat straw with elevated moisture content, mainly in the wavenumber region of 1800–1300 cm^{-1} (vibrations of C=C and C–H_n bonds), and also in the 1150–1050 cm^{-1} region (C–O bond vibrations). These changes were not found for chars produced at 600 °C, and the spectra for the four chars produced at 600 °C were approximately equivalent. The increase in C=C bonds on the char's surface could be produced by hydrocarbons suffering elimination

reactions, forming unsaturated compounds [351]. The increase in oxygen-containing functionalities in the 400 °C chars from the feedstock with increased moisture corroborated the increase in oxygen content for these chars (Table 4.16), which was not verified for the ones produced at 600 °C. It also connected to the pH value of the chars produced at 400 °C from elevated moisture content, which had significantly lower pH compared to chars from as-received feedstock.

It therefore seemed that pyrolysis temperature had a synergistic effect with feedstock moisture content in modifying char quality, with the lower temperature of 400 °C favouring reactions taking place between the vapours and the solid product. The reactions led to the differences in the elemental analysis of the chars from feedstock with elevated moisture content at 400 °C (mainly, increased oxygen content).

From the FTIR analyses it was verified that the solid products' surface suffered significant modifications with pyrolysis temperature and that it can also be affected by an elevated moisture content in the feedstock. With increasing pyrolysis temperature, surface functionalities on the surface of the solid were lost, mainly through the removal of O- and H-containing compounds. The removal of functionalities and increase in aromaticity promotes the stability of the char, making it more suitable for soil applications [198]. The functionalities gained for the chars produced at 400 °C and from wheat straw with elevated moisture content can lead to improvements in applications such as adsorption from aqueous phase due to an enhanced affinity for the adsorbates.

The changes in chemical surface features (e.g., polar groups) impact the basic/acidic character of the char's surface, and its hydrophobicity, and therefore influences potential applications [354]. The interaction of the char with a cationic compound, for example, can be improved, if the acidity of the char is increased, e.g., by introducing –OH functionalities on the surface [272]. Functional surface groups containing oxygen, such as –OH and –COOH, can act as binding sites for heavy metals, for example through complexation [355], which has benefits for liquid phase adsorption and soil applications. The processing of the wheat straw at lower pyrolysis temperatures and higher feedstock moisture contents can therefore possess advantages for these applications, in relation to higher pyrolysis temperatures and drier feedstock, since some potentially advantageous chemical functionalities were increased.

4.4.4. pH (in H₂O)

The solid products from the slow pyrolysis experiments with varying temperature and solid residence time were analysed in a water suspension for pH. The results of pH analysis are displayed in Figure 4.13. Error bars represent standard deviation, based on at least three measurements.

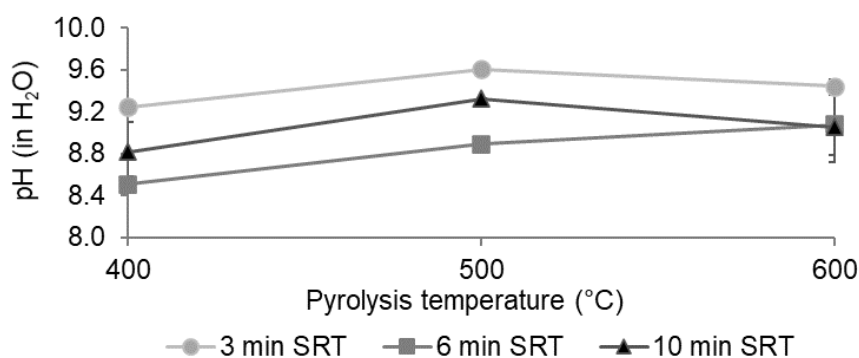


Figure 4.13: pH (in H₂O) of the produced chars with varying temperature and solid residence time.

The values of pH (in H₂O) for the chars from wheat straw slow pyrolysis with varying temperature and SRT were situated in the range 8.5–9.6, indicating a basic character of the chars. This represents an increase of pH when comparing to the wheat straw feedstock, which had a pH (in H₂O) of ≈7.3 (see section 4.2.3). The pH of the chars produced from the as-received wheat straw increase with pyrolysis temperature, however not regularly across all conditions, particularly between 500 and 600 °C. The cause can be the relatively low variation in ash contents between the chars produced at different temperatures, although there is a slight increase with pyrolysis temperature (values in Table 4.15). An increase of char pH with pyrolysis temperature was also found for several feedstocks for example by Ronsse *et al.* [307], which also verified that chars from pine wood had lower pH compared with wheat straw, green waste and algae chars. The pH values obtained in that study for wheat straw chars were in the range of 9.8–11.3 (450–600 °C pyrolysis temperature). Similar values of pH, of 9.0–10.0, were obtained by Budai *et al.* for chars from corn cob and *Miscanthus* produced in a retort at 400–600 °C [356]. The original feedstocks had a pH of 5.0–6.0, and the increase was found to be correlated with the loss of volatiles during pyrolysis, which reduced surface functionalities. In the work of Tag *et al.* [352], feedstocks with a higher ash content were found to produce chars with greater pH values. In terms of solid residence time influence, for the conditions used in the present work, the observed trend on char pH was 3 min > 10 min > 6 min, which does not correlate to the variation of char ash contents with SRT (highest ash content corresponds to a SRT of 6 min), unless the ash has an acidic character. Chars with basic character can be used in soil applications to reduce acidity in poor-quality soils, e.g., to rehabilitate former mine grounds [357]. Furthermore, chars with relatively high (basic) pH values have been found to reduce the mobility of heavy metals in soils [358].

The chars produced from the experiments with varying feedstock moisture content (“M”) were also analysed for pH in water suspension, with the results in Figure 4.14.

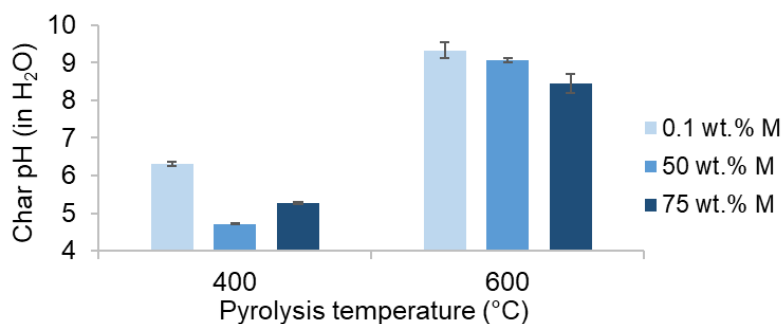


Figure 4.14: pH (in H₂O) of the produced chars with varying feedstock moisture content (“M”).

It was verified that the overall effect of increasing parameter M was a decrease in pH, i.e., the chars became more acidic than others. This occurred for both tested temperatures.

Comparing with the chars from as-received wheat straw, at 400 °C the chars with varying M became significantly more acidic (difference up to ≈3 pH units), which suggests that soaking the feedstock with water affected functional groups (and thus pH), potentially connected to particle disintegration and solubilisation (and re-precipitation) of inorganics. The effect was much less significant at 600 °C, which suggests different mechanisms occur with temperature and modify the char surface groups differently. These differences connect with the increase in char volatile matter and oxygen contents found through proximate and ultimate analysis, especially for 400 °C chars (Table 4.15 and Table 4.16).

Savova *et al.* studied one-step steam activation (120 mL/min flow, at 800 °C, for 1 hour) of five agricultural wastes, and found that solid products had a basic character (pH 8.1), and significant proportions of various oxygen-containing functional groups such as carbonyl and phenolic hydroxyl as analysed by Boehm titration [359].

The author would like to point out that the pH measurement of the chars in water was relatively challenging, due to different properties varying with production conditions, such as hydrophobicity. Furthermore, different research groups apply different procedures (i.e., different sample:water ratios, mixing and resting times, using aqueous solutions instead of only water), and the discrepancy in analysis methods limits comparisons between different studies. A recommended method for biochars [305] was found to have some limitations, for example due to a relatively low char:water ratio (1:10), which led to poor mixing. A char:water weight ratio of 1:100 (as used by Lima *et al.* [306]) was chosen to improve mixing. The mixing time was also prolonged (≈24 h) compared to the recommended method and other studies, to attempt to reach equilibrium, which however was not guaranteed. A method for pH quantification for char materials that can provide reliable and meaningful results should be developed and standardised.

As had occurred with surface functionalities analysed with FTIR, differences in char pH will affect its performance in various applications, including in liquid-phase adsorption, where the interaction with adsorbates in solution will be affected.

4.4.5. Porosity and surface area

The chars were analysed using nitrogen physisorption (77 K) to estimate porosity and surface area. For the chars produced with varying temperature and SRT, all isotherms and pore size distribution plots were similar, and an example for char produced at 600 °C and 10 minutes SRT from as-received feedstock is displayed in Figure 4.15. Isotherms and pore size distribution plots for all the analysed chars can be found in Appendix C.

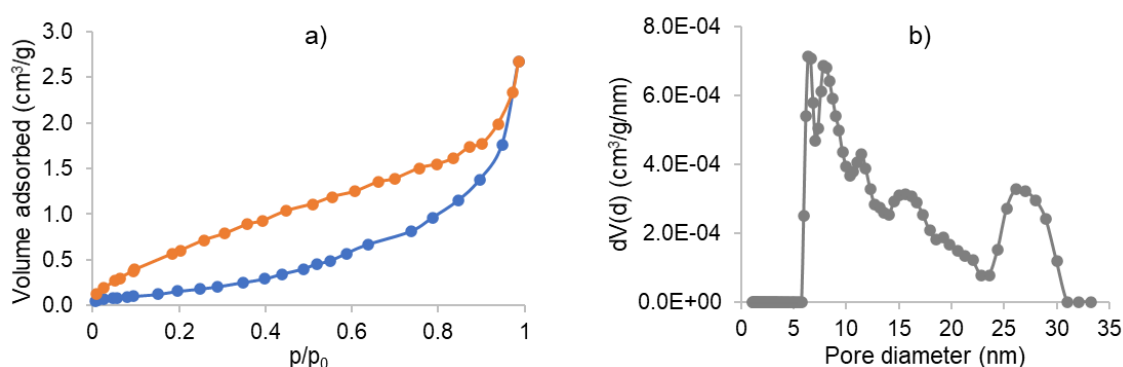


Figure 4.15: N₂ adsorption-desorption isotherm (a) and pore size distribution (QS-DFT applied on adsorption branch) (b) for char produced from as-received feedstock at 600 °C, 10 min SRT.

Overall, the low adsorbed volume showed that the chars had relatively very low porosity or can even be considered non-porous materials. Adsorption can also be occurring on uneven surfaces of the rough solid instead or on internal porosity [360]. The isotherms were either of type II or III, according to IUPAC designations, common of macroporous or non-porous materials [361]. Due to this, the BET theory which is commonly used to evaluate surface area of carbonaceous materials is likely to provide unreliable results [360], and the QS-DFT (Quenched Solid Density Functional Theory) was applied instead [311]. Furthermore, the QS-DFT considers surface heterogeneity in terms of heteroatoms and pore shapes [310].

The evaluated porosity on the chars was mainly due to mesoporosity, according to N₂ physisorption and QS-DFT model. Some hysteresis was also found for most analysed chars (in most of the whole range of p/p₀), which was related to intrapore condensation and/or odd-shaped pores (e.g., bottle-shaped) [360][361].

Regarding the effect of feedstock moisture content, some improvements were seen on the isotherms, although not that significant compared to porous materials. Overall, all nitrogen

physisorption analyses showed that the solid materials from slow pyrolysis with varying temperature, SRT, and feedstock moisture content were of low porosity.

A factor that can contribute to relatively low surface area and porosity is particle deformation and shrinkage during slow pyrolysis, which can modify pore structure [362].

The char produced with soaked and dry feedstock (0.1 wt.% M) at 400 °C produced a slightly different isotherm, with almost negligible adsorbed volume up to $p/p_0=0.9$ and then a sharp increase towards the end of the isotherm. This was regarded as adsorption on the external surface of the char, adsorption between particles, or even measurement errors. When this occurred for one of the chars produced at 600 °C, repeating the analysis resulted in an isotherm like the other ones. The analysis for the 400 °C char was not repeated due to the intrinsic low surface area.

The results obtained from applying the QS-DFT model to the adsorption branch of the isotherms are presented in Table 4.18. The chars in the table without an assigned feedstock moisture content are from wheat straw in as-received form (broken pellets, 4.8 wt.% M).

Table 4.18: Surface area, total pore volume and pore diameter (mode) of chars produced from slow pyrolysis of wheat straw with varying pyrolysis temperature (T), solid residence time (SRT), and feedstock moisture content (M).

T (°C)	SRT (min)	M (wt.%, wet basis)	Specific surface area (m ² /g)	Total pore volume (cm ³ /g)	Pore diameter (mode) (nm)
400	3	4.8 ^{b)}	1.1	0.004	5.0
	6	4.8	2.1	0.005	4.7
	10	4.8	3.3	0.007	5.4
	10 ^{a)}	0.1	N/A ^{c)}	N/A	N/A
	10	50	3.2	0.008	6.0
	10	75	8.8	0.020	5.4
500	3	4.8	1.8	0.005	5.6
	6	4.8	1.4	0.004	6.4
	10	4.8	2.8	0.007	5.6
600	3	4.8	1.9	0.005	5.0
	6	4.8	2.2	0.006	5.4
	10	4.8	2.3	0.007	6.4
	10 ^{a)}	0.1	2.0	0.005	4.2
	10	50	4.7	0.012	6.0
	10	75	4.9	0.013	5.2

Notes: a) Experiments performed in the second screw reactor.

b) Feedstock with 4.8 wt.% M was in as-received form (broken pellets).

c) Results unavailable due to isotherm measurement error.

The specific surface areas obtained for the produced chars were 1.1-8.8 m²/g, which was relatively low compared to what can be obtained from slow pyrolysis of biomass. Values

reported in the literature have considerable variation depending on process conditions, and can be up to hundreds of m^2/g [363]. Chars can then be modified to produce activated carbons with $>2,000 \text{ m}^2/\text{g}$ [364].

No significant difference was found comparing chars produced at different pyrolysis temperatures, and, although there is a trend of increasing surface area and pore volume with SRT, the variation is not significant due to being relatively small.

Values of surface area similar to the ones found in this work have been reported for chars from different feedstocks (poultry litter, vine prunings, orange pomace, and seaweed) and produced at temperatures up to $600 \text{ }^\circ\text{C}$ in a fixed bed reactor [352]. In a study with agricultural residues by Fu *et al.* [353], char surface areas only reached values $>20 \text{ m}^2/\text{g}$ when pyrolysis temperatures were ≥ 800 or $900 \text{ }^\circ\text{C}$, depending on the feedstock. On the other hand, Mohanty *et al.* performed pyrolysis of wheat straw (10 g , $\leq 1.3 \text{ mm}$ particle sizes) in a fixed bed reactor at $450 \text{ }^\circ\text{C}$, and obtained a char surface area of $\approx 180 \text{ m}^2/\text{g}$ [335]. The difference compared to the results in this work is probably due to the type of reactor and the feedstock particle size used, which is lower than the one used in this work. Low surface areas indicate that most of the pores are blocked, or that they are very narrow, not allowing adsorption of nitrogen at 77 K [333]. The ash content of the feedstock was found by Ronsse *et al.* [307] to be correlated with low surface areas, in chars produced from wood biomass and other biomasses with higher ash contents, such as wheat straw and algae. In that study, at $600 \text{ }^\circ\text{C}$ pyrolysis temperature, the woody feedstock (low ash content of $0.2 \text{ wt.}\%$) produced chars with up to $127 \text{ m}^2/\text{g}$, while the chars from wheat straw ($7.9 \text{ wt.}\%$ ash content) and the algae ($38.4 \text{ wt.}\%$ ash content) had 22 and $19 \text{ m}^2/\text{g}$, respectively. The inorganic contents could be deposited in the pores after being molten and re-fused. In the present study, however, the ash content of the wheat straw feedstock is not significantly high ($4.3 \text{ wt.}\%$, in Table 4.1), and so this effect would not be as noticeable. However, the effect of pore blocking could be potentiated during the pyrolysis process due to the lack of carrier gas, which increases the contact time between the solids and the produced vapours and reactions in which volatiles can be deposited on the char surface and pores.

A study of slow pyrolysis of coffee silverskin performed with the same screw reactor as this work [365] also obtained chars with low surface area ($<4 \text{ m}^2/\text{g}$), for both 400 and $500 \text{ }^\circ\text{C}$ operating temperatures (10 min SRT, no carrier gas). This suggests that the reactor configuration and consequential high degree of contact between vapours and solids could be the source of pore blocking, due to deposited volatiles or trapped inorganic content.

Regarding the effect of feedstock moisture, overall, there was an increase in surface area and pore volume for higher M , for both pyrolysis temperatures. The porosity increase was mainly in the region of mesoporosity ($2\text{-}50 \text{ nm}$), which has higher relevance for the adsorption of organic contaminants from water [235], however, the improvement was not that

significant to obtain relevant mesoporosity. Steam is known to provoke pore widening, typically yielding more mesoporosity compared for example to CO₂ activation [244]. This effect may be exacerbated in this work for chars from feedstock with elevated moisture content, in which water may have entered the lignocellulosic structure and thus be devolatilised with increased internal pressure.

The increase in surface area and pore volume, despite being relatively small, did correlate with the changes seen in char yields when using elevated M. For 75 wt.% M, char yields were significantly lower compared to using soaked and dried feedstock, while for 50 wt.% M the decrease in char yields was smaller, but still significant, especially at 600 °C. Indeed, the char produced at 400 °C with 50 wt.% M obtained surface area and pore volume similar to other 400 °C chars.

Some level of char activation during slow pyrolysis of wheat straw with elevated moisture content was hypothesized to have occurred due to gasification reactions, in which the solid develops a higher porosity and surface area compared to the chars from the experiments with lower feedstock M and as-received feedstock. This was suggested by the lower char yields, especially for 75 wt.% M (subsection 4.3.3). However, the relatively low surface areas and pore volumes observed for chars produced from feedstock with elevated M suggest that for the employed conditions, activation of the char due to the presence of steam from feedstock moisture did not occur inside the screw reactor. A steam activation process requires high temperatures, with 600 °C regarded as the minimum necessary [225][240], and this temperature was the maximum used in this work. Relatively long exposure times of the solid to steam (i.e., ≥ 1 hour) are also typically employed. Furthermore, the longer contact time between vapours and solid product due to the relatively long residence times, potentially promote entrapment of volatiles within the char matrix and consequent covering of the surface and closure of pores. The increased feedstock M, particularly at 75 wt.%, did cause a slight increase in surface area for both the pyrolysis temperatures tested, which was however not very significant for applications requiring high surface area such as gas adsorption.

Li *et al.* [195] found that steam activation (750 °C, 1 hour) of rice husk char led to a ≈ 7.8 -fold increase in surface area (to 351 m²/g), and a ≈ 5.6 -fold increase in pore volume. The increase in pore volume was due to micro- and mesoporosity, with micropores accounting for $\approx 44\%$ of total pores, and mesopores $\approx 56\%$.

One-step activation with steam (120 mL/min) at 800 °C for 1 hour was explored by Savova *et al.* for five agricultural wastes [359]. The study found that 1-step steam treatment could obtain relatively large BET surface area (497-1190 m²/g) and pore volume (0.58-0.83 cm³/g), and that pore sizes depended on the type of feedstock, specifically on the proportion of lignocellulosic compounds. One of the feedstocks (apricot stones) was subjected

to 2-step steam activation, and it was found that the 1-step process developed comparatively greater porosity and surface area. This was explained by the fact that after carbonisation (1st step), the solid material has a more ordered structure. This leads to higher stability and lowers reaction rates, for example of carbon consumption through steam gasification. It was also found that steam increased liquid and gas yields, which likely contributed to developing fissures and pores on the solid product. Furthermore, the flow of steam, removing primary volatiles, prevented those fissures and pores from being blocked by deposition of compounds from secondary reactions. Compared to the literature examples, the steam evolved in the screw reactor in this work did not significantly enhance char porosity evaluated with N₂ adsorption.

For testing the micropore range on chars, and especially narrow microporosity (or ultramicroporosity), CO₂ physisorption (273 K) is often employed in conjunction with N₂ physisorption (77 K) [203,360]. It was however not possible to test the produced chars with CO₂ physisorption in this work. Ultramicroporosity (pores ≤ 0.7 nm) can be found on chars and activated carbons with low activation degree [203]. However, for materials with polar surface chemical functionalities (such as the chars produced in this work), the CO₂ molecule is subjected to different surface interactions due to its quadrupole moment being larger than N₂, causing challenges in data interpretation [360]. Furthermore, for the application of the chars for adsorption of an organic contaminant from liquid phase, micropores (especially smaller micropores) are not as relevant as larger pores due to the size of the target contaminants compared for example to gas molecules in a gaseous stream [233][235].

Despite the relatively low porosity found on the chars, applications such as use as an adsorbent do not rely solely on porosity and surface area, but also on surface chemical functionalities [98,354,366].

4.4.6. Microscopic analyses with SEM

A selected number of the produced chars were analysed with Scanning Electron Microscopy (SEM) to assess morphological features at microscopic level. Due to limited availability of the SEM equipment and few morphological differences between samples, not all chars were evaluated, for example, only one SRT (3 minutes) was studied. Examples of micrographs from chars from slow pyrolysis of wheat straw with varying pyrolysis temperature are presented in Figure 4.16. The pictures on the left correspond to zoomed-in areas from the pictures on the right. The highlighted pore in the zoomed-in area of the 600 °C char micrograph has a diameter of ≈ 3.6 μm , according to SEM measurement.

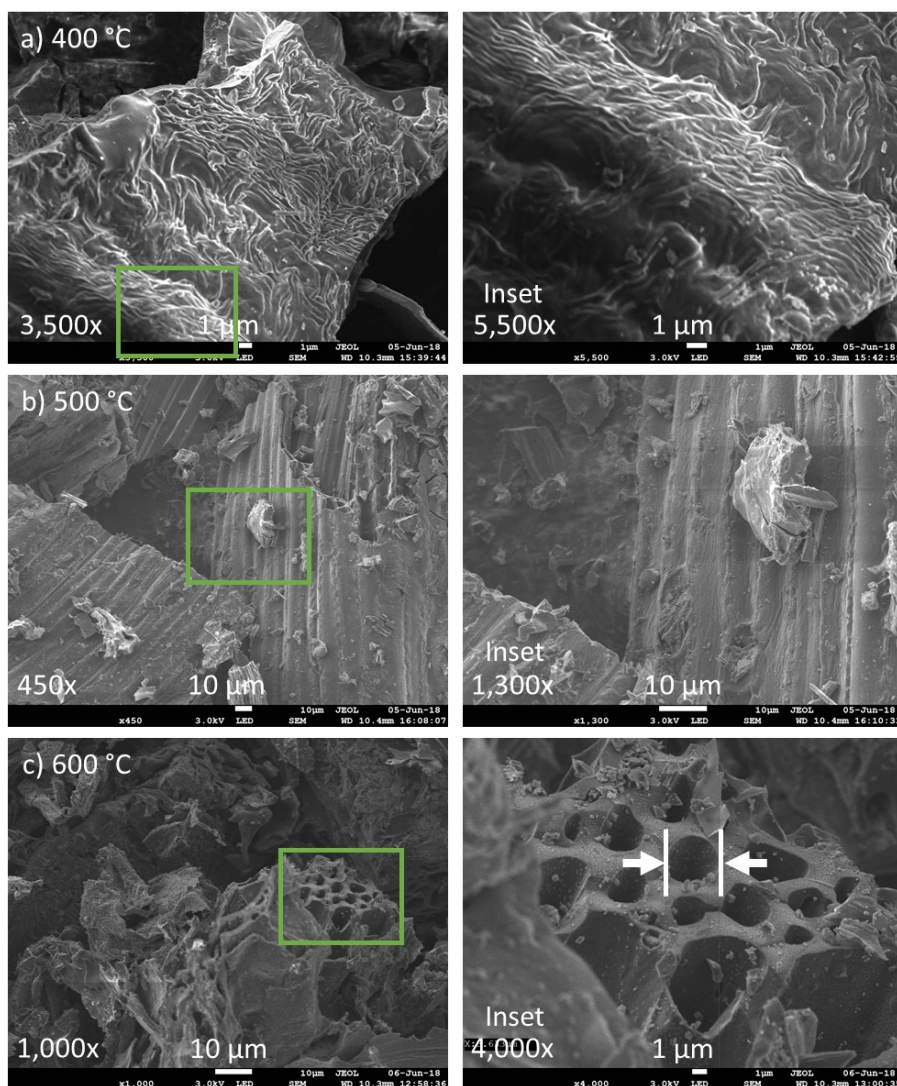


Figure 4.16: SEM micrographs of chars produced at (a) 400, (b) 500 and (c) 600 °C in the screw reactor with 3 minutes SRT and no carrier gas.

Zoomed-in areas highlighted in green rectangles are depicted on the right. The highlighted pore has $\approx 3.6 \mu\text{m}$ diameter.

The size of microscopic particles varied significantly, generally ranging 0.5-300 μm , with fractures seen on some particles, especially the larger ones. Particles were irregularly shaped, some with rough external surfaces and others with smoother surfaces. The particle sizes and shapes were influenced by the post-production grinding and sieving of the char (425 μm sieve). The char particles produced at the lowest temperature possessed smoother surfaces and less fractures compared to chars from 500 and 600 °C. This could be related to lignin, which goes through different processes such as softening, plasticisation and glass transition, depending on temperature [115][333][367]. Cellulose and hemicellulose are already thermally decomposed at $\approx 400 \text{ }^\circ\text{C}$ [105].

Pores were seen on some particles, which appeared to be channels from the original lignocellulosic matrix of the feedstock, through which the plant would conduct water and nutrients through. The micrographs suggest the pyrolysis process did not produce new pores besides the already existing ones from the biomass skeletal structure, and process temperature had little effect on microscopic appearance. This was in line with the results obtained from N₂ physisorption, which showed low porosity development regardless of process temperature.

Selected chars from experiments with elevated feedstock moisture content were also analysed with SEM, with micrographs presented in Figure 4.17.

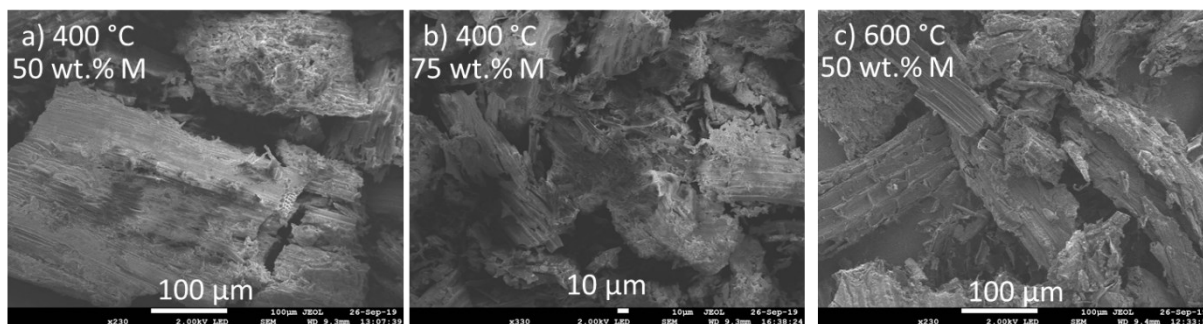


Figure 4.17: SEM micrographs of chars produced at (a) 400 °C and feedstock with 50 wt.% M, (b) 400 °C and feedstock with 75 wt.% M, and (c) 600 °C and feedstock with 50 wt.% M (10 minutes SRT, no carrier gas).

The chars produced from feedstock with elevated moisture content had the same overall microscopic appearance as the ones with as-received feedstock. An increase in particle fractures and roughness was verified on the micrographs, likely related to particle disintegration due to soaking with water during feedstock preparation. Feedstock moisture content did not have a significant effect on the microscopic appearance of the chars.

4.5. Characterisation of gaseous products

The gas product was analysed by the online MicroGC during each pyrolysis experiment. The data from the chromatograms was integrated afterwards and it was possible to obtain the proportions between the gaseous components (normalised to 100%).

The distribution of the gaseous species that comprise the gas product from the slow pyrolysis experiments with varying temperature and solid residence time are presented in Table 4.19. For each pair of pyrolysis conditions, the average density, molecular weight and HHV of the gas product are also indicated. The product yields corresponding to these slow pyrolysis experiments were presented in subsection 4.3.1 (Table 4.7).

Table 4.19: Distribution of gaseous species (vol.%) and main calculated properties from slow pyrolysis experiments using as-received wheat straw with varying temperature and SRT (n=2).

T (°C)	400			500			600		
SRT (min)	3	6	10	3 ^{a)}	6	10	3 ^{a)}	6	10
CO ₂	77.2 ± 0.6	76.4 ± 0.0	73.6 ± 0.9	70.8	65.6 ± 0.6	62.4 ± 2.1	57.5	48.3 ± 0.2	51.8 ± 0.0
CO	20.0 ± 0.3	19.5 ± 0.5	20.7 ± 0.7	17.2	19.3 ± 1.0	20.7 ± 0.1	18.1	22.7 ± 0.1	15.4 ± 0.1
CH ₄	1.8 ± 0.5	2.7 ± 0.3	3.7 ± 0.1	7.9	9.9 ± 0.3	11.7 ± 1.6	18.0	18.0 ± 0.2	20.1 ± 0.1
C _n H _m	0.9 ± 0.2	1.3 ± 0.2	2.0 ± 0.1	4.0	4.5 ± 0.1	4.5 ± 0.3	6.4	6.3 ± 0.1	6.4 ± 0.0
H ₂	0.1 ± 0.0	0.1 ± 0.0	0.1 ± 0.0	0.1	0.6 ± 0.1	0.7 ± 0.1	0.1	4.7 ± 0.2	6.3 ± 0.0
Density (g/cm ³)	1.68 ± 0.01	1.67 ± 0.00	1.65 ± 0.01	1.61	1.56 ± 0.00	1.53 ± 0.02	1.48	1.37 ± 0.00	1.36 ± 0.00
Molecular weight (g/mol)	40.2 ± 0.1	39.9 ± 0.0	39.4 ± 0.2	38.6	37.4 ± 0.0	36.6 ± 0.5	35.3	32.6 ± 0.1	32.6 ± 0.0
HHV (MJ/Nm ³)	3.6 ± 0.3	4.2 ± 0.2	5.0 ± 0.1	7.6	9.1 ± 0.0	9.8 ± 0.8	13.0	14.0 ± 0.0	14.2 ± 0.0

Notes: a) Only one experiment was performed due to exchange of screw motor.

Overall, in terms of composition, CO₂ was the main fraction, comprising at least half of the gas product, followed by CO, CH₄, light hydrocarbons (sum of ethene, ethane, propene and propane), and H₂.

CO₂ proportion decreased with pyrolysis temperature, while the proportions of CH₄, other light hydrocarbons and H₂ increased. Similar trends were found by Yu *et al.* on their study of corn stalks and rice husks in the same screw reactor for pyrolysis temperatures of 350–600 °C [178], with CH₄ having a noticeable increase and CO₂ suffering a pronounced decrease. The fraction of CO in this work did not show a clear trend with temperature. CO concentrations in pyrolysis gas from rice husks and corn stalks in the work by Yu *et al.* [178] were found to increase slowly with pyrolysis temperature: 14 to 19 vol.%, and 24 to 31 vol.%, respectively.

Hydrogen gas in this work was found to only be produced in significant amounts (≈1 vol.%) when pyrolysis temperature was ≥500 °C, and with a considerable increase to ≈5–6 wt.% at 600 °C. The relatively low fraction of H₂ obtained for 500 and 600 °C and 3 minutes SRT was due to a detection issue in the MicroGC equipment. Yu *et al.* found that H₂ concentration was negligible until ≈550 °C, when it suddenly increased to ≈1.8 vol.%, and then to 6.6 vol.% at 600 °C (for corn stalks) [178]. H₂ can be produced from cracking of hydrocarbons but requires more energy and relatively high temperatures [105]. Obtaining H₂ in pyrolysis gas is important since it has a greater heating value (per volume) than other gases.

Lignin was found by Yang *et al.* to be the main contributor to CH₄ and H₂ production due to having more aromatic structure and higher proportion of methoxyl groups [105], which correlates with a significant increase of those gaseous species with pyrolysis temperature in this work.

As was verified in section 4.3.1 regarding slow pyrolysis product yields, gas production increased for higher values of SRT, at the expense of liquid product. The reactions taking place caused an increase in the proportion of lower molecular weight gaseous species such as H₂, CH₄, and light hydrocarbons, based on MicroGC results. CO₂ was found to decrease with SRT, for 400 and 500 °C, while for 600 °C the trend was not verified, with a minimum being verified for 6 min SRT. This was attributed to integration errors in the MicroGC and other measurement anomalies, which could cause the CO₂ peak to be smaller for the 6 min SRT experiment, or other peaks to be higher, and thus decrease the CO₂ concentration to a greater extent. CO proportion showed different trends with SRT depending on temperature: at 400 °C there were no significant changes; at 500 °C it increased; and at 600 °C the CO fraction went through a maximum at 6 min SRT.

According to a TGA study of thermochemical decomposition of lignocellulosic components, Yang *et al.* found that CO₂ was more connected to primary pyrolysis reactions of cellulose and hemicellulose, while CO and CH₄ originated more from secondary reactions and their proportion increased upon extending the residence time of gaseous products [105]. Although the proportion of CO did not show an increasing trend with SRT for all temperatures, CH₄ proportion did increase with SRT.

According to the current knowledge, in cellulose pyrolysis, char yield originates mainly from secondary reactions, since the yield can be greatly minimised if secondary reactions are not favoured [115]. Secondary charring reactions of tar cracking in gas phase (homogeneous) create mainly CO and H₂, at >500 °C, and other secondary reactions, within the char structure (heterogeneous), can create CO₂, H₂O and PAHs [115]. These reactions are enhanced when VRT is increased, which occurs for higher SRT in this work (VRT values in Table 4.8). The fact that CO was not found to increase for higher SRT in this work can be related to the contribution of heterogeneous secondary reactions and/or of decomposition of other biomass components, e.g., lignin.

The heating value of the product gas increased significantly with pyrolysis temperature (due to increasing of combustible fraction), and with SRT as well, although not as significantly as with temperature. The gas product, especially from 500 and 600 °C, has a valuable heating value for energy production, which can be higher than for example typical gas products from gasification (4–13 MJ/Nm³) [368]. Using gas product HHV and density, it was possible to convert HHV to MJ/kg and calculate the energy yield from the gas product, which was 2-21%

of the feedstock energy content. Both the increase in gas product yield and concentration of combustible compounds with pyrolysis temperature contribute to the gas energy yield increasing. The energy yield from the gaseous product was significantly smaller compared to the char product (40-51%, see page 142), but comparable to what was obtained by Park *et al.* for rice straw slow pyrolysis [347].

Regarding the effect of feedstock moisture content (M), the gas products distribution for those experiments (400 and 600 °C, 10 minutes SRT) is indicated in Table 4.20. The product yields corresponding to these slow pyrolysis experiments were presented in subsection 4.3.3 (Table 4.11).

Table 4.20: Gas products distribution (vol.%) and main calculated properties from the slow pyrolysis experiments using wheat straw with varying feedstock moisture content (n=2).

T (°C)	400			600		
M (wt.%, w.b.)	0.1	50	75	0.1	50	75
CO ₂	58.5 ± 0.7	59.7 ± 3.1	60.9 ± 1.4	37.0 ± 0.5	50.5 ± 0.6	36.5 ± 1.7
CO	36.8 ± 1.2	34.7 ± 1.4	34.1 ± 0.3	31.8 ± 1.5	16.2 ± 0.0	26.2 ± 6.3
CH ₄	1.9 ± 0.1	1.4 ± 0.4	1.7 ± 0.0	15.5 ± 0.1	18.7 ± 0.2	11.0 ± 0.9
C _n H _m	1.0 ± 0.0	1.7 ± 0.6	3.2 ± 0.1	5.1 ± 0.2	6.6 ± 0.0	3.7 ± 0.4
H ₂	0.3 ± 0.0	0.5 ± 0.0	1.2 ± 0.5	10.6 ± 1.0	8.0 ± 0.3	22.6 ± 9.3
Density (g/cm ³)	1.54 ± 0.03	1.54 ± 0.05	1.56 ± 0.01	1.24 ± 0.01	1.34 ± 0.01	1.12 ± 0.11
Molecular weight (g/mol)	36.7 ± 0.6	36.9 ± 1.3	37.4 ± 0.2	29.5 ± 0.2	32.1 ± 0.2	26.8 ± 2.6
HHV (MJ/Nm ³)	5.8 ± 0.0	6.1 ± 0.2	6.3 ± 1.3	14.0 ± 0.1	14.1 ± 0.2	12.2 ± 0.2

The experiments using soaked and dried feedstock resulted in a decrease in CO₂, CH₄, and C_nH_m production, and an increase in CO and H₂ production, comparing to the experiments using as-received feedstock (Table 4.19), for both pyrolysis temperatures studied. The differences were more pronounced for 600 °C. The fact that the concentrations of the gas species changed for both pyrolysis temperatures employed, and that the liquid and gas yields were only significantly impacted for the highest pyrolysis temperature of 600 °C (Table 4.11), suggests that different mechanisms of lignocellulosic decomposition occurred depending on pyrolysis temperature and particle size, as reported in literature [107,115,340].

For 400 °C pyrolysis temperature, gas species concentrations did not change significantly with elevated M, besides a relatively small increase in C_nH_m and H₂ for the pyrolysis with 75 wt.% M. CO suffered a small decrease with increasing M at 400 °C. For the pyrolysis temperature of 600 °C, however, the gaseous product distribution suffered significant changes with M. The gaseous species CO₂, CH₄ and C_nH_m suffered an increase between using dried feedstock and using 50 wt.% M, and then a decrease when M was further raised. For CH₄ and C_nH_m, the decrease was even greater than the first increase. As for CO and H₂,

they suffered the opposite: firstly, a decrease when M was raised to 50 wt.%, and then an increase when M was further raised to 75 wt.%. It should be noted however that especially for the experiments with 75 wt.% M there were significant standard deviations for the peak areas registered by the MicroGC. This was especially noticed for CO and H₂ at 600 °C, and variations in the peak areas of some gaseous compounds affect the other ones due to the normalisation of results that is performed in this work. Nevertheless, even considering the high standard deviations for CO and H₂ at 600 °C with 75 wt.% M, the trend that was mentioned with M was still verified.

The steam gasification reaction ($C + H_2O \leftrightarrow CO + H_2$) can account for increased CO and H₂ yields, and there were probably contributions from other reactions, such as the water-gas-shift reaction ($H_2O + CO \leftrightarrow CO_2 + H_2$) [369]. The water-gas-shift reaction is exothermic, and therefore favoured by lower temperatures, which could account for the decrease in CO yield for the 400 °C experiments, and the increase in H₂ yields, however, without an increased CO₂ yield.

Ibrahim *et al.* did not verify differences in the molecular weight of the gas product from pyrolysis (475-575 °C) of wheat straw when the feedstock moisture content was increased to 15 wt.% [140]. Yang *et al.* found that gas distribution was not significantly influenced by feedstock moisture content (12.7, 22.8, 34.6, and 45.8 wt.%) in a slow pyrolysis study (450-850 °C) of the organic fraction of MSW in the same (first) screw reactor used in this work [142]. Pyrolysis temperature significantly affected gas product yields, however, the proportion of CO was found to not be greatly influenced neither by pyrolysis temperature nor feedstock moisture content [142].

4.6. Summary of Chapter 4

Different chars were produced from wheat straw slow pyrolysis in a continuous bench-scale screw reactor with varying pyrolysis temperature, solid residence time (SRT) and feedstock moisture content (M).

The dominant variable in terms of determining product distribution was pyrolysis temperature, with a more significant effect than SRT and M. As expected, char yields decreased with temperature, while gas yields increased. Liquid yields achieved a maximum yield at 500 °C slow pyrolysis temperature. SRT had a much smaller effect than temperature, and affected liquid and gas product yields more than char yield. The differences were connected to secondary reactions favoured by the longer contact time between vapours and char: gas yields increased and liquid yields decreased, while char suffered relatively small increases or remained equal (variation comparable to standard deviation).

The change in feedstock M content had consequences on the process, modifying VRT for example, and it also changed the particle size/shape, which also influenced the slow pyrolysis process. The particle size/shape change due to soaking the feedstock in water was found not to have significant influence for low feedstock moisture contents (i.e., between as-received and soaked and dried feedstock), however it could influence the process at higher values of feedstock moisture content. The use of elevated feedstock moisture content resulted in a significant decrease of char yields, especially with 75 wt.% M, for both 400 and 600 °C experiments.

Comparing product yields between soaked and dried feedstock with feedstock with 50 wt.% M, the differences were significantly smaller compared to 75 wt.% M, and were even similar to when processing feedstock with lower M. This suggests that it is possible with the screw reactor to obtain similar char yield from biomass whether it is wet or dry, which leads to savings in production cost due to avoiding feedstock drying. There were however consequences for the other products which can be detrimental, such as decreased liquid yield and quality.

The process parameters, especially pyrolysis temperature, also affected the char quality. A carbon content increase and a decrease in the hydrogen and oxygen fractions with increasing pyrolysis temperature led to an increase in the char's calorific value and stability. Increasing SRT caused a decrease in volatile matter and oxygen content, along with increased fixed carbon and carbon content. This was attributed to continuing devolatilisation reactions. Secondary reactions between the produced vapours and the char due to the extended contact time could also be occurring for higher SRT, since char yields did not decrease, and gas yields increased and liquid decreased. Surface chemical functionalities decreased with operation temperature quite significantly compared to the feedstock, and did not suffer significant changes with SRT. The pH value of the chars increased with pyrolysis temperature, and there was some effect from SRT, although the trend differed according to temperature.

When the feedstock was pyrolysed with elevated moisture content, solid product quality also changed, mainly by decreased in carbon content and increased oxygen content, which led to changes in FTIR spectra. The intensity of spectral features corresponding to surface chemical functionalities such as C–O and C–H_n suffered an increase. These changes were verified only for chars produced at pyrolysis temperatures of 400 °C, indicating that different thermal degradation mechanisms take place for different temperatures. The pH analysis of the chars found that elevated feedstock moisture content led to a pH decrease, likely connected to the increase in oxygen-containing functionalities.

All the produced chars obtained relatively low surface areas analysed with N₂ physisorption, with mesoporosity (2-50 nm) being the greatest contributor. This was likely due to the relatively low process temperature, and also due to high contact time between vapours

and solids within the reactor, which can lead to deposition of volatiles and other compounds on the char surface and pores. Chars produced from wheat straw with elevated moisture content had slightly higher surface area, however, the increase was not very significant (maximum was 8.8 m²/g). This suggests the steam evolved from the feedstock interacted with the solid material, for example by pore expansion during its evaporation, however, activation did not occur.

The chars described in this Chapter were tested in adsorption of an organic contaminant from water (Chapter 7). The changes in char properties observed for chars from feedstock with elevated moisture content can potentially lead to improved adsorption performance.

Chapter 5 – Slow pyrolysis with CO₂ as reaction atmosphere

5.1. Introduction

In the processes of physical activation for activated carbon production, usually the feedstock is firstly carbonised, and then goes through a second process where the atmosphere is CO₂ or steam (see Chapter 2, subsection 2.3.3.). For the experimental work of this thesis, it was not possible to do this with the screw reactor, because the solids are going to the char pot continuously with the screw movement. Hence, the slow pyrolysis process was carried out using CO₂ as reaction atmosphere/environment (injected in the gas inlet of the reactor system), and its effect on product yields and properties was analysed. It was hypothesised that having CO₂ during carbonisation could potentially modify char properties such as surface area (i.e., working as physical activation) and surface functionalities, in advantageous ways for the target application of adsorption of contaminants from liquid phase. Producing an efficient adsorbent through this one-step method can have potential advantages (time and resource-savings) over the standard two-step activation method.

This chapter discusses the results obtained from the slow pyrolysis experiments performed using CO₂ as reaction atmosphere (injected into the reactor). The experiments were performed in the second screw reactor described in Chapter 3, at 400 and 600 °C and with 10 minutes SRT. They are compared with the slow pyrolysis experiments performed without injected gas, and with the ones with N₂ as injected (carrier) gas. The wheat straw feedstock was used as-received (broken pellet form).

5.2. Product yields

Slow pyrolysis experiments described in this Chapter were performed with as-received wheat straw feedstock, at 400 and 600 °C, with 10 minutes SRT, and with different gases injected to the reactor: either N₂, CO₂, or no injected gas. These experiments were performed with the second screw reactor.

The temperature profiles inside the reactor for experiments with and without injected gas were similar to the one shown in Chapter 4 for experiments with the second screw reactor. The temperature measurements closer to the reactor exit (T3) and inlet (T2) were lower (≈ 40 °C) than the desired pyrolysis temperature, meaning the time during which the material inside the reactor was exposed to the maximum operating temperature was lower than SRT. Nevertheless, regarding carbonisation, it was considered that it was complete at the middle of the reactor tube, i.e., at ≈ 5 minutes for each fed feedstock batch, considering 10 min SRT.

This was because the temperature measured in the middle of the reactor (inside; T2) did not decrease significantly during operation, and the same occurred with the temperature at the end of the reactor (T3). Furthermore, the solid product is exposed to ≈ 400 °C inside the heated char pot. The temperature measurement closest to the start of the reactor did at times decrease, and when this occurred the furnace temperature was slightly increased (≈ 2 °C) as happened for experiments from Chapter 4. These remarks are valid if overall the process is considered endothermic, based on literature information and as discussed in Chapter 4.

The product yields (dry feedstock basis) obtained from the slow pyrolysis experiments using CO₂ or N₂ as injected gas, as well as without injecting gas, are presented in Table 5.1. Standard deviation is based on two experiments for each pair of conditions tested.

The losses for experiments with CO₂ reaction atmosphere at 400 °C were significantly higher than other experiments due to gas yields underestimation. The calculation of gas yields for experiments with CO₂ reaction atmosphere involved higher error because of uncertainty in operation time and in the CO₂ peak area corresponding to injected gas flow, which had to be subtracted.

Table 5.1: Product yields from slow pyrolysis experiments in the screw reactor without injecting gas or with N₂ or CO₂ as injected gases (number of experiments, n=2).

T (°C)	400			600		
	None	N ₂	CO ₂	None	N ₂	CO ₂
Char	36.8 ± 1.0	33.8 ± 0.3	34.1 ± 0.0	28.3 ± 1.5	28.9 ± 1.7	26.7 ± 1.7
Total liquid product	40.4 ± 0.8	45.4 ± 2.2	46.5 ± 0.3	36.2 ± 3.9	40.1 ± 1.2	40.1 ± 0.2
Aqueous phase	35.9 ± 0.1	40.5 ± 3.7	41.2 ± 0.4	28.4 ± 2.9	33.4 ± 1.0	34.6 ± 1.2
Organic phase	4.5 ± 0.7	4.9 ± 1.5	5.2 ± 0.8	7.9 ± 1.0	6.7 ± 0.2	5.5 ± 1.4
Gas product	20.2 ± 0.8	19.1 ± 1.4	9.6 ± 3.7	29.7 ± 5.0	28.9 ± 5.2	25.7 ± 0.2
Losses	2.6 ± 0.6	1.8 ± 3.3	9.9 ± 4.1	5.7 ± 0.5	2.1 ± 8.1	7.5 ± 1.2

The overall effect of injecting gas compared to not injecting, was an increase in liquid product yield, by ≈ 4 -6 wt.% for both tested temperatures. Char yields decreased, mainly at 400 °C, using N₂ or CO₂, while gas yields were impacted (decreased) by the use of CO₂ as reaction atmosphere, and not N₂. Despite a significant uncertainty associated with gas yields from CO₂ experiments, the overall trend was a decrease for both temperatures, compared to not injecting gas or using N₂.

For better visualisation of differences in char yields caused by using injected gases, the differences to the “control” experiments (without injected gas) are shown in Figure 5.1.

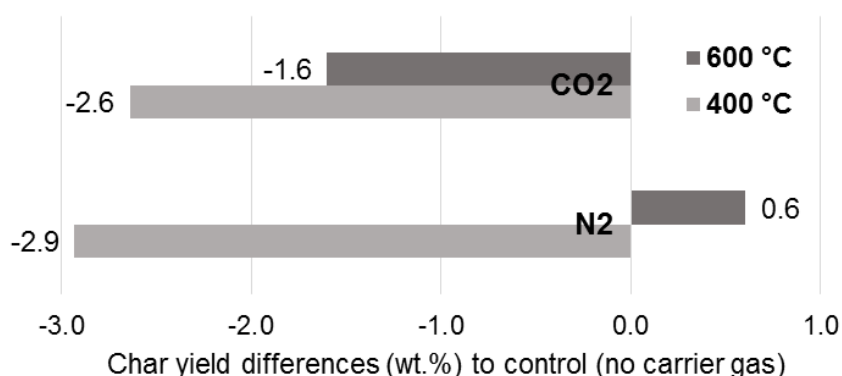


Figure 5.1: Differences in char yield (wt.%) between experiments with different injected gases and experiments without injecting gas.

Using CO₂ instead of not injecting gas caused char yields to decrease, especially at the lowest tested temperature of 400 °C. Using N₂ only caused relevant change in char yields for 400 °C, with a decrease similar to the one when using CO₂ as reaction atmosphere. The differences at 600 °C between injecting any gas (CO₂ or N₂) or not using one were not as significant, since they were within standard deviation for char yield (maximum 1.7 wt.%, from Table 5.1), especially for experiments with N₂.

Changes in VRT due to injecting gas could contribute to differences in product yields. Due to the higher gas flow rate from injecting gas, pyrolytic vapours were driven away from the reactor quicker (i.e., lower VRT), lowering contact time between pyrolysis vapours and solids inside the reactor, compared to when no gas is injected. This could decrease the occurrence of secondary reactions (e.g., volatile cracking and deposition) that typically form char and gas products at the expense of liquid product [13][29][116]. VRT values from both the visual method and from calculation using experimental gas flow rate are in Table 5.2.

Table 5.2: VRT values for experiments without injected gas or with N₂ or CO₂ as injected gases (n=2).

T (°C)	Injected gas	VRT, visual (min)	VRT, visual (s)	VRT, calc (s)
400	None	3.1 ± 0.2	188 ± 11	54 ± 0
	N ₂	3.0 ± 0.0	180 ± 0	46 ± 12
	CO ₂	3.3 ± 0.3	195 ± 21	87 ± 15
600	None	1.9 ± 0.2	113 ± 11	52 ± 30
	N ₂	2.0 ± 0.7	120 ± 42	33 ± 7
	CO ₂	2.4 ± 0.3	135 ± 21	25 ± 6

In terms of process temperature, higher temperature decreased VRT, which had been verified in previous experiments due to the evolution of more vapours from lignocellulosic compounds (Chapter 4).

The less significant effect of injecting gas on char yields for the highest temperature could be related to the fact that, at 600 °C, a greater vapour production occurs compared to lower temperature, due to the devolatilization of more lignocellulosic material, with VRT consequently reduced at the highest temperature.

In terms of the effect of injecting gas, a reduction of VRT could not be verified. VRT values estimated from the visual method were comparable between experiments with and without injected gas. As for calculated VRT, it was not possible to determine the effect of injecting gas due to relatively high standard deviations. It should be noted that injected gas flow was turned off during feeding, for safety reasons (gas could escape through the biomass inlet during feeding), which impacts VRT values, especially the visual method ones.

For 600 °C, injecting CO₂ caused char yields to decrease compared to not injecting gas, while using N₂ did not cause a significant change. However, comparing between CO₂ and N₂, the difference was significant (≈2.2 wt.% reduction), which suggests there could have been interactions between the injected CO₂ and pyrolysis products. Furthermore, the gas yield at 600 °C when using N₂ was more similar to the case of not injecting gas, than to the case of using CO₂.

For 400 °C, on the other hand, the effect on char yields of using CO₂ or N₂ was the same (a decrease), which suggests different reaction pathways depending on process temperature and type of injected gas.

To help identify possible causes for the differences in product yields, the distribution of gaseous species in the gas product analysed with MicroGC for each experiment is shown in Table 5.3. Calculated density, molecular weight, and higher heating value (HHV) are also shown. For experiments in which CO₂ was injected into the reactor, the determination of CO₂ produced by the pyrolysis process involved subtracting the peak area of the injected CO₂, as explained in Chapter 3 (subsection 3.3.3). For the experiments without injected gas at 400 °C there were some technical issues which limited the data that could be obtained during the experiments and caused increased standard deviation for CO and CO₂.

Table 5.3: Gas products distribution (vol.%) and main calculated properties from slow pyrolysis experiments using N₂ or CO₂ as injected gases or not injecting gas (n=2).

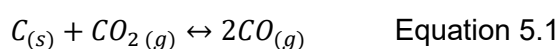
T (°C)	400			600		
Injected gas	None	N ₂	CO ₂	None ^{a)}	N ₂	CO ₂
CO ₂	59.4 ± 3.8	57.6 ± 1.2	54.4 ± 1.5	30.6	32.3 ± 0.3	27.5 ± 2.0
CO	37.9 ± 3.9	39.2 ± 1.4	42.3 ± 1.3	45.0	44.4 ± 0.5	47.8 ± 1.5
CH ₄	1.7 ± 0.0	2.1 ± 0.1	2.2 ± 0.1	12.4	11.3 ± 0.0	12.5 ± 0.1
C _n H _m	0.7 ± 0.0	0.8 ± 0.0	0.9 ± 0.0	4.4	4.0 ± 0.1	4.3 ± 0.1
H ₂	0.3 ± 0.1	0.3 ± 0.0	0.2 ± 0.0	7.6	8.0 ± 0.3	7.9 ± 0.2
Density (g/cm ³)	1.56 ± 0.03	1.54 ± 0.01	1.52 ± 0.01	1.24	1.25 ± 0.00	1.21 ± 0.02
Molecular weight (g/mol)	37.3 ± 0.6	36.9 ± 0.2	36.4 ± 0.3	29.6	29.9 ± 0.0	29.0 ± 0.4
HHV (MJ/Nm ³)	5.6 ± 0.4	5.9 ± 0.1	6.4 ± 0.2	13.6	12.9 ± 0.1	13.9 ± 0.3

Notes: a) MicroGC did not record data for one of the experiments due to equipment error (null standard deviation)

As had occurred for experiments from Chapter 4, higher pyrolysis temperature had significant influence on gas species distribution: CO, CH₄, C_nH_m and H₂ increased, while CO₂ decreased.

Regarding the effect of injecting gas or not, the differences were less significant compared to the influence of operating temperature, and the differences were mostly within standard deviation, especially when comparing absence of injected gas and using N₂. This is in line with the fact that N₂ is an inert gas, and that the effect of N₂ on the slow pyrolysis process was only a reduction of secondary reactions and consequent increase in liquid yield. On the other hand, when CO₂ was employed as injected gas, there was a more significant decrease in CO₂ and rise in CO (≥3 vol.%), for both temperatures. Other gaseous species were not significantly affected. The modification of gaseous product distribution suggests that besides reducing secondary reactions, there could have been interactions between the injected CO₂ gas and pyrolysis products.

The reverse Boudouard reaction (Equation 5.1), could increase CO yield and decrease char yield [244][332], and has been used in some research work to explain decreased char yields, even for relatively low temperatures [370]. The higher CO₂ concentration and partial pressure favours the Boudouard reaction in the reverse direction. However, this gasification-type reaction, based on theoretical calculations, is promoted by higher temperatures and only thermodynamically favourable at ≥710 °C, and can be relatively slow even at higher temperatures [371].



A lack of interaction at relatively low temperature between CO₂ and carbonaceous material had been verified by Duan *et al.* investigating coal pyrolysis [372]. The TG-FTIR study found that when comparing N₂ and CO₂ atmospheres, the only difference at <700 °C was an increased rate of volatile release at ≈480 °C, which correlated with increased CO production.

For the screw reactor used in this work, two main factors did not favour the occurrence of reactions between carbon in the char and CO₂, which are the basis for physical activation with CO₂. Firstly, the employed temperatures were relatively low compared to the ones typically used for CO₂ activation, i.e., >600 °C [240][225]. Secondly, the time of exposure of the solids inside the reactor to the CO₂ atmosphere was relatively short compared to traditional activation (usually >1 hour).

It should be noted that in this work, when not injecting gas, there was also a significant proportion of CO₂ in the pyrolysis vapours, the difference was that the flow rate was significantly lower than when using CO₂ as injected gas, especially at 400 °C. This was based on the findings from Chapter 4, in which CO₂ proportion in the pyrolysis gas was ≈48-77 vol.% and decreased with pyrolysis temperature (subsection 4.5, Table 4.19, page 156). The same was true for when using N₂ or CO₂ as injected gases, although the injected gas flow rate dilutes the pyrolysis gases. Thus, when CO₂ was not injected, there was still some contribution from CO₂ from the product gases, although less significant, due to the higher flow rate when injecting CO₂ gas and the higher contact time across the whole reactor.

A study comparing different atmospheres in pyrolysis of corncobs at 550 °C found that CO₂ produced the least char compared to using N₂, CO, CH₄, or H₂ as reaction atmosphere, which was attributed to the gasification reaction [370]. The production of CO and CH₄ was relatively high compared to using other atmospheres, although the total gas yield was not the highest, which was explained by a significant decrease in CO₂ product. That work however was performed in a fluidised bed reactor using 1-2 mm feedstock particles and silica sand as bed material.

A study of the same wheat straw feedstock used in this work, processed in a fixed bed reactor at 400-550 °C, found that switching from a N₂ atmosphere to a mixture of CO₂/N₂ (maximum 60 vol.% CO₂) did not significantly change char, liquid or gas yields [128]. The relatively small difference in char yield at 400 °C in this work is in line with those findings. However, injecting CO₂ and N₂ mixture of instead of using only N₂ as carrier gas caused higher CO gas yield [128][332]. This increase was hypothesised to be due to different processes: a) thermal cracking of volatile intermediates (e.g., carboxylic acids and phenolics); b) reverse water-gas-shift reactions (thermodynamically favoured, and likely promoted by a relatively high partial pressure of CO₂); and c) reverse Boudouard reaction (also promoted by high CO₂ concentration, despite being thermodynamically unfavoured and slow at the employed

temperatures) [332]. Furthermore, in that research, a decrease in water as pyrolysis product suggested that CO₂ promoted steam reforming (consuming water) and/or steam gasification reactions [128][332]. The role of CO₂ in promoting devolatilisation reactions has been mentioned by other research groups as the cause for the effect of CO₂ atmosphere on product yields from biomass pyrolysis [128][373][374].

The reverse water-gas-shift reaction (Equation 5.2), which is also favoured by higher temperatures and CO₂ partial pressure [128], could have occurred in the slow pyrolysis process. This reaction would contribute to increased CO yields and decreased CO₂, which occurred in this work.



Several researchers have reported increased CO yield when performing pyrolysis of biomass in a reactor with CO₂ atmosphere. Increased CO production was found in a TGA study comparing the effect of N₂ and CO₂ atmospheres on spent coffee grounds [371]. This was attributed to thermal cracking of VOCs and reactions with CO₂, since condensable hydrocarbons (tars) were reduced.

A TGA and batch reactor study with sewage sludge comparing N₂ and CO₂ atmospheres at 350-650 °C found that using CO₂ accelerated feedstock decomposition and led to lower char yields and higher liquid and gas yields (especially CO, H₂ and CH₄) [373]. CO₂ gas yield was reduced with increasing temperature for experiments with CO₂ atmosphere. It was postulated that CO₂ reacted with carbon through gasification, and also with H₂ and CH₄, through reverse WGS and methane dry reforming reactions, respectively. The CO₂ atmosphere could also promote volatile cracking and contribute to the increased CH₄ yield. These reactions could be favoured by the significant presence of inorganic elements in the sewage sludge feedstock. The observed differences in product yields under CO₂ atmosphere were more pronounced for higher temperatures (particularly, 550-650 °C), which was in line with the postulated reactions which are favoured by temperature increase.

Yang *et al.* performed a study in a fixed bed reactor with increasing CO₂ concentrations in the pyrolysis atmosphere for rape straw, corn stalks and camphorwood at 450, 550 and 650 °C [375]. They found that char yields increased with CO₂ concentration up to 50 vol.% CO₂, and then stabilised or decreased when only CO₂ was injected. The overall effect comparing using only N₂ or CO₂ as reaction atmosphere, was an increase in char yields, except for rape straw which did not have significant difference. The increases in char yield were connected to an inhibition of thermal degradation when CO₂ was present, since gas yields decreased as well. The differences to the results in this thesis are likely due to the

different reactor and process conditions, for example: the reactor was fixed bed, and the feedstock flow rate and total quantity were smaller (0.1 g/min for 15 min).

Cho *et al.*, in a TGA study of thermal decomposition of spent coffee grounds, found no significant difference comparing N₂ and CO₂ atmosphere, with only a slight further weight loss with CO₂ at ≥ 750 °C [371]. However, the presence of CO₂ led to increased CO gas production and reduction of condensable hydrocarbons (tars), which was attributed to thermal cracking of VOCs and possible reactions between VOCs and the CO₂ itself. Another study using several lignocellulosic feedstocks found the same results [374].

A study with rice straw comparing N₂ and CO₂ atmospheres in a fixed bed reactor at 300-450 °C found that using CO₂ atmosphere increased the liquid yields and decreased gas yields, which is in line with what was found in this work, however the trend for char yields was opposite (increased in that work) [376]. The effect on product yields was attributed to the occurrence of competing reactions, such as reactions between CO₂ and product gases, increasing condensable (liquid) products, and enhanced fragmentation and repolymerisation reactions which formed liquid and char products and decreased gas product.

Therefore, the effect of using CO₂ as injected gas on product yields, compared to using N₂, was considered as interactions with the solid product inside the reactor, promoting devolatilization, and thus decreasing solid yield and increasing the fraction of condensable vapour products. Analysing the characteristics of char products (subsection 5.3) can help verify if interactions occurred with the injected CO₂ gas.

5.3. Characterisation of solid products

The appearance of the chars was the same as the ones produced from varying temperature, SRT and feedstock moisture content in Chapter 4, so pictures of char produced from varying reaction atmosphere are not presented. The electrostatic properties and hygroscopicity verified in Chapter 4 were also noticed for chars produced with N₂ or CO₂ as injected gases.

5.3.1. TGA profiles and proximate analyses

The solid products obtained from the slow pyrolysis experiments with different injected gases, after being ground and sieved to particle sizes under 425 μm , were analysed by TGA with the temperature programmes described in Chapter 3. The TGA profiles (under nitrogen atmosphere) of char products produced at 400 °C (top graph) and 600 °C (bottom graph) with different injected gases (none, N₂ and CO₂) can be seen in Figure 5.2.

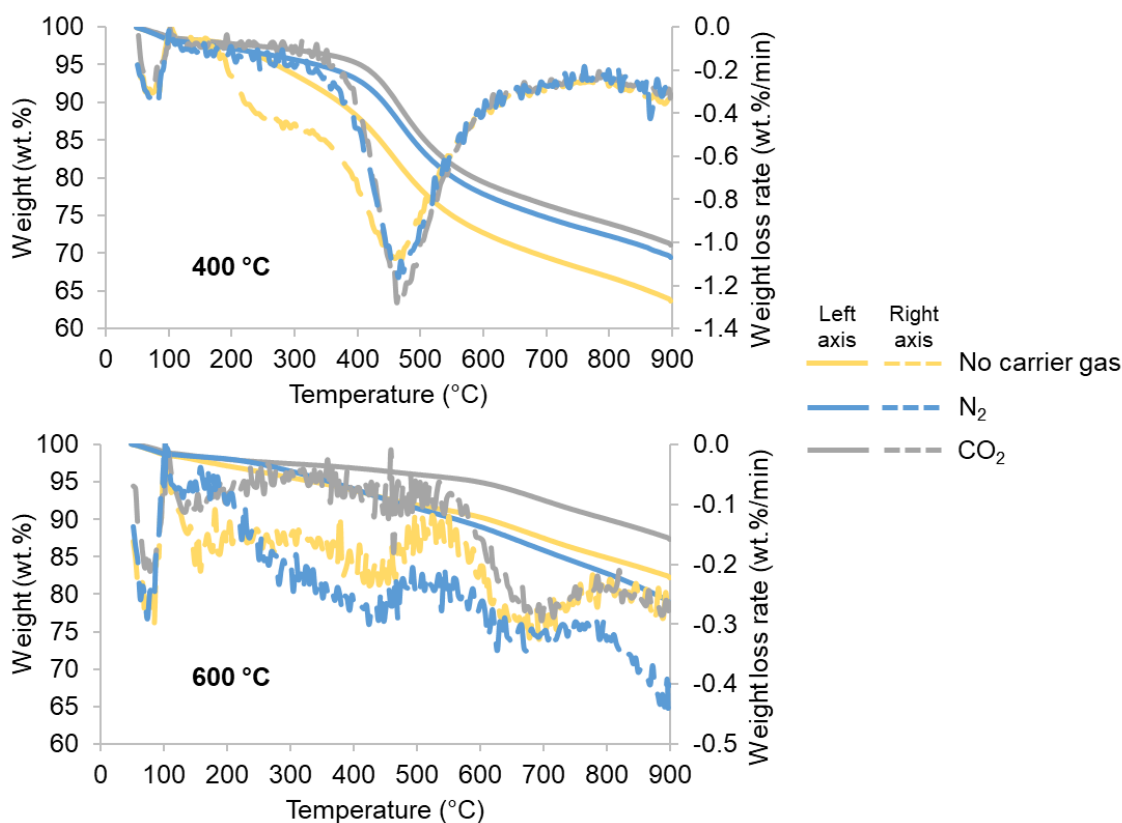


Figure 5.2: TGA profiles (N_2 atmosphere) for chars produced at 400 and 600 °C with N_2 or CO_2 as injected gases or without injected gas.

In the TGA profiles for chars produced at 400 °C the most significant difference was a weight loss at 200–400 °C for the char produced without injecting gas, which was not observed for chars produced with injected gases. This had been detected in Chapter 4 (subsection 4.4.1) when comparing 400 °C chars produced in both screw reactors used in this work (without injecting gas). The weight loss had been attributed to secondary char (due to higher VRT and contact time between solids and vapours) or carbonisation occurring to a lower extent in the second reactor (leaving more volatile matter in the solid to be devolatilised during TGA analysis), with the former being more likely due to design differences.

The second reactor was seen to have different heat transfer capability compared to the first reactor due to different design (subsection 4.3.2, Chapter 4). The heating up of the second reactor was slower, and there were significant temperature gradients between the temperature measurements along the reactor tube and thus the solids were exposed to the desired temperature for shorter time. This could lead to carbonisation occurring to a lower extent, leaving more lignocellulosic material unreacted. However, the temperature profiles inside the reactor (temperature of middle and final thermocouples, T2 and T3, not decreasing throughout experiments, see Figure 4.4, page 120) suggested carbonisation was complete, which was corroborated by visual inspection of char particles (black interior). Furthermore, the

char pot was also heated to ≈ 400 °C during those experiments. The fact that the weight loss did not occur for chars produced with injected gases suggests the injection of gases into the reactor promotes carbonisation.

For the 600 °C chars, the impact of injecting gas or not was not as significant. In this case, chars produced with N₂ as injected gas had weight loss more similar to chars from experiments without injecting gas, although the rate of weight loss was more distinct from the other chars, with greater weight loss at 200-350 °C and 800-900 °C. These weight loss regions did however not cause greater total weight loss for the chars from N₂ experiments.

Overall, the chars produced with CO₂ as injected gas (for both temperatures) had less weight loss, which suggests using CO₂ atmosphere increased the thermal stability of the solid product from wheat straw slow pyrolysis. This has been verified in other research examples [376]. The increase in stability benefits applications such as use as solid fuel and as soil amendment [198].

The proximate analysis results (dry basis) from solid products from slow pyrolysis experiments using CO₂ and N₂ (separately) as injected gases, as well as the ones from experiments without injecting gas, are presented in Table 5.4. The ash contents were determined with ASTM method (using an oven) instead of with TGA, which was the equipment used for volatile matter content determination (details in Chapter 3).

Table 5.4: Proximate analysis (wt.%, dry basis) of the chars produced from slow pyrolysis without injected gas and using N₂ or CO₂ as injected gases (n=3).

T (°C)	Injected gas	Volatile Matter	Ash	Fixed Carbon
400	None	39.8 ± 1.0	10.9 ± 0.1	49.9 ± 2.2
	N ₂	36.3 ± 4.4	12.6 ± 0.6	51.6 ± 4.8
	CO ₂	31.3 ± 1.0	11.8 ± 0.2	56.9 ± 0.4
600	None	22.6 ± 3.8	14.4 ± 0.8	65.0 ± 0.3
	N ₂	25.0 ± 0.6	14.5 ± 0.1	60.0 ± 0.0
	CO ₂	15.4 ± 1.1	14.3 ± 0.1	70.2 ± 0.1

The effect of temperature was the same as had been verified in the previous Chapter 4, of decreased volatile matter content and increased fixed carbon and ash contents for increasing slow pyrolysis temperature.

It was verified that the absence or presence of injected gas during pyrolysis in the screw reactor did not significantly interfere with the ash contents, while volatile matter and fixed carbon contents were altered.

The effect of injecting gas on volatile matter and fixed carbon contents depended on which gas was used, and the effect of using CO₂ was greater than using N₂. When using CO₂, the volatile matter content was decreased, while the fixed carbon content increased, for both

temperatures. The changes using N₂ at 400 °C were within standard deviation, and at 600 °C the trend inverted (volatile matter content increased compared to not injecting gas). The findings were correlated with the changes in product distribution from injecting gases (Table 5.1, subsection 5.2, page 163): using CO₂ decreased char yields at both temperatures, which only happened at 400 °C when using N₂. The results suggested CO₂ atmosphere promoted the release of volatile matter from the carbonaceous feedstock, which has been observed by other researchers even at relatively low temperatures [128][373][374].

5.3.2. Ultimate analyses

The ultimate analysis results (wt.%, dry ash-free basis) of chars produced under the different pyrolysis atmospheres are presented in Table 5.5, along with atomic H:C and O:C ratios and calculated high heating value (HHV). Sulphur contents are not presented due to no significant change for different injected gases, with ≈ 0.1 wt.% (d.a.f.) throughout all experiments presented here. Nitrogen contents did also not change depending on injected gas: 1.6 ± 0.1 wt.% for 400 °C chars, and 1.3 ± 0.2 wt.% for 600 °C chars.

Table 5.5: Elemental analysis (wt.%, dry ash-free) and HHV of chars produced from slow pyrolysis without injected gas and using N₂ or CO₂ as injected gas (n=3).

T (°C)	Injected gas	C	H	O (by diff.)	H:C	O:C	HHV (MJ/kg)
400	None	75.1 ± 0.9	4.4 ± 0.1	18.8 ± 0.8	0.70 ± 0.01	0.19 ± 0.01	26.0 ± 0.4
	N ₂	75.2 ± 2.9	4.1 ± 0.4	18.9 ± 0.9	0.65 ± 0.04	0.19 ± 0.01	25.2 ± 0.8
	CO ₂	69.6 ± 0.9	3.7 ± 0.1	25.0 ± 0.7	0.63 ± 0.00	0.27 ± 0.01	21.8 ± 0.4
600	None	84.2 ± 3.9	3.1 ± 0.0	11.3 ± 4.7	0.44 ± 0.03	0.10 ± 0.05	27.2 ± 1.8
	N ₂	85.9 ± 2.6	3.1 ± 0.1	9.4 ± 1.9	0.43 ± 0.02	0.08 ± 0.02	27.6 ± 0.6
	CO ₂	79.9 ± 3.0	2.8 ± 0.1	15.9 ± 1.9	0.42 ± 0.01	0.15 ± 0.02	23.8 ± 0.8

For the elemental analysis of the chars, it was verified that for both tested temperatures, only CO₂ atmosphere produced significant changes compared to not injecting gas, while using N₂ did not change elemental distribution significantly. The effect of temperature was the same as for Chapter 4: increased carbon contents and decreased hydrogen, nitrogen, and oxygen contents.

The effect of injecting CO₂ gas was that C and H contents were decreased, and O content increased (compared to not injecting gas). Nitrogen content in the char suffered no significant changes compared to other chars. The changes that occurred led to the higher heating value of the chars produced with CO₂ atmosphere dropping significantly compared to the other chars, mainly due to the decrease in carbon and increase in oxygen contents.

Connecting to changes in product distribution (Table 5.1, subsection 5.2, page 163), using CO₂ as injected gas was found to decrease char yields for both temperatures, and the elemental analysis of the chars suggests that the char yield decrease was likely due to loss of compounds containing greater proportions of carbon and hydrogen than oxygen. Changes in gaseous species production were however not in line with this suggestion because light hydrocarbons and hydrogen were not increased in the gas product for experiments using CO₂. Nevertheless, CO production increased, while CO₂ decreased, which can be connected to the increased oxygen content in the char.

Biswas *et al.* in a study comparing N₂ and CO₂ atmospheres in rice straw pyrolysis (300-450 °C) found that using CO₂ caused higher carbon, hydrogen, and nitrogen content, and lower oxygen content in the char product [376]. The changes were attributed to devolatilisation reactions and aromatisation of the char product.

From proximate analysis, it had been verified that chars from CO₂ experiments had lower VM content and higher FC content, especially compared to chars from experiments without injecting gas. Usually, when this occurs, it is allied to an increase in carbon content and decrease in oxygen content [29], however, this was not the case for the chars from using CO₂ as injected gas: VM decreased, however, oxygen content increased and so did O:C ratio. These results suggest oxygen was embedded into the carbonaceous matrix of the char, preventing oxygen from being released as volatile matter. This finding has implications for applications such as adsorption of contaminants due to potentially favoured interactions for example with polar groups, allied with higher stability based on lower VM content.

The observed changes in elemental distribution of the chars will likely affect adsorption performance, since they correlate with changes in surface functionalities, pH (in H₂O), and cation exchange capacity. For example, increased oxygen content and O:C ratio, found on chars produced with CO₂ as reaction atmosphere, was found to favour the adsorption of cations from water, due to higher cation exchange capacity [348].

5.3.3. Surface functional groups

The chars from slow pyrolysis of wheat straw pellets under no injected gas or with N₂ or CO₂ as injected gases were analysed with FTIR and the spectra are presented in Figure 5.3. The green spectra correspond to 400 °C chars, while the orange-brown spectra belong to 600 °C chars. The lighter coloured spectra correspond to experiments without injecting gas, the darkest coloured spectra to experiments injecting CO₂, and the middle one to injecting N₂.

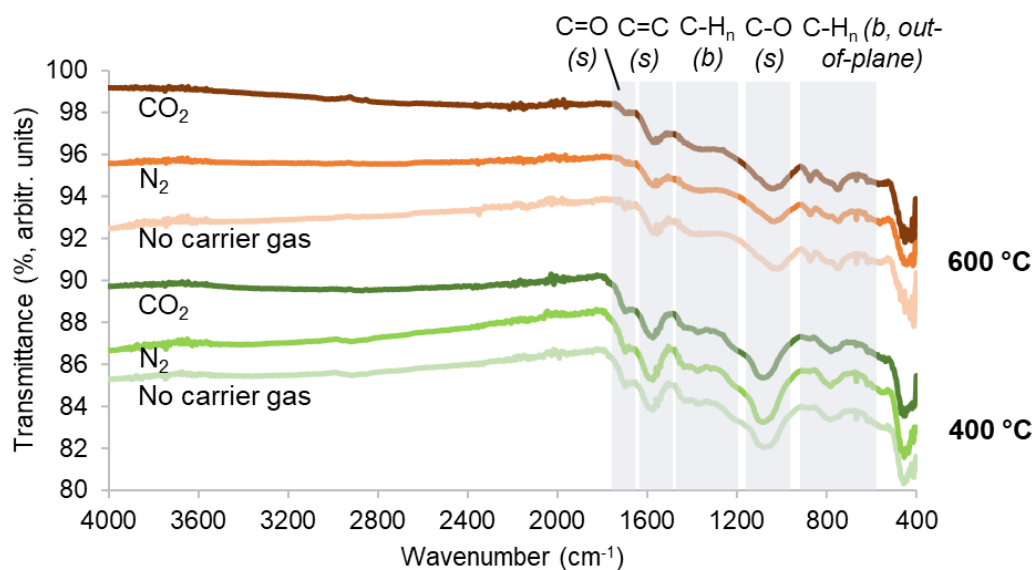


Figure 5.3: FTIR spectra of chars produced at 400 and 600 °C and absence of injected gas or using N₂ or CO₂ as injected gas.

Significant FTIR manifestation was only observed at 2000–400 cm⁻¹, as had occurred for the chars in Chapter 4. This signifies a diminishing of O–H and C–H_n functionalities for all chars.

Comparing chars produced at different temperatures, a lowering of surface chemical functionalities was observed, in line with the chars in Chapter 4. This was linked to loss of volatile matter and increase in aromatic structure on the char surface. The appearance of peaks for 600 °C chars in the region 900–700 cm⁻¹, corresponding mainly to vibration of out-of-plane C–H_n bonds from aromatic compounds, suggest a greater aromatisation degree. Manifestation of C–O bonds (1150–1050 cm⁻¹) suffered a significant decrease with pyrolysis temperature, indicating loss of volatile matter as CO or with C–O groups (from carboxylic and ester groups) [335].

Comparing between the different injected gases (or absence of), for the same pyrolysis temperature, the spectra were similar. The only observed difference was for chars produced at 600 °C with CO₂ as injected gas, in the 1750–1650 cm⁻¹ region, corresponding to carbonyl (C=O) stretching bond vibrations. In Chapter 4 (Figure 4.12, subsection 4.4.3, page 144), it was seen that these functionalities were found for chars produced at 400 and 500 °C, however not for the ones produced at 600 °C. In the case of chars from different injected gases at 600 °C, using CO₂ was found to increase FTIR manifestation in this region, comparing to using N₂ or not injecting gas. An increase was also noticed for the C–O region. This can be correlated with the higher oxygen content found for chars produced with CO₂ atmosphere, and suggests oxygen-containing groups were incorporated on the char surface, or that those groups suffered lower devolatilisation during slow pyrolysis.

Other research work studying chars produced from the same wheat straw pellets used in this work in a fixed bed reactor had also found greater FTIR manifestation of bond vibrations corresponding to oxygen-containing functional groups in chars produced with CO₂ atmosphere (mixed with N₂ 60:40 vol.%), compared to N₂ atmosphere [128]. For chars produced at 400 °C, this occurred for C-O and C=O bond vibrations corresponding to functional groups such as carboxyl, lactones, aldehydes and ketones. For 550 °C pyrolysis temperature, it occurred mostly for C-O bonds, because other functionalities decreased with pyrolysis temperature. The increases in oxygen-containing functional groups were explained by some oxidation occurring on the char surface.

In a study of 1-step CO₂ activation of oil palm stones (15 g) at 650-950 °C in a vertical tube furnace (0.5-3 hours activation time), activation temperature significantly reduced the presence of surface functionalities, and at 950 °C only carbonyl (C=O) groups attributed to quinones were detected [270]. Changes in surface functionalities such as an increase in oxygen-containing ones can lead to benefits in adsorption through favouring of electrostatic interactions.

5.3.4. pH (in H₂O)

The produced chars were analysed in terms of their pH in a water suspension and the results can be visualised in Figure 5.4.

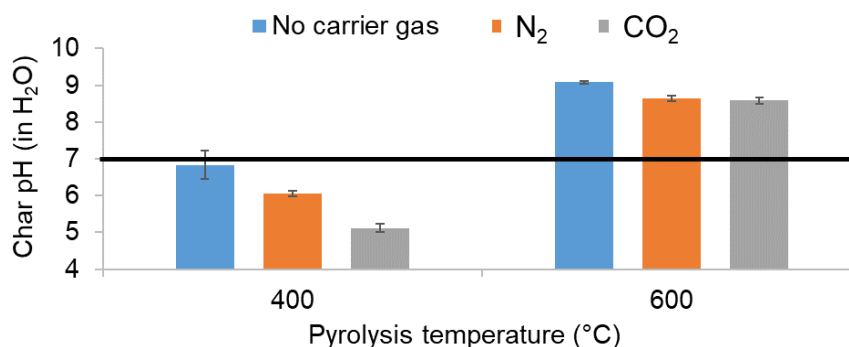


Figure 5.4: pH (in H₂O) of chars produced from slow pyrolysis without injected gas and using N₂ or CO₂ as injected gas.

The chars became more alkaline (i.e., pH increased) with pyrolysis temperature, which was due to the loss of surface functionalities [189][198], and had already been observed and explained for chars produced in Chapter 4. If applied to soils, the chars produced at higher temperature would be more favourable in acidic soils, with the opposite for lower temperature chars.

With the presence of injected gases (either N_2 or CO_2), chars became more acidic (i.e., pH decreased) compared to chars from experiments without injecting gas. Using CO_2 as injected gas had a greater effect than using N_2 , especially at 400 °C. The decrease in pH, particularly for chars produced with CO_2 as injected gas, can be related to increased oxygen content found through elemental analysis (Table 5.5, page 172). Oxygen in the char structure can be present in different forms, most with acidic character, such as carbonyls and carboxylic acids. The presence of oxygen functionalities was confirmed with FTIR for chars from experiments with CO_2 as injected gas. An increased oxygen content was however not found for chars produced with N_2 as injected gas, so this did not cause lower pH for those chars. Changes in pH of the chars in water can modify adsorption mechanisms and consequently the removal of contaminants from water.

5.3.5. Porosity and surface area

The chars were analysed with N_2 physisorption (77 K) and the produced isotherms for chars produced with N_2 and CO_2 as injected gas can be visualised respectively in Figure 5.5 and Figure 5.6. The results from chars produced without injected gas can be seen in Chapter 4, subsection 4.4.5.

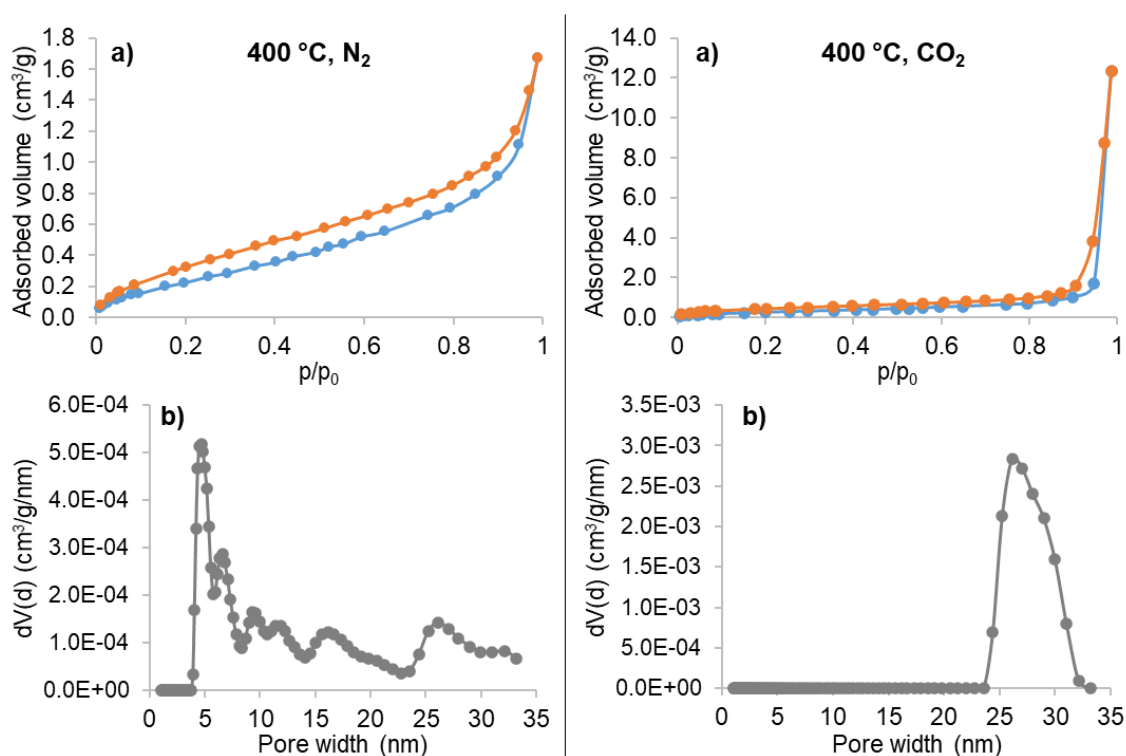


Figure 5.5: N_2 adsorption-desorption isotherms (a), and pore size distribution (QS-DFT applied on adsorption branch) (b), for chars produced from as-received feedstock at 400 °C with N_2 (left-hand side) or CO_2 (right-hand side) as injected gas.

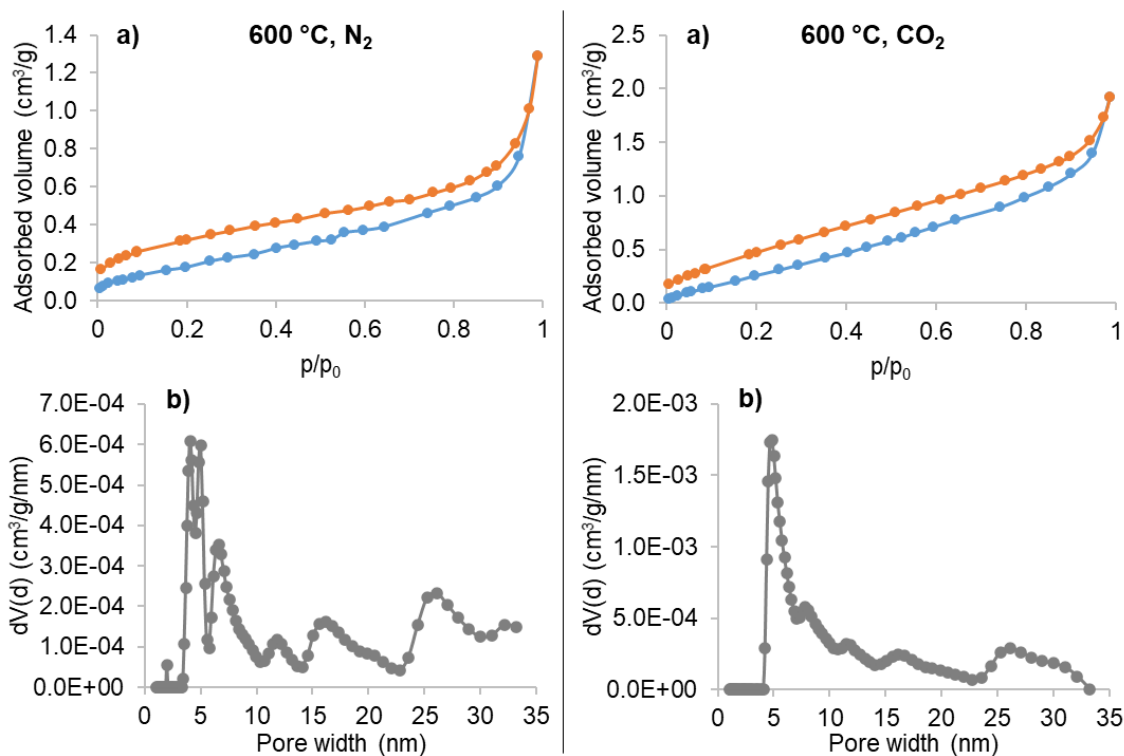


Figure 5.6: N₂ adsorption-desorption isotherms (a), and pore size distribution (QS-DFT applied on adsorption branch) (b), for chars produced from as-received feedstock at 600 °C with N₂ (left-hand side) or CO₂ (right-hand side) as injected gas.

Relatively low adsorbed volume was verified for all the chars, suggesting the materials are non-porous or with very low porosity analysed by N₂ physisorption. This was what occurred for chars analysed in Chapter 4, produced with varying temperature, SRT, and feedstock moisture content. The isotherms were also similar between each other, either of type II or III, according to IUPAC designations, common of macroporous or non-porous materials [361]. Some hysteresis was also found for chars produced with the different injected gases, indicating odd-shaped pores or capillary condensation [360][361].

No significant differences were found in the isotherms of chars produced with different injected gases or without injected gas. The char produced at 400 °C and with CO₂ as injected gas, however, had a different isotherm, with great increase in adsorbed volume close to the maximum partial pressure. This was observed also for one of the chars produced at 400 °C in Chapter 4 and explained by possible measurement errors or adsorption on external surface area or between char particles. The analysis was not repeated due to the intrinsic low surface area.

Table 5.6 shows the main N₂ physisorption results for chars from as-received wheat straw slow pyrolysis with N₂ or CO₂ or no injected gas, applying the QS-DFT model to the adsorption branch of the isotherm.

Table 5.6: Results from nitrogen physisorption at 77 K applied to chars produced using N₂ or CO₂ as injected gases or without injected gas.

T (°C)	Injected gas	Specific surface area (m ² /g)	Total pore volume (cm ³ /g)	Pore diameter (mode) (nm)
400	None	1.4	0.003	4.7
	N ₂	1.4	0.004	4.7
	CO ₂	N/A ^{a)}	N/A	N/A
600	None	1.5	0.004	4.1
	N ₂	1.8	0.005	4.1
	CO ₂	3.8	0.009	4.8

Note: a) Results unavailable due to isotherm measurement error.

The trend of surface area and total pore volume with temperature was overall of an increase, as had occurred for chars produced at different temperatures analysed in Chapter 4. The effect of temperature was however more noticeable when injecting gas, which was likely correlated to the lower VRT and thus contact time between vapours and char, which can lead to surface and pore covering by volatiles/tar.

As for the effect of injected gas, CO₂ resulted in the largest surface area and pore volume, especially at 600 °C. This was connected to a greater consumption of solid material when using CO₂, which had been observed in product yields (Table 5.1 and Figure 5.1). The increase, however, was not very significant and lower than what was observed in chars from feedstock with elevated moisture content (maximum 8.8 m²/g, Chapter 4).

It is known (see subsection 2.3.3, Chapter 2) that, overall, activation with CO₂ creates char with increased surface area compared to when using steam, due to the contribution of both pore widening and pore creation, with the latter occurring to a lower extent with steam [40][244]. This was, however, not the case in this work, although the chars produced from feedstock with elevated moisture content (acting as steam in the reactor during slow pyrolysis) had more wider pores than the ones produced from experiments with CO₂. This suggests pore creation when using CO₂ was very limited.

A study of CO₂ activation with almond shells found that the solid products had comparable or higher surface area when produced in 1-step, compared to 2-step activation, in the tested temperature range of 750-900 °C [377].

Lua and Guo analysed 1-step CO₂ activation of oil palm stones (15 g) at 650-950 °C in a vertical tube furnace, with activation time of 0.5-3 hours [270]. Different particle sizes (≤1.0 to 4.7 mm) and heating rates (5-20 °C/min) did not significantly affect char porosity, while temperature, activation time and CO₂ flow rate did. The gasification reaction between carbon and CO₂ was only favoured at ≥750 °C since the impact of activation time on solid yields was less significant at lower temperatures. Activation time had overall a negative effect on surface

area only when temperature was ≥ 900 °C, especially when using ≥ 2 h. Using ≤ 1 h caused a plateau on surface area for ≥ 900 °C. The effect of flow rate depended on temperature and was connected to the gasification reaction and thus burn-off as well. At 650 °C, surface area increased with flow rate, while at 850 °C it went through a maximum for 0.1 L/min, and at 950 °C it continuously decreased. The more severe burn-off was thus found for ≥ 850 °C and especially at 950 °C. The burn-off resulted in destruction of micropores and creation of meso and macropores, resulting in a broader pore size distribution for solids produced at relatively high temperatures and activation times. Optimal conditions for producing an activated carbon for application in gas-phase adsorption were 850 °C, 2 h activation time, and 0.1 L/min CO₂ flow rate.

Yang *et al.* studied 1-step CO₂ activation of coconut shells at 750-950 °C, using 30 g of precursor in a horizontal tube furnace. Optimal conditions for maximum BET surface area (1667 m²/g) and micropore volume (0.895 cm³/g) were found to be 900 °C, 140 min, 0.2 L/min CO₂ flow rate and 10 °C/min [378]. At 950 °C, the solid yield went down significantly (≈ 13 wt.% at 900 °C, to ≈ 6 wt.%), as well as BET surface area, total and micropore volume. This was attributed to excessive gasification reactions and expansion and eventual collapse of pore walls. Furthermore, microporosity was dominated by ultramicroporosity (≤ 0.7 nm) for activation temperatures of 750-850 °C, while for 900 °C, larger micropores, particularly 1-2 nm, became more relevant. Despite ultramicroporosity decreasing with activation temperature, micropore volume increased up to 900 °C, due to formation and enlarging of pores.

The micro and mesoporosity improvement with CO₂ as injected gas, although relatively small, could favour the adsorption of organic contaminants from liquid phase, which in general benefits from large micropores and mesoporosity [233][235][270].

5.4. Summary of Chapter 5

The injection of gases (CO₂ or N₂) into the reactor during slow pyrolysis overall decreased the char yields, also reduced gas yields, and increased liquid yields. This outcome was likely due to the lower vapour residence time when using injected gas flow, which reduced secondary reactions that produce char and gas at the expense of liquid product.

Char properties were more significantly modified for experiments using CO₂ comparing with using N₂ or no injected gas: volatile matter content decreased, and fixed carbon increased, although oxygen contents increased. The increase in oxygen contents was corroborated by changes in FTIR spectra, for which there was an increase in manifestation of C=O and C-O bond vibrations, at least for 600 °C chars. The porosity and surface area of the chars when using N₂ were similar to when not injecting gas, and there was a slight increase

when using CO₂ (maximum 3.8 m²/g, for 600 °C char). This suggested there were some interactions between the injected CO₂ and char, although not in a very pronounced way.

The results observed in this experimental chapter did not allow to confirm that it is possible to use the lab-scale continuous screw reactor to significantly increase the surface area of the char product, at least for the milder process conditions used (e.g., relatively low processing temperature and time) compared to the traditional process of activation. Although not in the scope of this work, exploring higher slow pyrolysis temperatures and injected gas flows could confirm or not that traditional activation can be performed in 1-step in the screw reactor system.

The results were also connected to the reactor configuration, which promotes contact between product vapours and solids inside the reactor tube (even though injecting gas reduced this to some extent). The prolonged contact can lead to secondary reactions (e.g., tar cracking and deposition of matter on solid products) and can also lead to the surface and pores of the chars becoming covered and blocked by volatiles and other deposited compounds (e.g., tars).

Although char surface area was not significantly improved with the injection of CO₂ in the slow pyrolysis process, other char properties were modified. Changes in properties such as surface functional groups and pH affect char applications, e.g., water decontamination. The effect of the observed changes will be explored in the experimental chapter regarding application of the chars for removal of an organic dye from water (Chapter 7).

Chapter 6 – Slow pyrolysis of KOH-impregnated feedstock

6.1. Introduction

Feedstock modification by KOH impregnation was performed to evaluate its effects on slow pyrolysis product yields and properties, focusing on the char product. The presence of KOH was hypothesised to potentially increase surface area (i.e., working as chemical activation), and/or add surface chemical functionalities, which could be advantageous for applying the chars in liquid phase adsorption.

Traditional chemical activation is done in a 1- or 2-step process, adding the activating agent to the feedstock, or to the carbonised feedstock (char), respectively. Doing activation in 1-step has lower costs, and a continuous process such as using a screw reactor can also have economic advantages compared to batch processing.

For chemical activation, KOH was chosen as the chemical agent. When using basic chemicals, there can be problems of corrosion, especially if temperature is relatively high. Using lower concentrations (0.1 and 1 M) of KOH reduces the risk of corrosion and related issues, and it should not affect the reactor materials and operation significantly. A lower KOH concentration also helps reduce production costs and can even serve to avoid the char washing step, which when performed creates harmful liquid waste streams and further adds to production cost.

If an adequate adsorbent can be produced under the conditions employed in this work, with performance comparable to a commercial activated carbon, then production costs compared to traditional activated carbon production can be lowered and the process becomes more sustainable.

In this chapter, the results obtained from slow pyrolysis experiments using KOH-impregnated wheat straw feedstock are discussed. The experiments were performed in the second screw reactor described in Chapter 3, at 400 and 600 °C, with 10 minutes SRT, and without carrier/injected gas. They are compared with the slow pyrolysis experiments performed without KOH impregnation, on soaked and dried feedstock. Product yields are presented, as well as char characterisation (proximate and ultimate analyses, FTIR, pH (in H₂O), and N₂ physisorption).

6.2. Characterisation of KOH-impregnated feedstock

Due to the modification of the feedstock by adding KOH, analyses were performed to evaluate if changes in proximate and ultimate analyses occurred. Table 6.1 presents

proximate analyses results for feedstock samples impregnated with different KOH solution concentrations ([KOH]), and Table 6.2 presents ultimate analyses. Also included are the analyses from KOH-free feedstock, from Chapter 4.

Table 6.1: Proximate analysis (wt.%, d.b.) of feedstock impregnated with different concentrations of KOH solution (number of experiments, n=3).

[KOH] (M)	Volatile Matter	Ash	Fixed Carbon (by diff.)
0 (Chapter 4)	79.4 ± 2.1	4.3 ± 0.3	16.3
0.1	80.6 ± 1.5	5.4 ± 0.4	14.1
1	76.6 ± 0.3	11.4 ± 3.1	12.0

Table 6.2: Ultimate analysis (wt.%, d.a.f.) and HHV (MJ/kg, d.b.) of feedstock impregnated with different concentrations of KOH solution (n=3).

[KOH] (M)	C	H	N	O (by diff.)	H:C	O:C	HHV
0 (Chapter 4)	49.3 ± 1.2	6.7 ± 0.0	0.9 ± 0.0	43.0	1.63	0.65	19.7
0.1	49.4 ± 0.5	6.0 ± 0.0	1.0 ± 0.1	43.5	1.46	0.66	18.7
1	50.5 ± 0.6	6.2 ± 0.1	1.1 ± 0.1	42.2	1.47	0.63	18.0

The addition of KOH to the feedstock, especially for 1 M KOH, caused ash contents to increase, since KOH is an inorganic material, and volatile matter and fixed carbon contents to decrease. As a consequence of greater ash contents, the HHV of KOH-impregnated feedstock was lowered compared to KOH-free feedstock, decreasing with KOH concentration.

In terms of elemental composition (organic material), the effects of KOH were less noticeable, besides a decrease in H contents for both KOH concentrations. The differences in other elements were within standard deviation. The decrease in H contents led to decreased H:C ratio for both KOH concentrations.

The changes in feedstock composition will affect the slow pyrolysis process, for example through favouring of secondary reactions by the increased inorganic contents.

6.3. Product yields

The slow pyrolysis experiments with KOH-impregnated feedstock were performed in the second screw reactor described in Chapter 3. The temperature profiles were similar to those observed with other experiments in that reactor, so they are not shown here.

The product yields from experiments using KOH-impregnated feedstock at 400 and 600 °C and with 10 minutes SRT are presented in Table 6.3. It includes the product yields from experiments with soaked and dried feedstock, which serve as control experiments (0 M KOH), without KOH impregnation but with water soaking and drying.

Table 6.3: Product yields (wt.%, dry and KOH-free feedstock basis) from experiments using KOH-impregnated feedstock in the second screw reactor (n=2).

T (°C)	400			600		
KOH solution concentration (M)	0	0.1	1	0	0.1	1
Char	36.8 ± 0.2	39.1 ± 1.3	40.9 ± 1.1	29.8 ± 0.5	31.0 ± 0.1	30.9 ± 0.5
Total liquid product	42.1 ± 2.0	41.6 ± 2.0	36.5 ± 1.6	34.2 ± 1.2	30.9 ± 6.4	29.7 ± 1.5
Aqueous phase	33.6 ± 1.8	31.3 ± 1.2	30.9 ± 0.5	27.1 ± 0.9	21.6 ± 7.6	21.1 ± 1.2
Organic phase	8.6 ± 0.2	10.3 ± 0.8	5.6 ± 1.1	7.1 ± 0.3	9.4 ± 1.2	8.6 ± 2.7
Gas product	20.2 ± 0.8	21.7 ± 0.3	21.4 ± 0.1	34.1 ± 0.1	31.5 ± 0.2	42.4 ± 0.4
Losses	0.9 ± 2.5	-2.4 ± 3.7	1.2 ± 0.7	1.8 ± 1.6	6.5 ± 6.7	-3.0 ± 1.7

It should be noted that gas and liquid yields have greater associated errors for experiments with KOH-impregnated feedstock. Product yields were calculated not only in dry feedstock basis, but also in KOH-free feedstock basis, to verify changes in the products themselves without KOH contribution. It was assumed that the KOH completely remained in the solid product, which may be a gross approximation. While the boiling point of KOH is 1327 °C [379], the melting point, depending on the presence of other compounds such as K₂CO₃, is in the range of 370-410 °C [380]. It would however not be collected as liquid product since it would have to be in vapour/gas form. During pyrolysis, depending on temperature, KOH-derived products are formed such as K₂CO₃, K₂O, K, and gases (e.g., CO, H₂O, CO₂) [249][250]. K₂CO₃ and K₂O have melting points >700 °C [256][381] and therefore likely stayed completely in the char product, however K₂O is reactive and decomposes at ≈350 °C [382]. The elemental form of potassium, although having 63.5 °C melting point, would not form liquid product on its own since it would have to be in vapour/gas form and be condensed after the reactor, and its boiling point is 759 °C [381]. Nevertheless, this assumption likely resulted in overestimation of gas product yields since part of the gaseous products were derived from the KOH. Liquid product yields could also be overestimated if unknown K-containing compounds were in vapour/gas form or if liquid droplets were transported to the condensing system by product vapours. It could also have occurred that with KOH there was greater production of H₂O or other gaseous compounds that are undetected by the MicroGC, which can also increase errors in the mass balances.

Comparing KOH absence with using KOH-impregnated feedstock (with the lowest KOH concentration), the main difference was in terms of char yields, which increased with the presence of KOH, especially at 400 °C. At 600 °C, the smaller increase could be due to more inorganic material devolatilising into vapour form from the higher temperature. However, comparing liquid and gas yields between KOH-free experiments with experiments using 0.1 M

KOH at 600 °C, there was a decrease (although standard deviation for liquid yields was high). This suggests devolatilization of inorganic material did not occur to a greater extent when using KOH. For 400 °C, there was only a small increase in gas yields when using KOH, and the liquid yields suffered no significant change.

Comparing experiments with increasing KOH concentration, at 400 °C char yields increased, although less than when comparing with KOH absence. For 600 °C, the change in char yield was not significant. In terms of liquid and gas products, the trends were contrasting: at 400 °C the liquid yield decreased when using 1 M KOH, while the gas yield did not change significantly; at 600 °C, the gas yield increased significantly, while the liquid yield did not change significantly (although the high standard deviation for 0.1 M KOH made it challenging to establish trends). Since the presence of KOH overall caused increased char yields, and not a decrease, this suggests activation reactions did not occur during the slow pyrolysis process. Activation reactions would also increase gas yield, which did not occur, except for 600 °C with 1 M KOH.

As explained in Chapter 2, the addition of a base such as KOH to a carbonaceous precursor and subjecting the mixture to pyrolysis is a method of chemical activation, producing a highly porous solid material due to the loss of carbonaceous material (as CO, CO₂, etc.) [22][239][379]. In summary, KOH activation is known to involve reactions between KOH and C forming CO, H₂ and K, and also reactions with CO₂, forming K₂CO₃ and H₂O [249][250][251]. Further reactions occur between the precursor material and CO₂, H₂O and K₂CO₃, forming more gaseous compounds, K-containing compounds such as K₂O and even metallic K, and increasing porosity [249][252].

Chemical activation is usually favoured by higher temperatures and agent:precursor (or agent:char) ratio, although these factors become detrimental once a certain value is reached [22][239][254]. The theoretical agent:char ratio was calculated in Chapter 3 (subsection 3.2.2.4) assuming a 30 wt.% char yield. The real (experimental) ratios considering the experimental char yields are presented in Table 6.4.

Table 6.4: Ratios between activating agent and char for experiments with KOH-impregnated wheat straw.

	Theoretical (from Chapter 3)		Experimental			
			400 °C		600 °C	
[KOH] (M)	0.1	1	0.1	1	0.1	1
KOH:Char ratio (wt.)	0.019	0.187	0.014	0.137	0.018	0.182

The ratios in Table 6.4 correspond to approximately 1:71 and 1:6, respectively, for 0.1 M KOH and 1 M KOH. In chemical activation, the agent:char ratios are typically between

1:0.5 and 1:3 [22], significantly higher than the ones used in this work (higher proportion of activating agent). The objective of this work was to evaluate the effect of KOH on product yields and properties, through feedstock impregnation with KOH solutions. The concentration of KOH in those solutions was relatively low, resulting in mild activation conditions, with the purpose of avoiding the post-washing step of the solid product, which creates waste liquid streams.

For 400 °C, a possible reason for increased char and gas yields and decreased liquid yields could be a favoured occurrence of secondary reactions due to KOH presence. Secondary reactions can reduce liquid yields and increase char and gas yields, for example through cracking reactions [13][104], and can be favoured by the presence of inorganics [77][90][99][108], with potassium (and sodium, calcium) being particularly important [90][104]. The use of KOH in pyrolysis has been verified to reduce tar yields and enhance thermal decomposition, increasing char and gas yields [22][245]. Tar reduction has been connected to the dehydration effect caused by KOH on the precursor, which reduces water presence [379]. A reduction of the aqueous phase was verified in this work at 600 °C production temperature.

One process variable that influences the occurrence of secondary reactions is VRT. For the experiments in this chapter with varying KOH concentration, the VRT values from both visual and calculated methods are presented in Table 6.5.

Table 6.5: VRT values for experiments with varying KOH concentration obtained through visual and calculated methods (n=2).

T (°C)	[KOH] (M)	VRT, visual (min)	VRT, vis (s)	VRT, calc (min)	VRT, calc (s)
400	0	4.2 ± 0.0	255 ± 0	1.5 ± 0.1	93 ± 6
	0.1	2.5 ± 0.4	150 ± 21	1.3 ± 0.2	78 ± 10
	1	3.8 ± 0.4	225 ± 21	1.5 ± 0.1	88 ± 9
600	0	2.5 ± 0.0	150 ± 0	0.8 ± 0.0	48 ± 0
	0.1	2.6 ± 0.2	158 ± 11	0.8 ± 0.1	49 ± 8
	1	2.8 ± 0.4	165 ± 21	0.7 ± 0.0	40 ± 2

The VRT results do not suggest secondary reactions were favoured when KOH was present, since VRT was either not significantly affected or decreased. Nevertheless, secondary reactions can occur inside the screw reactor due to the relatively long VRT, and depend on other factors such as temperature.

Since gas yields were not increased with KOH, this suggests KOH presence did not favour secondary reactions, but instead inhibited devolatilisation reactions, at least when comparing experiments at 400 °C, and at 600 °C when comparing KOH absence with 0.1 M KOH.

It had been suggested in Chapter 4 that the second screw reactor yielded higher char proportion and lower liquid and gas. The product yields, supported by temperature profiles and VRT values, suggested instead that carbonisation in the second screw reactor could occur to a lesser extent compared to the first reactor, due to the temperature gradients inside the reactor tube. The results in this chapter suggest KOH further inhibits devolatilisation, when char yields increased and gas yields decreased.

At 600 °C and with 1 M KOH, gas yields significantly increased (even considering overestimations), however the effect on char yields was not significant, which suggests that for those process conditions there could be competition between secondary and activation reactions, resulting in augmented gas yields but with contrasting effects on char yield. Upon activation, the char yield drops (burn-off), however, this was not verified in these results. The higher temperatures and KOH:char ratio favour the occurrence of both secondary and activation reactions.

Evaluating the effect of KOH on the distribution of gaseous species from the experiments can improve the understanding of what occurred during the process. The distribution of gaseous species (vol.%) for each experiment is presented in Table 6.6, along with gas product density, molecular weight, and HHV. The results for experiments without KOH impregnation are presented for comparison.

Table 6.6: Gaseous species distribution (vol.%), gas product density, molecular weight, and HHV for each slow pyrolysis experiment with KOH-impregnated feedstock (n=2).

T (°C)	400			600		
KOH solution concentration (M)	0	0.1	1	0	0.1	1 ^{a)}
CO ₂	58.5 ± 0.7	62.4 ± 5.1	60.2 ± 0.4	37.0 ± 0.5	31.0 ± 0.3	41.4
CO	36.8 ± 1.2	33.4 ± 5.5	36.6 ± 0.5	31.8 ± 1.5	41.8 ± 0.4	36.9
CH ₄	1.9 ± 0.1	2.2 ± 0.1	2.0 ± 0.1	15.5 ± 0.1	14.0 ± 0.1	12.7
C _n H _m	1.0 ± 0.0	1.1 ± 0.0	1.0 ± 0.1	5.1 ± 0.2	4.7 ± 0.1	4.8
H ₂	0.3 ± 0.0	0.8 ± 0.2	0.2 ± 0.0	10.6 ± 1.0	8.5 ± 0.2	4.2
Density (g/cm ³)	1.54 ± 0.03	1.57 ± 0.03	1.56 ± 0.00	1.24 ± 0.01	1.22 ± 0.00	1.34
Molecular weight (g/mol)	36.7 ± 0.6	37.6 ± 0.7	37.4 ± 0.1	29.5 ± 0.2	29.3 ± 0.0	32.2
HHV (MJ/Nm ³)	5.8 ± 0.0	5.5 ± 0.5	5.7 ± 0.0	14.0 ± 0.1	14.1 ± 0.1	12.6

Notes: a) MicroGC did not record data for one of the experiments due to equipment error (null standard deviation)

For 400 °C, the varying concentrations of KOH in impregnating solution did not produce significant changes in gaseous species. For 600 °C, however, significant changes occurred, and for some gaseous species the changes depended on KOH-impregnation degree.

For 600 °C experiments, CH₄ and H₂ decreased with increasing KOH concentration, and also C_nH_m but to a lower extent. For CO₂ and CO, however, the former decreased for 0.1 M KOH, and then increased for 1 M KOH experiments, while for the latter CO the opposite occurred, increasing for 0.1 M KOH and decreasing for the highest KOH concentration. This behaviour supports the hypothesis of competing secondary and activation reactions for 600 °C and 1 M KOH.

For 0.1 M KOH at 600 °C, comparing with absence of KOH, the results suggest CO-forming reactions occurred, which could be due to (activation) reactions between carbon and KOH, K₂CO₃, and K₂O. CO₂ could be consumed by reaction with KOH, producing K₂CO₃. Contributions from the reverse Boudouard reaction (C+CO₂↔2CO), favoured by higher temperature, could also contribute to CO₂ consumption and CO creation. However, at 600 °C it is not likely that this reaction occurred to a significant extent, since it is only spontaneous at ≥710 °C [371]. The reverse water-gas-shift reaction (H₂+CO₂↔H₂O+CO) could also have the same effect, and at the same time consume H₂, which did occur.

In chemical activation with KOH, reactions such as the one between carbon and KOH can produce gaseous H₂ and thus increase its yield [250]. However, except for the experiment with 0.1 M KOH at 400 °C, H₂ was seen to decrease with KOH impregnation. This suggests H₂-forming reactions did not occur, or, if they occurred, there were other reactions in which H₂ was consumed such as the reverse water-gas-shift reaction, especially at 600 °C.

Decreased CH₄ yields for increasing KOH concentration could be due to the dry methane reforming reaction (CO₂+CH₄↔2H₂+2CO), although KOH is not known to catalyse this reaction. Besides causing CH₄ yield to decrease, it also decreases CO₂ and increases CO, which is in line with the results for 0.1 M KOH. However, the reduction of H₂ yield found in this work does not support the occurrence of that reaction.

The suggested lack of activation will reflect on char properties such as porosity and surface area, which are analysed in the next section. Despite likely not having significant surface area development, the chars from experiments with KOH may have had other properties (e.g., surface chemical functionalities) affected in positive ways to improve liquid-phase adsorption performance.

6.4. Characterisation of solid products

As had occurred for other chars produced in this work (Chapter 4 and 5), the produced chars were overall black in colour, had electrostatic properties, and increased weight during weighing, which was attributed to moisture adsorption and probable hygroscopicity.

For the chars produced by feedstock impregnation with 1 M KOH solution at 600 °C, however, a different kind of particles were present, shaped like sheets, of different sizes but

in general longer than the char particles, with an overall dull dark grey colour. Figure 6.1 presents a picture of one of the chars produced from KOH-impregnated feedstock (1 M KOH solution) with marked particles, and a picture of a char from KOH-free feedstock.

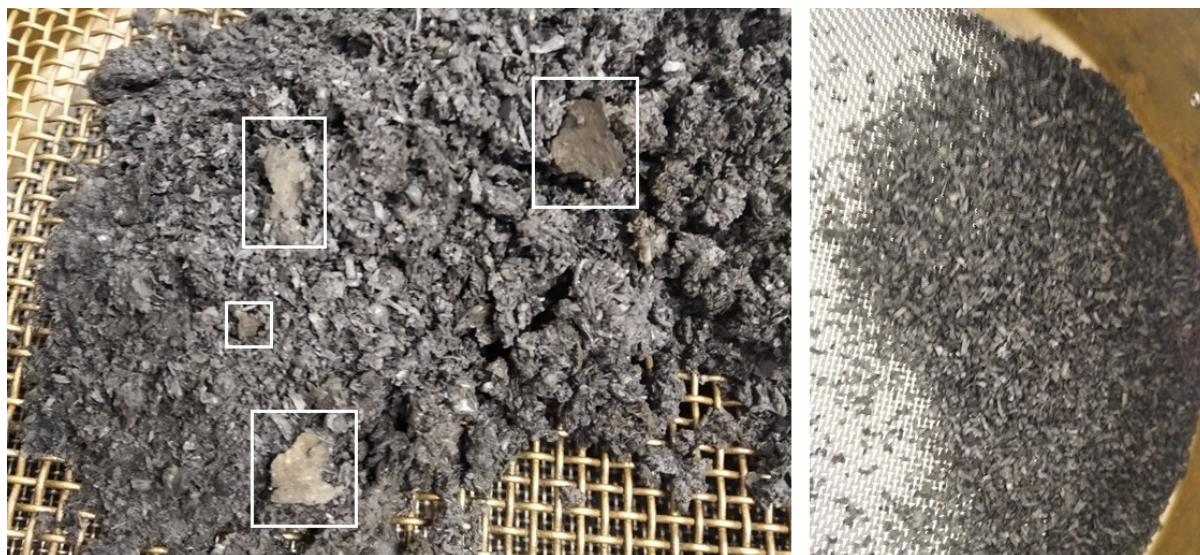


Figure 6.1: Left picture – char produced at 600 °C from feedstock impregnated with 1 M KOH solution, with different-looking particles marked; right picture – char produced at 600 °C from soaked and dried feedstock (0 M KOH).

Literature mentions potassium in its elemental form is solid at room temperature, as a silver metal, but with a dull grey colour (tarnished) due to oxidation upon air exposure [381][383]. The melting point of potassium is 63.5 °C and boiling point is 759 °C [381], so during slow pyrolysis potassium would be in liquid form, dragged by the solid product. Once in the char pot, since it was heated, pieces of still liquid potassium could merge between themselves. It was thus concluded that the different-looking particles were elemental (metallic) potassium. The different particles were not observed when chars originated from feedstock impregnated with 0.1 M KOH solution, due to the relatively lower amount of KOH used for that concentration.

The different-looking particles were not observed in 400 °C chars, suggesting their existence was temperature-dependant, which could be due to the temperature not being high enough for certain reactions to occur (such as the ones forming K_2CO_3 , K_2O or K), although K was likely to be integrated into the precursor structure from KOH dissociation during feedstock impregnation [384].

Typically, in chemical activation, the solid products are washed post-production with water or weak acid/base solution to remove the activating agent, free porosity and balance pH [22]. The char products from experiments with KOH-impregnated feedstock in this work were

not washed prior to analyses or application due to the relatively mild production conditions, i.e., relatively low ratio KOH:char. In this way, the creation of liquid waste streams that would increase production costs was avoided. Furthermore, washing solid products from chemical activation is usually performed not only due to high agent:precursor ratios, but also due to the nature of the activating agent, especially when it is highly corrosive, such as H_2SO_4 , H_3PO_4 or ZnCl_2 [239]. KOH, although being considered a strong base, is a milder activating agent comparatively to the mentioned activating agents and will cause fewer negative effects such as equipment corrosion [379]. Furthermore, KOH converts to other compounds such as K_2CO_3 and K_2O which represent fewer risks. There was no noticeable corrosion or other negative effects on the reactor or analysis equipment from the chars produced with KOH-impregnated feedstock.

One negative consequence from not washing the char products and having different kinds of particles (as seen in Figure 6.1) was that during sampling and sample preparation the heterogeneity of the sample likely increased.

6.4.1. TGA profiles and proximate analyses

The chars were analysed by TGA in inert atmosphere and the thermal degradation profiles are displayed in Figure 6.2. Results for chars produced without KOH impregnation (from soaked and dried feedstock) are also included for comparison.

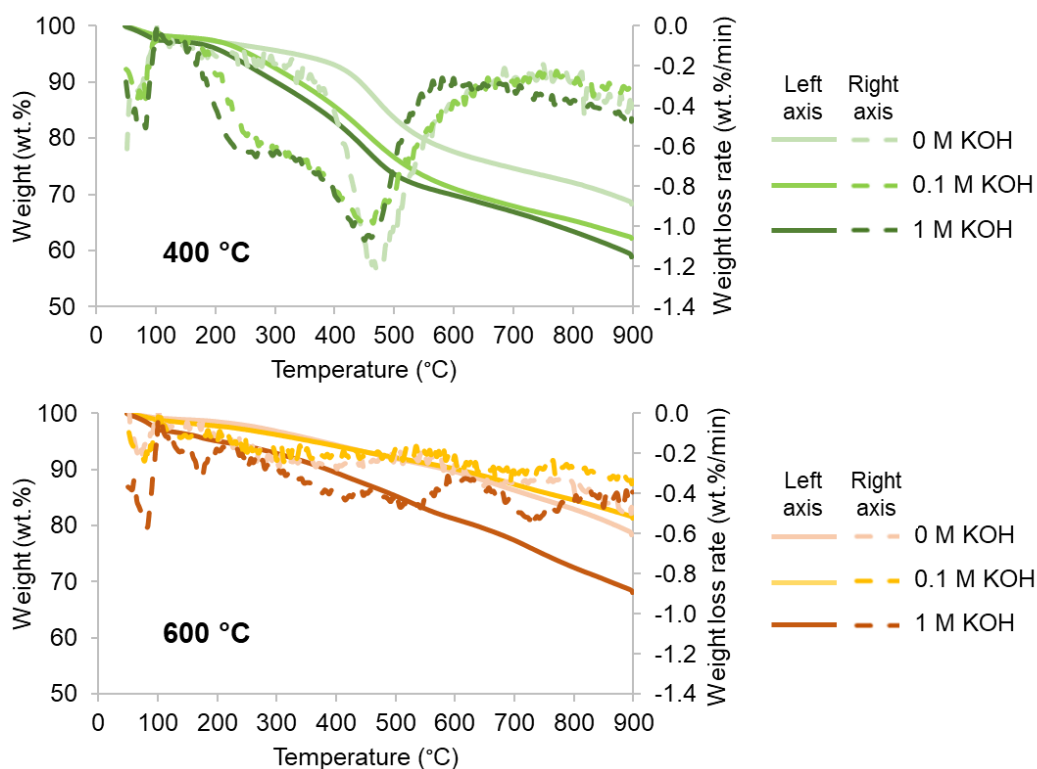


Figure 6.2: TGA profiles (N₂ atmosphere) for chars produced at 400 °C (top) and 600 °C (bottom) with varying concentration of KOH in the impregnation solution.

Comparatively, the chars produced at higher temperature had less weight loss than the ones from 400 °C, which correlates with increased stability during slow pyrolysis and was seen in Chapter 4 and 5.

Overall, using KOH-impregnated feedstock increased the total weight loss under inert atmosphere of the resulting chars, especially for 400 °C production temperature. For 400 °C, both chars produced from KOH-impregnated feedstock had greater weight loss than the char from KOH-free feedstock, while for 600 °C the char from feedstock impregnated with 1 M KOH solution had significantly higher weight loss than the chars from 0.1 M KOH solution impregnation and the char from KOH-free feedstock.

The chars produced at 400 °C with KOH-impregnated feedstock had significant weight loss at \approx 200-350 °C, which was already observed for chars produced from experiments in the second screw reactor with as-received feedstock without injected gas and using N₂ as injected/carrier gas (Chapter 5). This had not been observed in other chars produced in the first screw reactor with varying temperature, SRT or feedstock moisture content (Chapter 4), and had been attributed to heat transfer limitations being more pronounced in the second screw reactor (due to design differences), leading to a lower carbonisation degree. In this chapter the weight loss was observed for chars from experiments with KOH, suggesting the KOH acts as an inhibitor of thermal degradation in the screw reactor, by increasing heat

transfer limitations already relatively pronounced in the second screw reactor compared to the first one. This is however contrary to indications from literature mentioning a favouring of thermal degradation from KOH, although it is more related to cracking of tars and compounds in vapour form [22][245]. Inhibition of thermal degradation leads to more volatile matter remaining in the char product and leading to greater weight loss during TGA analysis under inert atmosphere. This correlated with the greater char yield observed for 400 °C and with KOH-impregnated feedstock (both concentrations).

The other (main) weight loss region was at $\approx 400\text{-}550$ °C, due to lignocellulosic material still present, shared by all chars produced at 400 °C. The peak of weight loss rate however shifted to lower temperatures for chars produced from KOH-impregnated feedstock, suggesting the presence of KOH or KOH-derived compounds in the char led to lower thermal stability. After ≈ 600 °C, only the char produced with 1 M KOH suffered significant weight loss, starting at ≈ 700 °C and continuing until 900 °C, attributed to K-containing compounds.

For 600 °C chars, the ones produced with 0.1 M KOH had thermal degradation similar to the ones without KOH, unlike 400 °C chars in which the chars produced from KOH-impregnated feedstock were more similar between themselves than with char from KOH-free feedstock. This could be because the higher temperature leads to greater degradation of KOH and K-containing compounds during slow pyrolysis, leaving less in the char product. For the char produced at 400 °C from feedstock impregnated with 1 M KOH solution there was a significant weight loss step starting at ≈ 700 °C, which could be due to devolatilization of metallic K (boiling point 759 °C [381]) present in the char structure or derived from K_2O or K_2CO_3 formed during slow pyrolysis. This weight loss was also present for 600 °C char with 1 M KOH. Furthermore, there was also significant weight loss at $\approx 350\text{-}600$ °C for char produced at 600 °C with 1 M KOH, which, similarly to chars produced at 400 °C with KOH, was related to a lower carbonisation degree due to the presence of KOH.

The weight losses identified for chars with KOH could also be due to volatiles adsorbed on the surface, however if the proportion of adsorbed compounds is unlikely to be as significant as the observed weight loss. The lower thermal stability of chars produced with KOH was in contrast with chars produced with CO_2 as injected gas, which had less weight loss than chars produced without injected gas or with N_2 as injected/carrier gas.

The proximate analyses of chars produced from slow pyrolysis of KOH-impregnated feedstock are presented in Table 6.7. For comparison, the results for chars from soaked and dried feedstock (KOH-free during soaking) are also presented.

Table 6.7: Proximate analyses (wt.%, dry basis) of the chars produced from experiments from feedstock with varying KOH solution concentrations (n=3).

T (°C)	[KOH] (M)	Volatile Matter	Ash	Fixed Carbon
400	0	34.0 ± 1.4	13.4 ± 0.6	52.6 ± 2.5
	0.1	40.2 ± 2.1	12.4 ± 0.5	47.4 ± 0.2
	1	44.2 ± 1.9	23.3 ± 0.8	32.5 ± 2.9
600	0	21.6 ± 0.6	18.0 ± 0.3	60.3 ± 0.7
	0.1	22.7 ± 1.8	15.7 ± 0.0	61.6 ± 1.1
	1	37.2 ± 3.3	27.1 ± 0.0	35.7 ± 1.5

The char proximate analyses were significantly affected by the presence of KOH in the feedstock, especially for the highest KOH solution concentration. Overall, with KOH, volatile matter (VM) content increased, and fixed carbon (FC) content decreased. The final difference was greater for 600 °C production temperature, but less gradual than for 400 °C, since there was no significant difference between chars produced at 600 °C with 0.1 M KOH or without KOH. These trends were in line with the TGA thermal degradation profiles. Ash contents were also affected significantly, however only for the highest KOH concentration. Since ash contents varied significantly, the proximate analysis was calculated in dry ash-free basis and converted to VM:FC ratio, with the results in Figure 6.3.

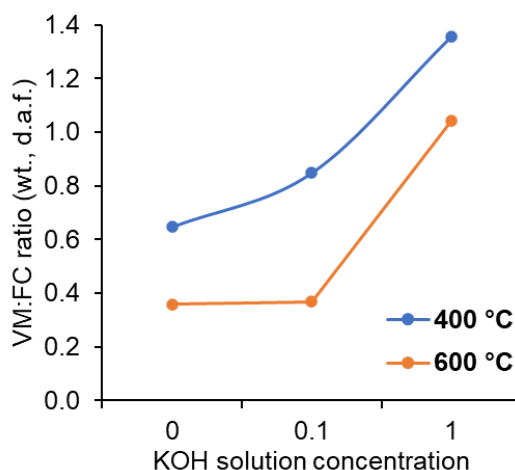


Figure 6.3: Ratio between volatile matter and fixed carbon contents (dry ash-free basis) for chars produced with varying KOH concentration.

The ratio VM:FC ratio corroborates the greater impact of 1 M KOH for 600 °C production temperature, compared to the negligible difference between 0 and 0.1 M KOH, and because the ratio increases very significantly for 1 M KOH. The proportion between VM and FC becomes approximately equal for 1 M KOH, while for 0 and 0.1 M KOH there was more than double the content of FC compared to VM. For 400 °C, a more gradual increase of VM:FC

ratio with KOH concentration occurred, with the difference that FC content becomes significantly greater than VM content for 1 M KOH.

The effects of KOH presence on char proximate analysis were connected to carbonisation likely occurring to a lower extent, which was already suggested by product yields and char TGA profiles. There could also be a contribution from adsorbed material on the char, from secondary reactions (e.g., cracking and deposition of volatiles, tars and other compounds) or just due to extended contact between solids and vapours during slow pyrolysis. However, the changes are likely too large to be explained by this second reason, at least on its own; there could be a simultaneous contribution from secondary reactions and inhibited carbonisation.

The fixed carbon content is often utilised as stability indicator, and it was verified that KOH presence inhibits its increase, especially for feedstock impregnated with higher KOH solution concentration.

Ash contents were mainly affected by the highest KOH concentration, increasing significantly, which was due to the significantly higher inorganic fraction in the feedstock, which mainly remained in the char. The significant increase in ash contents for 1 M KOH led to the more pronounced decrease in fixed carbon contents for those chars. However, comparing KOH absence with the lowest KOH concentration, the ash contents did not increase, and it even significantly decreased for 600 °C production temperature. Part of the inorganic material can suffer devolatilization during pyrolysis, and the KOH can be converted into other compounds such as K_2CO_3 and K_2O and release vapour products. Reactions with other inorganic compounds in the char could have occurred, creating other compounds that could be more easily devolatilised, thus lowering ash contents.

One observation made during ashing of chars from experiments with 1 M KOH was that the ashes had a blue colour, for both production temperatures but especially for 400 °C. The colours were seen both in ashing with the TGA equipment and with ASTM method in a muffle oven. Samples of chars from experiments with 1 M KOH at 400 and 600 °C ashed in the muffle oven can be seen in Figure 6.4.

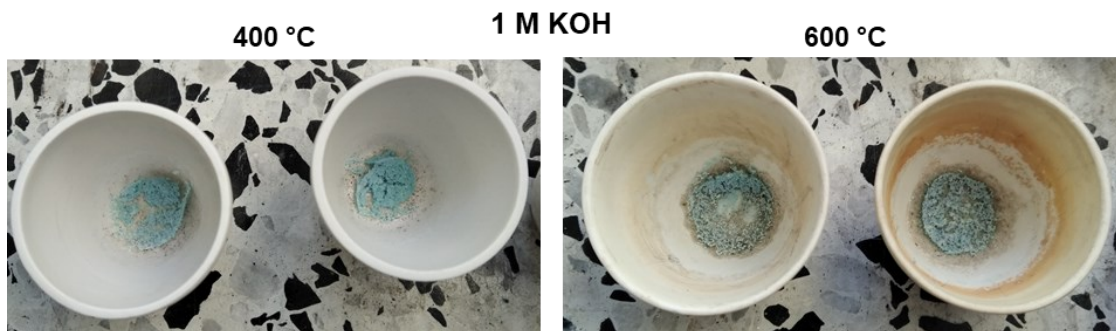


Figure 6.4: Ashes from chars produced from feedstock impregnated with 1 M KOH solution and at 400 (left) and 600 °C (right).

The colour only appeared for the chars with 1 M KOH due to the higher proportion of inorganic content on those chars. The blue coloured ashes were connected to KOH-related compounds in the char, and the fact that the colour was not as strong for the highest temperature suggests some of that inorganic material was devolatilised into vapour phase during slow pyrolysis. This may be connected to the increased gas yields verified for 600 °C and 1 M KOH. This could explain the decrease in ash content for the char from 0.1 M KOH, since the relatively low proportion of added inorganic material could suffer devolatilisation.

The nature of the compounds that compose the char structure can be investigated with ultimate analysis and FTIR.

6.4.2. Ultimate analyses and inorganic contents

The elemental analyses of chars produced from KOH-impregnated feedstock, along with atomic H:C and O:C ratios and HHV are presented in Table 6.8. For comparison, the results for chars from soaked and dried feedstock (no KOH in soaking) are also presented.

Table 6.8: Ultimate analyses (wt.%, dry ash-free basis) and calculated higher heating value (MJ/kg, dry basis) of the chars produced from experiments with varying KOH concentration (n=3).

T (°C)	[KOH] (M)	C	H	N	O (by diff.)	H:C	O:C	HHV
400	0	74.7 ± 1.9	4.2 ± 0.2	1.7 ± 0.1	19.3 ± 0.9	0.66	0.19	24.8
	0.1	73.7 ± 0.7	4.0 ± 0.0	1.4 ± 0.0	20.7 ± 0.7	0.65	0.21	24.6
	1	78.3 ± 2.9	4.8 ± 0.2	1.3 ± 0.1	15.5 ± 0.2	0.73	0.15	23.6
600	0	89.0 ± 1.3	3.0 ± 0.1	1.5 ± 0.0	6.5 ± 0.7	0.40	0.05	27.5
	0.1	88.0 ± 0.7	2.9 ± 0.1	1.4 ± 0.1	7.6 ± 0.6	0.39	0.07	27.7
	1	85.1 ± 1.8	2.6 ± 0.1	1.2 ± 0.1	11.0 ± 0.2	0.36	0.10	22.5

The effect of KOH impregnation on char elemental analyses was overall only significant for the case of highest KOH concentration. However, the effect was different depending on operating temperature: for 400 °C, feedstock impregnation with 1 M KOH

solution caused carbon and hydrogen contents to increase, while oxygen contents decreased; for 600 °C, carbon and hydrogen contents decreased, while oxygen increased. These differences were reflected on the H:C and O:C ratios as well. The effect on nitrogen contents was overall a decrease with KOH impregnation for both temperatures.

The changes in elemental composition were connected to changes in proximate analyses, mainly: increased volatile matter and decreased fixed carbon contents. At 400 °C, the chars kept more carbon and hydrogen-containing compounds, and there was a greater contribution from these compounds to volatile matter, while at 600 °C a greater carbon and hydrogen proportion was lost, and thus the increase in volatile matter was due to increased oxygen content. This could have been because the KOH or K-related compounds stabilised the carbon and hydrogen-containing elements at lower temperature, and the stabilisation could not be maintained for higher temperatures, maybe also due to devolatilisation of K-containing compounds. At higher temperature, production of gases such as hydrogen and hydrocarbons are known to increase in slow pyrolysis [105], which agrees with the findings.

The changes in proximate analyses occurred for 1 M KOH, however there was also an increase (to a lower extent) in volatile matter for 0.1 M KOH at 400 °C compared to KOH-free experiments, which was not accompanied by significant changes in elemental composition. This was probably because the volatile matter which was lost had equal proportions (by weight) of hydrogen, carbon and oxygen.

As a result of significantly increased ash contents for chars produced with highest KOH concentration (Table 6.7), the HHV (dry basis) decreased. At 400 °C, this occurred despite an increase in carbon and hydrogen contents and decreased oxygen content, which would increase HHV. At 600 °C, increased oxygen contents, besides increased ash content, contributed to the HHV decrease. The changes on elemental distribution of chars can affect their applications and have beneficial effects, for example, a greater O:C ratio has been correlated with higher cation exchange capacity and thus adsorption of cations from liquid-phase [348].

The chars from experiments with KOH-impregnated feedstock were analysed for K content and the results are presented in Figure 6.5 (bars, read on left axis). The K contents were compared to the ones from chars produced from KOH-free feedstock (results in Chapter 4, subsection 4.4.2) and included in the graph as a percentage of increase (dots, right secondary axis).

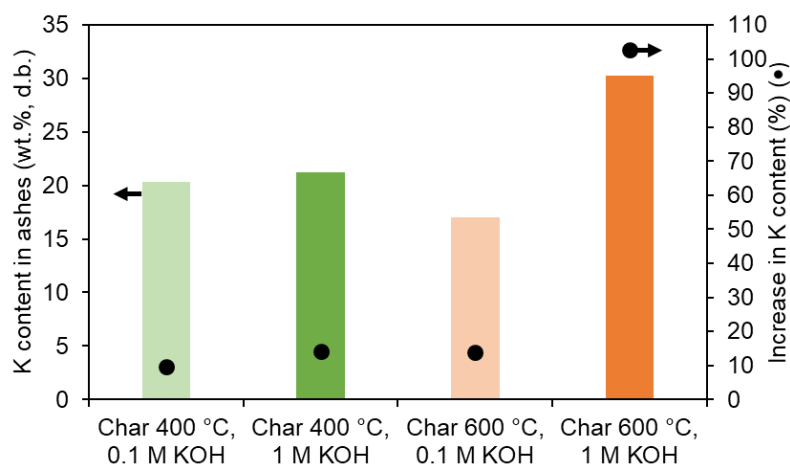


Figure 6.5: Potassium contents (wt.%, d.b.) in ash from chars produced from KOH-impregnated feedstock (bars, left axis) and increase (%) compared to chars from feedstock without KOH (dots, right axis).

The chars produced with the highest concentration of KOH had greater proportion of K in their ash contents, for both production temperatures, although the difference for 400 °C is relatively small. It was expected that the ashes of 400 °C char with 1 M KOH would have similar or even greater proportion of K compared to 600 °C, since the lower temperature would devolatilise a smaller proportion of inorganic materials. The lack of this effect could be due to sample heterogeneity.

Comparing with chars produced from KOH-free feedstock, an increase in K content was verified, especially for the char produced at 600 °C from 1 M KOH, for which it more than doubled. This was due to the addition of K from KOH and the lack of washing of the final solid product. The significant increase in K content can be advantageous for applying the char in soils, especially those that are K-deficient.

The changes in inorganic contents will affect other characteristics such as pH value and thus the behaviour of the char in water, impacting its performance in liquid-phase adsorption.

6.4.3. Surface functional groups

The produced chars from KOH-impregnated feedstock were analysed by FTIR for surface functional groups and the spectra is present in Figure 6.6. The green spectra correspond to 400 °C chars, while the orange-brown spectra belong to 600 °C chars. The colour gradient represents KOH concentration in the impregnation solution (darker is higher).

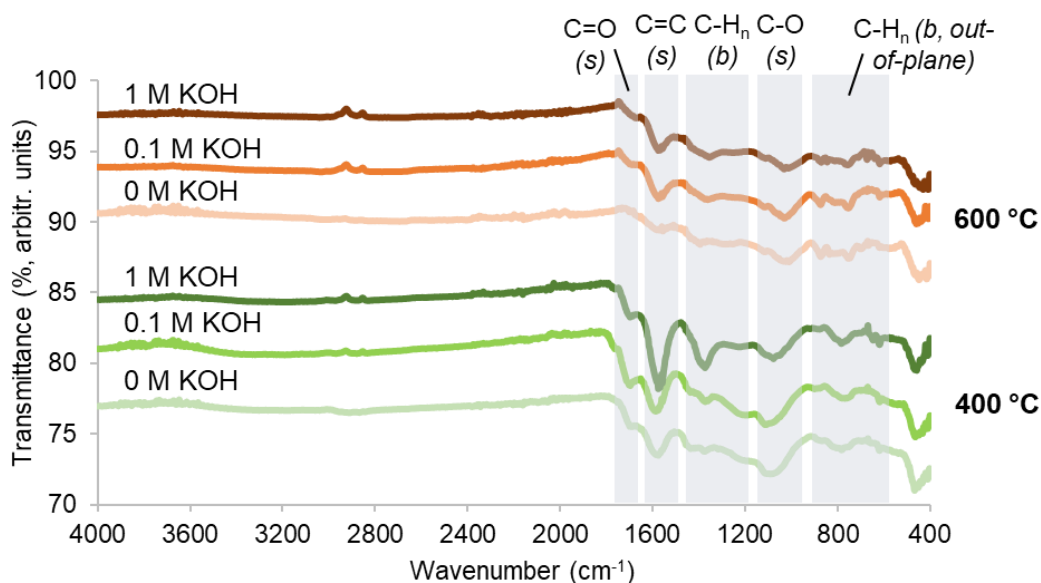


Figure 6.6: FTIR spectra of chars produced at 400 and 600 °C with varying KOH solution concentrations used for feedstock impregnation.

As had occurred for other produced chars in this work, only the IR manifestation at 2000-400 cm^{-1} was significant, due to loss of surface functionalities and increase in aromatisation during slow pyrolysis. Furthermore, the chars produced at higher temperature had overall lower IR manifestation, due to the same reason.

The effect of KOH on the FTIR spectrum varied depending on production temperature, and was more significant for 400 °C. For chars produced at 400 °C, the most noticeable difference was for $\approx 1650\text{-}1500 \text{ cm}^{-1}$, corresponding to C=C bond vibrations. For the char produced with 1 M KOH, the intensity was significantly higher than for the other chars, and the peak also moved to lower wavenumbers. The region $\approx 1420\text{-}1320 \text{ cm}^{-1}$ (bending C-H_n) also gained intensity for chars with 1 M KOH. The increases in these two regions correlated with the significant increase in volatile matter in chars from 1 M KOH, and to increased carbon and hydrogen contents for 400 °C chars from 1 M KOH. Another region corresponding to C-H_n bending vibrations ($\approx 1300\text{-}1200 \text{ cm}^{-1}$), however, decreased for 1 M KOH char, suggesting rearrangement of chemical bonds. The region for C-O bond vibrations ($\approx 1150\text{-}1050 \text{ cm}^{-1}$) decreased intensity for the highest KOH concentration. The bond vibrations of carboxyls (C=O, $\approx 1710 \text{ cm}^{-1}$), suffered an increase for 0.1 M KOH and then a decrease for 1 M KOH. This is in line with the elemental analysis, in which oxygen contents decreased for 400 °C chars from 1 M KOH and carbon and hydrogen contents increased.

For 600 °C, the effect of KOH concentration was considerably less significant than for 400 °C. Nevertheless, when produced at 600 °C, chars produced with KOH-impregnated feedstock had more manifestation from C=O ($\approx 1710 \text{ cm}^{-1}$) and C=C ($1650\text{-}1500 \text{ cm}^{-1}$) bond

vibrations compared to chars without KOH. This was linked to possible rearrangement of carbon-carbon bonds and incorporation of carbon-oxygen bonds, however with likely low structural and thermal resistance, since volatile matter content increased. The increase in C=O manifestation was in line with increased oxygen contents in chars with KOH-impregnated feedstock.

Between chars produced at the same temperature, no significant differences were found in the region $\approx 700\text{-}400\text{ cm}^{-1}$ typical of inorganic functionalities. Thus, FTIR could not be used to identify KOH-related compounds on the char surface.

Modifications in surface chemistry such as increased O-containing functionalities can be advantageous for liquid-phase adsorption, by for example favouring electrostatic interactions. Increased carboxyl functionalities, for example, have been found to positively correlate with adsorption of methylene blue from water [272].

6.4.4. pH (in H₂O)

The chars from slow pyrolysis experiments with KOH were analysed for pH (in H₂O) and the results are shown in Figure 6.7. The results for chars without KOH, from soaked and dried feedstock, are also presented for comparison.

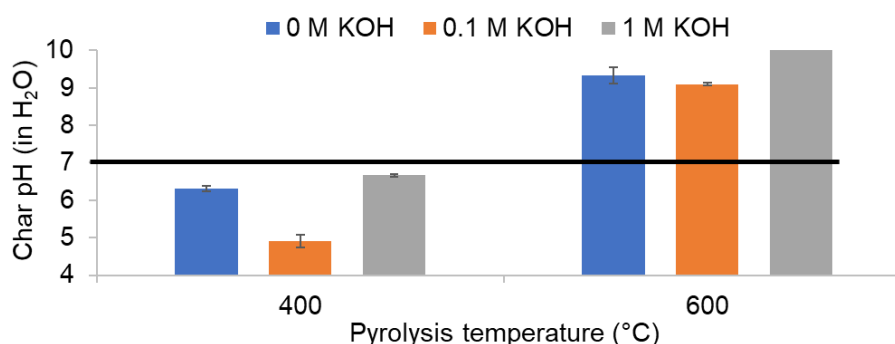


Figure 6.7: pH value (in H₂O) of chars produced with varying KOH solution concentration.

As occurred for other chars produced in this work, the pH value increased with process temperature, as a result of the solid material losing volatile matter and functional groups and increasing ash contents [189][198].

The feedstock, after impregnation with KOH, was also tested for pH (in H₂O): 8.4 ± 0.3 for 0.1 M KOH, and 6.2 ± 0.1 for 1 M KOH. The more acidic pH of feedstock with 1 M KOH could be due to changes in the lignocellulosic structure of the feedstock, leading to more acidic compounds being release into the measured water. For feedstock after impregnation with 0.1 M KOH, 400 °C slow pyrolysis caused significant decrease in pH, and 600 °C caused a

slight increase. For 1 M KOH, both temperatures caused pH to increase, although 600 °C caused a much more significant increase.

As for the effect of increasing KOH concentration, the pH value first decreased, comparing not using KOH with using 0.1 M KOH solution, and then increased significantly (surpassing the value for 0 M KOH chars) when using 1 M KOH solution. This was due to the much more significant amount of KOH used in the 1 M case, which the slow pyrolysis process was not capable of devolatilising to an extent comparable to using 0.1 M KOH. Since a greater proportion of KOH, a strong base, remained in the char, the pH was increased.

According to the results from proximate and ultimate analyses, the trends of pH values were mostly related to changes in volatile matter and ash contents. For 0.1 M KOH, the volatile matter increased, while ash contents did not change, and this caused decreased pH value. For 1 M KOH, on the other hand, while volatile matter contents also increased, the ash contents also significantly increased, and this caused an opposite effect, of increased pH value.

In Chapter 5, a decrease in pH for chars from experiments with CO₂ as injected gas was connected to increased oxygen content (found by ultimate analysis and FTIR). However, in this chapter, the trends of elemental composition from chars produced with KOH could not be connected to variations in pH.

Changes in char pH can lead to benefits in adsorption applications due to potentially favoured interactions with adsorbates in solution (e.g., a more acidic char becoming more attracted to cationic compounds).

6.4.5. Porosity and surface area

The isotherms and pore size distributions from chars produced from experiments with different KOH concentration are presented in Figure 6.8 (400 °C) and Figure 6.9 (600 °C).

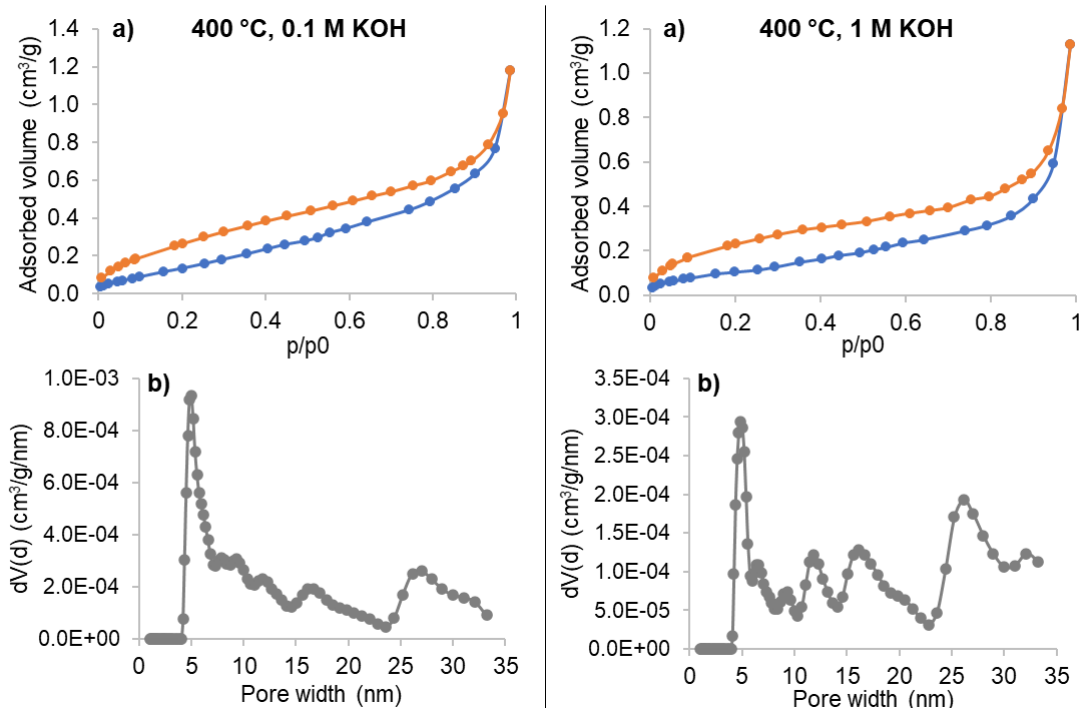


Figure 6.8: N₂ adsorption-desorption isotherms (a), and pore size distribution (QS-DFT applied on adsorption branch) (b), for chars produced from KOH-impregnated feedstock at 400 °C with 0.1 M KOH solution (left-hand side) and 1 M KOH solution (right-hand side).

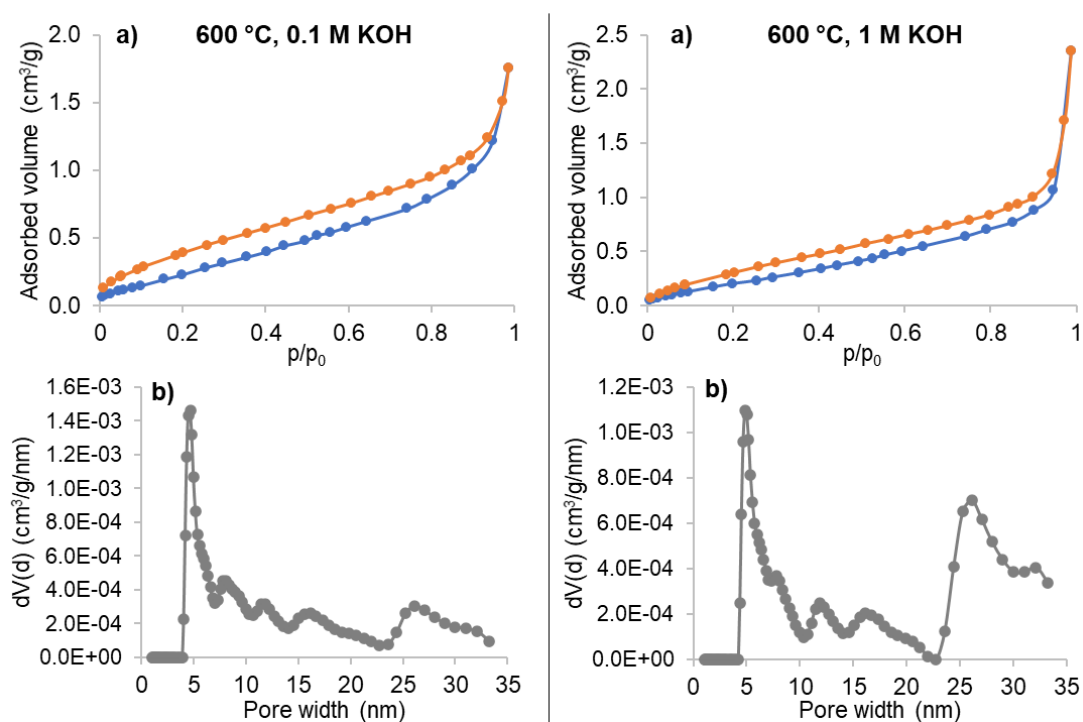


Figure 6.9: N₂ adsorption-desorption isotherms (a), and pore size distribution (QS-DFT applied on adsorption branch) (b), for chars produced from KOH-impregnated feedstock at 600 °C with 0.1 M KOH solution (left-hand side) and 1 M KOH solution (right-hand side).

Overall, the obtained isotherms were similar to the ones obtained from other experimental sets with varying temperature, solid residence time, feedstock moisture content, and reaction atmosphere/environment (by injecting gas into the reactor during slow pyrolysis). The chars had relatively low adsorbed volume, suggesting non-porous or very low porosity material. The isotherms had characteristics of type II or III according to IUPAC designations, which are common to macroporous or non-porous materials [361]. Hysteresis was also verified, suggesting capillary condensation or odd-shaped pores [360][361].

Comparing between KOH solution concentrations, few differences were found, although overall the adsorbed volume was lower for the case of 1 M KOH, and larger pores (i.e., ≈ 25 nm mesopores) gained relevance compared to micropores which were prominent for the cases of 0.1 M KOH.

The main results from N₂ physisorption (with QS-DFT model) of chars produced with KOH-impregnated feedstock are shown in Table 6.9. The results from chars produced without KOH impregnation are shown for comparison.

Table 6.9: Results from nitrogen physisorption at 77 K applied to chars produced from KOH-impregnated feedstock.

T (°C)	[KOH] (M)	Specific surface area (m ² /g)	Total pore volume (cm ³ /g)	Pore diameter (mode) (nm)
400	0	N/A ^{a)}	N/A	N/A
	0.1	2.2	0.006	5.1
	1	1.2	0.004	4.8
600	0	2.0	0.005	4.2
	0.1	3.4	0.008	4.6
	1	2.7	0.008	4.8

Note: a) Results unavailable due to isotherm measurement error.

The chars produced at higher temperature had slightly higher porosity than chars produced at lower temperature, which was consistent with what was observed in Chapter 4 and 5 for chars produced at different temperatures.

Comparing the effect of different KOH concentrations, it was found that using 0.1 M could slightly improve surface area and pore volume compared to not using KOH, however, when using higher KOH concentration (1 M), the surface area suffered a decrease. This was attributed to surface and pore covering due to the greater proportion of inorganic material present in the char. This negative effect has been verified in other instances, although for higher KOH:char ratios than the ones used in this work [254]. The results suggest that KOH can have detrimental effects on porosity development even at relatively low KOH:char ratios. If this is true, porosity could potentially be increased if inorganic material is removed from the

chars by washing post-production. The char washing process, however, creates waste liquid streams and increases production costs.

Literature indicates that solid products from chemical activation usually have wider pores compared to physical activation [37]. Despite not many differences being observed with N₂ physisorption, the chars produced from feedstock with 0.1 M KOH had results most similar to chars produced with CO₂ as injected gas, for both tested temperatures. To better evaluate the effect of KOH on porosity, CO₂ adsorption at 273 K would be required to assess microporosity, especially narrow micropores [203][360].

For the target application of the chars in this work, the slight improvement in surface area assessed by N₂ physisorption may be beneficial, since it is usually favoured by higher proportion of large micropores and mesopores [235].

6.5. Summary of Chapter 6

The addition of KOH to the feedstock prior to slow pyrolysis led to modified product yields (dry KOH-free basis), mainly: increased char yields, and decreased liquid yields. The yields and distribution of gaseous products suggest the contribution of activation reactions was relatively low, and that KOH could have inhibited carbonisation. Secondary reactions could also have been promoted by KOH presence. For 600 °C and 1 M KOH, however, the results suggested competition between secondary and activation reactions, due to the higher temperature and KOH:char ratio.

The char properties were also significantly affected by the presence of KOH. Volatile matter content increased for chars from experiments with KOH, while fixed carbon contents decreased, which corroborated the hypothesis of carbonisation inhibition. The ash contents were only modified for 1 M KOH, with a very significant increase, due to the greater proportion of KOH used. The elemental analysis was only modified for chars produced from 1 M KOH, for both temperatures, however with different trends depending on temperature. For 400 °C chars, carbon and hydrogen contents increased while oxygen contents decreased, and the opposite occurred for 600 °C chars. This could have been due to K-containing compounds stabilising carbon and hydrogen-containing compounds at lower temperatures. The K content in the char was also significantly increased, especially for 1 M KOH, which impacts other properties such as pH.

In terms of surface chemical functionalities, differences were mostly noticed for chars produced with 1 M KOH, and were more significant for 400 °C chars. Mainly, for 400 °C chars and 1 M KOH, chemical bond vibrations of C=C and C-H_n increased intensity, while C=O and C-O decreased, which was in line with elemental analysis. For 600 °C chars, the use of KOH (both concentrations) in feedstock impregnation led to increased intensity of C=O and C=C

bond vibrations, which agreed with increased oxygen contents and decreased hydrogen contents for chars produced at 600 °C with KOH. In terms of char pH (in H₂O), compared to not using KOH, the lowest KOH concentration caused the value to decrease, and the highest concentration caused an increase. The increase in pH was related to the significantly greater proportion of ash in the chars from 1 M KOH, while the decrease in pH for 0.1 M KOH was not only due to the smaller ash contents, but also to possible effects on the lignocellulosic material of the precursor during impregnation.

The results from N₂ physisorption (77 K) led to conclude that the KOH treatment did not make significant changes in surface area of the chars (both slow pyrolysis temperatures), although the results suggested it was slightly increased for 0.1 M KOH and that using 1 M KOH had a negative effect. The positive effect with 0.1 M KOH could be due to modifications of the surface of the precursor during impregnation and also slow pyrolysis, and the negative effect from 1 M KOH was due to the blocking of pores by K or K-related compounds.

The results indicate that traditional chemical activation could not be performed in this work, due to the relatively mild conditions employed, especially in terms of activation time and KOH:char ratio. The configuration of the reactor can also be related to this, due to promoted contact between vapours and solids and thus secondary reactions which can lead to surface and pore covering, besides the effect of inorganic material as well.

Although porosity and surface area were not significantly improved by the feedstock KOH treatment, the modification of other char properties (e.g., surface functional groups and pH) could lead to improvements in adsorption in liquid phase, investigated in the experimental chapter regarding adsorption of an organic dye from water with the chars (Chapter 7).

Chapter 7 – Adsorption of an organic contaminant from water using chars

7.1. Introduction

There is a growing demand for solutions for air and water pollution, due to increasing pollution levels and also more stringent limits on pollutants. Adsorption is one of the most effective techniques, with activated carbon being the popular adsorbent. However, producing activated carbon is time- and resource-consuming, and so there is interest in developing more sustainable and cost-effective production methods and adsorbents. The char from pyrolysis of biomass has been shown to have similar properties to activated carbon and usefulness for decontamination, and can be produced by slow pyrolysis in a relatively affordable manner, from agricultural residues for example.

The wheat straw chars produced in this work (Chapters 4, 5 and 6) were tested for adsorption of an organic contaminant from water, a cationic dye called methylene blue (also referred to as MB). The main objective was to achieve adsorption performance comparable to a commercial activated carbon, mainly in terms of maximum dye removal, and also adsorption capacity. Firstly, the performance of the chars from as-received wheat straw and unmodified slow pyrolysis process conditions is shown and discussed, followed by the chars from feedstock with modified moisture content (and consequently modified particle size/shape). This is followed by the chars from using CO₂ as injected gas (compared to using N₂ or not injecting gas), and finally by the chars from slow pyrolysis integrated with chemical activation, in which the feedstock was impregnated with KOH (in solution, testing 0.1 and 1 M KOH concentrations) prior to being processed.

The adsorption performance of all chars was tested using the same conditions: 10 mL of MB dye solution with 100 mg/L initial concentration, 25 mg of adsorbent (ground and sieved to $\leq 425 \mu\text{m}$ particle size) and mixing in a sonicator at 50 °C for 3 hours. A commercial activated carbon was also tested for adsorption performance using the same conditions.

After the first tests under the same conditions, a selected number of adsorbents with sufficiently good performance ($\geq 90\%$ dye removal) were further tested by modifying adsorption parameters: adsorbent mass and initial dye concentration. Adsorption of an anionic dye methyl orange was also tested to investigate the adsorption mechanism. Kinetics tests were also performed by investigating dye removal at certain time intervals.

The adsorption performances are discussed and connected to the respective char properties and process conditions, highlighting the impact of the different process and feedstock modifications. Possible adsorption mechanisms are discussed based on the performances and results from kinetics studies.

7.2. Adsorption performances of chars with a cationic dye as model compound

For the methylene blue (MB) dye, a calibration curve was created for the stock solution, by testing different concentrations in the UV-Vis spectrophotometer. The calibration can be seen in Figure 7.1.

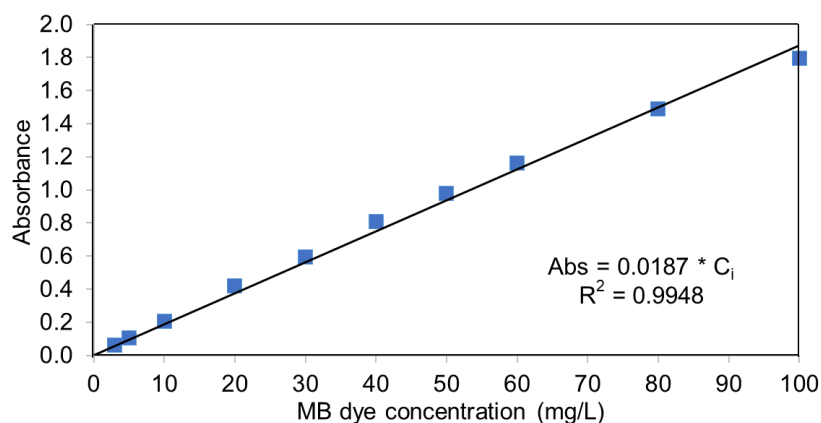


Figure 7.1: Calibration curve in UV-Visible spectrophotometry for the MB dye.

The obtained linear correlation was used to calculate the unknown MB concentration after adsorption tests with the produced chars. The agreement was considered sufficiently satisfactory ($R^2 \geq 0.99$). Pictures of samples of MB solutions with different concentrations used for calibration can be seen in Figure 7.2.

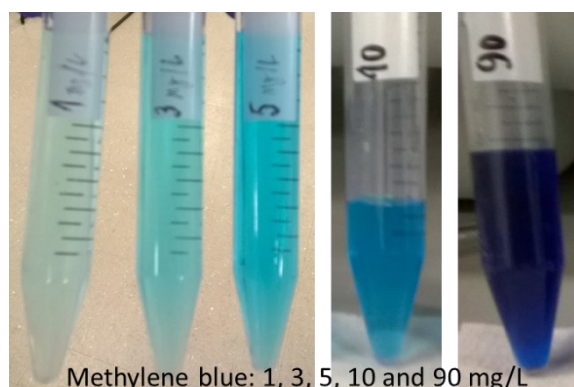


Figure 7.2: Samples of MB solutions with different concentrations (1, 3, 5, 10, and 90 mg/L).

7.2.1. Chars from slow pyrolysis of as-received wheat straw

The adsorption performances of the chars from slow pyrolysis of as-received wheat straw feedstock, in terms of maximum removal of dye (at equilibrium), are shown in Figure 7.3. The chars were produced with varying temperature (400-600 °C) and solid residence time

(SRT; 3-10 minutes). The performance of a commercial activated carbon (product details in Chapter 3) is also shown for comparison.

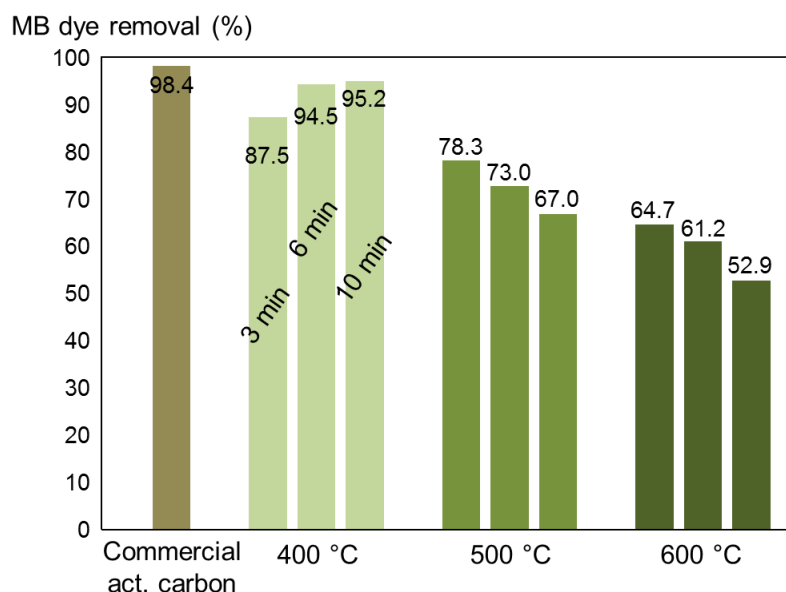


Figure 7.3: MB dye removal from water (at equilibrium) using commercial activated carbon and produced chars from varying T (°C) and SRT (minutes).

In parallel with maximum MB removal, adsorption capacity (mg/g) is an important parameter in adsorption, measuring how much adsorbate the adsorbent can remove, by weight. This depends greatly on the conditions used for adsorption, and for the tests performed here, the maximum capacity achieved was ≈ 38 mg/g, for the commercial activated carbon, and ≈ 37 mg/g, for the 400 °C chars. This value is relatively low compared to values found in literature: up to 366 mg/g with char or 2500 mg/g with a chitosan-bentonite composite [273]. However, adsorption capacity can be improved for example if high dye removal is still obtained when using lower adsorbent mass (evaluated in subsection 7.4.1).

The commercial activated carbon removed almost all (98.4%, from Figure 7.3) of the MB dye, and thus had the highest adsorption performance, as expected, since the product was commercialised as water decontaminant. It should however be noted that due to using a relatively high initial dye concentration of 100 mg/L, a >99% removal signifies that the final concentration was <1 mg/L (<1 ppm). For >90% removal, the final concentration was <10 mg/L. The presence of dyes such as MB imparts colour to drinking water even at concentrations ≈ 1 ppm, and in water bodies can affect dissolved oxygen and light penetration [385]. Legislation is very strict, with limits depending on region but virtually requiring complete removal/degradation [385]. Normally, if present, and depending on location, dyes are in much lower concentration in wastewater than the one used in this work. Adsorption is usually more

challenging when concentration is already relatively low (e.g., ≤ 1 mg/L) [41][267], and so it is necessary that the adsorbents have high performance even at those concentrations. Tests with lower dye concentrations were performed and shown in subsection 7.4.2.

In terms of the produced chars, it was verified that adsorption performance significantly decreased for chars produced at increasing pyrolysis temperature, and this parameter had the most influence on MB adsorption. The fact that lower temperature chars were more effective at removing the MB dye brings economic advantages to the production process since less energy is required to heat the pyrolysis reactor. To better understand the differences in adsorption performance using chars produced with low and high pyrolysis temperature (400 and 600 °C), photographs of samples of MB solutions after adsorption can be seen in Figure 7.4. A sample with the commercial activated carbon as adsorbent is also present for comparison (adsorption conditions: 100 mg/L initial MB concentration, 25 mg adsorbent, 50 °C, 180 minutes).

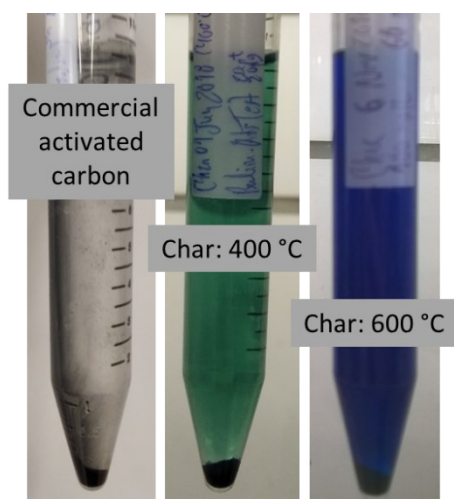


Figure 7.4: Samples of MB solution after adsorption using a commercial activated carbon (left), and chars produced with 400 and 600 °C pyrolysis temperature (middle and right tubes, respectively).

With Figure 7.4, and comparing with Figure 7.2, it is possible to see the visual changes that occur in the MB adsorption experiments. The commercial activated carbon yields an MB solution with no visual trace of MB (transparent solution), and the char produced at 600 °C produces practically no visual difference in the MB solution (dark blue solution). On the other hand, the char produced with 400 °C pyrolysis temperature yields a considerable removal of MB from solution, resulting in a light blue solution. The presence of solid particles on the sample tube walls results in a darkening of the solutions seen in Figure 7.4.

The influence of SRT was different according to the applied temperature, since adsorption performance increased with SRT for 400 °C chars, but decreased for 500 and 600 °C chars. The differences with SRT were however less significant than with temperature.

An important adsorbent property that is often viewed as necessary to obtain high adsorption performances is surface area, with activation being employed to increase the porosity of the solid material and produce activated carbons [40][202]. Furthermore, for increasing pyrolysis temperatures and as material is decomposed and removed from the solid product, porosity and surface area are known to increase [37][196][240]. However, for the chars produced in this work, significant surface area was not achieved with the screw reactor, even at 600 °C process temperature (maximum 8.8 m²/g, see Chapter 4, subsection 4.4.5). For the commercial activated carbon tested in this work, on the other hand, porosity was much more significant, with the results from N₂ physisorption (77 K) analysed with QS-DFT model presented in Table 7.1. The isotherm and pore size distribution for the commercial activated carbon can be found in Appendix E.

Table 7.1: Results from N₂ physisorption (77 K) analysed with QS-DFT model for commercial activated carbon.

	Surface area (m ² /g)	Total pore V (cm ³ /g)	Micropore V (%)
Commercial activated carbon	615.0	0.64	47

The commercial activated carbon had a type II adsorption branch, and hysteresis (type H4; capillary condensation), typical of micro-mesoporous carbons [361]. The adsorption performance of the commercial activated carbon was thus connected to high surface area and pore volume, significantly higher compared to the chars.

For adsorption of organic compounds from water such as MB, the porosity domain of interest is mainly mesoporosity (2-50 nm) [235]. This is due to the size of the adsorbate molecule (1.7 nm longest side [279][386]), compared for example to relatively smaller gas molecules, for which microporosity is more relevant [233]. For the chars produced in this work, the present porosity, besides being relatively small, was mostly narrow micropores (subsection 4.4.5, Chapter 4). For the commercial activated carbon, the mode of pore size was determined as 0.97 nm, however, the N₂ adsorption capacity across a wide range of pore sizes (2-30 nm) was significantly higher compared to the char products (see pore size distribution, Appendices C for all char products and Appendix E for commercial activated carbon).

FTIR analysis showed a lack of functional groups in the commercial activated carbon (spectrum in Appendix E) compared to the chars, and the pH value (in H₂O) was 3.24 (±0.14),

significantly lower than the value for chars from experiments varying temperature and SRT (8.5-9.6, from Chapter 4 subsection 4.4.4).

Since high adsorption performance was found using the produced wheat straw chars even without significant surface area, this suggests that internal porosity was not required for adsorption, and other features play a more important role. For the commercial activated carbon, however, surface area and porosity were the main driving forces for MB adsorption.

Based on char analyses, the higher performance obtained with lower temperature chars can be explained by a greater proportion of surface functional groups that can interact with MB molecules in solution. The importance of surface chemical functionalities in adsorption is known [98][354][366].

Increasing pyrolysis temperature removes volatile matter and functional groups, especially those with heteroatoms (e.g., O, N), increasing carbon content and char aromaticity [26][29][95][178][189]. Increasing pyrolysis temperature can modify or remove polar and oxygen-containing functional groups, which can interact with contaminants [387][388]. A greater presence of functional groups with C-O and C=O bond vibrations was verified with FTIR for the lower temperature chars, along with higher volatile matter content and H:C and O:C ratios (see Chapter 4, subsections 4.4.1. and 4.4.2.). Modifying functional groups changes the surface charge of the adsorbent, and thus the affinity towards water (hydrophobic/hydrophilic) and pH value, which are important factors in adsorption from water [388][389]. The pH value of chars (in H₂O) was found to increase with pyrolysis temperatures (i.e., the chars became more alkaline). Since the MB molecule in solution is cationic, it will be more attracted to anionic compounds and thus lower temperature chars with lower pH.

The different trends of MB removal with SRT for different pyrolysis temperatures could be explained in the following way: at 400 °C, a lower proportion of chemical functionalities relevant for MB adsorption was removed compared to higher temperature, and so increased SRT did not affect them significantly, while higher temperatures removed a greater proportion of functionalities, and keeping the higher temperature for longer time removed even more functionalities. Furthermore, for the lower temperature, due to the lower vapour production, VRT (vapour residence time) was longer than for higher temperature (see Chapter 4, subsection 4.3.1). Longer VRT can favour reactions between vapours and solids, which could add functionalities to the char surface and consequently improve MB adsorption.

To support these findings, linear correlations were made between various char properties and MB removal. This was performed for each set of produced chars, with the coefficients of determination (R^2) for chars produced with varying temperature and SRT from as-received feedstock indicated in Table 7.2. The graphs are presented in Appendix F, since the key result was the coefficient of determination, R^2 , and section 7.3 shows the same graphs but for all of the produced chars.

Table 7.2: Coefficients of determination for the linear relationship between char properties and MB removal for chars produced with varying temperature and SRT, and indication of positive (+) or negative (-) correlation.

	VM	FC	Ash	C	H	O	H:C	O:C
R ²	0.93 (+)	0.88 (-)	0.53 (-)	0.93 (-)	0.84 (+)	0.93 (+)	0.89 (+)	0.93 (+)
	pH (in H ₂ O)		Surface area		Total pore V		Pore size	
R ²	0.18 (-)		0.00 (+)		0.09 (-)		0.31 (-)	

The main char properties that had stronger correlations ($R^2 \geq 0.7$) with maximum MB removal were volatile matter and fixed carbon contents, elemental carbon, hydrogen and oxygen contents, and H:C and O:C ratios. On the other hand, pH value and porosity-related properties had the weakest correlations ($R^2 \leq 0.3$). These results overall agree with what was suggested based on the results from Figure 7.3, with the exception of the poor correlation with pH value. This was likely because of the non-monotonic trends of char pH value with temperature and SRT: the maximum pH value was at the middle SRT value, and the same occurred with temperature (see Chapter 4, subsection 4.4.4).

A study of five woody and herbaceous feedstocks had found a positive correlation between H:C and O:C ratios and iodine adsorption [390]. Iodine has a similar molecular size to methylene blue and is thus frequently used to probe similar porosity domains: iodine for pores >1 nm, MB for >1.5 nm [254].

Due to the better adsorption performance (in terms of maximum MB removal) of lower temperature chars and to the influence of volatile matter and functional groups, samples of feedstock and torrefied feedstock (300 °C) were also tested in MB adsorption, with results in Table 7.3.

Table 7.3: Maximum MB removal from solution (at equilibrium) with feedstock and torrefied feedstock (300 °C).

	Wheat straw feedstock	Torrefied feedstock (300 °C)
Max. MB dye removal (%)	89.4	97.6

Adsorption performance with torrefied feedstock surpassed the ones from the 400 °C chars, which further suggests surface functionalities and H:C and O:C ratios (which were higher in torrefied material, see Chapter 2, subsection 2.1.2) favour MB adsorption from water. However, the torrefaction process produces a material less stable than char, due to the higher remaining proportion of lignocellulosic material, prone to modification or degradation (e.g., biological, oxidation) [391]. Leaching of organic solutes could also occur, negatively affecting

the water by increasing chemical oxygen demand (COD) and potentially providing coloration [19].

The feedstock itself had significant MB removal from solution, even superior to 500 and 600 °C chars, however, the problem of degradation is exacerbated due to the greater cellulose and hemicellulose contents [5]. The feedstock, although having higher H:C and O:C ratios and more surface functionalities, could have its performance hindered due to volatile matter content being too high, inhibiting MB adsorption by stereochemistry or competition [41]. Furthermore, the feedstock has a more hydrophilic behaviour and this could lower the affinity towards the adsorbate [267].

A study with a mixture of sawdust and sugarcane straw [392] found that the feedstock had the highest removal of MB from solution, with the performance decreasing when using chars from that feedstock mixture (400, 600, 800 °C) due to the removal of oxygenated functional groups, e.g., carboxylates ($-\text{COO}^-$) and phenolates ($-\text{O}^-$). Moreover, for the 800 °C char, the performance slightly increased compared to other chars, which was connected to increased surface area.

As mentioned for the feedstock and the torrefied materials, the chars also have a certain volatile matter content, which can potentially leach into the water, especially for the chars produced at lower temperatures (which coincidentally were the ones with better adsorption performance). For traditional adsorbents such as activated carbon, the volatile matter content is significantly reduced during production, increasing the stability of the material and reducing potential leaching of compounds. Hence, although the surface functional groups (part of the volatile matter) were the main contributors for the adsorption performance of the chars, the issue of stability and compound leaching during adsorption must be considered.

To investigate how adsorption performance was affected and if it could be improved, chars from experiments with modified feedstock/process were evaluated by adsorption of MB as well. The modifications, including integrating slow pyrolysis with procedures used in activation, were meant to provoke changes in char properties that would improve adsorption performance (e.g., increased surface area, changes in surface chemical functionalities). The employed procedures were however considerably milder compared to traditional activation, since the purpose was also to produce more sustainable and affordable carbonaceous adsorbents to replace activated carbon for water contaminant removal.

7.2.2. Chars from slow pyrolysis of wheat straw with varying moisture content

The first modification on the feedstock/conditions of the slow pyrolysis experiments was feedstock moisture content (M), and the results of MB adsorption using chars from those experiments are shown in Table 7.4.

Table 7.4: Removal of MB dye from water (at equilibrium) for chars produced from experiments with varying feedstock moisture content ("M").

T (°C)	400			600		
M (wt.%, wet basis)	0.1	50	75	0.1	50	75
Max. MB dye removal (%)	98.3	96.4	96.1	68.9	72.6	67.1

The char with highest MB removal (400 °C, 0.1 wt.% M) obtained the greatest adsorption capacity of this set of chars, of ≈ 38 mg/g, which was similar to when using 400 °C chars (previous subsection), due to the adsorption conditions (e.g., solution volume and concentration, adsorbent amount) being the same and due to the similar maximum MB removal values.

It was verified that the lower pyrolysis temperature chars had higher MB removal than the higher temperature ones, consistent with what occurred with chars from as-received feedstock. Comparing with the chars from as-received feedstock, there was an improvement in maximum MB removal when using any of the chars from varying feedstock moisture content (M), however, the char produced with minimum M (0.1 wt.%) had the highest MB removal. Since the adsorption performance with 400 °C chars from feedstock with elevated M was significantly high (>95%), this indicates that feedstock drying can be avoided, which reduces production costs. However, drying the feedstock can have even higher MB removal if required, although with higher production costs.

Linear correlations between MB removal and char properties were established for this char set (graphs in Appendix F), with the coefficients of determination presented in Table 7.5.

Table 7.5: Coefficients of determination for linear relationships between char properties and MB removal for chars from varying feedstock moisture content (M), and indication of positive (+) or negative (-) correlation.

	VM	FC	Ash	C	H	O	H:C	O:C
R ²	0.91 (+)	0.87 (-)	0.84 (-)	0.96 (-)	0.92 (+)	0.94 (+)	0.99 (+)	0.91 (+)
	pH (in H ₂ O)		Surface area		Total pore V		Pore size	
R ²	0.86 (-)		0.10 (+)		0.35 (+)		0.24 (+)	

From char analyses in Chapter 4 (subsection 4.4.1.), chars from varying feedstock moisture content (M) had higher volatile matter content and oxygen content than the ones from as-received feedstock, which can be linked to the differences in MB adsorption. However, comparing only between the chars from pre-treated feedstock (0.1, 50 and 75 wt.% M), the chars from reduced M were the ones with highest volatile matter content, while the oxygen content (and O:C ratio) increased with feedstock M. This was also corroborated by FTIR

analysis, in which more oxygen-containing functional groups were seen for the chars from elevated reduced M, however not for the chars from reduced feedstock M. This suggests MB adsorption was affected by volatile matter content and oxygen content (and O:C ratio), with a compromise between both being necessary for best performance.

It should be noted that the chars from reduced feedstock M, unlike the other ones, were produced in the second screw reactor, and it was suggested (Chapter 4) that this reactor favoured secondary reactions or even inhibited carbonisation, which could lead to different char characteristics such as increased volatile matter.

For chars produced with varying feedstock moisture content, the strong correlations observed for the first char set were maintained, however the strongest correlation was now with H:C ratio. The coefficient of determination with ash contents increased significantly, to similar strength to the correlation with fixed carbon contents. Furthermore, the coefficient for pH also became significantly strong, becoming comparable to the other strong correlations.

MB removal was higher when using chars from varying feedstock M, which based on analyses was connected to increased volatile matter and oxygen contents, which were then connected to changes in surface functionalities (i.e., higher manifestation of O-containing groups such as C-O and C=O) and consequently in pH value (overall lower than chars from as-received feedstock).

A comparison of twenty one chars [348] had found that higher O:C ratios led to higher cation exchange capacity, which can benefit adsorption. Iodine adsorption also benefited from increased O:C and H:C ratios in a study with several biomass feedstocks [390]. Minkova *et al.* verified that for pyrolysis (750 °C) of several biomass types, using steam led to preferable removal of some oxygen-functional groups compared to others [387]. Carboxylic (-COOH) and lactonic (-C(=O)-O-) groups were absent from the chars, and only phenolic (-C₆H₅-OH) and carbonylic (-C=O) functional groups were found in significant amounts by Boehm titration. This signifies that the nature of the surface functional groups on char can change depending on production temperature, with consequences for the adsorption process.

7.2.3. Chars from slow pyrolysis with CO₂ as reaction atmosphere

The chars produced from experiments using CO₂ as reaction atmosphere (by injecting it as a gas into the reactor during slow pyrolysis) were tested for MB adsorption and the results of maximum dye removal are presented in Table 7.6, along with results from using chars from experiments using N₂ and without injecting gas. The adsorption capacities observed with chars from CO₂ experiments (and N₂) were similar to the previous ones, with maximum ≈38 mg/g for 400 °C with CO₂ as injected gas.

Table 7.6: Removal of MB dye from water (at equilibrium) for the chars produced from experiments with N₂ or CO₂ as injected gases, or using no injected gas.

T (°C)	400			600		
Injected gas	None	N ₂	CO ₂	None	N ₂	CO ₂
Max. MB dye removal (%)	93.5	92.6	95.4	72.1	71.6	70.8

The chars produced at lower pyrolysis temperature outperformed the ones from higher temperature, as had occurred for the other slow pyrolysis chars. This was connected to the greater presence of surface functionalities in the lower temperature chars, which allow for greater MB adsorption due to for example electrostatic attraction (see Figure 2.10, Chapter 2, subsection 2.4.3).

For the higher temperature chars, the results suggest that injecting gas reduces performance, which could be related to the removal of surface functional groups when gas is injected, or to less deposition of volatiles/tars on the chars, since the higher gas flow rate removes the vapours quicker and reduces VRT. The difference between using N₂ or CO₂ for 600 °C chars was less significant.

The fact that the differences in MB removal between 600 °C chars were lower can be due to greater formation of vapours at higher pyrolysis temperature, which already cause a reduced vapours residence time (as was seen by VRT in section 5.2, Chapter 5). This was added to the fact that the injected gas flow rate was relatively low (1 L/min), and that the pyrolysis vapours already had CO₂ in their composition (27-59 vol.%, see Chapter 5, section 5.2).

Linear correlations between MB removal and char properties were established for the chars produced with different injected gases (CO₂, N₂, or none), with the coefficients of determination presented in Table 7.7, and the graphs in Appendix F.

Table 7.7: Coefficients of determination for linear correlations between char properties and MB removal for chars produced with varying injected gas, and indication of positive (+) or negative (-) correlation.

	VM	FC	Ash	C	H	O	H:C	O:C
R ²	0.78 (+)	0.72 (-)	0.88 (-)	0.81 (-)	0.82 (+)	0.73 (+)	0.95 (+)	0.74 (+)
	pH (in H ₂ O)		Surface area		Total pore V		Pore size	
R ²	0.90 (-)		0.20 (-)		0.03 (+)		0.30 (+)	

For the chars produced with varying injected gas, the coefficients of determination for VM, carbon and oxygen contents and O:C ratio became weaker, and the strongest correlations were with H:C ratio and pH value. Contributing to this is the fact that comparing MB removal

for different injected gas, the trend was different depending on temperature. Using CO₂ resulted in the highest removal at 400 °C, however for 600 °C chars the ones produced with CO₂ as injected gas had the worst performance.

For the lowest temperature (400 °C), the chars produced with CO₂ as injected gas had higher MB removal than the ones from using N₂ or not injecting gas. This was related to the changes found in char properties (Chapter 5): the chars produced from using CO₂ had higher oxygen content and O:C ratio. This occurred even though the injection of gas (for both CO₂ and N₂) overall reduced volatile matter content and increased fixed carbon content, suggesting adsorption did not depend on volatile matter content as much as on O:C ratio. The H:C ratio was lower for chars produced with CO₂. The CO₂ chars also had lower pH than others (more acidic), which may have also benefited adsorption.

For 600 °C chars, the same property changes occurred for chars produced with CO₂: higher oxygen contents and O:C ratio, lower H:C ratio and pH. However, these changes did not correlate with adsorption performance, since the CO₂ ones had the lowest maximum MB removal. This was likely related to the significantly lower volatile matter content, which did not vary much between chars produced without injecting gas or with N₂ (23-25 wt.%) but decreased significantly for CO₂ ones (15 wt.%).

Cho *et al.*, in a study comparing chars produced from spent coffee grounds with N₂ or CO₂ atmospheres (900 °C), found that even though the CO₂ char had higher surface area, the MB adsorption was higher with the N₂ one [371]. Using ≈10-137 mg/L of initial MB concentration in 20 mL solution volume and 100 mg of adsorbent, the maximum adsorption capacities were: 4.5 mg/g for char from N₂ and 4.1 mg/g for char from CO₂. This was said to be due to the CO₂ atmosphere removing functional groups such as –OH, C–H, C=O, C–O from the char surface. From the FTIR analyses of chars produced in this work there was no indication that this occurred, since no significant differences were found between using different injected gases. Moreover, the oxygen contents were increased when injecting CO₂.

Franciski *et al.* [393] compared 800 °C char from barley malt bagasse with the same char after CO₂-activation, and found that char after activation was more suitable for MB adsorption. Surface area increased from 0.2 m²/g to 80.5 m²/g, and oxygen contents decreased (≈5 wt.%) compared to the unmodified char. However, the CO₂-activated char still had significant oxygen content, ≈28 wt.%, higher than the ≈25 wt.% in this work from 400 °C chars from wheat straw under CO₂ atmosphere. No differences were seen in FTIR analysis comparing the char with activated char. The maximum adsorption capacity was 161 mg/g (50 mg adsorbent, 50 mL solution, 0-500 mg/L initial dye concentration). Due to this, the differences in adsorption performance were connected to the increase surface area and

mesoporosity. Despite the higher adsorption capacity compared to this thesis, the maximum removal obtained was significantly lower, $\approx 70\%$.

7.2.4. Chars from slow pyrolysis of KOH-impregnated feedstock

The results of maximum dye removal with the chars from the slow pyrolysis experiments with KOH-impregnated feedstock are presented in Table 7.8. The results from using the chars from soaked and dry feedstock (0.1 wt.% feedstock moisture content, wet basis, here denoted as 0 M KOH concentration), are also shown for comparison, since the feedstock was also oven-dried after the wet impregnation with KOH solution and before the slow pyrolysis experiments. The adsorption capacities observed with chars from experiments using KOH were similar to the previous ones, with maximum ≈ 38 mg/g.

Table 7.8: Removal of MB dye from water (at equilibrium) for the chars produced from experiments with KOH-impregnated feedstock.

T (°C)	400			600		
KOH concentration (M)	0	0.1	1	0	0.1	1
Max. MB dye removal (%)	98.3	98.5	94.0	68.9	68.7	83.8

As had occurred for the other chars, the ones produced at 400 °C outperformed the 600 °C ones in terms of maximum MB removal. There was however a significant increase in MB removal with the char from 600 °C and 1 M KOH, although still lower than the 400 °C chars.

For the 400 °C chars, the one produced from feedstock impregnated with 0.1 M KOH solution had the highest MB removal of all the tested chars. The char produced from non-impregnated feedstock obtained slightly lower but similar performance. For the highest KOH concentration (1 M), the adsorption performance was decreased compared to other 400 °C chars, although still with acceptable results.

Considering char analyses (Chapter 6), oxygen contents significantly decreased for 400 °C chars with 1 M KOH, while carbon and hydrogen contents increased, with a consequent decrease in O:C ratio and increase in H:C ratio. These characteristics were confirmed with FTIR, through increased intensity of IR manifestation for C=C and C-H_n bonds and decreased for C=O and C-O ones. This suggests MB adsorption was affected by the removal of oxygen-containing functionalities. There could also have been a contribution of change in pH value (results in Chapter 6, subsection 6.4.4): the chars produced at 400 °C with 0.1 M KOH had the lowest pH, and lower pH was found to favour MB adsorption.

A very significant difference between chars was the ash proportion: the chars produced from 1 M KOH had significantly higher ash contents than 0 or 0.1 M KOH chars (see

subsection 6.4.1 in Chapter 6). The inorganic material likely covered the char surface and pores, which decreased the number of available sites for adsorption [254][307]. There could also have been competition between cationic MB and K^+ in solution [39], however, some research examples verified that MB adsorption was insensitive to several ions including K^+ [394]. A decrease in adsorption performance was indeed noticed for 1 M KOH chars produced at 400 °C, however, the opposite occurred for 600 °C. It was possible that the inorganic contents could have favoured MB adsorption, through ion exchange or other mechanisms [281].

Similarly, the improved performance for the 600 °C char with 1 M KOH could be due to the higher oxygen content and O:C ratio compared to other 600 °C chars (see subsection 6.4.2). The elemental composition of 600 °C chars with 0 and 0.1 M KOH were similar between themselves, and the adsorption performance as well, even though the ash contents were significantly higher for the 1 M KOH char compared to the other two.

Linear correlations between MB removal and char properties were established for the chars produced with feedstock impregnated with different concentrations of KOH solution (0, 0.1, or 1 M), with the coefficients of determination presented in Table 7.9, and the graphs in Appendix F.

Table 7.9: Coefficients of determination for linear correlations between char properties and MB removal for chars produced with varying KOH solution concentration, and indication of positive (+) or negative (-) correlation.

	VM	FC	Ash	C	H	O	H:C	O:C
R ²	0.75 (+)	0.34 (-)	0.02 (-)	0.94 (-)	0.59 (+)	0.94 (+)	0.72 (+)	0.93 (+)
	pH (in H ₂ O)		Surface area		Total pore V		Pore size	
R ²	0.67 (-)		0.01 (-)		0.15 (+)		0.75 (+)	

Coefficients of determination were significantly altered compared to other char sets. The correlations with fixed carbon and hydrogen contents were significantly weakened, likely due to effects of KOH addition, and to not performing the char washing step. There was now a strong correlation with pore size, however the main correlations were carbon and oxygen contents and O:C ratio.

A study of KOH-activated hemp fibers found that surface functional groups greatly contributed to pesticide adsorption from water, with adsorption capacity correlating positively with the proportion of oxygen-containing groups [395]. The authors concluded that the main driving force for adsorption was dispersion between π electrons of the adsorbent structure and of the pesticide molecules. Adsorbent-adsorbate interactions increased with the number

of aromatic rings, due to delocalised π electrons over the rings, and smaller number or absence of aromatic rings led to slower adsorption.

Xie *et al.* found that the addition of cations such as Na^+ (0.01-0.12 M) into the adsorption solution led to enhanced MB adsorption on char from sorghum straw, and there was a synergistic effect between adsorption of cations and MB [396].

Once a char produced from KOH-impregnated feedstock and used for adsorption is exhausted and not recyclable, it could be burned to obtain energy, and applying the ashes to rehabilitate soils could have positive results, especially if soils are K-deficient.

7.3. Potential mechanisms for MB adsorption with chars

The same linear correlations established for each set of chars were also established for the whole collection of produced chars, as shown in Figure 7.5.

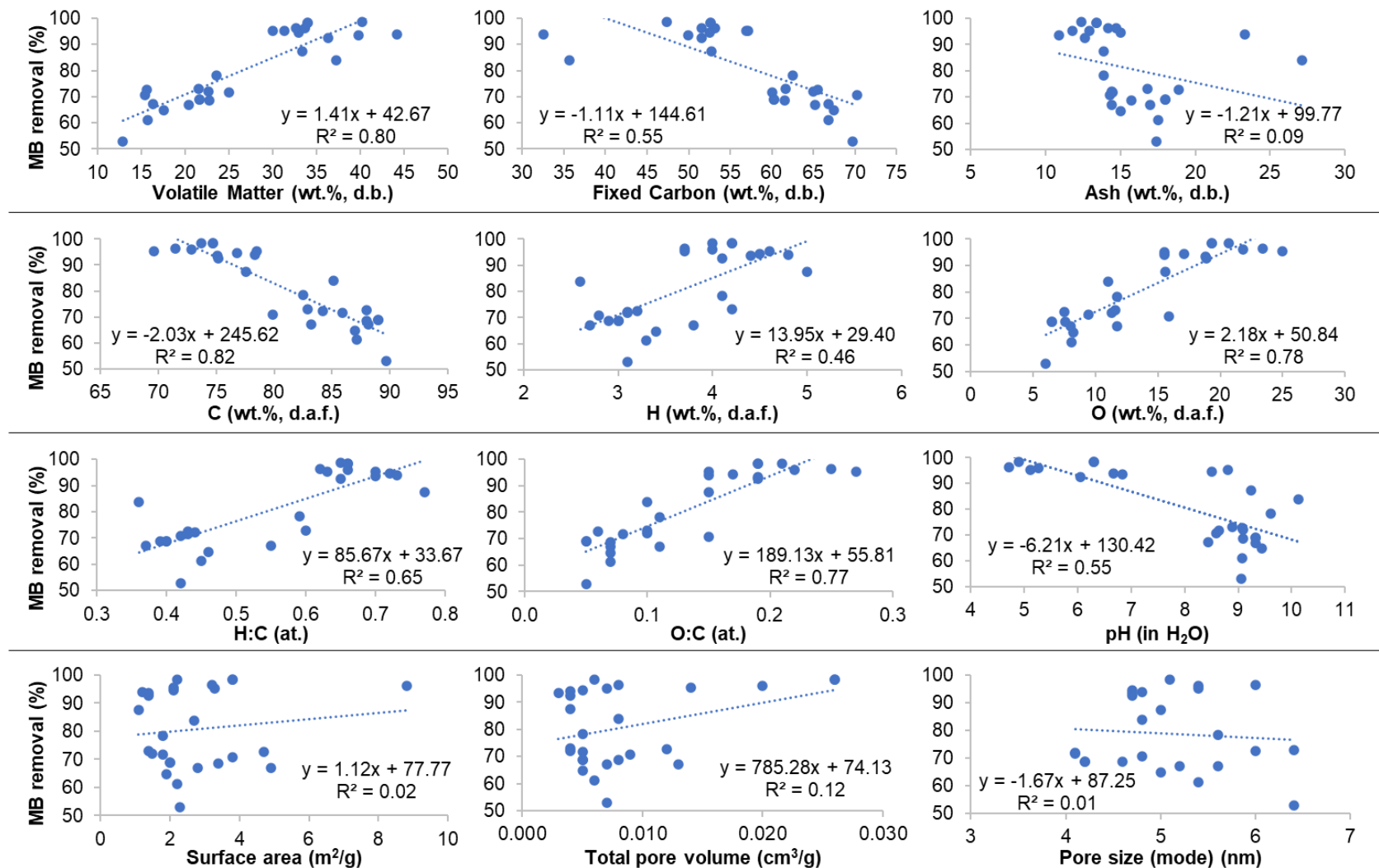


Figure 7.5: Correlations between MB removal from solution (% at equilibrium; vertical axis) and char properties (horizontal axis), for the whole collection of produced chars.

The only char properties with strong correlations ($R^2 \geq 0.7$) with maximum MB removal were volatile matter content, carbon and oxygen content, and O:C ratio. On the other hand, the weakest correlations ($R^2 \leq 0.3$) were with ash contents and porosity-related properties (surface area, total pore volume and pore size).

Overall, the correlations had the same trends (i.e., positive/negative) from the ones found for each char set, however, the coefficients of determination decreased. The trends and R^2 for the whole collection of chars were most similar to the ones from the first two sets of chars, produced with varying T and SRT, and also with different feedstock M. This was because, for those cases, the property changes were more linear both with temperature and with the varying parameter in study (SRT, M). For the other two char sets, from varying injected gas (reaction atmosphere) and different KOH solution concentration, the studied process variables produced some changes in char properties that were counter-intuitive, and produced less linear trends of the properties with temperature and the studied variables. For example, compared to chars from experiments without injected gas or using N_2 , the chars produced from CO_2 as injected gas had significantly lower volatile matter content, but higher oxygen contents and lower carbon contents (Chapter 5).

Overall, for the char properties in analysis, the points on the graph cluster into one large group or 2 or 3 smaller groups, linked to the char sets. However, the properties related to porosity had the least clustering and thus low coefficient of determination. Furthermore, especially for char sets of varying injected gas and KOH concentration, some properties can have significantly different value compared to chars from other sets.

The ash contents had overall low correlation with MB removal, with two points contributing strongly to this, corresponding to chars produced from feedstock impregnated with 1 M KOH solution. These chars had significantly higher ash contents than chars produced without KOH or with 0.1 M KOH solution concentration, and achieved relatively high MB removal values (94% and 84%, respectively, for 400 and 600 °C char). For other chars, increasing ash contents resulted overall in lower MB removal (negative correlation), which was because the ash content increase was connected with a loss of volatile matter and oxygen contents, and gain in fixed and elemental carbon contents. For the chars produced with 1 M KOH, however, the volatile matter contents were still significantly high, in agreement with the strong correlation between this property and MB removal. Adsorption tests using washed chars from KOH-impregnated feedstock would have been useful to investigate the role of inorganic material.

The correlations between char properties and MB removal allowed to investigate what contributed to the MB adsorption mechanisms (reviewed in subsection 2.4.3 Chapter 2). In this work, the main MB adsorption mechanisms (see Figure 2.10) were likely from electrostatic attraction and electron interactions ($n-\pi$ and $\pi-\pi$). Some contributions from hydrogen-bonding

interactions, MB attachment to hydrophobic/uncarbonized char segments, and filling of larger pores could also occur although to a significantly lower extent. The good performance of the char products in MB adsorption can be related to the possibility of simultaneous contribution of various mechanisms.

In the case of the chars produced in this work, since their pH was alkaline, oxygen-containing functional such as the ones depicted in Figure 2.10 (page 76, subsection 2.4.3) were negatively charged and thus the attraction of MB molecules was favoured. On the other hand, hydrogen-bonding interactions were less favoured.

To further investigate the adsorption mechanisms, analyses on the adsorbents after their use would have been useful, however, these were not performed due to time constraints and the already extensive list of experimental tests that had to be performed. Furthermore, regeneration and re-use of the adsorbents after adsorption would have also helped in identifying adsorption mechanisms.

7.4. Further adsorption studies

7.4.1. Varying adsorbent mass

Tests were performed using a selected number of best performing chars (maximum MB removal >90%), to investigate the effect of adsorbent mass on the maximum removal and adsorption capacity. The adsorbent mass was changed to 10 mg and compared to the already shown tests with 25 mg of adsorbent. The results are shown in Figure 7.6 and include the results for the commercial activated carbon tested previously. The bar graphs correspond to the maximum MB removal (%) and are read on the main vertical (left) axis, while the points are read on the secondary vertical (right) axis and correspond to adsorption capacity (at equilibrium; mg adsorbate per g of adsorbent). The bars that mention "400 °C" correspond to chars produced at 400 °C from unmodified process conditions and feedstock.

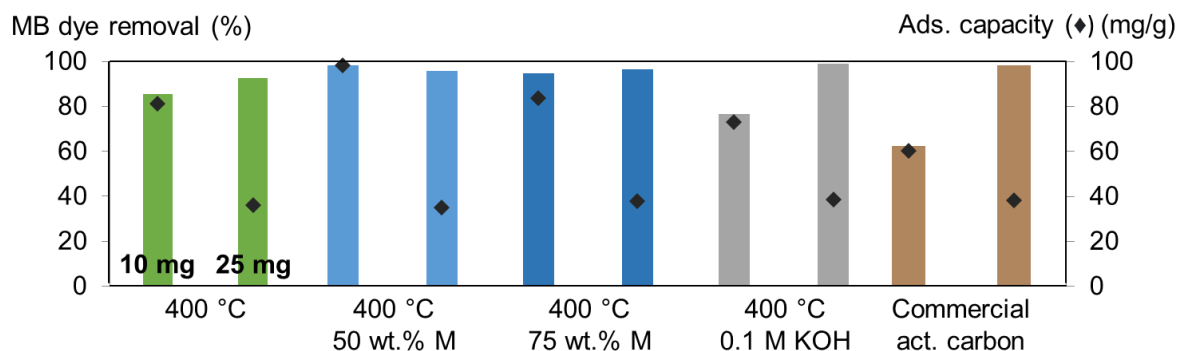


Figure 7.6: Removal of MB dye from water at equilibrium (bars; main vertical axis) and adsorption capacity (♦; secondary vertical axis) for selected chars using different adsorbent mass.

By testing lower adsorbent mass it was possible to enhance the differences between adsorption performances of different adsorbents, and to verify that in certain conditions the char products can have greater adsorption capacity than the commercial activated carbon.

The performance of the commercial activated carbon decreased significantly when 10 mg was used instead of 25 mg, and in those conditions the char performances were superior. This suggests that the available surface area in 10 mg activated carbon was not sufficient to adsorb the dye from solution with 100 mg/L initial concentration. It can be the case that a significant proportion of the internal surface area becomes unavailable due to filling of pores that could be used to access other pores, or because the pores do not serve for MB molecules due to being too small (i.e., ≤ 1.7 nm, size of longest side of MB molecule [279][386]). For the chars, however, it was verified that some of the tested chars kept a considerably high performance when lower mass was used, especially the ones from feedstock with elevated moisture content. This is very important since it allows using less adsorbent to remove the same dye concentration, which translates into higher adsorption capacity and economic savings. The decrease in maximum removal for the char produced with 0.1 M KOH when 10 mg was used could be linked to inorganic matter covering a greater proportion of surface and reducing the number of available active sites for MB adsorption.

In terms of adsorption capacity, differences are also very noticeable between the tested adsorbents. Comparing between the tests using 25 mg, the maximum capacity was ≈ 38 mg/g, for the commercial activated carbon, and the high performing chars also obtained comparable values of ≈ 37 mg/g. On the other hand, tests using 10 mg had much more noticeable differences. The char products were able to outperform the commercial activated carbon, which only increased its adsorption capacity by $\approx 59\%$. The 400 °C char from using 50 wt.% feedstock moisture content had the highest adsorption capacity of ≈ 98 mg/g, which was a $\approx 182\%$ increase. The adsorption capacity was still lower than other studies of MB removal with char in the literature (e.g., 366 mg/g [273]), however, it was increased significantly in this work.

These results suggest that the chars, although having lower surface area compared to the commercial activated carbon, have more available active sites for interaction with MB molecules. Perhaps what occurs with the commercial product is that the surface and most exposed pores become covered first, and then some of the inner porosity becomes inaccessible.

7.4.2. Varying initial dye concentration

Another parameter that was varied was the initial dye concentration, with tests performed with selected chars. The initial concentration was varied to 20 and 60 mg/L and

compared to the tests previously performed with 100 mg/L. The results in terms of maximum MB removal and final MB concentration are shown respectively in Figure 7.7 and Figure 7.8.

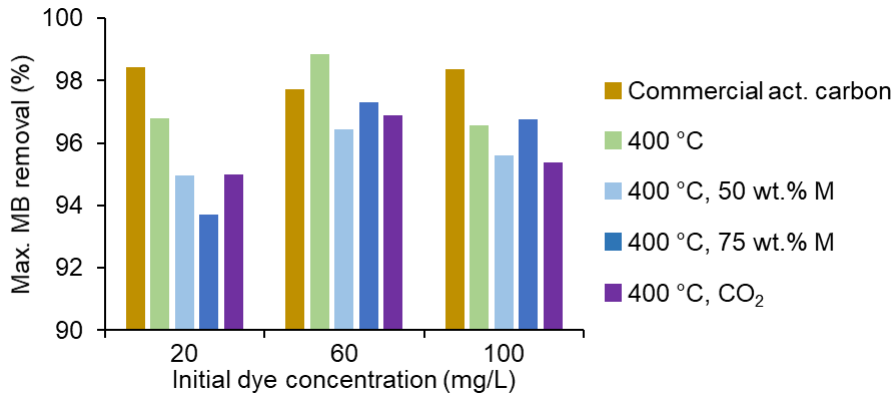


Figure 7.7: Maximum MB removal (% , at equilibrium) for adsorption tests with varying initial dye concentration.

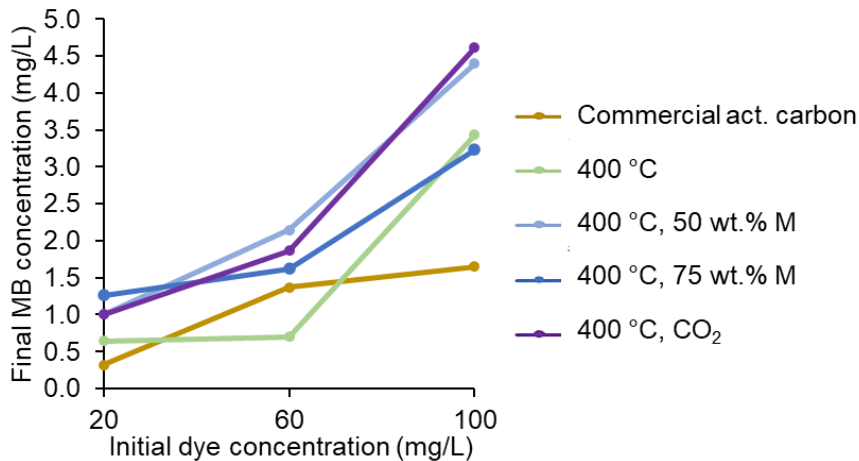


Figure 7.8: Final MB concentration (mg/L, at equilibrium) for adsorption tests with varying initial dye concentration.

Overall, for the tested chars, MB removal went through a maximum for 60 mg/L initial dye concentration, while for commercial activated carbon the opposite occurred, with a minimum for 60 mg/L. Because of this, for 60 mg/L the performances of all tested adsorbents were more similar, while for the other two initial dye concentrations the commercial activated carbon was superior (by 1-5%).

In terms of final dye concentration, improvements were possible compared to the preliminary tests with 100 mg/L since the maximum MB removal remained high. This allowed to obtain MB final concentrations using char as low as 0.6 mg/L (for 20 mg/L), while with the commercial activated carbon 0.3 mg/L final concentration was reached (also for 20 mg/L). For

60 mg/L, the char produced at 400 °C from unmodified feedstock and process even obtained lower final MB concentration compared to commercial activated carbon.

For both 20 and 60 mg/L, the differences between adsorbents were not as significant as for the highest initial dye concentration of 100 mg/L. This is important because removing dyes and other pollutants from water is usually more problematic for lower concentrations [41][267], and having the performance with chars in those cases comparable to commercial activated carbon means potential cost savings if replacing traditional adsorbents with char.

The performance with commercial activated carbon did not vary significantly comparing different initial dye concentrations, which correlates with the fact that the mechanism was more related to surface area and porosity. For adsorption with the commercial activated carbon, the governing step was likely diffusion within pores (internal diffusion) [397], more dependent on the adsorbent itself, which remained unchanged. On the other hand, for the chars, there were more significant differences in final dye concentration: the performance for lower initial dye concentrations was overall better (higher MB removal) compared to when starting with higher initial concentration. This could be explained by the mechanisms of adsorption when using the chars: the active sites were on the external surface, and when decreasing the quantity of dye molecules keeping the same amount of adsorbent, there were more free sites for adsorption and less competition between MB molecules.

In terms of adsorption capacity, compared to the preliminary tests (100 mg/L), it decreased since the same amount of adsorbent was used (25 mg) for smaller initial dye concentrations. For 20 mg/L, ≈ 8 mg/g was obtained, while for 60 mg/L adsorption capacity was ≈ 23 mg/g, with results similar for chars and commercial activated carbon.

The results from varying initial dye concentration are usually used to fit isothermal models such as Freundlich or Langmuir, however, due to only having three points for each char, it was not useful to do this in this work. The isothermal models help discern between adsorption mechanisms, e.g., mono- or multi-layer adsorption.

7.4.3. Adsorption of an acidic dye

In order to further understand the adsorption mechanism and corroborate the hypothesis of surface functionalities on the chars being the most influencing parameter, adsorption tests were carried out with an acidic dye, methyl orange. The employed adsorption conditions were the same as for the MB tests. MB is a dye with alkaline character and positive charge in solution (is cationic), while methyl orange (MO) has negative charge in solution (is anionic) and acidic character. If the char functional groups are contributing to the adsorption of the alkaline dye MB, e.g., by electrostatic interactions, then it is likely that the same functional groups will not be able to adsorb the acidic dye MO since they would repel MO

molecules. The results of MO adsorption in terms of maximum removal with selected char products are indicated in Figure 7.9.

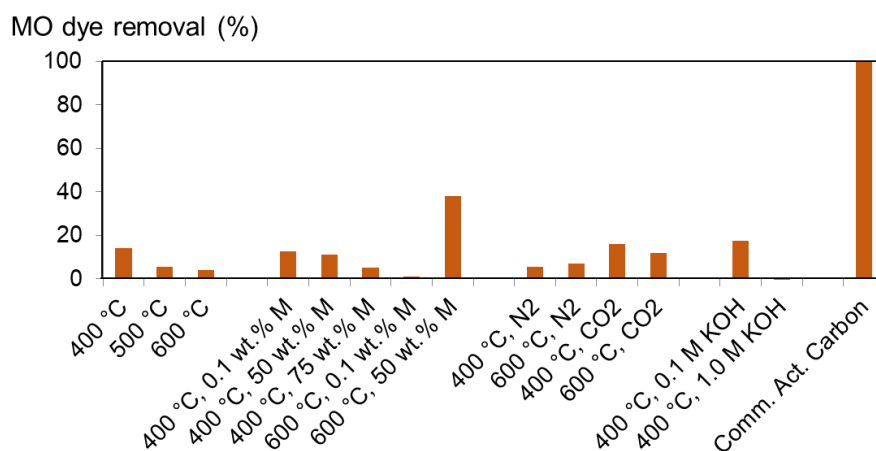


Figure 7.9: Removal of methyl orange dye from water (at equilibrium) by produced chars and a commercial activated carbon.

For the acidic dye, similarly to the alkaline MB dye, the commercial activated carbon was able to remove it almost entirely ($\approx 100\%$ removal), due to its high porosity and surface area. The chars produced in this work, on the other hand, could not achieve comparable performance to the commercial adsorbent, and their performance was much lower than with the MB dye.

The maximum MO dye removal obtained with the chars was $\approx 38\%$, with a char produced at 600 °C and from wheat straw with 50 wt.% feedstock moisture content (wet basis). With the 400 °C chars, the maximum removal was $\approx 14\%$, which was lower compared to the performances with the alkaline MB dye.

For the chars from as-received feedstock without process modifications, the results suggest a negative correlation between adsorption performance and pyrolysis temperature, which also occurred for MB, however, the maximum removal values are significantly lower for MO. This trend with pyrolysis temperature did not remain, however, for the other experiments with process or feedstock modifications, which did occur for MB.

None of the feedstock and process modifications led to significant improvements of MO adsorption with the chars produced at 400 °C, which was always $< 20\%$. The use of 400 °C char from feedstock impregnated with 1 M KOH solution even led to negative MO removal values (assumed as 0%). This could be due to compounds being released from the char into solution and leading to interference with the absorbance of MO during UV-Vis spectrophotometry.

The results obtained from MO dye adsorption corroborate the hypothesis of surface chemistry being responsible for the high adsorption performances of the lower temperature chars with the MB dye. The surface of the chars produced at lower temperatures has more O-containing chemical functionalities than the ones produced at higher temperatures, which relates to a greater pH in solution. These features ultimately result in greater electrostatic attraction to the cationic MB dye, removing more of this dye from solution, contrarily to the anionic MO dye, which has greater electrostatic repulsion to the lower temperature chars. This was true for the chars, but not for the commercial activated carbon, which removed both dyes efficiently, due to its significantly higher porosity and surface area compared to the chars. There can be some contribution of surface chemistry with the activated carbon, however based on performed analyses the main driver for adsorption was porosity and surface area.

A study comparing feedstock and chars produced at 400, 600 and 800 °C from a mixture of sawdust and sugarcane straw [392] also verified that the adsorption of an anionic dye was significantly lower than that of MB. The removal of anionic dye increased with production temperature, while for MB the highest removal was with the feedstock, and removal decreased with temperature until 600 °C. MB adsorption was favoured by greater presence of oxygenated functionalities on the feedstock and lower temperature chars, while the anionic dye adsorption was favoured by increased surface area.

Faria *et al.* and Pereira *et al.* [398][399] studied the adsorption of cationic and anionic dyes and found that besides surface area and porosity, the basicity or acidity of the adsorbents, derived from surface functionalities, play a key role. For anionic dyes, oxygen-free Lewis base sites related to delocalised π -electrons on basal planes of the adsorbent were the main contributors, with oxygen-containing groups having a negative effect. For cationic dyes, on the other hand, acidic oxygen-containing groups (e.g., carboxylic) had a positive effect, and adsorption could also be favoured by delocalised π -electrons.

In conclusion, the produced chars were much more efficient for a cationic dye than an anionic one, suggesting its use in adsorption would be suitable for compounds with positive charge in solution (e.g., other cationic dyes [398], heavy metals such as As, Cd, Cu, Cr, Pb, Zn [400][401]). The chars could also potentially be efficient for organic compounds with aromatic structures for electron delocalisation to favour the mechanism of electron interactions with the adsorbent, e.g., aromatic hydrocarbons such as phenol and its derivatives [402][403], some pesticides [235][395] and pharmaceuticals [404].

7.4.4. Kinetics studies

The evolution of adsorption with time was evaluated for a selected number of chars with highest performance, by sampling at certain time intervals until equilibrium. The removal

of MB dye with time for different chars and the commercial activated carbon can be visualised in Figure 7.10. Only values ≤ 5 minutes are shown, to highlight the different performances; dye removal continued until equilibrium (180 minutes). The full graph (0-180 minutes) is shown in Appendix G.

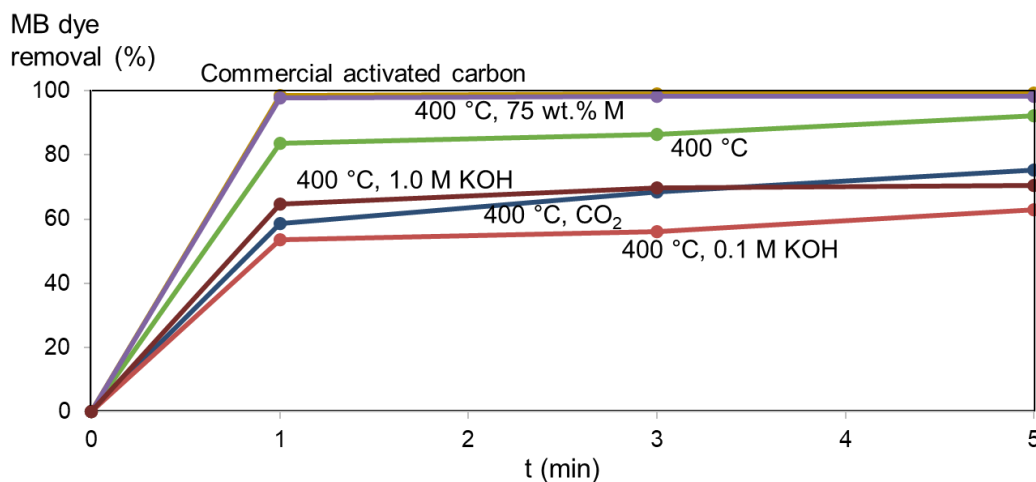


Figure 7.10: Evolution of MB dye removal from water with time (≤ 5 min) for selected chars and commercial activated carbon.

While within the first minute all the adsorbents achieved significant dye removal values, the commercial activated carbon practically achieved maximum removal (99%). Fast adsorption is a positive aspect, however, the downside is that investigating adsorption kinetics becomes more challenging. Nevertheless, these results are useful for the design and engineering of adsorption processes.

The adsorption with char products was overall slower than with commercial activated carbon, with some chars taking up to 100 minutes to reach maximum MB removal. However, the char produced with 75 wt.% feedstock moisture content achieved equilibrium similarly to the commercial activated carbon, within the first 5 minutes ($\approx 98\%$). Relatively fast adsorption (i.e., $\approx 95\%$ within 5 minutes) has been verified in other studies using chars [273]. Fast adsorption rate suggests adsorption occurred through chemisorption instead of physisorption, which is usually slower and governed by a diffusion mechanism [282][405].

Kinetics models were fitted to the results, which helps investigate the adsorption mechanism, e.g., if it is diffusion limited. The graphs representing the fitting to pseudo-first order and pseudo-second order models are presented in Appendix G. The coefficients of determination for selected chars are indicated in Table 7.10.

Table 7.10: Coefficients of determination (R^2) for data fitting to pseudo-first and -second order kinetics models.

	Pseudo-first order model	Pseudo-second order model
Commercial act. carbon	0.83	1.0
400 °C	0.89	1.0
400 °C, 75 wt.% M	0.54	1.0
400 °C, CO ₂	0.38	0.99
400 °C, 0.1 M KOH	0.79	0.99
400 °C, 1 M KOH	0.0	0.99

The adsorption data for all tested adsorbents had the best fitting with the pseudo-second order kinetics model, which suggests a chemisorption mechanism. It should be noted, however, that the pseudo-second order model is mathematically biased for cases with fast equilibrium [406]. This was the case for the commercial activated carbon, while for the chars equilibrium was reached slower, except for char produced with 75 wt.% feedstock moisture content. Many studies arrive to the erroneous conclusion that an adsorption process is governed by the pseudo-second order model, however, a good fitting is not enough to prove this, especially if points near equilibrium are used. Further investigations are suggested, for example by analysing the effect of different adsorbent particle sizes on adsorption.

7.5. Comparison of adsorption performance with the literature

In the previous subsections, comparisons of the MB adsorption results with the literature have been made, in text form, however, it was considered useful to have a comparison in table form (Table 7.11). Selected results from this thesis work have been included, to compare with relevant literature examples, with a column presenting the most relevant conclusions from each reference.

Table 7.11: Comparison of MB adsorption performance in this work with relevant literature examples.

Adsorbent	Feedstock	MB adsorption conditions	MB removal (max.; %)	MB ads. capacity (max.; mg/g)	Comments/conclusions	Reference
Char (400 °C, 10 min SRT, no injected gas)	Wheat straw pellets (no modification)	100 mg/L initial MB concentration; 25 mg adsorbent	95	37	MB adsorption favoured by functional groups, more relevant in lower temperature chars; modifying feedstock by KOH-impregnation improved adsorption, due to greater presence of oxygenated functional groups; CO ₂ environment during pyrolysis produced char with slightly better adsorption performance than using N ₂ environment, also due to functional groups	This work
Char (400 °C, 10 min SRT, CO ₂ flow)			95	38		
KOH-modified char (400 °C, 10 min SRT, no injected gas)			KOH-impregnated wheat straw (0.1 M solution)	99		
Char (400 °C, 10 min SRT, no injected gas)	Wheat straw (increased moisture content to 50 wt.% w.b.)	10 mg adsorbent (other variables as before)	98	98		
Char (700 °C, N ₂ flow)	Spent coffee grounds	9.9-136.6 mg/L initial MB concentration; 100 mg adsorbent	N/A	5		
Char (700 °C, CO ₂ flow)			N/A	4		
Chars produced at different temperatures (400-800 °C, 1h hold time, N ₂ flow)	Sawdust and sugarcane straw (pre-washed with HCl to remove soluble metals; pH neutralised with NaOH, NaHCO ₃ and distilled H ₂ O)	25 mg/L initial MB concentration; 10 mg adsorbent	N/A	10	Chars produced at 400 and 800 °C had the best performance, the former due to functional groups, the latter to increased porosity and surface area (590 m ² /g compared to 30 m ² /g); adsorption of an anionic dye was worst with 400 °C char and best with 800 °C char, due to a lack of favourable interactions with functional groups in the 400 °C chars and to being favoured by the surface area increase in the 800 °C chars	Mendonça <i>et al.</i> (2017) [392]

Table 4.11 (cont.): Comparison of MB adsorption performance in this work with relevant literature examples.

Adsorbent	Feedstock	MB adsorption conditions	MB removal (max.; %)	MB ads. capacity (max.; mg/g)	Comments/conclusions	Reference
Char (800 °C, 1h hold time, N ₂ flow)	Barley malt bagasse	Up to 500 mg/L initial MB concentration;	40	N/A	Mediocre MB removal with char, due to diminished volatile matter and surface groups, and small surface area (≤ 1 m ² /g); CO ₂ activation of char increased surface area (80 m ² /g; mainly mesoporous) and led to improved adsorption	Franciski <i>et al.</i> (2018) [393]
CO ₂ -activated char (900 °C, 1h, CO ₂ flow)		50 mg adsorbent (1 g/L)	70	161		
Char (500 °C; washed to neutrality)	Corn stalk (washed, dried, and cut to pass 100 mesh sieve)	50-500 mg/L initial MB concentration; 15-120 mg adsorbent (0.5-4.0 g/L)	59	43	KOH produced a more microporous structure, and increased surface area from 24 m ² /g (for unmodified char) to 474 m ² /g; H ₃ PO ₄ modification decreased surface area to 3 m ² /g; H ₃ PO ₄ -modified char performed worse than KOH-modified char, due to less favourable porosity, however, the performance was better than unmodified char due to surface functional groups, e.g., -OH, -COOH, -P-OH	Liu <i>et al.</i> (2019) [407]
KOH-activated char (700 °C, 2h, washed to neutrality)			100	406		
H ₃ PO ₄ -activated char (700 °C, 2h, washed to neutrality)			100	230		
Char (800 °C, 2h, N ₂ flow)	Sorghum waste (root and stem)	20 mg/L initial MB concentration;	Low (colour similar to initial)		KOH-impregnated feedstock led to chars with higher surface area (168 m ² /g for root-derived char and 949 m ² /g for stem-derived char, compared to <1 m ² /g for root- and stem-derived chars from unmodified feedstock) and greater presence of oxygenated functional groups on the surface, which contributed to higher adsorption performance	Hou <i>et al.</i> (2020) [408]
Char from KOH-impregnated feedstock (800 °C, 2h, N ₂ flow)	Sorghum waste (root and stem; KOH-impregnated, 1 M KOH solution)	20 mg adsorbent	98	93 and 98 (root and stem, respectively)		

For increased adsorption performance, the usefulness of modifying the slow pyrolysis process has been verified by other authors, including the use of CO₂ as reaction environment, and modifying the feedstock, e.g., through KOH-impregnation. This was due, overall, to increased surface area and adequate porosity domains, but also due to the contribution of surface functional groups, mainly O-containing ones. This conclusion agreed with the results in this thesis work. The adsorption performances achieved in this work were above some of the literature examples, especially in terms of percentage of MB removal.

7.6. Limitations of the adsorption studies

It is recognised by the author that the adsorption tests performed in this work have limitations and were mainly of preliminary nature, because the main purpose was only to assess the potential of the solid products from slow pyrolysis of wheat straw (unmodified or not) in a screw reactor for water decontamination.

Other parameters besides the ones studied here are usually evaluated, such as pH and ionic strength in solution. It was chosen not to study these parameters because the purpose was not to perform an in-depth evaluation, but to investigate the applicability of the chars as adsorbents, as more affordable and sustainable alternatives to traditional activated carbons. Changing parameters such as pH and ionic strength in a real wastewater treatment process makes the process more costly and this was not desired. It was also not considered necessary since some preliminary tests obtained adsorption performance comparable to commercial activated carbon. Furthermore, some researchers that studied pH and ionic strength found that these parameters did not significantly influence dye adsorption [39][284].

An adsorbent property that is considered relevant for adsorption in liquid phase is the pH at the point of zero charge (pH_{pzc}), i.e., the pH value at which the adsorbent surface has neutral charge. This property is used to determine the pH range in which the adsorbent is more likely to attract the adsorbate, and is thus used to optimise pH conditions during adsorption. For cationic dyes such as MB, attraction occurs when $pH > pH_{pzc}$, since the adsorbent has negative charge [27][272][273]. Since it was chosen not to control or vary solution pH during adsorption, char pH_{pzc} was not measured.

In terms of adsorption conditions, temperature can have significant influence on adsorption performance, and its impact has been evaluated in some adsorption studies. Temperature often positively affects adsorption [272], however, it has also been verified to have a negative effect [273]. In this work, adsorption temperature was kept constant, and at 50 °C due to using a sonicator as mixing method (the equipment naturally heats up during operation, see Chapter 3, subsection 3.4.2, for more information). It would be ideal to use room temperature, in a real water decontamination process, which is usually done in

continuous columns, because it is costly to keep a constant higher temperature during adsorption. Preliminary tests were performed at room temperature (with mechanical mixing, as described in Chapter 3), and adsorption performance with the commercial activated carbon was also high (99%).

It is also recognised that the use of a sonicator as mixing method in adsorption was not the most adequate, since in a larger scale application this equipment is likely to not be suitable and rather energy intensive. Furthermore, at a small scale, due to the features of sonication, e.g., cavitation (provides high mixing efficiency), changes may occur on the surface of the adsorbent material:

1) Erosion. This has been recognised to occur in certain conditions [326][409], and could increase the surface area of the adsorbent and lead to over-estimations of adsorption performance. It was considered, however, that this did not occur in this work, since the adsorbent particles already have a relatively small particle size ($\leq 425 \mu\text{m}$), and if it occurred the higher temperature chars would have had increased adsorption performance, which was not verified. The surface area could have been analysed after adsorption, however for N_2 physisorption (77 K) the amount of adsorbent available after the test was not sufficient.

2) Desorption of compounds from the char structure. Another consequence of sonication, due to its highly energetic nature, is the potential release of compounds from the solid [327]. Sonication is often used to degas and clean materials, as well as to extract substances [289][327][409][410]. Examples of compounds potentially desorbed from chars would be water (moisture), CO_2 , PAHs and VOCs, which could be present from char production or storage. Compound desorption could lead to interference with the adsorption process due to competition for adsorption sites and even attraction between desorbed compounds and the target adsorbate(s). This could however also increase the number of available sites for adsorption, due to the release of adsorbed substances, which would be advantageous for adsorption performance if competition and interference with MB adsorption would not occur.

7.7. Summary of Chapter 7

Char from slow pyrolysis of unmodified feedstock (wheat straw in broken pellet form) was effective at removing the organic dye MB from solution. The maximum dye removal and adsorption capacity were comparable to a commercial activated carbon, although lower (95% maximum removal compared to 98%, and 37 mg/g adsorption capacity compared to 38 mg/g).

The main char properties contributing to adsorption were surface functionalities based on oxygen-containing groups, due to greater oxygen content and O:C ratio. Linear correlations between MB removal and char properties corroborated this finding. For the commercial

activated carbon, on the hand, porosity-related properties such as surface area and mesoporosity were the main factors favouring adsorption.

Adsorption performance using the chars was improved (maximum 99% MB removal) through some of the modifications applied on process conditions or feedstock, especially soaking the feedstock with water or with a KOH solution with low concentration (0.1 M). The improved adsorption was mainly connected to increased oxygen contents in the chars, which resulted in greater presence of favourable surface chemical functionalities and higher O:C ratios, known to be connected to increased cation exchange capacity [348]. Even though the process and feedstock modifications did not significantly improve porosity-related char properties, as could be expected, MB adsorption performance was increased. Higher KOH solution concentration (1 M) during feedstock soaking decreased the maximum MB removal likely due to surface and pore coverage by inorganic material. The maximum adsorption capacity obtained was ≈ 38 mg/g for the conditions applied (relatively high initial dye concentration of 100 mg/L, 25 mg of adsorbent, 10 mL solution volume).

Adsorption with the chars produced in this work was successful for a cationic organic contaminant, however not for an anionic one. This was due to char properties, such as presence of polar and negatively-charged surface groups, and the nature of the contaminant, which resulted in repulsion of the anionic molecules. The results suggest the chars were more suitable for contaminants with cationic nature (e.g., positive charge) and aromatic rings for electron delocalisation.

The adsorption capacity using char was increased to ≈ 98 mg/g when decreasing the amount of adsorbent from 25 to 10 mg, which was a $\approx 182\%$ increase compared to the other conditions. Such a significant increase did not occur when using the commercial activated carbon, which suggested the active sites on the activated carbon became occupied faster, and/or became inaccessible. This finding supported the potential of chars to replace traditional activated carbon in decontaminating water.

When testing lower initial dye concentrations (20 and 60 mg/L), the chars obtained comparable performance to the commercial activated carbon, in terms of final dye concentration. This further supported the idea that traditional adsorbents such as activated carbon could be replaced by biobased materials such as biomass chars without needing to modify the process, potentially lowering costs.

The tested adsorbents had overall high initial adsorption rate, with commercial activated carbon being the fastest ($\approx 99\%$ within the first minute) and one of the chars in particular having a comparable initial adsorption rate ($\approx 98\%$ in 1 minute). Most chars had slower MB uptake, with some needing up to 100 minutes to achieve removal close to the maximum (i.e., equilibrium) value.

Traditionally, for decontaminating water, a property of carbonaceous materials that is desired is high porosity and surface area, however according to the results in this work other features such as surface chemistry can be crucial in adsorption and must also be considered. Char properties such as surface functionalities were significantly changed with feedstock and process modifications, with impact in adsorption, which suggests modifications can be used to tailor char to a desired application (for example, specific contaminant(s)).

It was thus concluded that chars derived from low-value biomass such as agricultural wastes (wheat straw) have the potential to replace traditional adsorbents used for water decontamination such as activated carbon. Besides improving sustainability, using char instead of traditional activated carbons could result in cost savings due to milder production conditions, and the use of affordable and accessible feedstocks.

Chars were effective for an organic cationic dye which suggested they could be useful to remove other compounds such as heavy metals or aromatic hydrocarbons, as long as positive charge and/or aromatic rings are present. However, due to the lack of significant surface area and porosity, the adsorption capacity for other/multiple contaminants is likely limited compared to adsorbents with relatively high surface areas. Further studies are needed, especially by testing chars produced from different biobased feedstocks, and applying chars for other contaminants, in multi-contaminant adsorption, and using real wastewater.

Chapter 8 – Future work and recommendations

This chapter summarises suggestions regarding further work based on the results obtained in this work, and also recommendations about the reactor system, char analyses, and adsorption tests.

8.1. Reactor system

The screw reactors used in this work performed well, however, improvements could be made. Some improvements were implemented in the second screw reactor version (as explained in Chapter 3).

Feeding of the biomass feedstock into the reactor was performed manually in this work, and it would be better to have a hopper and an automatic continuous feeding system (e.g., with a screw). Feeding manually allowed for better process control, especially for the first experiments when the responses from the reactor to the process variables were not very known. Afterwards, and especially for the second screw reactor used, it would be better to have automated feeding to save time and allow the user to focus on other tasks during the experiment (e.g., analysing temperature profiles, the gas meter, and the MicroGC results). The feeding system would however need previous calibration and also potentially being able to adjust the feeding rate during operation. Having a dedicated feeding system could also help isolate the reactor from air ingress, keeping the process atmosphere oxygen-free, and also protect the user, since during feeding the inlet valve was opened and could let vapours pass through.

The experiments in which different injected gases were studied would also benefit from having an automated feeding system, since there would be no need to turn off the injected gases when feeding. This would improve the study of the effect of reaction atmosphere/environment (by injection of different gases). For enhanced contact with the char product, gases could be injected at the reactor front-end instead of in the feeding tube.

During operation, the joints and connections between different pieces of the reactor system had to be tight, to prevent vapours from coming out and air going in. Some of these connections were more problematic than others. For example, the sealing for the char pot consisted of a gasket, and there were some issues with the type of material used. A tanged graphite gasket was not successful in keeping the sealing because it was damaged during operation, since it only was designed for operating temperatures up to 450 °C. The usual temperatures of the char pot area, heated with a heating tape, were ≈400-600 °C, depending on the pyrolysis temperatures employed. It was thus necessary to use gaskets of materials that could withstand higher temperatures, and so we were supplied with a galvanised gasket

(Novaform SK) with a mesh insert and high-quality aramid fibre, which could operate at up to 650 °C.

Other suggested improvements for the screw reactor systems were:

a) A barrier to the passage of fine solid (char) particles through the vapour outlet.

The barrier could be a metallic mesh or a cotton filter, that would at the same time retain solids and be permeable to vapours from the reactor passing through it.

b) A fractionated condensation system for the liquid products.

During the pyrolysis experiments performed, it was noticed many times that the liquid product collected in the first flask was mostly made up of the aqueous phase, and that the organic phase would be mainly stuck to the condenser. This hinders the amount of liquid collected, although the viscous organic phase could be collected by heating the condenser.

A possible solution for this would be to have two condensers instead of one, working at different temperatures: the first one at a higher temperature and second one at lower temperature. This would in principle allow to collect heavier liquids in a first flask located after the first condenser, and then lighter compounds in the second flask after the second condenser. Operating temperatures of the condensers would be chosen considering the compounds present in the pyrolysis liquid phases and their boiling points. A possibility would be to have the first condenser at a temperature higher than the boiling point of water, so that it would condense compounds with boiling points higher than that and virtually none of the water, and the second condenser would retain all of the water and compounds with the same or lower boiling points than that of water. Since the focus of the work was the solid and not the liquid or gaseous product, these improvements were not trialled, but it is something to consider in the future to improve the overall process and for possible scaling-up.

c) A cooling system for the feedstock inlet tube.

Especially closer to the end of a pyrolysis experiment with the screw reactors, the feedstock inlet tube would get particularly hot (by conduction from the furnace and reactor tube), especially in the bottom where the feedstock enters the reactor. If the temperature became too high, vapours could start forming from the feedstock, and accumulate and condense in the inlet tube. This could lead to greater losses and be potentially dangerous to the operator (especially if manually feeding). To prevent this, the inlet tube could be cooled, or better insulated from the reactor and furnace heat.

d) Installing a pressure sensor to monitor pressure changes and identify possible leaks/blockages.

Monitoring pressure inside the reactor, especially if gas is injected into the reactor and the system is relatively sealed (e.g., after installing an automatic feeding system), could be used to check for blockages and other problems inside the system.

e) A monitoring system for the gas meter.

Gas production rate is an important parameter when pyrolysis is occurring. If during the process the gas production stops when feedstock should be inside the reactor, it signifies that something occurred and is preventing pyrolysis from continuing or the vapours are going somewhere else, i.e., there is a leak. Gas production can be used to monitor the progress of the pyrolysis process and can be compared between different reactors, feedstocks, and process conditions.

For the pyrolysis process, it is also important to determine vapour residence time (VRT), which is better checked at the start of the operation. In this work, VRT determination was usually done visually, by watching moisture and vapours appear in the reactor outlet, however this method was not the most accurate. Some produced gases are not visible and therefore will be undetected visually, however, the gas meter will detect them. A way to constantly monitor the gas meter, e.g., by digitally recording it, would improve gas production rate and VRT determination.

f) Improved reactor and char pot insulation.

If the heated areas of the system are not properly insulated, it may lead to cold spots and consequently allow condensation of vapour products. If there is condensation in the reactor or in the vapour outlet, it may lead to blockages and cause operation to stop. The reactor and the char pot had custom-made insulation, however, due to the architecture of the parts it was difficult to fully cover all exposed areas. Thermocouples (T4, in the case of the second screw reactor) can be used to monitor the temperatures in these areas.

8.2. Slow pyrolysis process conditions and modifications

It was verified that char quality for adsorption was improved by lower pyrolysis temperatures, and it would be of interest to test other feedstocks and see if the same trend would be obtained.

Elevated feedstock moisture content was tested in this work by soaking the feedstock in water prior to the experiment. It was verified that char yields were not modified significantly when feedstock moisture content up to 50 wt.% was processed. It would be interesting to test as-received feedstocks with relatively high moisture contents, without the need to soak them in water, which in the case of the wheat straw pellets in this work resulted in modified particle size and shape. This would allow to study the impact of feedstock moisture content without other parameters being changed.

For experiments with varying reaction atmosphere/environment (by injection of different gases), higher temperatures should be tested (e.g., 700-900 °C), to evaluate if activation with CO₂ or another activating agent would occur in the screw reactor and with the feedstock being studied. Using higher injected gas flow rates may also favour activation.

Testing 2-step physical activation with the screw reactor would also be valuable, i.e., by carbonising the feedstock and then activating the char. If char quality benefitted from this 2-step method, a two-reactor system could be designed, i.e., having in sequence a carbonisation reactor and an activation reactor.

Regarding experiments with KOH-impregnated feedstock, higher concentration of KOH solution should be tested in order to have greater KOH:char ratios and promote activation reactions. This will however result in more aggressive process conditions and material corrosion becomes more likely. However, the adsorption results showed that too much KOH could be detrimental for adsorption, which was likely due to repulsion or competition effects from the excess of inorganic material when using 1 M KOH solution in feedstock impregnation. This could potentially be avoided if the char product was washed after production to remove inorganic material, however, waste streams will be created and have a negative impact on process sustainability and even higher costs.

8.3. Char quality

The char or char-derived products should be analysed for PAH and other potentially harmful compounds in their structure. This is particularly important for the application chosen in this work, in order to avoid other compounds leaching into the water that is being decontaminated.

As discussed in Chapter 4, some analyses are not suitable for all chars, and researchers tend to develop different protocols according to the materials and experience they possess. Standardised analysis methods should be developed for chars, in order to have more comparable results between laboratories and researchers.

Finally, as char materials are being developed all over the world for various applications, standards should be produced according to the application. This would allow to better tailor chars for different uses and develop commercialisation.

8.4. Liquid and gas products from slow pyrolysis

When performing slow pyrolysis of biomass, it is important to take advantage not only of the main product char, but also of the vapours produced in the process. What to do with the co-products will depend on the reactor system (e.g., available equipment, scale), location, and possible local demand for energy/heat.

The main options for the product vapours are: burning right after production, by directing the vapours to a combustion chamber; or separating them into condensable and non-condensable products, producing respectively a liquid and a gas product. If separated, the liquid product can be stored (appropriately) for usage at a different time, and the gaseous

product should be used right away (e.g., burned by combustion) due to limited storage possibilities (i.e., required volume).

The heat from burning of pyrolytic products can be used for the process itself, e.g., to dry biomass or to heat the reactor or another equipment. This is common in several slow pyrolysis reactor systems due to typically being economically and environmentally friendly. Another option is to conduct combustion in a boiler to produce steam, which would then be used as heat source or with another end in the facility, e.g., electricity generation. When combusting pyrolysis products, it is however important to have appropriate emissions control, by monitoring combustion products and cleaning the flue gas before using and releasing to the atmosphere.

The liquid and gas products from other slow pyrolysis experiments should be analysed, in order to obtain deeper knowledge regarding the slow pyrolysis mechanisms and optimising the process. The analysis will also allow to perform energy and elemental balances, determining for example the energy yields from the process and how much heat can be recovered from the co-products.

8.5. Adsorption with char products

Regarding adsorption, in future work, the effect of pH would be interesting to investigate, although the chars produced in this work had high apparent performance for the adsorption of the cationic dye methylene blue (MB), without modifying solution pH. Nevertheless, determination of pH_{pzc} and studying the effect of pH could help better understand adsorption mechanisms.

Another relevant parameter in large scale adsorption is processing time, and it was seen that the commercial activated carbon samples were much faster at achieving equilibrium in the batch tests compared to the chars (≈ 60 min versus ≈ 180 min). It is recommended that the adsorption time is optimised using as a benchmark the equilibrium time of the commercial samples, and so the optimum conditions for fastest adsorption with the chars should be investigated.

Regarding the adsorption tests performed with chars from KOH-impregnated feedstock, to investigate the role of inorganic material, it is recommended to perform adsorption tests using char (from as-received feedstock) to which KOH was added post-production.

After adsorption and separating the solid from solution, the solution could be analysed for compounds that may have been from char or MB degradation, or even leached from the chars. It is critically important that other compounds do not contaminate the water during

adsorption. Analyses could be done e.g., for heavy metals using Ion Chromatography (IC) or ICP, and analysing for PAHs with HPLC or GC-MS.

Different biobased feedstocks should be explored for adsorbent production, and process conditions potentially tailored for different applications and/or contaminants. From the results in this work, lower temperatures and milder process conditions or feedstock treatments were better for adsorbent production. This should be investigated for other feedstocks, evaluating the possibility of developing replacements for traditional adsorbents such as activated carbon. Besides likely being more sustainable than using fossil coal to run the plant, the mild or absence of treatments make the process more economically attractive for investment.

Other contaminants should be explored, especially emerging contaminants and/or micropollutants: pesticides, herbicides, pharmaceuticals, organic dyes, etc. Testing the adsorption performance under continuous conditions (e.g., with column and breakthrough studies) is recommended in order to make the study more realistic. Furthermore, also with the previously stated purpose, water samples from industrial or commercial sites should be used for decontamination with the bioadsorbents. Although the multi-component decontamination will become more challenging to analyse, it will allow for more advanced studies and to gather further results regarding the performance of the bioadsorbents.

After adsorption, the adsorbents are saturated, and it is necessary to either dispose or reutilise the product. To improve process economics, it is recommended that products are regenerated, although regeneration can create waste streams and thus costs. After adsorption, the chars could also be utilised in another common char application, e.g., as solid fuel (as long as there is a suitable fuel gas treatment method). Furthermore, there is interest in utilising chars from adsorption in soils (cascaded use), however the contaminants need to be compatible with the soils, e.g., phosphates and nitrates (especially in soils that are deficient in those fertilising compounds).

Chapter 9 – Conclusions

This work had the aim of studying the slow pyrolysis of a biomass feedstock in a continuous screw reactor and explore the potential of using the product char for removal of contaminants from water. The feedstock was wheat straw pellets, and the impact of temperature and solid residence time on product yields and properties was studied. Furthermore, feedstock and process modifications were explored in terms of their impact on product yields and properties (focusing on the char) and on the performance of chars in contaminant removal from water. The feedstock was modified by increasing its moisture content (which consequently also changed particle size and shape), and also by impregnating it with KOH solutions. In the process, the use of CO₂ as reaction atmosphere/environment (injected gas) was explored and compared to using N₂ or no injected gas (static reaction atmosphere, comprised of slow pyrolysis vapour products).

The unmodified slow pyrolysis process obtained 26-35 wt.% char, 39-49 wt.% liquid, and 16-36 wt.% gas yields (dry feedstock basis). Temperature increased gas yields at the expense of char, and liquid yields were maximum at 500 °C. Solid residence time overall increased char and gas yields and decreased liquid yields.

The liquid and gaseous products, viewed as co-products in this work, should be utilised, if possible, for improved process economics. Due to the presence of considerable proportions of compounds with significant heating value, the main application for the co-products would be to use as fuel. Based on the heating values obtained in this work (in subsection 4.6 for the gas product and Appendix D for the liquid), the gaseous and liquid products possess 9-29% of the energy yield from the slow pyrolysis process, with the highest value from the highest temperature (process conditions: 400-600 °C, 3 min SRT, without modifying feedstock moisture content or adding KOH, and without injecting gas into the reactor). The vapours or gaseous products could be combusted in a combustion chamber downstream from the slow pyrolysis reactor, while the liquid product could be stored for later use. The hot flue gas from combusting the co-products could be used as heating medium to dry the feedstock before pyrolysis, or to heat the reactor itself (externally) or another equipment. The flue gas could also be used in a boiler to produce steam, which would be used as heat source or to generate electricity in a turbine. The liquid products also possess compounds with added value (e.g., phenolics, aromatics, sugars) and could potentially be refined or separated into groups of compounds. These options are worth exploring in future work. Utilising the pyrolysis co-products results in environmental and economic benefits: it avoids the release of harmful pyrolytic vapours into the atmosphere, which occurs in traditional slow pyrolysis systems (e.g., pits and mounds in the ground); and allows cost savings in terms

of energy/heat, or even by adding revenue sources (e.g., from selling valuable compounds separated from the liquid product or selling the heat to the grid from burning the co-products).

Elevated feedstock moisture content decreased char yields (up to ≈ 5 wt.%), however it was verified that up to 50 wt.% moisture content can be utilised without significantly decreasing char yields. This is advantageous due to reduced production costs from avoiding drying the feedstock (although transportation of the biomass would become more costly), which pyrolysis processes sometimes require. However, liquid yields (dry feedstock basis) decreased when feedstock with elevated moisture content was used.

Using gas injection overall decreased char yields (up to ≈ 3 wt.%), likely due to prevented secondary reactions from the reduced vapour residence time. The addition of KOH to the process increased char yields (up to ≈ 4 wt.%), however only for 400 °C. This could have been from promoted secondary reactions or even some degree of carbonisation inhibition.

Increasing temperature and solid residence time led to loss of volatile matter in the char, with hydrogen, nitrogen and oxygen proportions decreasing, while elemental and fixed carbon contents increased. Due to the loss of heteroatoms as volatile matter, surface functionalities decreased, and pH increased, i.e., the chars became more alkaline.

Processing feedstock with elevated moisture content led to greater manifestation of oxygenated surface groups in FTIR analysis, which was in line with the increased volatile matter and oxygen contents. Using CO₂ as injected gas overall increased the oxygen contents in the chars, although volatile matter content was decreased. Pre-treating the feedstock with a KOH solution led to increased volatile matter contents in the char, and oxygen contents decreased at 400 °C and increased for 600 °C production temperature. The ash content of the chars was significantly increased when using 1 M KOH solution in feedstock impregnation.

All the product chars had relatively low surface area (maximum 8.8 m²/g). The process and feedstock modifications were thought to increase surface area, since activating agents were introduced into the process, however, this did not occur. This was mainly due to a) the mild conditions applied (low activation temperature and time, low KOH:char ratio, low CO₂ flow rate), b) reactor configuration, which led to relatively high contact between solids and vapours, potentially leading to surface and pore coverage, and c) the nature of the feedstock, which could prevent porosity from developing. Nevertheless, other char properties were changed such as elemental distribution and pH, some with positive effects on adsorption performance.

The chars produced from unmodified process conditions and feedstock were able to effectively remove the organic dye methylene blue (MB) from solution, used as proxy for other organic contaminants. The maximum removal was comparable to a commercial activated carbon, although lower (95% compared to 98%). For the applied conditions (100 mg/L initial dye concentration, 25 mg adsorbent, 10 mL MB solution volume), the maximum adsorption

capacity was ≈ 38 mg/g. Although having similar maximum dye removal values, the commercial activated carbon was faster at reaching equilibrium, which is a feature that should be developed for the char products.

The chars with best performance were produced at the lowest temperature of 400 °C, with higher SRT providing higher MB removal at this temperature. This was due to the key role of oxygen content and O:C ratio, which gave the lower temperature chars more oxygen-containing surface functionalities and thus active sites for MB adsorption. Linear correlations established between MB removal and char properties corroborated this. The adsorption with the commercial activated carbon, however, relied mainly on its significantly greater surface area (≈ 615 m²/g) and mesopore volume.

Improvements in adsorption performance occurred when using char from feedstock with modified moisture content, and feedstock impregnated with KOH solution (lowest concentration of 0.1 M KOH only). MB removal reached 99% with chars produced with process/feedstock modifications. This was mainly due to increased O:C ratio and oxygen-containing surface functionalities.

It was possible, by changing adsorption conditions, to improve adsorption capacity. Using 10 mg of char, capacity was increased to ≈ 98 mg/g, which was a $\approx 182\%$ increase compared to using 25 mg. For the commercial activated carbon, however, the maximum removal was only $\approx 62\%$, which resulted in ≈ 62 mg/g adsorption capacity (only a $\approx 59\%$ increase). This suggested that the active sites on the commercial activated carbon became depleted or inaccessible faster than with the chars.

From the adsorption results it was concluded that chars from wheat straw can have comparable efficiency in removing an organic dye from water to a commercial activated carbon. Relatively high temperatures were detrimental for performance, and, although further treatment provided further improvement, the chars from unmodified process conditions and feedstock were very efficient ($\approx 95\%$ removal). Thus, chars have the potential to replace traditional adsorbents, which would make water decontamination more sustainable and economically favourable.

Char composition and surface chemical functionalities were found to be key for the positive adsorption performance achieved with the chars. The performance with the commercial activated carbon, on the other hand, relied more on its relatively high surface area and porosity. The development of sustainable carbonaceous materials for adsorption should consider not only surface area but also the interaction of the contaminants with the surface chemistry of the adsorbents. Feedstock and process conditions should be explored in order to tailor chars for the desired applications, such as decontaminating gas or aqueous streams and removing organic or inorganic contaminants.

Considering char properties and the high adsorption performance of the chars for a cationic dye, the chars are potentially suitable to remove from water other substances with positive charge in solution, such as heavy metals (e.g., Cu, Cr, Ni, Pb). Since the performance for an anionic dye was relatively low, adsorption of other anionic compounds (even with aromatic structures and electron delocalisation) is likely to be low. Nevertheless, the chars could also potentially remove organic compounds with aromatic structures such as aromatic hydrocarbons (e.g., phenol and its derivatives), some pharmaceuticals and pesticides.

Future work on using chars for water decontamination should focus on testing different biobased feedstocks, other types of contaminants, mono- and multi-contaminated water, and using real wastewater samples (e.g., from river and storm water).

References

- [1] IPCC. Intergovernmental Panel on Climate Change Fourth Assessment Report, "What is the Greenhouse Effect?" FAQ 1.3 – AR4 WGI Chapter 1: Historical Overview of Climate Change Science. 2007.
- [2] Morice CP, Kennedy JJ, Rayner NA, Jones PD. Quantifying uncertainties in global and regional temperature change using an ensemble of observational estimates: The HadCRUT4 data set. *J Geophys Res Atmos* 2012;117. <https://doi.org/10.1029/2011JD017187>.
- [3] Sosdian SM, Greenop R, Hain MP, Foster GL, Pearson PN, Lear CH. Constraining the evolution of Neogene ocean carbonate chemistry using the boron isotope pH proxy. *Earth Planet Sci Lett* 2018;498:362–76. <https://doi.org/https://doi.org/10.1016/j.epsl.2018.06.017>.
- [4] Bereiter B, Eggleston S, Schmitt J, Nehrbass-Ahles C, Stocker TF, Fischer H, et al. Revision of the EPICA Dome C CO₂ record from 800 to 600 kyr before present. *Geophys Res Lett* 2015;42:542–9. <https://doi.org/10.1002/2014GL061957>.
- [5] Basu P. Biomass Gasification and Pyrolysis: Practical Design and Theory. Elsevier Inc.; 2010. <https://doi.org/10.1017/CBO9781107415324.004>.
- [6] Pant KK, Mohanty P. Chapter 1: Biomass, Conversion Routes and Products - An Overview. In: Hornung A, editor. *Transform. Biomass Theory to Pract.*, vol. 9781119973, John Wiley & Sons, Inc.; 2014, p. 1–30. <https://doi.org/10.1002/9781118693643.ch1>.
- [7] IRENA, IEA Bioenergy, FAO. Bioenergy for Sustainable Development. 2017. <https://doi.org/10.1007/978-94-007-2181-4>.
- [8] de Jong W, van Ommen JR. Chapter 1 - Introduction. In: de Jong W, van Ommen JR, editors. *Biomass as a Sustain. Energy Source Futur. - Fundam. Convers. Process.* First, New Jersey: Wiley; 2015, p. 3–35.
- [9] Harris ZM, Spake R, Taylor G. Land use change to bioenergy: A meta-analysis of soil carbon and GHG emissions. *Biomass and Bioenergy* 2015;82:27–39. <https://doi.org/https://doi.org/10.1016/j.biombioe.2015.05.008>.
- [10] Verstegen JA, van der Laan C, Dekker SC, Faaij APC, Santos MJ. Recent and projected impacts of land use and land cover changes on carbon stocks and biodiversity in East Kalimantan, Indonesia. *Ecol Indic* 2019;103:563–75. <https://doi.org/https://doi.org/10.1016/j.ecolind.2019.04.053>.
- [11] Hayes DJM. Second-Generation Biofuels: Why They are Taking so Long. *WIREs Energy Env* 2013;2:304–34. <https://doi.org/10.1002/9781118957844.ch12>.
- [12] Demirbas A. Biomass resource facilities and biomass conversion processing for fuels

- and chemicals. *Energy Convers Manag* 2001;42:1357–78.
- [13] Tripathi M, Sahu JN, Ganesan P. Effect of process parameters on production of biochar from biomass waste through pyrolysis: A review. *Renew Sustain Energy Rev* 2016;55:467–81. <https://doi.org/10.1016/j.rser.2015.10.122>.
- [14] Lee RA, Lavoie J-M. From first- to third-generation biofuels: Challenges of producing a commodity from a biomass of increasing complexity. *Anim Front* 2013;3:6–11. <https://doi.org/10.2527/af.2013-0010>.
- [15] Alam F, Mobin S, Chowdhury H. Third generation biofuel from Algae. 6th BSME Int. Conf. Therm. Eng. (ICTE 2014), vol. 105, Elsevier B.V.; 2015, p. 763–8. <https://doi.org/10.1016/j.proeng.2015.05.068>.
- [16] Kaza S, Yao LC, Bhada-Tata P, Van Woerden F. *What a Waste 2.0 : A Global Snapshot of Solid Waste Management to 2050*. Washington DC: World Bank; 2018.
- [17] Kumar S, Smith SR, Fowler G, Velis C, Kumar SJ, Arya S, et al. Challenges and opportunities associated with waste management in India. *R Soc Open Sci* 2017;4:160764. <https://doi.org/10.1098/rsos.160764>.
- [18] Mohanty AK, Misra M, Hinrichsen G. Biofibres, biodegradable polymers and biocomposites: An overview. *Macromol Mater Eng* 2000;276–277:1–24. [https://doi.org/10.1002/\(SICI\)1439-2054\(20000301\)276:1<1::AID-MAME1>3.0.CO;2-W](https://doi.org/10.1002/(SICI)1439-2054(20000301)276:1<1::AID-MAME1>3.0.CO;2-W).
- [19] Tran HN, Nguyen HC, Woo SH, Nguyen TV, Vigneswaran S, Hosseini-Bandegharaei A, et al. Removal of various contaminants from water by renewable lignocellulose-derived biosorbents: a comprehensive and critical review. *Crit Rev Environ Sci Technol* 2019;49:2155–219. <https://doi.org/10.1080/10643389.2019.1607442>.
- [20] Thornley P, Gilbert P, Thornley P. Biofuels: balancing risks and rewards. *Interface Focus* 2012;3. <https://doi.org/http://dx.doi.org/10.1098/rsfs.2012.0040>.
- [21] Dahlquist E. Chapter 1 - An overview of thermal biomass conversion technologies. In: Dahlquist E, editor. *Technol. Convert. Biomass to Useful Energy*, CRC Press; 2013.
- [22] Hagemann N, Spokas K, Schmidt HP, Kägi R, Böhler MA, Bucheli TD. Activated carbon, biochar and charcoal: Linkages and synergies across pyrogenic carbon's ABCs. *Water (Switzerland)* 2018;10:1–19. <https://doi.org/10.3390/w10020182>.
- [23] European Biochar Foundation (EBC). *European Biochar Certificate - Guidelines for a Sustainable Production of Biochar*. Arbaz, Switzerland: 2012. <https://doi.org/10.13140/RG.2.1.4658.7043>.
- [24] International Biochar Initiative. *Standardized Product Definition and Product Testing Guidelines for Biochar That Is Used in Soil*. 2015. <https://doi.org/http://www.biochar-international.org/characterizationstandard>.
- [25] Khalil LB. Porosity characteristics of chars derived from different lignocellulosic

- materials. *Adsorpt Sci Technol* 1999;17:729–39. <https://doi.org/10.1177/026361749901700904>.
- [26] Manyà JJ. Pyrolysis for biochar purposes: A review to establish current knowledge gaps and research needs. *Environ Sci Technol* 2012;46:7939–54. <https://doi.org/10.1021/es301029g>.
- [27] Martins A, Nunes N. Adsorption of a textile dye on commercial activated carbon: A simple experiment to explore the role of surface chemistry and ionic strength. *J Chem Educ* 2015;92:143–7. <https://doi.org/10.1021/ed500055v>.
- [28] Schmidt HP, Wilson K. The 55 uses of biochar. *Biochar J* 2014. <https://www.biochar-journal.org/en/ct/2> (accessed June 4, 2020).
- [29] Antal MJ, Grønli M. The Art, Science, and Technology of Charcoal Production †. *Ind Eng Chem Res* 2003;42:1619–40. <https://doi.org/10.1021/ie0207919>.
- [30] Kotrba R. Fighting climate change with ancient technology. *Biomass Mag (BBI Int March/April, Vol 14, Issue 2 2020)*:16–25.
- [31] Taylor P. Chapter 1 - Biochar: Ancient Origins, Modern Solution, in Part I: Ancient origins, modern inspirations. In: Taylor P, editor. *Biochar Revolut. - Transform. Agric. Environ. First Edit, Queensland, Australia: NuLife Publishing; 2010*.
- [32] Mehmood K, Chávez Garcia E, Schirrmann M, Ladd B, Kammann C, Wrage-Mönnig N, et al. Biochar research activities and their relation to development and environmental quality. A meta-analysis. *Agron Sustain Dev* 2017;37. <https://doi.org/10.1007/s13593-017-0430-1>.
- [33] Track 0. A compendium of solutions for achieving the sustainable development goals and staying below 2 °C or 1.5 °C. London: 2017.
- [34] IPCC. 15th IPCC special report on Global Warming of 1.5 °C. 2018.
- [35] Schmidt HP. Biochar and PyCCS included as negative emission technology by the IPCC. *Biochar J* 2018. <https://www.biochar-journal.org/en/ct/94> (accessed June 4, 2020).
- [36] Ragan S, Megonnell N. Activated Carbon From Renewable Resources – Lignin. *Cellul Chem Technol* 2011;45:7–8.
- [37] Prauchner MJ, Rodríguez-Reinoso F. Chemical versus physical activation of coconut shell: A comparative study. *Microporous Mesoporous Mater* 2012;152:163–71. <https://doi.org/10.1016/j.micromeso.2011.11.040>.
- [38] Dias JM, Alvim-ferraz MCM, Almeida MF, Sa M. Waste materials for activated carbon preparation and its use in aqueous-phase treatment: A review 2007;85:833–46. <https://doi.org/10.1016/j.jenvman.2007.07.031>.
- [39] Lakshmiathy R, Sarada NC. Adsorptive removal of basic cationic dyes from aqueous solution by chemically protonated watermelon (*Citrullus lanatus*) rind biomass. *Desalin*

- Water Treat 2014;52:6175–84. <https://doi.org/10.1080/19443994.2013.812526>.
- [40] Schröder E, Thomauske K, Oechsler B, Herberger S, Baur S, Hornung A. Chapter 18 - Activated Carbon from Waste Biomass. In: Shaukat S, editor. Prog. Biomass Bioenergy Prod., InTech; 2011. <https://doi.org/10.5772/20594>.
- [41] Luo Y, Guo W, Ngo HH, Nghiem LD, Hai FI, Zhang J, et al. A review on the occurrence of micropollutants in the aquatic environment and their fate and removal during wastewater treatment. Sci Total Environ 2014;473–474:619–41. <https://doi.org/10.1016/j.scitotenv.2013.12.065>.
- [42] CPL Industries. CPL Industries 2020. <http://www.cplindustries.co.uk/cpl/> (accessed June 23, 2020).
- [43] Calgon Carbon. Calgon Carbon 2020. <https://www.calgoncarbon.com/> (accessed June 23, 2020).
- [44] Cabot Corporation. Cabot Corp. 2020. <https://www.cabotcorp.com/> (accessed June 23, 2020).
- [45] Sunmark Environmental Services LLC. Sunmark Environmental 2020. <http://sunmarkenvironmental.com/> (accessed October 27, 2020).
- [46] Stormwater Biochar. StormwaterBIOCHAR 2020. <https://stormwaterbiochar.com/> (accessed December 14, 2020).
- [47] EINPresswire. Glanris raises \$2 million to produce world's first green hybrid water filtration media. Online 2021.
- [48] Brigano F, Glanris. Rice husk biochar: an ecological solution to remove metals from water (Webinar presentation) 2021.
- [49] Lehmann J. Science-to-action through global and regional biochar networks. Biochar 2019;1:337–337. <https://doi.org/10.1007/s42773-019-00029-y>.
- [50] Wang S, Luo Z. Chapter 1 - Biomass components and characteristics. In: Wang S, Luo Z, editors. Pyrolysis of biomass, De Gruyter; 2017.
- [51] Isikgor FH, Becer CR. Lignocellulosic biomass: a sustainable platform for the production of bio-based chemicals and polymers. Polym Chem 2015;6:4497–559. <https://doi.org/10.1039/C5PY00263J>.
- [52] Smokefoot. Lignin (<https://commons.wikimedia.org/wiki/File:Lignin.png>) 2011.
- [53] Rowell RM, Pettersen R, Han JS, Rowell JS, Tshabalala MA. Chapter 3 - Cell Wall Chemistry. In: Rowell RM, editor. Handb. wood Chem. wood Compos., CRC Press; 2005. <https://doi.org/10.1201/b12487-5>.
- [54] Van Loo S, Koppejan J. Chapter 8 - Biomass Ash Characteristics and Behaviour in Combustion Systems. In: Van Loo S, Koppejan J, editors. Handb. Biomass Combust. Co-firing, Earthscan; 2008.
- [55] Hon D, Shiraishi N. Wood and cellulosic chemistry. New York: Marcel Dekker, Inc.;

- 1991.
- [56] Dhyani V, Bhaskar T. A comprehensive review on the pyrolysis of lignocellulosic biomass. *Renew Energy* 2018;129:695–716. <https://doi.org/10.1016/j.renene.2017.04.035>.
- [57] Chiamonti D, Oasmaa A, Solantausta Y. Power generation using fast pyrolysis liquids from biomass. *Renew Sustain Energy Rev* 2007;11:1056–86. <https://doi.org/10.1016/j.rser.2005.07.008>.
- [58] Holubcik M, Jandacka J, Malcho M. Ash Melting Temperature Prediction from Chemical Composition of Biomass Ash. *Holist Approach to Environ* 2015;5:119–25.
- [59] Yao X, Zhao Z, Li J, Zhang B, Zhou H, Xu K. Experimental investigation of physicochemical and slagging characteristics of inorganic constituents in ash residues from gasification of different herbaceous biomass. *Energy* 2020;198:117367. <https://doi.org/https://doi.org/10.1016/j.energy.2020.117367>.
- [60] de Jong W. Chapter 8 - Physical Pretreatment of Biomass. In: de Jong W, van Ommen R, editors. *Biomass as a Sustain. Energy Source Futur. - Fundam. Convers. Process. First*, New Jersey: Wiley; 2015, p. 233–67.
- [61] Cai J, He Y, Yu X, Banks SW, Yang Y, Zhang X, et al. Review of physicochemical properties and analytical characterization of lignocellulosic biomass. *Renew Sustain Energy Rev* 2017;76:309–22. <https://doi.org/10.1016/j.rser.2017.03.072>.
- [62] Bakker R, Elbersen W, Poppens R, Lesschen J. Rice straw and Wheat straw - Potential feedstocks for the biobased economy. 2013.
- [63] Ritchie H. Agricultural Production. *Our World Data* 2020. <https://ourworldindata.org/agricultural-production> (accessed July 15, 2020).
- [64] Renewable Fuels Agency. The indirect effect of “wastes.” 2010.
- [65] Copeland J, Turley D. National and regional supply/demand balance for agricultural straw in Great Britain. 2008.
- [66] Glithero NJ, Wilson P, Ramsden SJ. Straw use and availability for second generation biofuels in England. *Biomass and Bioenergy* 2013;55:311–21. <https://doi.org/https://doi.org/10.1016/j.biombioe.2013.02.033>.
- [67] Scarlat N, Martinov M, Dallemand JF. Assessment of the availability of agricultural crop residues in the European Union: Potential and limitations for bioenergy use. *Waste Manag* 2010;30:1889–97. <https://doi.org/10.1016/j.wasman.2010.04.016>.
- [68] Liu R, Yu H, Huang Y. Structure and morphology of cellulose in wheat straw. *Cellulose* 2005;12:25–34. <https://doi.org/10.1007/s10570-004-0955-8>.
- [69] Amit R P, Prabir S, Harpreet S, Himanshu T, Sagi S. Life Cycle Assessment of Intermediate Pyrolysis of Wheat Straw for Sustainable Energy Alternate and Emission Mitigation. *Int Rev Appl Eng Res* 2014;4:325–30.

- [70] Kim S, Dale BE. Global potential bioethanol production from wasted crops and crop residues. *Biomass and Bioenergy* 2004;26:361–75. <https://doi.org/10.1016/j.biombioe.2003.08.002>.
- [71] Whittaker C, Shield I. Factors affecting wood, energy grass and straw pellet durability – A review. *Renew Sustain Energy Rev* 2017;71:1–11. <https://doi.org/10.1016/j.rser.2016.12.119>.
- [72] Gilbert P, Ryu C, Sharifi V, Swithenbank J. Effect of process parameters on pelletisation of herbaceous crops. *Fuel* 2009;88:1491–7. <https://doi.org/10.1016/j.fuel.2009.03.015>.
- [73] Miranda T, Montero I, Sepúlveda FJ, Arranz JI, Rojas CV, Nogales S. A review of pellets from different sources. *Materials (Basel)* 2015;8:1413–27. <https://doi.org/10.3390/ma8041413>.
- [74] El-Sayed SA, Khairy M. An Experimental Study of Combustion and Emissions of Wheat Straw Pellets in High-Temperature Air Flows. *Combust Sci Technol* 2018;190:222–51. <https://doi.org/10.1080/00102202.2017.1381953>.
- [75] Zhu Y, Hu J, Yang W, Zhang W, Zeng K, Yang H, et al. Ash Fusion Characteristics and Transformation Behaviors during Bamboo Combustion in Comparison with Straw and Poplar. *Energy & Fuels* 2018;acs.energyfuels.8b00371. <https://doi.org/10.1021/acs.energyfuels.8b00371>.
- [76] Biswas B, Pandey N, Bisht Y, Singh R, Kumar J, Bhaskar T. Pyrolysis of agricultural biomass residues: Comparative study of corn cob, wheat straw, rice straw and rice husk. *Bioresour Technol* 2017;237:57–63. <https://doi.org/10.1016/j.biortech.2017.02.046>.
- [77] Jensen A, Dam-Johansen K, Wójtowicz MA, Serio MA. TG-FTIR study of the influence of potassium chloride on wheat straw pyrolysis. *Energy and Fuels* 1998;12:929–38. <https://doi.org/10.1021/ef980008i>.
- [78] Wang L, Becidan M, Skreiberg Ø. Sintering behavior of agricultural residues ashes and effects of additives. *Energy and Fuels* 2012;26:5917–29. <https://doi.org/10.1021/ef3004366>.
- [79] Gollakota ARK, Kishore N, Gu S. A review on hydrothermal liquefaction of biomass. *Renew Sustain Energy Rev* 2018;81:1378–92. <https://doi.org/https://doi.org/10.1016/j.rser.2017.05.178>.
- [80] Nicolae S, Wang X, Hedin N, Titirici M. Chapter 7: Refined biocarbons for gas adsorption and separation. In: Manyà JJ, editor. *Adv. Carbon Mater. from Biomass an Overv.*, GreenCarbon Project and Consortium; 2019.
- [81] Bridgwater A V. Review of fast pyrolysis of biomass and product upgrading. *Biomass and Bioenergy* 2012;38:68–94. <https://doi.org/10.1016/j.biombioe.2011.01.048>.
- [82] Miandad R, Rehan M, Barakat MA, Aburiazza AS, Khan H, Ismail IMI, et al. Catalytic

- pyrolysis of plastic waste: Moving toward pyrolysis based biorefineries. *Front Energy Res* 2019;7:1–17. <https://doi.org/10.3389/fenrg.2019.00027>.
- [83] Martínez JD, Murillo R, García T, Veses A. Demonstration of the waste tire pyrolysis process on pilot scale in a continuous auger reactor. *J Hazard Mater* 2013;261:637–45. <https://doi.org/10.1016/j.jhazmat.2013.07.077>.
- [84] Recycling Technologies. Technology 2020. <https://recyclingtechnologies.co.uk/technology/> (accessed July 7, 2020).
- [85] Bridgwater T. Challenges and opportunities in fast pyrolysis of biomass: Part I. *Johnson Matthey Technol Rev* 2018;62:150–60. <https://doi.org/10.1595/205651318X696738>.
- [86] Bridgwater A V. Renewable fuels and chemicals by thermal processing of biomass. *Chem Eng J* 2003;91:87–102. [https://doi.org/10.1016/S1385-8947\(02\)00142-0](https://doi.org/10.1016/S1385-8947(02)00142-0).
- [87] Bridgwater A V. *Biomass Pyrolysis (Presentation)*. York: 2010.
- [88] Hossain AK, Davies PA. Pyrolysis liquids and gases as alternative fuels in internal combustion engines - A review. *Renew Sustain Energy Rev* 2013;21:165–89. <https://doi.org/10.1016/j.rser.2012.12.031>.
- [89] Oasmaa A, Czernik S. Fuel oil quality of biomass pyrolysis oils - state of the art for the end users. *Energy and Fuels* 1999;13:914–21. <https://doi.org/10.1021/ef980272b>.
- [90] Banks SW, Nowakowski DJ, Bridgwater A V. Impact of Potassium and Phosphorus in Biomass on the Properties of Fast Pyrolysis Bio-oil. *Energy and Fuels* 2016;30:8009–18. <https://doi.org/10.1021/acs.energyfuels.6b01044>.
- [91] Reumerman P, Frederiks B. Charcoal production with reduced emissions. 12th Eur. Conf. Biomass Energy, Ind. Clim. Prot. Amsterdam, Amsterdam: 2002.
- [92] Schmidt HP, Hagemann N, Draper K, Kammann C. The use of biochar in animal feeding. *PeerJ* 2019;2019:1–54. <https://doi.org/10.7717/peerj.7373>.
- [93] Straka TJ. Charcoal as a Fuel in the Ironmaking and Smelting Industries. *Adv Hist Stud* 2017;06:56–64. <https://doi.org/10.4236/ahs.2017.61004>.
- [94] Szymkowski CJ, Bultitude-Paull JM. The Production of High-quality Silicon Metal at Simcoa. *Infacon 6 - Proc. from 6th Int. Ferroalloys Congr. Cape T., vol. I, Johannesburg: SAIMM; 1992, p. 185–91.*
- [95] Demirbaş A, Arin G. An overview of biomass pyrolysis. *Energy Sources* 2002;24:471–82. <https://doi.org/10.1080/00908310252889979>.
- [96] Neumann J, Meyer J, Ouadi M, Apfelbacher A, Binder S, Hornung A. The conversion of anaerobic digestion waste into biofuels via a novel Thermo-Catalytic Reforming process. *Waste Manag* 2016;47:141–8. <https://doi.org/10.1016/j.wasman.2015.07.001>.
- [97] Oasmaa A, Van De Beld B, Saari P, Elliott DC, Solantausta Y. Norms, standards, and legislation for fast pyrolysis bio-oils from lignocellulosic biomass. *Energy and Fuels* 2015;29:2471–84. <https://doi.org/10.1021/acs.energyfuels.5b00026>.

- [98] Guo F, Li X, Liu Y, Peng K, Guo C, Rao Z. Catalytic cracking of biomass pyrolysis tar over char-supported catalysts. *Energy Convers Manag* 2018;167:81–90. <https://doi.org/10.1016/j.enconman.2018.04.094>.
- [99] Oudenhoven S, Kersten S. Chapter 11 - Thermochemical conversion: An introduction to fast pyrolysis. In: de Jong W, van Ommen J, editors. *Biomass as a Sustain. Energy Source Futur. - Fundam. Convers. Process.* First, John Wiley & Sons, Inc.; 2015.
- [100] ASTM. ASTM D7544-09 - Standard specification for pyrolysis liquid biofuel. *ASTM Int* 2009.
- [101] IEA Bioenergy. IEA Bioenergy Task 34 - Pyrolysis. 2014.
- [102] Mahmood ASN, Brammer JG, Hornung A, Steele A, Poulston S. The intermediate pyrolysis and catalytic steam reforming of Brewers spent grain. *J Anal Appl Pyrolysis* 2013;103:328–42. <https://doi.org/10.1016/j.jaap.2012.09.009>.
- [103] Radlein D, Quignard A. A Short Historical Review of Fast Pyrolysis of Biomass. *Oil Gas Sci Technol* 2013;68:765–83. <https://doi.org/10.2516/ogst/2013162>.
- [104] Di Blasi C. Modeling chemical and physical processes of wood and biomass pyrolysis. *Prog Energy Combust Sci* 2008;34:47–90. <https://doi.org/10.1016/j.pecs.2006.12.001>.
- [105] Yang H, Yan R, Chen H, Lee DH, Zheng C. Characteristics of hemicellulose, cellulose and lignin pyrolysis. *Fuel* 2007;86:1781–8. <https://doi.org/10.1016/j.fuel.2006.12.013>.
- [106] Mok WSL, Antal MJ, Szabo P, Varhegyi G, Zelei B. Formation of Charcoal from Biomass in a Sealed Reactor. *Ind Eng Chem Res* 1992;31:1162–6. <https://doi.org/10.1021/ie00004a027>.
- [107] Wang S, Dai G, Yang H, Luo Z. Lignocellulosic biomass pyrolysis mechanism: A state-of-the-art review. *Prog Energy Combust Sci* 2017;62:33–86. <https://doi.org/10.1016/j.pecs.2017.05.004>.
- [108] White JE, Catallo WJ, Legendre BL. Biomass pyrolysis kinetics: A comparative critical review with relevant agricultural residue case studies. *J Anal Appl Pyrolysis* 2011;91:1–33. <https://doi.org/10.1016/j.jaap.2011.01.004>.
- [109] Bradury A, Sakai Y, Shafizadeh F. A kinetic model for pyrolysis of cellulose. *J Appl Polym Sci* 1979;23:3271–80. <https://doi.org/https://doi.org/10.1002/app.1979.070231112>.
- [110] Wang S, Dai G, Ru B, Zhao Y, Wang X, Zhou J, et al. Effects of torrefaction on hemicellulose structural characteristics and pyrolysis behaviors. *Bioresour Technol* 2016;218:1106–14. <https://doi.org/https://doi.org/10.1016/j.biortech.2016.07.075>.
- [111] de Caprariis B, De Filippis P, Herce C, Verdone N. Double-Gaussian Distributed Activation Energy Model for Coal Devolatilization. *Energy & Fuels* 2012;26:6153–9. <https://doi.org/10.1021/ef301092r>.
- [112] Ru B, Wang S, Dai G, Zhang L. Effect of Torrefaction on Biomass Physicochemical

- Characteristics and the Resulting Pyrolysis Behavior. *Energy and Fuels* 2015;29:5865–74. <https://doi.org/10.1021/acs.energyfuels.5b01263>.
- [113] Wang S, Ru B, Dai G, Lin H, Zhang L. Influence mechanism of torrefaction on softwood pyrolysis based on structural analysis and kinetic modeling. *Int J Hydrogen Energy* 2016;41:16428–35. <https://doi.org/https://doi.org/10.1016/j.ijhydene.2016.02.082>.
- [114] Evans RJ, Milne TA. Molecular Characterization of the Pyrolysis of Biomass. 1. Fundamentals. *Energy & Fuels* 1987;1. <https://doi.org/10.1021/ac00126a800>.
- [115] Anca-Couce A. Reaction mechanisms and multi-scale modelling of lignocellulosic biomass pyrolysis. *Prog Energy Combust Sci* 2016;53:41–79. <https://doi.org/10.1016/j.pecs.2015.10.002>.
- [116] Di Blasi C. Modeling intra- and extra-particle processes of wood fast pyrolysis. *AIChE J* 2002;48:2386–97. <https://doi.org/10.1002/aic.690481028>.
- [117] Schmidt M, Noack A. Black carbon in soils and sediments: Analysis, distribution, implications, and current challenges. *Global Biogeochem Cycles* 2000;14:777–93.
- [118] Antal MJ, Varhegyi G. Cellulose Pyrolysis Kinetic: The Current State of Knowledge. *Ind Eng Chem Res* 1995;34:703–17. <https://doi.org/10.1021/ie00042a001>.
- [119] Raveendran K, Ganesh A, Khilar KC. Influence of mineral matter on biomass pyrolysis characteristics. *Fuel* 1995;74:1812–22. [https://doi.org/10.1016/0016-2361\(95\)80013-8](https://doi.org/10.1016/0016-2361(95)80013-8).
- [120] Sekiguchi Y, Shafizadeh F. The effect of inorganic additives on the formation, composition, and combustion of cellulosic char. *J Appl Polym Sci* 1984;29:1267–86. <https://doi.org/10.1002/app.1984.070290421>.
- [121] Butler E, Devlin G, Meier D, McDonnell K. Characterisation of spruce, salix, miscanthus and wheat straw for pyrolysis applications. *Bioresour Technol* 2013;131:202–9. <https://doi.org/10.1016/j.biortech.2012.12.013>.
- [122] Van de Velden M, Baeyens J, Brems A, Janssens B, Dewil R. Fundamentals, kinetics and endothermicity of the biomass pyrolysis reaction. *Renew Energy* 2010;35:232–42. <https://doi.org/10.1016/j.renene.2009.04.019>.
- [123] Zhao L, Cao X, Mašek O, Zimmerman A. Heterogeneity of biochar properties as a function of feedstock sources and production temperatures. *J Hazard Mater* 2013;256–257:1–9. <https://doi.org/10.1016/j.jhazmat.2013.04.015>.
- [124] Manyà JJ, Ruiz J, Arauzo J. Some peculiarities of conventional pyrolysis of several agricultural residues in a packed bed reactor. *Ind Eng Chem Res* 2007;46:9061–70. <https://doi.org/10.1021/ie070811c>.
- [125] Stenseng M, Jensen A, Dam-Johansen K. Investigation of biomass pyrolysis by thermogravimetric analysis and differential scanning calorimetry. *J Anal Appl Pyrolysis* 2001;58–59:765–80. [https://doi.org/10.1016/S0165-2370\(00\)00200-X](https://doi.org/10.1016/S0165-2370(00)00200-X).
- [126] Puy N, Murillo R, Navarro M V., López JM, Rieradevall J, Fowler G, et al. Valorisation

- of forestry waste by pyrolysis in an auger reactor. *Waste Manag* 2011;31:1339–49. <https://doi.org/10.1016/j.wasman.2011.01.020>.
- [127] Solar J, de Marco I, Caballero BM, Lopez-Urionabarrenechea A, Rodriguez N, Agirre I, et al. Influence of temperature and residence time in the pyrolysis of woody biomass waste in a continuous screw reactor. *Biomass and Bioenergy* 2016;95:416–23. <https://doi.org/10.1016/j.biombioe.2016.07.004>.
- [128] Greco G, Di Stasi C, Rego F, González B, Manyà JJ. Effects of slow-pyrolysis conditions on the products yields and properties and on exergy efficiency: A comprehensive assessment for wheat straw. *Appl Energy* 2020;279. <https://doi.org/10.1016/j.apenergy.2020.115842>.
- [129] Bahng MK, Mukarakate C, Robichaud DJ, Nimlos MR. Current technologies for analysis of biomass thermochemical processing: A review. *Anal Chim Acta* 2009;651:117–38. <https://doi.org/10.1016/j.aca.2009.08.016>.
- [130] Azuara M, Saiz E, Manso JA, Garcia-Ramos FJ, Manyà JJ. Study on the effects of using a carbon dioxide atmosphere on the properties of vine shoots-derived biochar. *J Anal Appl Pyrolysis* 2017;124:719–25. <https://doi.org/10.1016/j.jaap.2016.11.022>.
- [131] Resende FLP. Recent advances on fast hydrolysis of biomass. *Catal Today* 2016;269:148–55. <https://doi.org/https://doi.org/10.1016/j.cattod.2016.01.004>.
- [132] Wang L, Skreiberg O, Gronli M, Specht GP, Antal MJ. Is elevated pressure required to achieve a high fixed-carbon yield of charcoal from biomass? Part 2: The importance of particle size. *Energy and Fuels* 2013;27:2146–56. <https://doi.org/10.1021/ef400041h>.
- [133] Di Blasi C, Signorelli G, Di Russo C, Rea G. Product distribution from pyrolysis of wood and agricultural residues. *Ind Eng Chem Res* 1999;38:2216–24. <https://doi.org/10.1021/ie980711u>.
- [134] Antal MJ, Croiset E, Dai X, DeAlmeida C, Mok WSL, Norberg N, et al. High-yield biomass charcoal. *Energy and Fuels* 1996;10:652–8. <https://doi.org/10.1021/ef9501859>.
- [135] Demirbas A. Effects of temperature and particle size on bio-char yield from pyrolysis of agricultural residues. *J Anal Appl Pyrolysis* 2004;72:243–8. <https://doi.org/10.1016/j.jaap.2004.07.003>.
- [136] Mani T, Murugan P, Abedi J, Mahinpey N. Pyrolysis of wheat straw in a thermogravimetric analyzer: Effect of particle size and heating rate on devolatilization and estimation of global kinetics. *Chem Eng Res Des* 2010;88:952–8. <https://doi.org/10.1016/j.cherd.2010.02.008>.
- [137] Onay O, Kockar OM. Slow, fast and flash pyrolysis of rapeseed. *Renew Energy* 2003;28:2417–33. [https://doi.org/10.1016/S0960-1481\(03\)00137-X](https://doi.org/10.1016/S0960-1481(03)00137-X).
- [138] Westerhof RJM, Kuipers NJM, Kersten SRA, Van Swaaij WPM. Controlling the water

- content of biomass fast pyrolysis oil. *Ind Eng Chem Res* 2007;46:9238–47. <https://doi.org/10.1021/ie070684k>.
- [139] Gray MR, Corcoran WH, Gavalas GR. Pyrolysis of a Wood-Derived Material. Effects of Moisture and Ash Content. *Ind Eng Chem Process Des Dev* 1985;24:646–51. <https://doi.org/10.1021/i200030a020>.
- [140] Ibrahim N, Jensen PA, Johansen DM, Ali RR, Kasmani MR. Influence of Reaction Temperature and Water Content on Wheat Straw Pyrolysis. *World Acad Sci Eng Technol* 2012;6:10–21.
- [141] Várhegyi G, Szabó P, Mok WS-L, Antal MJ. Kinetics of the thermal decomposition of cellulose in sealed vessels at elevated pressures. Effects of the presence of water on the reaction mechanism. *J Anal Appl Pyrolysis* 1993;26:159–74. [https://doi.org/10.1016/0165-2370\(93\)80064-7](https://doi.org/10.1016/0165-2370(93)80064-7).
- [142] Yang Y, Heaven S, Venetsaneas N, Banks CJ, Bridgwater A V. Slow pyrolysis of organic fraction of municipal solid waste (OFMSW): Characterisation of products and screening of the aqueous liquid product for anaerobic digestion. *Appl Energy* 2018;213:158–68. <https://doi.org/10.1016/j.apenergy.2018.01.018>.
- [143] Hatakeyama H, Hatakeyama T. Interaction between water and hydrophilic polymers. *Thermochim Acta* 1998;308:3–22. [https://doi.org/10.1016/s0040-6031\(97\)00325-0](https://doi.org/10.1016/s0040-6031(97)00325-0).
- [144] Antal MJ, Allen SG, Dai X, Shimizu B, Tam MS, Grønli M. Attainment of the theoretical yield of carbon from biomass. *Ind Eng Chem Res* 2000;39:4024–31. <https://doi.org/10.1021/ie000511u>.
- [145] Antal MJ, Mok WSL, Varhegyi G, Szekely T. Review of Methods for Improving the Yield of Charcoal from Biomass. *Energy and Fuels* 1990;4:221–5. <https://doi.org/10.1021/ef00021a001>.
- [146] Czernik S, Bridgwater A V. Overview of applications of biomass fast pyrolysis oil. *Energy and Fuels* 2004;18:590–8. <https://doi.org/10.1021/ef034067u>.
- [147] Bridgwater A V. The production of biofuels and renewable chemicals by fast pyrolysis of biomass. *Int J Glob Energy Issues* 2007;27:160–203. <https://doi.org/10.1504/IJGEI.2007.013654>.
- [148] Garcia-Nunez JA, Pelaez-Samaniego MR, Garcia-Perez ME, Fonts I, Abrego J, Westerhof RJM, et al. Historical Developments of Pyrolysis Reactors: A Review. *Energy and Fuels* 2017;31:5751–75. <https://doi.org/10.1021/acs.energyfuels.7b00641>.
- [149] Abdelhafez A, Abbas M, Li J. Chapter 2 - Biochar: The Black Diamond for Soil Sustainability, Contamination Control and Agricultural Production. In: Huang W-J, editor. *Eng. Appl. Biochar*, IntechOpen; 2017. <https://doi.org/http://dx.doi.org/10.5772/intechopen.68803>.
- [150] Ronsse F. Introduction to thermal and catalytic waste conversion - Conference

- presentation (Re-Source Webinars) 2020.
- [151] Thangalazhy-Gopakumar S, Adhikari S, Ravindran H, Gupta RB, Fasina O, Tu M, et al. Physiochemical properties of bio-oil produced at various temperatures from pine wood using an auger reactor. *Bioresour Technol* 2010;101:8389–95. <https://doi.org/10.1016/j.biortech.2010.05.040>.
- [152] Badger PC, Fransham P. Use of mobile fast pyrolysis plants to densify biomass and reduce biomass handling costs - A preliminary assessment. *Biomass and Bioenergy* 2006;30:321–5. <https://doi.org/10.1016/j.biombioe.2005.07.011>.
- [153] Marshall A. Commercial applications of Pyrolysis Technology in Agriculture. Ontario: 2013.
- [154] Campuzano F, Brown RC, Martínez JD. Auger reactors for pyrolysis of biomass and wastes. *Renew Sustain Energy Rev* 2019;102:372–409. <https://doi.org/10.1016/j.rser.2018.12.014>.
- [155] Sirijanusorn S, Sriprateep K, Pattiya A. Pyrolysis of cassava rhizome in a counter-rotating twin screw reactor unit. *Bioresour Technol* 2013;139:343–8. <https://doi.org/10.1016/j.biortech.2013.04.024>.
- [156] Yang Y, Brammer JG, Ouadi M, Samanya J, Hornung A, Xu HM, et al. Characterisation of waste derived intermediate pyrolysis oils for use as diesel engine fuels. *Fuel* 2013;103:247–57. <https://doi.org/10.1016/j.fuel.2012.07.014>.
- [157] Funke A, Tomasi Morgano M, Dahmen N, Leibold H. Experimental comparison of two bench scale units for fast and intermediate pyrolysis. *J Anal Appl Pyrolysis* 2017;124:504–14. <https://doi.org/10.1016/j.jaap.2016.12.033>.
- [158] Lakshmanan C, Gal-Or B, Hoelscher H. Production Of Levoglucosan By Pyrolysis Of Carbohydrates. *I&EC Prod Res Dev* 1969;8:261–7. <https://doi.org/10.1021/i360031a010>.
- [159] Brassard P, Godbout S, Raghavan V. Pyrolysis in auger reactors for biochar and bio-oil production: A review. *Biosyst Eng* 2017;161:80–92. <https://doi.org/10.1016/j.biosystemseng.2017.06.020>.
- [160] Hammond J, Rödger J. Biochar - climate saving soils - Newsletter 1. vol. 1. 2012.
- [161] IEA Bioenergy. Thermal Pre-treatment of Biomass for Large-scale Applications - Summary and Conclusions from the ExCo66 Workshop. 2011.
- [162] ETIA Group. Spirajoule: electrically heated screw conveyor 2019. <https://etia-group.com/our-products/spirajoule> (accessed December 9, 2020).
- [163] Biogreen, ETIA Group. The pyrolyzer Spirajoule®. An exclusive process for thermal treatment 2020. <http://www.biogreen-energy.com/spirajoule/> (accessed December 9, 2020).
- [164] Roggero CM, Tumiatti V, Scova A, De Leo C, Binello A, Cravotto G. Characterization

- of oils from haloclean pyrolysis of biomasses. *Energy Sources, Part A Recover Util Environ Eff* 2011;33:467–76. <https://doi.org/10.1080/15567030903096980>.
- [165] Hornung A, Bockhorn H, Appenzeller K, Roggero CM, Tumiatti W. Patent EP 1 217 318 A1 - Plant for the thermal treatment of material and operation process thereof. EP 1 217 318 A1, 2002.
- [166] Hornung A, Koch W, Seifert H. Haloclean and PYDRA - a dual staged pyrolysis plant for the recycling waste electronic and electrical equipment (WEEE). *Met. Energy Recover. Internat.Symp.in North. Sweden, Skelleftea: 2003*, p. 7.
- [167] Sea Marconi. Haloclean BioEnergy - Pyrolysis Liquid for Power Generation. *PyNe IEA Bioenergy*; 2007.
- [168] Hornung A, Apfelbacher A, Koch W, Linek K, Sagi S, Schoner J, et al. Thermo-chemical conversion of straw – Haloclean , an optimised low temperature pyrolysis. *14th Eur. Biomass Conf., Paris: 2005*, p. 5.
- [169] Schmitt N, Apfelbacher A, Jäger N, Daschner R, Stenzel F, Hornung A. Thermo-chemical conversion of biomass and upgrading to biofuel: The Thermo-Catalytic Reforming process – A review. *Biofuels, Bioprod Biorefining* 2019;13:822–37. <https://doi.org/10.1002/bbb.1980>.
- [170] Hornung A, Apfelbacher A. EP2300560B1 - Thermal treatment of biomass. EP2300560B1, 2009.
- [171] Hornung A, Apfelbacher A, Sagi S. Intermediate pyrolysis: A sustainable biomass-to-energy concept-biothermal valorisation of biomass (BtVB) process. *J Sci Ind Res (India)* 2011;70:664–7.
- [172] Yang Y, Brammer JG, Mahmood ASN, Hornung A. Intermediate pyrolysis of biomass energy pellets for producing sustainable liquid, gaseous and solid fuels. *Bioresour Technol* 2014;169:794–9. <https://doi.org/10.1016/j.biortech.2014.07.044>.
- [173] Conti R, Jäger N, Neumann J, Apfelbacher A, Daschner R, Hornung A. Thermocatalytic Reforming of Biomass Waste Streams. *Energy Technol* 2017;5:104–10. <https://doi.org/10.1002/ente.201600168>.
- [174] Binder S, Ouadi M, Hornung A. Biobattery - Integration of TCR, PSA and HDO for the production of 100% green fuels, biochar, heat and power. *25th EUBCE, Stockholm: ETA-Florence; 2017*.
- [175] Li B, Lv W, Zhang Q, Wang T, Ma L. Pyrolysis and catalytic upgrading of pine wood in a combination of auger reactor and fixed bed. *Fuel* 2014;129:61–7. <https://doi.org/10.1016/j.fuel.2014.03.043>.
- [176] Fassinou WF, Van de Steene L, Toure S, Volle G, Girard P. Pyrolysis of Pinus pinaster in a two-stage gasifier: Influence of processing parameters and thermal cracking of tar. *Fuel Process Technol* 2009;90:75–90. <https://doi.org/10.1016/j.fuproc.2008.07.016>.

- [177] Tomasi Morgano M, Leibold H, Richter F, Seifert H. Screw pyrolysis with integrated sequential hot gas filtration. *J Anal Appl Pyrolysis* 2015;113:216–24. <https://doi.org/10.1016/j.jaap.2014.12.019>.
- [178] Yu Y, Yang Y, Cheng Z, Blanco PH, Liu R, Bridgwater A V., et al. Pyrolysis of Rice Husk and Corn Stalk in Auger Reactor. 1. Characterization of Char and Gas at Various Temperatures. *Energy and Fuels* 2016;30:10568–74. <https://doi.org/10.1021/acs.energyfuels.6b02276>.
- [179] Dalluge DL, Daugaard T, Johnston P, Kuzhiyil N, Wright MM, Brown RC. Continuous production of sugars from pyrolysis of acid-infused lignocellulosic biomass. *Green Chem* 2014;16:4144–55. <https://doi.org/10.1039/c4gc00602j>.
- [180] Yang Y. Energy production from biomass and waste derived intermediate pyrolysis. Aston University, 2014.
- [181] Tomasi Morgano M, Leibold H, Richter F, Stapf D, Seifert H. Screw pyrolysis technology for sewage sludge treatment. *Waste Manag* 2017. <https://doi.org/10.1016/j.wasman.2017.05.049>.
- [182] Ouadi M, Brammer JG, Yang Y, Hornung A, Kay M. The intermediate pyrolysis of deinking sludge to produce a sustainable liquid fuel. *J Anal Appl Pyrolysis* 2013;102:24–32. <https://doi.org/10.1016/j.jaap.2013.04.007>.
- [183] Neumann J, Binder S, Apfelbacher A, Gasson JR, Ramírez García P, Hornung A. Production and characterization of a new quality pyrolysis oil, char and syngas from digestate - Introducing the thermo-catalytic reforming process. *J Anal Appl Pyrolysis* 2015;113:137–42. <https://doi.org/10.1016/j.jaap.2014.11.022>.
- [184] Ouadi M, Jaeger N, Greenhalf C, Santos J, Conti R, Hornung A. Thermo-Catalytic Reforming of municipal solid waste. *Waste Manag* 2017;68:198–206. <https://doi.org/10.1016/j.wasman.2017.06.044>.
- [185] Liaw SS, Wang Z, Ndegwa P, Frear C, Ha S, Li CZ, et al. Effect of pyrolysis temperature on the yield and properties of bio-oils obtained from the auger pyrolysis of Douglas Fir wood. *J Anal Appl Pyrolysis* 2012;93:52–62. <https://doi.org/10.1016/j.jaap.2011.09.011>.
- [186] Enders A, Hanley K, Whitman T, Joseph S, Lehmann J. Characterization of biochars to evaluate recalcitrance and agronomic performance. *Bioresour Technol* 2012;114:644–53. <https://doi.org/10.1016/j.biortech.2012.03.022>.
- [187] World Nuclear Association. Heat Values of Various Fuels 2021. <https://www.world-nuclear.org/information-library/facts-and-figures/heat-values-of-various-fuels.aspx> (accessed March 30, 2021).
- [188] Bjorkman E, Stromberg B. Release of chlorine from biomass at pyrolysis and gasification conditions. *Energy & Fuels* 1997;10:26–32.
- [189] Manyà JJ, Laguarta S, Ortigosa MA, Manso JA. Biochar from slow pyrolysis of two-

- phase olive mill waste: Effect of pressure and peak temperature on its potential stability. *Energy and Fuels* 2014;28:3271–80. <https://doi.org/10.1021/ef500654t>.
- [190] Mukherjee A, Zimmerman AR, Harris W. Surface chemistry variations among a series of laboratory-produced biochars. *Geoderma* 2011;163:247–55. <https://doi.org/10.1016/j.geoderma.2011.04.021>.
- [191] Boehm H-P, Diehl E, Heck W, Sappok R. Surface Oxides of Carbon. *Angew Chemie Int Ed English* 1964;3:669–77. <https://doi.org/10.1002/anie.196406691>.
- [192] Boehm HP. Surface oxides on carbon and their analysis: A critical assessment. *Carbon* N Y 2002;40:145–9. [https://doi.org/10.1016/S0008-6223\(01\)00165-8](https://doi.org/10.1016/S0008-6223(01)00165-8).
- [193] Jiang SF, Sheng GP, Jiang H. Advances in the characterization methods of biomass pyrolysis products. *ACS Sustain Chem Eng* 2019;7:12639–55. <https://doi.org/10.1021/acssuschemeng.9b00868>.
- [194] Fidel RB, Laird DA, Thompson ML. Evaluation of modified boehm titration methods for use with biochars. *J Environ Qual* 2013;42:1771–8. <https://doi.org/10.2134/jeq2013.07.0285>.
- [195] Li J, Li Q, Qian C, Wang X, Lan Y, Wang B, et al. Volatile organic compounds analysis and characterization on activated biochar prepared from rice husk. *Int J Environ Sci Technol* 2019;16:7653–62. <https://doi.org/10.1007/s13762-019-02219-4>.
- [196] Ahmad M, Rajapaksha AU, Lim JE, Zhang M, Bolan N, Mohan D, et al. Biochar as a sorbent for contaminant management in soil and water: A review. *Chemosphere* 2014;99:19–33. <https://doi.org/10.1016/j.chemosphere.2013.10.071>.
- [197] Ahmad M, Lee SS, Dou X, Mohan D, Sung JK, Yang JE, et al. Effects of pyrolysis temperature on soybean stover- and peanut shell-derived biochar properties and TCE adsorption in water. *Bioresour Technol* 2012;118:536–44. <https://doi.org/10.1016/j.biortech.2012.05.042>.
- [198] Li Y, Hu S, Chen J, Müller K, Li Y, Fu W. Effects of biochar application in forest ecosystems on soil properties and greenhouse gas emissions: a review. *Springer* 2018:546–63.
- [199] Allaire S, Lange S, Auclair I, Quinche M, Greffard L. Analyses of biochar properties. Quebec: 2015. <https://doi.org/10.13140/RG.2.1.2789.4241>.
- [200] Rouquerol J, Avnir D, Fairbridge CW, Everett DH., Haynes JH, Pernicone N, et al. Recommendations for the characterization of porous solids (technical report). *Pure Appl Chem* 1994;66:1739–58.
- [201] Fitzer E, Kochling K-H, Boehm HP, Marsh H. Recommended terminology for the description of carbon as a solid (IUPAC Recommendations 1995). *Pure Appl Chem* 1995;67:473–506. <https://doi.org/10.1351/pac199567030473>.
- [202] Marsh H, Rodríguez-Reinoso F. *Activated Carbon*. Elsevier Science & Technology

- Books; 2006. <https://doi.org/10.1016/B978-008044463-5/50018-2>.
- [203] Lozano-Castelló D, Cazorla-Amorós D, Linares-Solano A. Usefulness of CO₂ adsorption at 273 K for the characterization of porous carbons. *Carbon N Y* 2004;42:1233–42. <https://doi.org/10.1016/j.carbon.2004.01.037>.
- [204] Kim KC, Yoon TU, Bae YS. Applicability of using CO₂ adsorption isotherms to determine BET surface areas of microporous materials. *Microporous Mesoporous Mater* 2016;224:294–301. <https://doi.org/10.1016/j.micromeso.2016.01.003>.
- [205] Sun H, Hockaday WC, Masiello CA, Zygourakis K. Multiple controls on the chemical and physical structure of biochars. *Ind Eng Chem Res* 2012;51:3587–97. <https://doi.org/10.1021/ie201309r>.
- [206] Novak J. Biochar formulations as a soil amendment in the agricultural, forestry and environmental sectors - Conference presentation n.d.
- [207] Ma Q, Song W, Wang R, Zou J, Yang R, Zhang S. Physicochemical properties of biochar derived from anaerobically digested dairy manure. *Waste Manag* 2018;79:729–34. <https://doi.org/10.1016/j.wasman.2018.08.023>.
- [208] Spokas KA, Novak JM, Stewart CE, Cantrell KB, Uchimiya M, DuSaire MG, et al. Qualitative analysis of volatile organic compounds on biochar. *Chemosphere* 2011;85:869–82. <https://doi.org/10.1016/j.chemosphere.2011.06.108>.
- [209] Pathy A, Ray J, Paramasivan B. Biochar amendments and its impact on soil biota for sustainable agriculture. *Biochar* 2020;2:287–305. <https://doi.org/10.1007/s42773-020-00063-1>.
- [210] Bucheli TD, Hilber I, Schmidt HP. Polycyclic aromatic hydrocarbons and polychlorinated aromatic compounds in biochar. In: Lehmann J, Joseph S, editors. *Biochar Environ. Manag.* 2nd Ed, Routledge (Taylor and Francis group); 2015, p. 593–622. <https://doi.org/10.4324/9780203762264-28>.
- [211] David E, Kopac J. Activated carbons derived from residual biomass pyrolysis and their CO₂ adsorption capacity. *J Anal Appl Pyrolysis* 2014;110:322–32. <https://doi.org/10.1016/j.jaap.2014.09.021>.
- [212] Kan T, Strezov V, Evans TJ. Lignocellulosic biomass pyrolysis: A review of product properties and effects of pyrolysis parameters. *Renew Sustain Energy Rev* 2016;57:1126–40. <https://doi.org/10.1016/j.rser.2015.12.185>.
- [213] Keown DM, Hayashi J ichiro, Li CZ. Effects of volatile-char interactions on the volatilisation of alkali and alkaline earth metallic species during the pyrolysis of biomass. *Fuel* 2008;87:1187–94. <https://doi.org/10.1016/j.fuel.2007.05.056>.
- [214] Lohri CR, Rajabu HM, Sweeney DJ, Zurbrügg C. Char fuel production in developing countries - A review of urban biowaste carbonization. *Renew Sustain Energy Rev* 2016;59:1514–30. <https://doi.org/10.1016/j.rser.2016.01.088>.

- [215] Lehmann J. A handful of carbon. *Nature* 2007;447:143–4. <https://doi.org/10.1038/447143a>.
- [216] Ippolito JA, Laird DA, Busscher WJ. Environmental Benefits of Biochar. *J Environ Qual* 2012;41:967–72. <https://doi.org/10.2134/jeq2012.0151>.
- [217] Lehmann J, Joseph S. Biochar for environmental management: An introduction. *Biochar Environ Manag - Sci Technol* 2009;1:1–12. <https://doi.org/10.1016/j.forpol.2009.07.001>.
- [218] Park JH, Choppala GK, Bolan NS, Chung JW, Chuasavathi T. Biochar reduces the bioavailability and phytotoxicity of heavy metals. *Plant Soil* 2011;348:439. <https://doi.org/10.1007/s11104-011-0948-y>.
- [219] Lehmann J, Gaunt J, Rondon M. Bio-char sequestration in terrestrial ecosystems - A review. *Mitig Adapt Strateg Glob Chang* 2006;11:403–27. <https://doi.org/10.1007/s11027-005-9006-5>.
- [220] Tian X, Li C, Zhang M, Wan Y, Xie Z, Chen B, et al. Biochar derived from corn straw affected availability and distribution of soil nutrients and cotton yield. *PLoS One* 2018;13:1–19. <https://doi.org/10.1371/journal.pone.0189924>.
- [221] Gray M, Johnson MG, Dragila MI, Kleber M. Water uptake in biochars: The roles of porosity and hydrophobicity. *Biomass and Bioenergy* 2014;61:196–205. <https://doi.org/10.1016/j.biombioe.2013.12.010>.
- [222] European Biochar Foundation (EBC). Biochar for use as a feed-additive - Guidelines for EBC-feed certification. 2018.
- [223] Stevenson KJ, Ozoliņš V, Dunn B. Chapter 23 - Electrochemical Energy Storage. In: Bottani E, Tascon J, editors. *Adsorpt. by Carbons*, vol. 46, Elsevier Ltd; 2008, p. 1051–2. <https://doi.org/10.1021/ar400100z>.
- [224] Jiang J, Zhang L, Wang X, Holm N, Rajagopalan K, Chen F, et al. Highly ordered macroporous woody biochar with ultra-high carbon content as supercapacitor electrodes. *Electrochim Acta* 2013;113:481–9. <https://doi.org/https://doi.org/10.1016/j.electacta.2013.09.121>.
- [225] Ioannidou O, Zabaniotou A. Agricultural residues as precursors for activated carbon production — A review 2007;11:1966–2005. <https://doi.org/10.1016/j.rser.2006.03.013>.
- [226] Derbyshire F, Jagtoyen M, Andrews R, Rao A, Martin-Gullón I, Grulke E. 1. Carbon Materials in Environmental Applications. In: Radovic L, editor. *Chem. Phys. Carbon - Vol. 27*, Marcel Dekker, Inc.; 2001.
- [227] Huang Q, Song S, Chen Z, Hu B, Chen J, Wang X. Biochar-based materials and their applications in removal of organic contaminants from wastewater: state-of-the-art review. *Biochar* 2019;1:45–73. <https://doi.org/10.1007/s42773-019-00006-5>.
- [228] Di Stasi C, Alvira D, Greco G, González B, Manyà JJ. Physically activated wheat straw-

- derived biochar for biomass pyrolysis vapors upgrading with high resistance against coke deactivation. *Fuel* 2019;255:115807. <https://doi.org/10.1016/j.fuel.2019.115807>.
- [229] Jasim SM, Ali NA. Properties characterization of plasticized polylactic acid/Biochar (bio carbon) nano-composites for antistatic packaging. *Iraqi J Phys* 2019;17:13–26. <https://doi.org/10.20723/ijp.17.42.13-26>.
- [230] Giorcelli M, Bartoli M. Development of coffee biochar filler for the production of electrical conductive reinforced plastic. *Polymers (Basel)* 2019;11:1–17. <https://doi.org/10.3390/polym11121916>.
- [231] Ziegler D, Palmero P, Giorcelli M, Tagliaferro A, Tulliani JM. Biochars as innovative humidity sensing materials. *Chemosensors* 2017;5:1–16. <https://doi.org/10.3390/chemosensors5040035>.
- [232] Qian K, Kumar A, Zhang H, Bellmer D, Huhnke R. Recent advances in utilization of biochar. *Renew Sustain Energy Rev* 2015;42:1055–64. <https://doi.org/10.1016/j.rser.2014.10.074>.
- [233] Garg S, Das P. Microporous carbon from cashew nutshell pyrolytic biochar and its potential application as CO₂ adsorbent. *Biomass Convers Biorefinery* 2020;10:1043–61. <https://doi.org/10.1007/s13399-019-00506-1>.
- [234] Koehlert K. Activated Carbon : Fundamentals and New Applications. *Chem Eng Online* 2017:32–40.
- [235] Li S, Lü J, Zhang T, Cao Y, Li J. Relationship between biochars' porosity and adsorption of three neutral herbicides from water. *Water Sci Technol* 2017;75:482–9. <https://doi.org/10.2166/wst.2016.535>.
- [236] Kim P, Johnson A, Edmunds CW, Radosevich M, Vogt F, Rials TG, et al. Surface functionality and carbon structures in lignocellulosic-derived biochars produced by fast pyrolysis. *Energy and Fuels* 2011;25:4693–703. <https://doi.org/10.1021/ef200915s>.
- [237] Nam H, Capareda SC, Ashwath N, Kongkasawan J. Experimental investigation of pyrolysis of rice straw using bench-scale auger, batch and fluidized bed reactors. *Energy* 2015;93:2384–94. <https://doi.org/10.1016/j.energy.2015.10.028>.
- [238] Santos J, Ouadi M, Jahangiri H, Hornung A. Integrated intermediate catalytic pyrolysis of wheat husk. *Food Bioprod Process* 2019;114:23–30. <https://doi.org/10.1016/j.fbp.2018.11.001>.
- [239] Di Stasi C, Greco G, Manyà JJ, González B. Chapter 8 - Biochar as sustainable platform for pyrolysis vapours upgrading. In: Manyà JJ, editor. *Adv. Carbon Mater. from Biomass an Overv.*, GreenCarbon Project and Consortium; 2019.
- [240] Suhas, Carrott PJM, Ribeiro Carrott MML. Lignin - from natural adsorbent to activated carbon: A review. *Bioresour Technol* 2007;98:2301–12. <https://doi.org/10.1016/j.biortech.2006.08.008>.

- [241] Pilon G, Lavoie JM. Pyrolysis of switchgrass (*Panicum virgatum* L.) at low temperatures within N₂ and CO₂ environments: Product yield study. *ACS Sustain Chem Eng* 2013;1:198–204. <https://doi.org/10.1021/sc300098e>.
- [242] Bouchelta C, Medjram MS, Bertrand O, Bellat J-P. Preparation and characterization of activated carbon from date stones by physical activation with steam. *J Anal Appl Pyrolysis* 2008;82:70–7. <https://doi.org/https://doi.org/10.1016/j.jaap.2007.12.009>.
- [243] Kumar A, Jones DD, Hanna MA. Thermochemical biomass gasification: A review of the current status of the technology. *Energies* 2009;2:556–81. <https://doi.org/10.3390/en20300556>.
- [244] Rodríguez-Reinoso F, Molina-Sabio M, González MT. The use of steam and CO₂ as activating agents in the preparation of activated carbons. *Carbon N Y* 1995;33:15–23. [https://doi.org/10.1016/0008-6223\(94\)00100-E](https://doi.org/10.1016/0008-6223(94)00100-E).
- [245] Ahmadpour A, Do DD. The preparation of active carbons from coal by chemical and physical activation. *Carbon N Y* 1996;34:471–9. [https://doi.org/10.1016/0008-6223\(95\)00204-9](https://doi.org/10.1016/0008-6223(95)00204-9).
- [246] Dehkoda AM, Gyenge E, Ellis N. A novel method to tailor the porous structure of KOH-activated biochar and its application in capacitive deionization and energy storage. *Biomass and Bioenergy* 2016;87:107–21. <https://doi.org/10.1016/j.biombioe.2016.02.023>.
- [247] Lillo-Ródenas MA, Lozano-Castelló D, Cazorla-Amorós D, Linares-Solano A. Preparation of activated carbons from Spanish anthracite - II. Activation by NaOH. *Carbon N Y* 2001;39:751–9. [https://doi.org/10.1016/S0008-6223\(00\)00186-X](https://doi.org/10.1016/S0008-6223(00)00186-X).
- [248] Maiti S, Purakayastha S, Ghosh B. Production of low-cost carbon adsorbents from agricultural wastes and their impact on dye adsorption. *Chem Eng Commun* 2008;195:386–403. <https://doi.org/10.1080/00986440701707917>.
- [249] Otowa T, Tanibata R, Itoh M. Production and adsorption characteristics of MAXSORB: High-surface-area active carbon. *Gas Sep Purif* 1993;7:241–5. [https://doi.org/https://doi.org/10.1016/0950-4214\(93\)80024-Q](https://doi.org/https://doi.org/10.1016/0950-4214(93)80024-Q).
- [250] Wang J, Kaskel S. KOH activation of carbon-based materials for energy storage. *J Mater Chem* 2012;22:23710–25. <https://doi.org/10.1039/c2jm34066f>.
- [251] Lillo-Ródenas MA, Cazorla-Amorós D, Linares-Solano A. Understanding chemical reactions between carbons and NaOH and KOH: An insight into the chemical activation mechanism. *Carbon N Y* 2003;41:267–75. [https://doi.org/10.1016/S0008-6223\(02\)00279-8](https://doi.org/10.1016/S0008-6223(02)00279-8).
- [252] Hayashi J, Kazehaya A, Muroyama K, Watkinson AP. Preparation of activated carbon from lignin by chemical activation. *Carbon N Y* 2000;38:1873–8. [https://doi.org/10.1016/S0008-6223\(00\)00027-0](https://doi.org/10.1016/S0008-6223(00)00027-0).

- [253] Maciá-Agulló JA, Moore BC, Cazorla-Amorós D, Linares-Solano A. Activation of coal tar pitch carbon fibres: Physical activation vs. chemical activation. *Carbon N Y* 2004;42:1367–70. <https://doi.org/https://doi.org/10.1016/j.carbon.2004.01.013>.
- [254] Arauzo P, Olszewski M, Lucian M, Rodriguez-Correa C, Ringelspacher Y, Kruse A, et al. Chapter 6 - Review of the conversion from hydrochar to activated carbon. In: Manyà JJ, editor. *Adv. Carbon Mater. from Biomass an Overv., GreenCarbon Project and Consortium*; 2019.
- [255] Oh GH, Park CR. Preparation and characteristics of rice-straw-based porous carbons with high adsorption capacity. *Fuel* 2002;81:327–36. [https://doi.org/https://doi.org/10.1016/S0016-2361\(01\)00171-5](https://doi.org/https://doi.org/10.1016/S0016-2361(01)00171-5).
- [256] Robau-Sánchez A, Aguilar-Elguézabal A, Aguilar-Pliego J. Chemical activation of *Quercus agrifolia* char using KOH: Evidence of cyanide presence. *Microporous Mesoporous Mater* 2005;85:331–9. <https://doi.org/10.1016/j.micromeso.2005.07.003>.
- [257] Teng H, Yeh T-S, Hsu L-Y. Preparation of activated carbon from bituminous coal with phosphoric acid activation. *Carbon N Y* 1998;36:1387–95. [https://doi.org/https://doi.org/10.1016/S0008-6223\(98\)00127-4](https://doi.org/https://doi.org/10.1016/S0008-6223(98)00127-4).
- [258] Sudaryanto Y, Hartono SB, Irawaty W, Hindarso H, Ismadji S. High surface area activated carbon prepared from cassava peel by chemical activation. *Bioresour Technol* 2006;97:734–9. <https://doi.org/https://doi.org/10.1016/j.biortech.2005.04.029>.
- [259] Fierro V, Torné-Fernández V, Celzard A, Montané D. Influence of the demineralisation on the chemical activation of Kraft lignin with orthophosphoric acid. *J Hazard Mater* 2007;149:126–33. <https://doi.org/https://doi.org/10.1016/j.jhazmat.2007.03.056>.
- [260] Unur E. Functional nanoporous carbons from hydrothermally treated biomass for environmental purification. *Microporous Mesoporous Mater* 2013;168:92–101. <https://doi.org/https://doi.org/10.1016/j.micromeso.2012.09.027>.
- [261] Jain A, Balasubramanian R, Srinivasan MP. Hydrothermal conversion of biomass waste to activated carbon with high porosity: A review. *Chem Eng J* 2016;283:789–805. <https://doi.org/https://doi.org/10.1016/j.cej.2015.08.014>.
- [262] Laine J, Simoni S, Calles R. Preparation of Activated carbon from coconut shell in a small scale co-current flow rotary kiln. *Chem Eng Commun* 1991;99:15–23. <https://doi.org/10.1080/00986449108911575>.
- [263] Jung SH, Kim JS. Production of biochars by intermediate pyrolysis and activated carbons from oak by three activation methods using CO₂. *J Anal Appl Pyrolysis* 2014;107:116–22. <https://doi.org/10.1016/j.jaap.2014.02.011>.
- [264] Ma Y. Comparison of Activated Carbons Prepared from Wheat Straw via ZnCl₂ and KOH Activation. *Waste and Biomass Valorization* 2017;8:549–59. <https://doi.org/10.1007/s12649-016-9640-z>.

- [265] Grand View Research Inc. Activated Carbon Market Analysis and Segment Forecasts To 2024. San Francisco: 2016.
- [266] Pescod M, FAO. Wastewater treatment and use in agriculture - FAO irrigation and drainage paper 47. Rome: 1992.
- [267] Das S, Ray N, Wan J, Khan A, Chakraborty T, Ray M. Chapter 5 - Micropollutants in Wastewater: Fate and Removal Processes. In: Farooq R, Ahmad Z, editors. Physico-Chemical Wastewater Treat. Resour. Recover., IntechOpen; 2017. <https://doi.org/10.5772/67803>.
- [268] Rouquerol F, Rouquerol J, Sing K. Adsorption by powders and porous solids - Principles, methodology and apps. Academic Press; 1999. <https://doi.org/10.15713/ins.mmj.3>.
- [269] Markets And Markets. Adsorbent Market by Type, by Application, and by Region - Global Forecast to 2020 2015.
- [270] Lua AC, Guo J. Activated carbon prepared from oil palm stone by one-step CO₂ activation for gaseous pollutant removal. Carbon N Y 2000;38:1089–97. [https://doi.org/10.1016/S0008-6223\(99\)00231-6](https://doi.org/10.1016/S0008-6223(99)00231-6).
- [271] Reljic S, et al. CO₂ Adsorption in Activated Carbons. In: Moreno-Piraján J, Giraldo-Gutierrez L, Gómez-Granados F, editors. Porous Mater., Springer; 2021. <https://doi.org/10.1007/978-3-030-65991-2>.
- [272] Zhu Y, Yi B, Yuan Q, Wu Y, Wang M, Yan S. Removal of methylene blue from aqueous solution by cattle manure-derived low temperature biochar. RSC Adv 2018;8:19917–29. <https://doi.org/10.1039/c8ra03018a>.
- [273] Manna S, Roy D, Saha P, Gopakumar D, Thomas S. Rapid methylene blue adsorption using modified lignocellulosic materials. Process Saf Environ Prot 2017;107:346–56. <https://doi.org/10.1016/j.psep.2017.03.008>.
- [274] Thompson KA, Shimabuku KK, Kearns JP, Knappe DRU, Summers RS, Cook SM. Environmental Comparison of Biochar and Activated Carbon for Tertiary Wastewater Treatment. Environ Sci Technol 2016;50:11253–62. <https://doi.org/10.1021/acs.est.6b03239>.
- [275] Wu S, Wu H. Incorporating Biochar into Wastewater Eco-treatment Systems: Popularity, Reality, and Complexity. Environ Sci Technol 2019;53:3345–6. <https://doi.org/10.1021/acs.est.9b01101>.
- [276] Xue Y, Gao B, Yao Y, Inyang M, Zhang M, Zimmerman AR, et al. Hydrogen peroxide modification enhances the ability of biochar (hydrochar) produced from hydrothermal carbonization of peanut hull to remove aqueous heavy metals: Batch and column tests. Chem Eng J 2012;200–202:673–80. <https://doi.org/https://doi.org/10.1016/j.cej.2012.06.116>.

- [277] Hale SE, Lehmann J, Rutherford D, Zimmerman AR, Bachmann RT, Shitumbanuma V, et al. Quantifying the Total and Bioavailable Polycyclic Aromatic Hydrocarbons and Dioxins in Biochars. *Environ Sci Technol* 2012;46:2830–8. <https://doi.org/10.1021/es203984k>.
- [278] Raposo F, De La Rubia MA, Borja R. Methylene blue number as useful indicator to evaluate the adsorptive capacity of granular activated carbon in batch mode: Influence of adsorbate/adsorbent mass ratio and particle size. *J Hazard Mater* 2009;165:291–9. <https://doi.org/10.1016/j.jhazmat.2008.09.106>.
- [279] Sych N V., Trofymenko SI, Poddubnaya OI, Tsyba MM, Sapsay VI, Klymchuk DO, et al. Porous structure and surface chemistry of phosphoric acid activated carbon from corncob. *Appl Surf Sci* 2012;261:75–82. <https://doi.org/10.1016/j.apsusc.2012.07.084>.
- [280] Brewer CE, Chuang VJ, Masiello CA, Gonnermann H, Gao X, Dugan B, et al. New approaches to measuring biochar density and porosity. *Biomass and Bioenergy* 2014;66:176–85. <https://doi.org/10.1016/J.BIOMBIOE.2014.03.059>.
- [281] Wang X, Guo Z, Hu Z, Zhang J. Recent advances in biochar application for water and wastewater treatment: a review. *PeerJ* 2020;8:e9164. <https://doi.org/10.7717/peerj.9164>.
- [282] Ma J, Yu F, Zhou L, Jin L, Yang M, Luan J, et al. Enhanced adsorptive removal of methyl orange and methylene blue from aqueous solution by alkali-activated multiwalled carbon nanotubes. *ACS Appl Mater Interfaces* 2012;4:5749–60. <https://doi.org/10.1021/am301053m>.
- [283] Tran HN, You SJ, Nguyen TV, Chao HP. Insight into the adsorption mechanism of cationic dye onto biosorbents derived from agricultural wastes. *Chem Eng Commun* 2017;204:1020–36. <https://doi.org/10.1080/00986445.2017.1336090>.
- [284] Tran HN, You S-J, Chao H-P. Fast and efficient adsorption of methylene green 5 on activated carbon prepared from new chemical activation method. *J Environ Manage* 2017;188:322–36. <https://doi.org/https://doi.org/10.1016/j.jenvman.2016.12.003>.
- [285] Zubair M. Biochar-LDH composites for water purification (Webinar presentation) 2020.
- [286] University I. NEW Tech project proposes better water treatment system 2020. <https://www.lib.uidaho.edu/digital/uinews/item/n-e-w-tech-project-proposesbetter-water-treatment-system.html>.
- [287] Ahmed MB, Zhou JL, Ngo HH, Guo W, Chen M. Progress in the preparation and application of modified biochar for improved contaminant removal from water and wastewater. *Bioresour Technol* 2016;214:836–51. <https://doi.org/10.1016/j.biortech.2016.05.057>.
- [288] Mohan D, Kumar H, Sarswat A, Alexandre-Franco M, Pittman CU. Cadmium and lead remediation using magnetic oak wood and oak bark fast pyrolysis bio-chars. *Chem Eng*

- J 2014;236:513–28. <https://doi.org/10.1016/j.cej.2013.09.057>.
- [289] Oesterle P, Lindberg RH, Fick J, Jansson S. Extraction of active pharmaceutical ingredients from simulated spent activated carbonaceous adsorbents. *Environ Sci Pollut Res* 2020;27:25572–81. <https://doi.org/10.1007/s11356-020-08822-0>.
- [290] Mohan D, Sarswat A, Ok YS, Pittman CU. Organic and inorganic contaminants removal from water with biochar, a renewable, low cost and sustainable adsorbent - A critical review. *Bioresour Technol* 2014;160:191–202. <https://doi.org/10.1016/j.biortech.2014.01.120>.
- [291] IHS Markit. *Activated Carbon - Chemical Economics Handbook* 2017.
- [292] Ahmed MB, Zhou JL, Ngo HH, Guo W. Insight into biochar properties and its cost analysis. *Biomass and Bioenergy* 2016;84:76–86. <https://doi.org/10.1016/j.biombioe.2015.11.002>.
- [293] McLaughlin H. Understanding activated carbon reactivation and low-temperature regeneration technology. *Int Sugar J* 2005.
- [294] Pei-Jen L, Hsin-Chien L, Wen-Te Y, Jia-Ming C. Chemical regeneration of activated carbon used for dye adsorption. *J Taiwan Inst Chem Eng* 2011;42:305–11.
- [295] Sühnholz S, Kopinke FD, Weiner B. Hydrothermal treatment for regeneration of activated carbon loaded with organic micropollutants. *Sci Total Environ* 2018;644:854–61. <https://doi.org/10.1016/j.scitotenv.2018.06.395>.
- [296] Zhang XN, Mao GY, Jiao YB, Shang Y, Han RP. Adsorption of anionic dye on magnesium hydroxide-coated pyrolytic bio-char and reuse by microwave irradiation. *Int J Environ Sci Technol* 2014;11:1439–48. <https://doi.org/10.1007/s13762-013-0338-5>.
- [297] Ronsse F, Manyà JJ. Deliverable 4.1: 1st specific report in WP 4. Report on the selection of the dry biomass feedstocks. 2017.
- [298] The Linde Group. *Safety Advice - 12. Working with CO₂*. n.d.
- [299] Sigma-Aldrich. *KOH (221473)* 2020. <https://www.sigmaaldrich.com/catalog/product/sigald/221473> (accessed April 14, 2020).
- [300] ASTM. ASTM International, E1131-08 Standard Test Method for Compositional Analysis by Thermogravimetry. *Annu B ASTM Stand* 2008:8–12. <https://doi.org/10.1520/E1131-08>.
- [301] ASTM D 1762-84. Standard Test Method for Chemical Analysis of Wood Charcoal. *ASTM Int* 2011;84:1–2. <https://doi.org/10.1520/D1762-84R07>.
- [302] ASTM. ASTM E1755-01 Standard Test Method for Ash in Biomass. *Annu B ASTM Stand* 2012;01:1–3. <https://doi.org/10.1520/E1755-01R07.2>.
- [303] Channiwala SA, Parikh PP. A unified correlation for estimating HHV of solid, liquid and gaseous fuels. *Fuel* 2002;81:1051–63. [https://doi.org/10.1016/S0016-2361\(01\)00131-](https://doi.org/10.1016/S0016-2361(01)00131-)

- 4.
- [304] Ragland K, Bryden K. Combustion Engineering. 2nd Ed. CRC Press; 2011.
- [305] Singh B, Lehmann J, Camps-Arbestain M. Biochar - A Guide to Analytical Methods. CRC Press; 2017.
- [306] Lima IM, Boateng AA, Klasson KT. Physicochemical and adsorptive properties of fast-pyrolysis bio-chars and their steam activated counterparts. *J Chem Technol Biotechnol* 2010;85:1515–21. <https://doi.org/10.1002/jctb.2461>.
- [307] Ronsse F, van Hecke S, Dickinson D, Prins W. Production and characterization of slow pyrolysis biochar: Influence of feedstock type and pyrolysis conditions. *GCB Bioenergy* 2013;5:104–15. <https://doi.org/10.1111/gcbb.12018>.
- [308] Stella Mary G, Sugumaran P, Niveditha S, Ramalakshmi B, Ravichandran P, Seshadri S. Production, characterization and evaluation of biochar from pod (*Pisum sativum*), leaf (*Brassica oleracea*) and peel (*Citrus sinensis*) wastes. *Int J Recycl Org Waste Agric* 2016;5:43–53. <https://doi.org/10.1007/s40093-016-0116-8>.
- [309] Gor GY, Thommes M, Cychosz KA, Neimark A V. Quenched solid density functional theory method for characterization of mesoporous carbons by nitrogen adsorption. *Carbon N Y* 2012;50:1583–90. <https://doi.org/10.1016/j.carbon.2011.11.037>.
- [310] Landers J, Gor GY, Neimark A V. Density functional theory methods for characterization of porous materials. *Colloids Surfaces A Physicochem Eng Asp* 2013;437:3–32. <https://doi.org/10.1016/j.colsurfa.2013.01.007>.
- [311] Maziarka P, Wurzer C, Arauzo PJ, Dieguez-Alonso A, Mašek O, Ronsse F. Do you BET on routine? The reliability of N₂ physisorption for the quantitative assessment of biochar's surface area. *Chem Eng J* 2021;418. <https://doi.org/10.1016/j.cej.2021.129234>.
- [312] ASTM. ASTM E203-Standard Test Method for Water Using Volumetric Karl Fischer Titration. *ASTM Int* 2011;04:1–9. <https://doi.org/10.1520/C1366-04R09.2>.
- [313] Sigma-Aldrich. Methylene blue (M9140) 2020. <https://www.sigmaaldrich.com/catalog/product/sial/m9140> (accessed April 13, 2020).
- [314] IARC. Methylene Blue - Monograph 108. 2016.
- [315] Dutta S, Bhattacharyya A, Ganguly A, Gupta S, Basu S. Application of Response Surface Methodology for preparation of low-cost adsorbent from citrus fruit peel and for removal of Methylene Blue. *Desalination* 2011;275:26–36. <https://doi.org/https://doi.org/10.1016/j.desal.2011.02.057>.
- [316] Pelekani C, Snoeyink VL. Competitive adsorption between atrazine and methylene blue on activated carbon: The importance of pore size distribution. *Carbon N Y* 2000;38:1423–36. [https://doi.org/10.1016/S0008-6223\(99\)00261-4](https://doi.org/10.1016/S0008-6223(99)00261-4).
- [317] Cazetta AL, Vargas AMM, Nogami EM, Kunita MH, Guilherme MR, Martins AC, et al.

- NaOH-activated carbon of high surface area produced from coconut shell: Kinetics and equilibrium studies from the methylene blue adsorption. *Chem Eng J* 2011;174:117–25. <https://doi.org/10.1016/j.cej.2011.08.058>.
- [318] Ellis R. Reagent and Dye Solubility Chart. IHC World 2011. http://www.ihcworld.com/_technical_tips/solubility_chart.htm (accessed April 14, 2020).
- [319] Martinez V, Henary M. Nile Red and Nile Blue: Applications and Syntheses of Structural Analogues. *Chem - A Eur J* 2016;22:13764–82. <https://doi.org/10.1002/chem.201601570>.
- [320] National Library of Medicine. Methyl Red. PubChem 2020. <https://pubchem.ncbi.nlm.nih.gov/compound/Methyl-red> (accessed April 14, 2020).
- [321] Sigma-Aldrich. Methyl orange (C.I. 13025) (101322) 2020. <https://www.sigmaaldrich.com/catalog/product/mm/101322> (accessed April 13, 2020).
- [322] Kahlert H, Meyer G, Albrecht A. Colour maps of acid–base titrations with colour indicators: how to choose the appropriate indicator and how to estimate the systematic titration errors. *ChemTexts* 2016;2:1–28. <https://doi.org/10.1007/s40828-016-0026-4>.
- [323] Ai L, Zhang C, Meng L. Adsorption of methyl orange from aqueous solution on hydrothermal synthesized Mg-Al layered double hydroxide. *J Chem Eng Data* 2011;56:4217–25. <https://doi.org/10.1021/je200743u>.
- [324] Sigma-Aldrich. Activated Charcoal Norit® (96831) 2020. <https://www.sigmaaldrich.com/catalog/product/sigald/96831> (accessed April 15, 2020).
- [325] Teanmetawong S, Chantaramanee T, Lhosupasirirat S, Wongariyakawee A, Sriksirin T. A Comparison Study of Magnetic Stirrer and Sonicator Technique to Disperse 1% Span20 Treated Layered Double Hydroxides (LDHs). *IOP Conf Ser Mater Sci Eng* 2019;654. <https://doi.org/10.1088/1757-899X/654/1/012005>.
- [326] Mejia J, Valembois V, Piret JP, Tichelaar F, Van Huis M, Masereel B, et al. Are stirring and sonication pre-dispersion methods equivalent for in vitro toxicology evaluation of SiC and TiC? *J Nanoparticle Res* 2012;14. <https://doi.org/10.1007/s11051-012-0815-7>.
- [327] Ashokkumar M. *Ultrasonic Synthesis of Functional Materials*. Springer; 2016. <https://doi.org/10.1007/978-3-319-28974-8>.
- [328] Yildiz G, Ronsse F, Venderbosch R, Duren R van, Kersten SRA, Prins W. Effect of biomass ash in catalytic fast pyrolysis of pine wood. *Appl Catal B Environ* 2015;168–169:203–11. <https://doi.org/10.1016/j.apcatb.2014.12.044>.
- [329] de Jong W. Chapter 2 - Biomass Composition, Properties, and Characterization. In: de Jong W, van Ommen R, editors. *Biomass as a Sustain. Energy Source Futur. - Fundam. Convers. Process. First*, New Jersey: Wiley; 2015, p. 36–68.
- [330] Lu D, Tabil L, Wang D, Wang G. *Manufacturing Wheat Straw Pellet with Wood Waste*

- and Binders. CSBE/SCGAB 2013 Annu. Conf., 2013, p. 1–15.
- [331] Sarkanen K V, Tillman DA, Jahn EC. Progress in Biomass Conversion: Volume 3. First Ed. Academic Press; 1982.
- [332] Greco G, Videgain M, Di Stasi C, González B, Manyà JJ. Evolution of the mass-loss rate during atmospheric and pressurized slow pyrolysis of wheat straw in a bench-scale reactor. *J Anal Appl Pyrolysis* 2018;136:18–26. <https://doi.org/10.1016/j.jaap.2018.11.007>.
- [333] Sharma RK, Wooten JB, Baliga VL, Lin X, Chan WG, Hajaligol MR. Characterization of chars from pyrolysis of lignin. *Fuel* 2004;83:1469–82. <https://doi.org/10.1016/j.fuel.2003.11.015>.
- [334] Lou K, Rajapaksha AU, Ok YS, Chang SX. Pyrolysis temperature and steam activation effects on sorption of phosphate on pine sawdust biochars in aqueous solutions. *Chem Speciat Bioavailab* 2016;28:42–50. <https://doi.org/10.1080/09542299.2016.1165080>.
- [335] Mohanty P, Nanda S, Pant KK, Naik S, Kozinski JA, Dalai AK. Evaluation of the physiochemical development of biochars obtained from pyrolysis of wheat straw, timothy grass and pinewood: Effects of heating rate. *J Anal Appl Pyrolysis* 2013;104:485–93. <https://doi.org/10.1016/j.jaap.2013.05.022>.
- [336] Chen B, Zhou D, Zhu L. Transitional adsorption and partition of nonpolar and polar aromatic contaminants by biochars of pine needles with different pyrolytic temperatures. *Environ Sci Technol* 2008;42:5137–43. <https://doi.org/10.1021/es8002684>.
- [337] Himmelsbach D, Khalili S, Akin D. The use of FT-IR microspectroscopic mapping to study the effects of enzymatic retting of flax *Linum usitatissimum* L stems. *J Sci Food Agric* 2002;82:685–96. <https://doi.org/10.1002/jsfa.1090>.
- [338] Stefanidis SD, Kalogiannis KG, Iliopoulou EF, Michailof CM, Pilavachi PA, Lappas AA. A study of lignocellulosic biomass pyrolysis via the pyrolysis of cellulose, hemicellulose and lignin. *J Anal Appl Pyrolysis* 2014;105:143–50. <https://doi.org/10.1016/j.jaap.2013.10.013>.
- [339] Hornung U, Schneider D, Hornung A, Tumiatti V, Seifert H. Sequential pyrolysis and catalytic low temperature reforming of wheat straw. *J Anal Appl Pyrolysis* 2009;85:145–50. <https://doi.org/10.1016/j.jaap.2008.11.006>.
- [340] Collard FX, Blin J. A review on pyrolysis of biomass constituents: Mechanisms and composition of the products obtained from the conversion of cellulose, hemicelluloses and lignin. *Renew Sustain Energy Rev* 2014;38:594–608. <https://doi.org/10.1016/j.rser.2014.06.013>.
- [341] Júnior AFD, Pirola LP, Takeshita S, Lana AQ, Brito JO, de Andrade AM. Hygroscopicity of charcoal produced in different temperatures. *Cerne* 2016;22:423–30.

- <https://doi.org/10.1590/01047760201622032175>.
- [342] Xie T. Characterization of biochar and its application in yellow water treatment. Tsinghua University, 2015.
- [343] Sohi S, Lopez-Capel E, Krull E, Bol R. Biochar's roles in soil and climate change: A review of research needs. 2009.
- [344] Jindo K, Mizumoto H, Sawada Y, Sonoki T. Physical and chemical characterization of biochars derived from different agricultural residues. *Biogeosciences* 2014;6613–21. <https://doi.org/10.5194/bg-11-6613-2014>.
- [345] Crombie K, Mašek O, Sohi SP, Brownsort P, Cross A. The effect of pyrolysis conditions on biochar stability as determined by three methods. *GCB Bioenergy* 2013;5:122–31. <https://doi.org/10.1111/gcbb.12030>.
- [346] Tan P, Zhang C, Xia J, Fang Q, Chen G. Estimation of higher heating value of coal based on proximate analysis using support vector regression. *Fuel Process Technol* 2015;138:298–304. <https://doi.org/10.1016/j.fuproc.2015.06.013>.
- [347] Park J, Lee Y, Ryu C, Park YK. Slow pyrolysis of rice straw: Analysis of products properties, carbon and energy yields. *Bioresour Technol* 2014;155:63–70. <https://doi.org/10.1016/j.biortech.2013.12.084>.
- [348] Wang Y, Liu R. Comparison of characteristics of twenty-one types of biochar and their ability to remove multi-heavy metals and methylene blue in solution. *Fuel Process Technol* 2017;160:55–63. <https://doi.org/10.1016/j.fuproc.2017.02.019>.
- [349] Nanda S, Mohanty P, Pant KK, Naik S, Kozinski JA, Dalai AK. Characterization of North American Lignocellulosic Biomass and Biochars in Terms of their Candidacy for Alternate Renewable Fuels. *Bioenergy Res* 2013;6:663–77. <https://doi.org/10.1007/s12155-012-9281-4>.
- [350] Li X, Shen Q, Zhang D, Mei X, Ran W, Xu Y, et al. Functional Groups Determine Biochar Properties (pH and EC) as Studied by Two-Dimensional ¹³C NMR Correlation Spectroscopy. *PLoS One* 2013;8. <https://doi.org/10.1371/journal.pone.0065949>.
- [351] Zhu X, Liu Y, Zhou C, Luo G, Zhang S, Chen J. A novel porous carbon derived from hydrothermal carbon for efficient adsorption of tetracycline. *Carbon N Y* 2014;77:627–36. <https://doi.org/10.1016/j.carbon.2014.05.067>.
- [352] Tag AT, Duman G, Ucar S, Yanik J. Effects of feedstock type and pyrolysis temperature on potential applications of biochar. *J Anal Appl Pyrolysis* 2016;120:200–6. <https://doi.org/10.1016/j.jaap.2016.05.006>.
- [353] Fu P, Yi W, Bai X, Li Z, Hu S, Xiang J. Effect of temperature on gas composition and char structural features of pyrolyzed agricultural residues. *Bioresour Technol* 2011;102:8211–9. <https://doi.org/10.1016/j.biortech.2011.05.083>.
- [354] Li H, Dong X, da Silva EB, de Oliveira LM, Chen Y, Ma LQ. Mechanisms of metal

- sorption by biochars: Biochar characteristics and modifications. *Chemosphere* 2017;178:466–78. <https://doi.org/10.1016/j.chemosphere.2017.03.072>.
- [355] Sun J, Lian F, Liu Z, Zhu L, Song Z. Biochars derived from various crop straws: Characterization and Cd(II) removal potential. *Ecotoxicol Environ Saf* 2014;106:226–31. <https://doi.org/10.1016/J.ECOENV.2014.04.042>.
- [356] Budai A, Wang L, Gronli M, Strand LT, Antal MJ, Abiven S, et al. Surface properties and chemical composition of corncob and miscanthus biochars: Effects of production temperature and method. *J Agric Food Chem* 2014;62:3791–9. <https://doi.org/10.1021/jf501139f>.
- [357] Ippolito JA, Cui L, Johnson MG. Biochar for Mine-land Reclamation. *Biochar from Biomass Waste* 2019:75–90. <https://doi.org/10.1016/B978-0-12-811729-3.00005-4>.
- [358] Zhang X, Wang H, He L, Lu K, Sarmah A, Li J, et al. Using biochar for remediation of soils contaminated with heavy metals and organic pollutants. *Environ Sci Pollut Res Int* 2013;20:8472–83. <https://doi.org/10.1007/s11356-013-1659-0>.
- [359] Savova D, Apak E, Ekinici E, Yardim F, Petrov N, Budinova T, et al. Biomass conversion to carbon adsorbents and gas. *Biomass and Bioenergy* 2001;21:133–42. [https://doi.org/10.1016/S0961-9534\(01\)00027-7](https://doi.org/10.1016/S0961-9534(01)00027-7).
- [360] Thommes M, Kaneko K, Neimark A V., Olivier JP, Rodriguez-Reinoso F, Rouquerol J, et al. Physisorption of gases, with special reference to the evaluation of surface area and pore size distribution (IUPAC Technical Report). *Pure Appl Chem* 2015;87:1051–69. <https://doi.org/10.1515/pac-2014-1117>.
- [361] Sing K, Everett DH., Haul R, Moscou L, Pierotti R, Rouquerol J, et al. Reporting physisorption data for gas/solid systems with Special Reference to the Determination of Surface Area and Porosity. *Pure Appl Chem* 1985;57:603–19.
- [362] Barr MR, Jervis R, Zhang Y, Bodey AJ, Rau C, Shearing PR, et al. Towards a mechanistic understanding of particle shrinkage during biomass pyrolysis via synchrotron X-ray microtomography and in-situ radiography. *Sci Rep* 2021;11:2656. <https://doi.org/10.1038/s41598-020-80228-x>.
- [363] Tomczyk A, Sokołowska Z, Boguta P. Biochar physicochemical properties: pyrolysis temperature and feedstock kind effects. *Rev Environ Sci Biotechnol* 2020;19:191–215. <https://doi.org/10.1007/s11157-020-09523-3>.
- [364] Hwang H, Sahin O, Choi JW. Manufacturing a super-active carbon using fast pyrolysis char from biomass and correlation study on structural features and phenol adsorption. *RSC Adv* 2017;7:42192–202. <https://doi.org/10.1039/c7ra06910c>.
- [365] del Pozo C, Rego F, Yang Y, Puy N, Bartrolí J, Fàbregas E, et al. Converting coffee silverskin to value-added products by a slow pyrolysis-based biorefinery process. *Fuel Process Technol* 2021;214. <https://doi.org/10.1016/j.fuproc.2020.106708>.

- [366] Plaza MG, Pevida C, Martín CF, Feroso J, Pis JJ, Rubiera F. Developing almond shell-derived activated carbons as CO₂ adsorbents. *Sep Purif Technol* 2010;71:102–6. <https://doi.org/10.1016/J.SEPPUR.2009.11.008>.
- [367] Gellerstedt G, Sjöholm E, Brodin I. The Wood-Based Biorefinery : A Source of Carbon Fiber? *Open Agric J* 2010;3:119–24.
- [368] Ruiz JA, Juárez MC, Morales MP, Muñoz P, Mendivil MA. Biomass gasification for electricity generation: Review of current technology barriers. *Renew Sustain Energy Rev* 2013;18:174–83. <https://doi.org/https://doi.org/10.1016/j.rser.2012.10.021>.
- [369] Morf P, Hasler P, Nussbaumer T. Mechanisms and kinetics of homogeneous secondary reactions of tar from continuous pyrolysis of wood chips. *Fuel* 2002;81:843–53. [https://doi.org/10.1016/S0016-2361\(01\)00216-2](https://doi.org/10.1016/S0016-2361(01)00216-2).
- [370] Zhang H, Xiao R, Wang D, He G, Shao S, Zhang J, et al. Biomass fast pyrolysis in a fluidized bed reactor under N₂, CO₂, CO, CH₄ and H₂ atmospheres. *Bioresour Technol* 2011;102:4258–64. <https://doi.org/10.1016/j.biortech.2010.12.075>.
- [371] Cho DW, Cho SH, Song H, Kwon EE. Carbon dioxide assisted sustainability enhancement of pyrolysis of waste biomass: A case study with spent coffee ground. *Bioresour Technol* 2015;189:1–6. <https://doi.org/10.1016/j.biortech.2015.04.002>.
- [372] Duan L, Zhao C, Zhou W, Qu C, Chen X. Investigation on coal pyrolysis in CO₂ atmosphere. *Energy and Fuels* 2009;23:3826–30. <https://doi.org/10.1021/ef9002473>.
- [373] Jindarom C, Meeyoo V, Rirksomboon T, Rangsunvigit P. Thermochemical decomposition of sewage sludge in CO₂ and N₂ atmosphere. *Chemosphere* 2007;67:1477–84. <https://doi.org/10.1016/j.chemosphere.2006.12.066>.
- [374] Lee J, Oh JI, Ok YS, Kwon EE. Study on susceptibility of CO₂-assisted pyrolysis of various biomass to CO₂. *Energy* 2017;137:510–7. <https://doi.org/10.1016/j.energy.2017.01.155>.
- [375] Yang M, Luo B, Shao J, Zeng K, Zhang X, Yang H, et al. The influence of CO₂ on biomass fast pyrolysis at medium temperatures. *J Renew Sustain Energy* 2018;10. <https://doi.org/10.1063/1.5005013>.
- [376] Biswas B, Singh R, Kumar J, Singh R, Gupta P, Krishna BB, et al. Pyrolysis behavior of rice straw under carbon dioxide for production of bio-oil. *Renew Energy* 2018;129:686–94. <https://doi.org/10.1016/j.renene.2017.04.048>.
- [377] Linares-Solano A, De D. López-González J, Molina-Sabio M, Rodríguez-Reinoso F. Active carbons from almond shells as adsorbents in gas and liquid phases. *J Chem Technol Biotechnol* 1980;30:65–72. <https://doi.org/https://doi.org/10.1002/jctb.503300109>.
- [378] Yang K, Peng J, Xia H, Zhang L, Srinivasakannan C, Guo S. Textural characteristics of activated carbon by single step CO₂ activation from coconut shells. *J Taiwan Inst Chem*

- Eng 2010;41:367–72. <https://doi.org/10.1016/j.jtice.2009.09.004>.
- [379] Hui TS, Zaini MAA. Potassium hydroxide activation of activated carbon: A commentary. *Carbon Lett* 2015;16:275–80. <https://doi.org/10.5714/CL.2015.16.4.275>.
- [380] Seward RP, Martin KE. The Melting Point of Potassium Hydroxide. *J Am Chem Soc* 1949;71:3564–5. <https://doi.org/10.1021/ja01178a530>.
- [381] Lide D. Physical Constants of Inorganic Compounds (in Section 4). In: Lide D, editor. *CRC Handb. Chem. Phys.* 88th Editi, CRC Press; 2007. <https://doi.org/10.7788/boehlau.9783412301989.abbr>.
- [382] Ltd. W. WebElements n.d. <https://www.webelements.com> (accessed May 31, 2021).
- [383] Greenwood N, Earnshaw A. *Chemistry of the Elements*. Butterworth-Heinemann; 1997.
- [384] Heidarinejad Z, Dehghani MH, Heidari M, Javedan G, Ali I, Sillanpää M. Methods for preparation and activation of activated carbon: a review. *Environ Chem Lett* 2020;18:393–415. <https://doi.org/10.1007/s10311-019-00955-0>.
- [385] Pereira L, Alves M. Dyes-environmental impact and remediation. In: Malik A, Grohmann E, editors. *Environ. Prot. Strateg. Sustain. Dev.*, Springer; 2012, p. 111–62. https://doi.org/10.1007/978-94-007-1591-2_4.
- [386] Arias M, López E, Nuñez A, Rubinos D, Soto B, Barral MT, et al. Adsorption of Methylene Blue by Red Mud, An Oxide- Rich Byproduct of Bauxite Refining. In: Berthelin J, Huang P, Bollag J, Andreux F, editors. *Eff. Miner. Interact. Soil Freshw. Environ.*, Springer; 1999, p. 361–5. https://doi.org/10.1007/978-1-4615-4683-2_39.
- [387] Minkova V, Marinov SP, Zanzi R, Björnbom E, Budinova T, Stefanova M, et al. Thermochemical treatment of biomass in a flow of steam or in a mixture of steam and carbon dioxide. *Fuel Process Technol* 2000;62:45–52. [https://doi.org/10.1016/S0378-3820\(99\)00065-X](https://doi.org/10.1016/S0378-3820(99)00065-X).
- [388] Dai Y, Wang W, Lu L, Yan L, Yu D. Utilization of biochar for the removal of nitrogen and phosphorus. *J Clean Prod* 2020;257. <https://doi.org/10.1016/j.jclepro.2020.120573>.
- [389] Zhou H lei, Zhen W juan, Zhu Q, Wu X bin, Chang Z dong, Li W jun. Role of the surface chemistry of activated carbons in dye removal from aqueous solution. *Int J Miner Metall Mater* 2015;22:770–6. <https://doi.org/10.1007/s12613-015-1133-8>.
- [390] Raveendran K, Ganesh A. Adsorption characteristics and pore-development of biomass-pyrolysis char. *Fuel* 1998;77:769–81. [https://doi.org/10.1016/S0016-2361\(97\)00246-9](https://doi.org/10.1016/S0016-2361(97)00246-9).
- [391] Kymäläinen M, Havimo M, Keriö S, Kemell M, Solio J. Biological degradation of torrefied wood and charcoal. *Biomass and Bioenergy* 2014;71:170–7. <https://doi.org/https://doi.org/10.1016/j.biombioe.2014.10.009>.
- [392] Mendonça FG de, Cunha IT da, Soares RR, Tristão JC, Lago RM. Tuning the surface properties of biochar by thermal treatment. *Bioresour Technol* 2017;246:28–33.

- <https://doi.org/10.1016/j.biortech.2017.07.099>.
- [393] Franciski MA, Peres EC, Godinho M, Perondi D, Foletto EL, Collazzo GC, et al. Development of CO₂ activated biochar from solid wastes of a beer industry and its application for methylene blue adsorption. *Waste Manag* 2018;78:630–8. <https://doi.org/10.1016/j.wasman.2018.06.040>.
- [394] Kuang Y, Zhang X, Zhou S. Adsorption of methylene blue in water onto activated carbon by surfactant modification. *Water (Switzerland)* 2020;12:1–19. <https://doi.org/10.3390/w12020587>.
- [395] Vukčević MM, Kalijadis AM, Vasiljević TM, Babić BM, Laušević Z V., Laušević MD. Production of activated carbon derived from waste hemp (*Cannabis sativa*) fibers and its performance in pesticide adsorption. *Microporous Mesoporous Mater* 2015;214:156–65. <https://doi.org/10.1016/j.micromeso.2015.05.012>.
- [396] Xie J, Lin R, Liang Z, Zhao Z, Yang C, Cui F. Effect of cations on the enhanced adsorption of cationic dye in Fe₃O₄-loaded biochar and mechanism. *J Environ Chem Eng* 2021;105744. <https://doi.org/10.1016/j.jece.2021.105744>.
- [397] Khraisheh MAM, Al-Degs YS, Allen SJ, Ahmad MN. Elucidation of controlling steps of reactive dye adsorption on activated carbon. *Ind Eng Chem Res* 2002;41:1651–7. <https://doi.org/10.1021/ie000942c>.
- [398] Faria PCC, Órfão JJM, Pereira MFR. Adsorption of anionic and cationic dyes on activated carbons with different surface chemistries. *Water Res* 2004;38:2043–52. <https://doi.org/10.1016/j.watres.2004.01.034>.
- [399] Pereira MFR, Soares SF, Órfão JJM, Figueiredo JL. Adsorption of dyes on activated carbons: Influence of surface chemical groups. *Carbon N Y* 2003;41:811–21. [https://doi.org/10.1016/S0008-6223\(02\)00406-2](https://doi.org/10.1016/S0008-6223(02)00406-2).
- [400] Zhang C, He C, Qiao Y. Lower-Temperature Pyrolysis to Prepare Biochar from Agricultural Wastes and Adsorption for Pb²⁺. *BioResources* 2018;13:5543–53.
- [401] Nyamunda BC, Chivhanga T, Guyo U, Chigondo F. Removal of Zn (II) and Cu (II) Ions from Industrial Wastewaters Using Magnetic Biochar Derived from Water Hyacinth. *J Eng (United Kingdom)* 2019;2019. <https://doi.org/10.1155/2019/5656983>.
- [402] Liu WJ, Zeng FX, Jiang H, Zhang XS. Preparation of high adsorption capacity bio-chars from waste biomass. *Bioresour Technol* 2011;102:8247–52. <https://doi.org/10.1016/j.biortech.2011.06.014>.
- [403] Zhao L, Xiao D, Liu Y, Xu H, Nan H, Li D, et al. Biochar as simultaneous shelter, adsorbent, pH buffer, and substrate of *Pseudomonas citronellolis* to promote biodegradation of high concentrations of phenol in wastewater. *Water Res* 2020;172:115494. <https://doi.org/10.1016/j.watres.2020.115494>.
- [404] Wurzer C, Mašek O. Feedstock doping using iron rich waste increases the pyrolysis

- gas yield and adsorption performance of magnetic biochar for emerging contaminants. *Bioresour Technol* 2021;321. <https://doi.org/10.1016/j.biortech.2020.124473>.
- [405] Alghamdi AA, Al-Odayni A-B, Abduh NAY, Alramadhan SA, Aljboar MT, Saeed WS. Adsorptive Performance of Polypyrrole-Based KOH-Activated Carbon for the Cationic Dye Crystal Violet: Kinetic and Equilibrium Studies. *Adsorpt Sci & Technol* 2021;2021:5527594. <https://doi.org/10.1155/2021/5527594>.
- [406] Simonin JP. On the comparison of pseudo-first order and pseudo-second order rate laws in the modeling of adsorption kinetics. *Chem Eng J* 2016;300:254–63. <https://doi.org/10.1016/j.cej.2016.04.079>.
- [407] Liu L, Li Y, Fan S. Preparation of KOH and H₃PO₄ modified biochar and its application in methylene blue removal from aqueous solution. *Processes* 2019;7. <https://doi.org/10.3390/PR7120891>.
- [408] Hou J, Hou J, Liu Y, Wen S, Li W, Liao R, et al. Sorghum-Waste-Derived High-Surface Area KOH-Activated Porous Carbon for Highly Efficient Methylene Blue and Pb(II) Removal. *ACS Omega* 2020;5:13548–56. <https://doi.org/10.1021/acsomega.9b04452>.
- [409] Stephens DL, McFadden T, Heath OD, Mauldin RF. The effect of sonication on the recovery of polycyclic aromatic hydrocarbons from coal stack ash surfaces. *Chemosphere* 1994;28:1741–7. [https://doi.org/https://doi.org/10.1016/0045-6535\(94\)90022-1](https://doi.org/https://doi.org/10.1016/0045-6535(94)90022-1).
- [410] Martínez-Parreño M, Llorca-Pórcel J, Valor I. Analysis of 51 persistent organic pollutants in soil by means of ultrasonic solvent extraction and stir bar sorptive extraction GC-MS. *J Sep Sci* 2008;31:3620–9. <https://doi.org/10.1002/jssc.200800355>.

Appendices

Appendix A – Properties of gaseous species

Table A.1 presents values of molecular weight, density and high heating value (HHV) for individual gaseous species (normal temperature and pressure conditions (20 °C and 1 atm) [1]. Density values were used to obtain gas yield based on the MicroGC results (description in Chapter 3, subsection 3.2.2), and to characterise the gas product, along with molecular weight and HHV.

Table A.1: Molecular weight, density and high heating value of individual gaseous species at normal temperature and pressure conditions (20 °C and 1 atm) [1].

	Density (g/cm ³)	Molecular weight (g/mol)	High heating value (MJ/Nm ³)
CO ₂	1.842	44.010	a)
CO	1.165	28.011	11.6
CH ₄	0.668	16.043	36.4
C ₂ H ₆	1.264	30.070	63.8
C ₂ H ₄	1.260	28.054	57.7
C ₃ H ₁₀	1.882	44.097	90.8
C ₃ H ₈	1.748	42.080	84.2
H ₂	0.0899	2.016	11.7

a) CO₂ is a non-combustible gas.

Appendix B – Screw reactor operation

As described in Chapter 3, some operational parameters were determined prior to performing the slow pyrolysis experiments (in non-heating conditions), such as feeding rate and solid residence time of the wheat straw feedstock. Another operational parameter was vapour residence time, which can be estimated during or after pyrolysis experiments, visually or by calculation.

B.1. Feeding rate

The appropriate feeding rate was determined from the amount which could be fed into the reactor without causing blockages in the inlet tube, and which at the same time allowed material to enter continuously into the reactor tube itself. Feeding is done manually by opening the inlet tube valve and inserting a certain amount of feedstock, with the weight measured in a tared beaker.

For the wheat straw used for the slow pyrolysis experiments, the maximum rate of feeding was determined to be ≈ 10 g every 2 minutes, which corresponds to a feeding rate of 300 g/h. This feeding rate was maintained for both screw reactors used in this work.

B.2. Solid residence time

To determine solid residence time (SRT), portions of feedstock were fed into the system (cold run), and collected into a container on the outlet side, while the screw is operating at a certain speed. The time it takes for the portion to reach the container can be an estimate of SRT. Another way of measuring SRT is by measuring the time it takes for a section of the screw to traverse a certain distance (screw speed), visually, even without the need to feed material.

For the latter method (visual determination of screw speed), the movement of the screw is observed through the opening of the inlet tube and it is possible to time how long it takes for a turn in the screw to traverse the distance corresponding to that opening. The total time inside the reactor tube is then calculated proportionally, knowing the (inner) diameter of the opening and the length of the heated section of the reactor tube through which the material is transported. Although the furnace only covers ≈ 40.0 cm of the reactor tube, it is assumed that the whole tube (≈ 61.0 cm, see Chapter 3) is heated to at least 300 °C, which is considered an adequate temperature for which there is considerable degradation of the lignocellulosic compounds of the feedstock. This assumption is based on a study on the pyrolysis of individual lignocellulosic compounds, which found that hemicellulose has its main weight loss between 220 and 315 °C, and cellulose has a maximum degradation rate at ≈ 355 °C [2]. This method of determining SRT assumes that the fed material continuously moves with the screw, at the

same rate, without any disturbance (similarly to plug flow). This assumption does not provide an accurate representation of the movement of solid material inside the screw, which varies due to the different particle sizes and shapes, feeding rate, interactions between particles, and other factors. The residence time determined by this method can, however, give a good approximation of the minimum time it takes for the material to be transported through the reactor tube.

The first motor used for the first screw reactor described in Chapter 3 had 10 levels for speed selection, however, only 6 of them were tested due to concerns of motor overheating and system integrity due to the vibration caused by the motor running. Furthermore, very high screw speed (smaller SRT) was not desired, because of the risk of not having enough time for carbonisation to occur. For the first screw reactor, the SRT corresponding to each level of the motor was determined for the wheat straw as-received feedstock with both above-described methods, and the values are indicated in Table B.1.

Table B.1: Values of solid residence time for the first screw reactor based on screw speed and on cold runs with wheat straw feedstock.

Level	SRT from screw speed (min)	SRT from cold runs (min)
1	5.4	5.6
2	4.4	4.6
3	3.8	3.8
4	3.4	3.5
5	3.2	3.5
6	3.0	3.0

The results showed that the two employed methods do not yield significant differences between themselves, and that for higher motor levels the difference in SRT between levels gets more and more reduced. Furthermore, although six motor levels were tested, the impact on SRT was not as significant as expected, since it was only between 3 to 6 minutes. Higher SRT values were desired for the study of the impact of this parameter on the slow pyrolysis process, and so additional levels between level 0 and level 1 were tested, that were marked manually on the level selection dial: levels 0.5 and 0.25. Using the visual screw speed method, without material being fed, the SRT obtained was 7.2 and 9.4 minutes, respectively, for level 0.5 and level 0.25. By doing cold runs with the wheat straw feedstock, the resulting SRT was ≈ 7.1 and ≈ 10.0 minutes for levels 0.5 and 0.25, respectively. From these results, the selected SRT values to be used for the slow pyrolysis experiments were 3, 6 and 10 minutes, as represented in Table B.2.

Table B.2: Selected solid residence times used for the slow pyrolysis experiments with wheat straw feedstock in the first screw reactor.

Level	SRT from screw speed (min)	SRT from cold runs (min)	SRT value (min)
0.25	9.4	10.0	10
1	5.4	5.6	6
6	3.0	3.0	3

The SRT values mentioned in this work are rounded-up to the nearest unit based on the estimated SRT values from the cold runs, which are more realistic than the ones calculated with the visual screw speed method.

Tests performed under cold conditions with feedstock with reduced particle size (after soaking and drying) resulted in ≈ 4.3 min SRT for motor level 1, which corroborated what was mentioned in Chapter 3 regarding the effect of feedstock moisture content and particle size on SRT (subsection 3.2.2): the reduced particle size caused by soaking counteracts the likely increase in SRT caused by an elevated feedstock moisture content. A cold test with wet particles was not performed to avoid leaving unreacted biomass inside the reactor.

After some months, due to a malfunction, the motor for the screw reactor had to be replaced with a new one. The new motor did not have levels on the selector dial and was calibrated based on the first motor and using the methods described above. It was found that it was no longer possible to have a SRT inferior to 5 minutes, so only values of SRT of 6 and 10 minutes were used from then on for the slow pyrolysis experiments. The calibration consisted in determining the dial positions corresponding to 6 and 10 minutes SRT.

For the second screw reactor system (described in subsection 3.2.1.2), the respective motor had 10 positions in the speed selection dial, and cold tests were performed with the wheat straw feedstock to determine which positions corresponded to which SRT. For the SRT calculation with the screw speed (visual) method, 61.0 cm was the length used (same as for the first reactor). The results of SRT estimation based on screw speed and cold runs for the second screw reactor are presented in Table B.3. The slow pyrolysis experiments performed with the second screw reactor only required using a SRT of 10 minutes, which corresponded to level 2.

Table B.3: Values of solid residence time for the second screw reactor based on screw speed and on cold runs with wheat straw feedstock.

Level	SRT from screw speed (min)	SRT from cold runs (min)
1	15.3	16.7
2	10.0	10.7
3	7.4	7.9
5	4.9	5.3
8	3.1	3.4

B.3. Vapour residence time

A preliminary estimation of the vapour residence time (VRT) can be done by using the free space volume in the reactor (calculated in Chapter 3, subsection 3.2.2.) and by assuming a gas flow rate, as explained in Chapter 3. Assuming different gas flow rates it is possible to calculate the corresponding VRT by dividing by the free space volume. Some examples of VRT estimation for the first screw reactor are indicated in Table B.4.

Table B.4: VRT estimation for the first screw reactor for different assumed gas flow rates.

Gas flow rate (L/min)	VRT (min)	VRT (s)
0.1	2.6	158
0.2	1.3	79
0.5	0.5	32
1.0	0.3	16
2.0	0.1	8
3.0	0.1	5

VRT values decrease when gas flow rate increases, which was because the more vapours the pyrolysis process produces, the faster they come out of the reactor, which remains the same. The VRT value is considerably sensitive to changes in the gas flow rate: a doubling of the gas flow rate from 0.1 to 0.2 causes the VRT to drop from 2.6 to 1.3 minutes. This sensitivity occurs mainly for low gas flow rates, with asymptotic behaviour of VRT in function of the gas flow rate, towards an infinite value (for increasingly lower flow rates) or zero (for increasingly higher flow rates). If higher gas flow rates are employed, VRT becomes more similar to the typical VRT in fast pyrolysis (e.g., in a fluidised bed), which is at most 2 seconds [3]. These calculations were not performed for the second screw reactor due to not having an estimation of the screw volume.

Once a slow pyrolysis experiment had been performed and the volume of produced gas was known, it was possible to obtain a gas flow rate by dividing the gas volume by the experiment duration. The results from this method are presented in the corresponding sections for each experimental set in Chapter 4. Another way of estimating VRT was by visually

checking the time at which the first vapours appeared in the reactor outlet at the start of a slow pyrolysis experiment. The results are also presented in each experimental subsection. Changes in the gas meter can also be used for the VRT estimation, and are considered more reliable than the former methods, since some gases from pyrolysis are not visible. However, the gas meter is not monitored all the time and so this option was not available for this work.

Appendix C – Char properties

C.1 – FTIR spectra for chars produced with varying slow pyrolysis temperature and SRT

Figure C.1 presents the full FTIR spectra for chars produced with varying slow pyrolysis temperature in the first screw reactor (10 minutes SRT), along with the feedstock spectrum. FTIR spectra for chars produced with different SRT due to relatively small differences between them. In Chapter 4 (subsection 4.4.3), these spectra were shown, however, only for the wavenumber range of 2000-400 cm^{-1} , due to there being very little IR manifestation in the range 4000-2000 cm^{-1} in the case of chars.

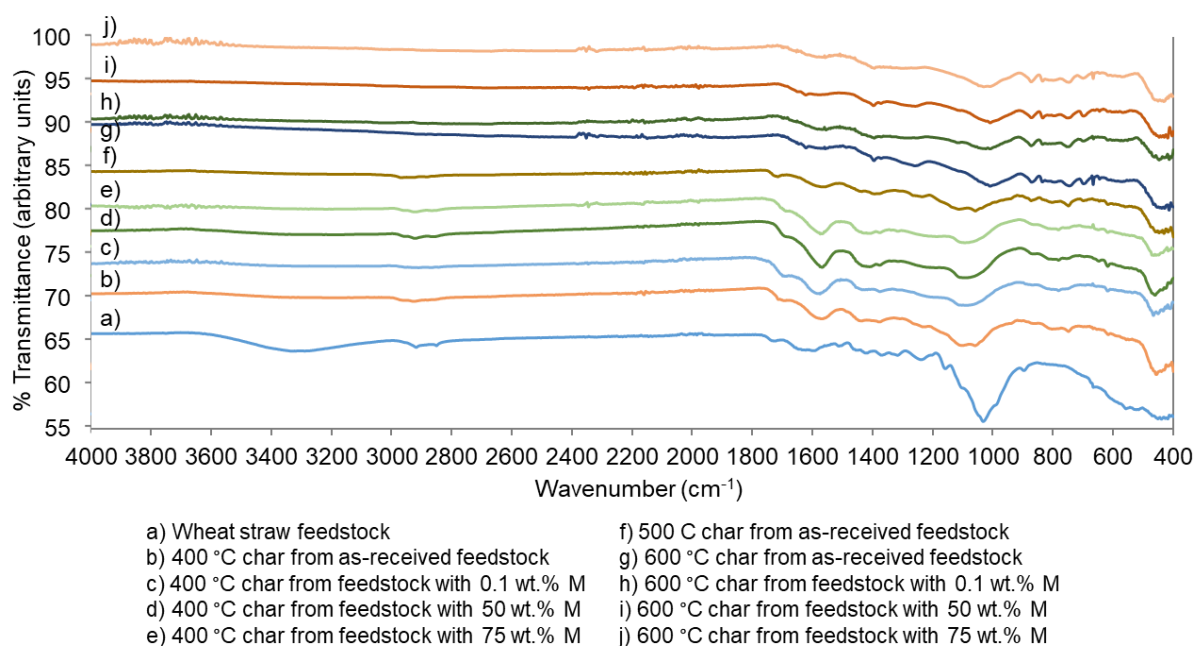


Figure C.1: FTIR spectra for the wheat straw feedstock and chars produced from slow pyrolysis with 10 minutes SRT and varying temperature and feedstock moisture content.

C.2 – N_2 physisorption (77 K) isotherms and pore size distribution for chars produced with varying slow pyrolysis temperature, SRT, and feedstock moisture content

Figure C.2 presents the isotherms for chars produced with varying slow pyrolysis temperature and SRT. In Chapter 4 (subsection 4.4.5), only one example was shown, due to the high similarity between graphs. Figure C.3 presents the pore size distribution (PSD) graphs for chars produced with varying slow pyrolysis SRT. In Chapter 4 (subsection 4.4.5), one example was shown due to the high similarity between graphs.

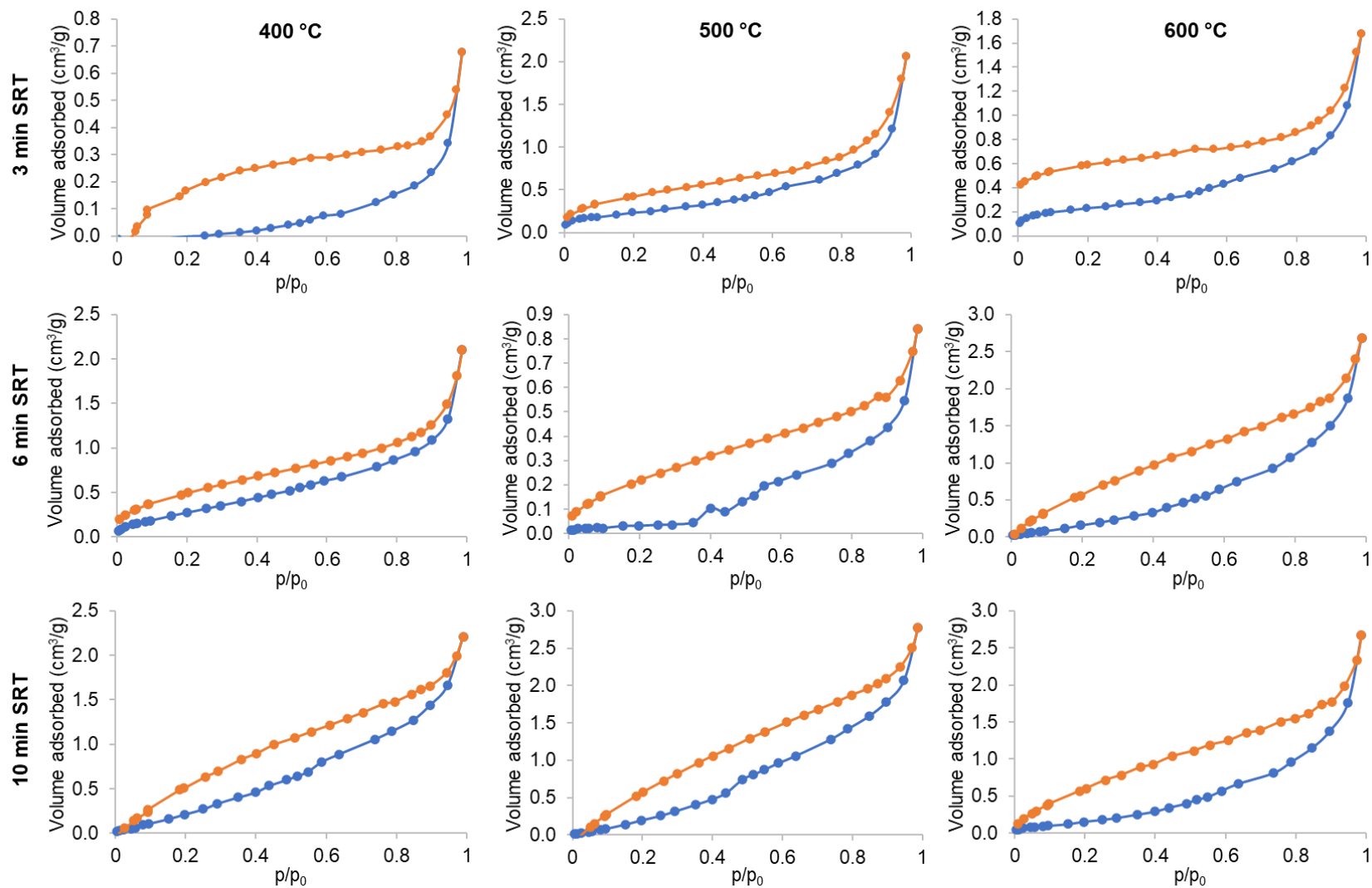


Figure C.2: N₂ adsorption-desorption isotherm for chars produced from as-received feedstock at 400, 500, and 600 °C, and 3, 6 and 10 min SRT.

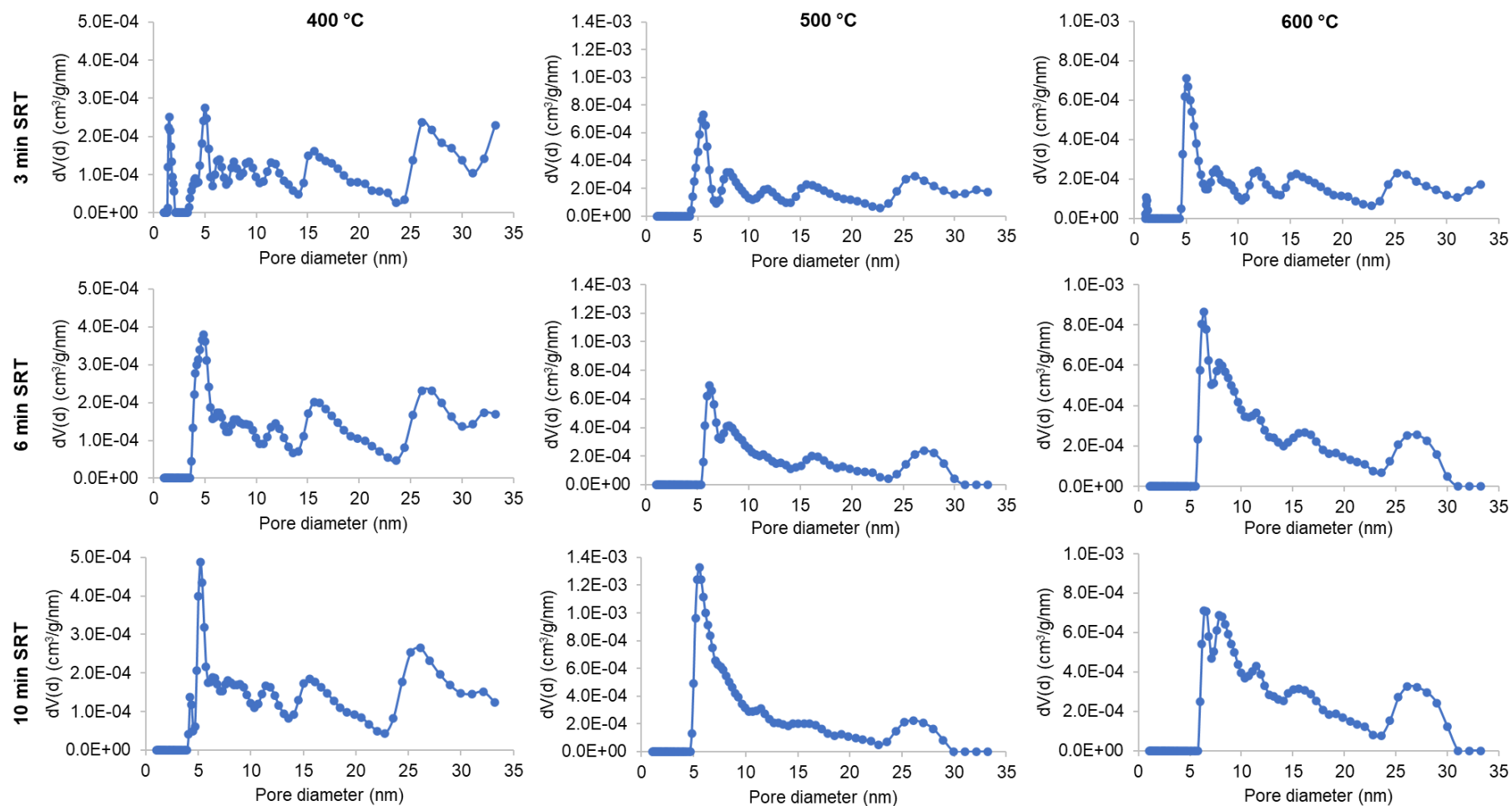


Figure C.3: Pore size distribution (QS-DFT applied on N_2 adsorption branch) for chars produced from as-received feedstock at 400, 500, and 600 °C, and 3, 6 and 10 min SRT.

C.3 – N₂ physisorption (77 K) isotherms and pore size distribution for chars produced without injected gas in the second screw reactor

Figure C.4 presents the isotherms and pore size distribution (PSD) graphs for chars produced without injected gas in the second screw reactor. In Chapter 5 (subsection 5.3.5), the graphs for chars produced with CO₂ and N₂ as injected gases (separately) were shown with these ones not being shown due to the similarity between all graphs.

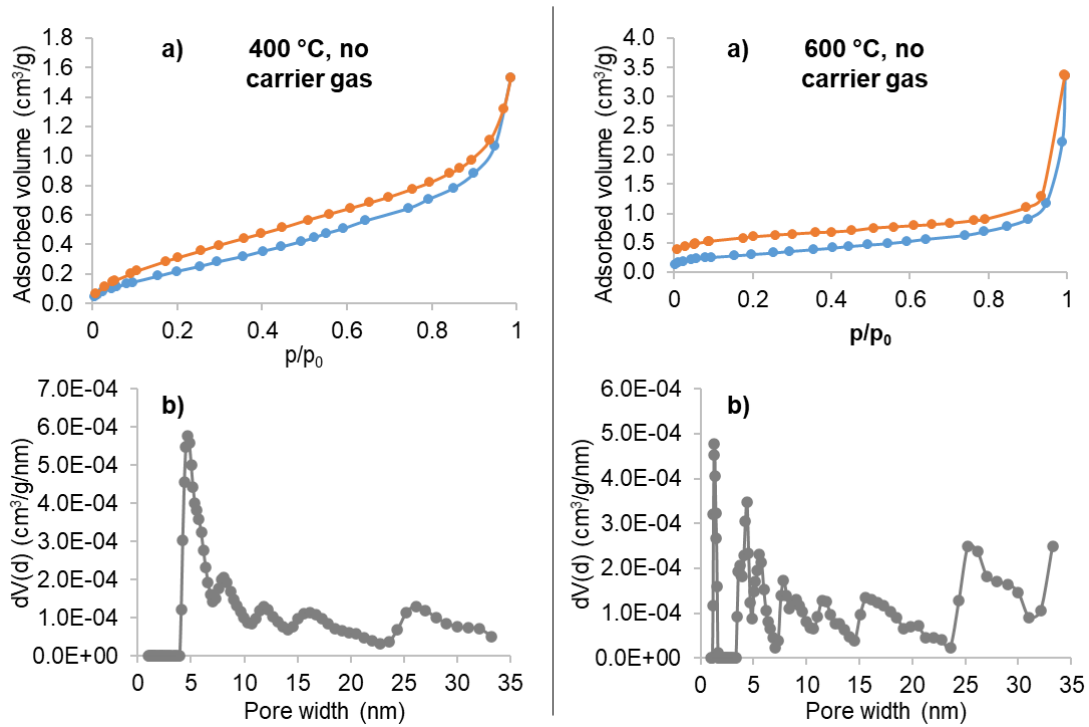


Figure C.4: N₂ adsorption-desorption isotherms (a), and pore size distribution (QS-DFT applied on adsorption branch) (b), for chars produced from as-received feedstock at 400 °C (left-hand side) and 600 °C (right-hand side) without injected gas.

Appendix D – Liquid product analyses

D.1. Liquid products from varying slow pyrolysis temperature and solid residence time

D.1.1. Physical aspects

When a pyrolysis experiment was taking place, it was possible to visualise liquid product being condensed and collected. At least two different phases were seen in the produced liquids, a clearer phase (orange/yellow-ish), and a darker-coloured phase (brown). The clearer phase was mainly comprised of water and water-soluble compounds and was considered the aqueous phase. The darker-coloured phase was composed by heavier oil-based organic compounds and was considered the organic phase. The aqueous phase in each experiment was produced in larger quantities than the organic phase. The higher viscosity of the organic phase caused part of it to become trapped in the first cold spot (water-cooled condenser). The first collection flask was where most ($\geq 90\%$) of the pyrolysis liquid product was collected (both aqueous and organic phases). The aqueous phase was commonly on top of the organic phase, meaning the organic phase was of higher density. The organic phase, besides sitting on the bottom of the collection flask, also got stuck to the flask walls, and parts of it were also found on the surface of the aqueous phase, which occurred due to phase immiscibility and density differences.

For some of the experiments, with time, the appearance of the pyrolysis liquids in the first collection flask changed slightly, mainly, the aqueous phase became darker (more brownish). This was a consequence of contact with the organic phase and aging, that occurs for pyrolysis liquids that are stored for long periods of time, which can cause changes in water content and viscosity of the liquid product [4][5].

The liquids produced from slow pyrolysis experiments possessed a strong odour resembling vinegar due to organic volatiles (e.g., aldehydes). This characteristic has been reported in literature, and the odour is indicated to be non-toxic [6].

Comparing between experiments, with increasing pyrolysis temperatures, the colour of the liquid, especially the aqueous phases, got slightly lighter. In contrast, the colour of the vapours coming from the reactor outlet during pyrolysis were darker for higher pyrolysis temperatures. The particles trapped on the cotton filter also got darker with increasing pyrolysis temperatures. The darker vapours and particles are probably due to a higher production of heavier compounds (e.g., naphthalene) and to the possible transport of solid particles (i.e., char) with the vapours produced in the reactor, which have a higher flow rate at higher temperatures. The lighter colour of the liquids from experiments at higher temperatures are probably due to a higher water content,

produced from fragmentation, dehydration, and other reactions that are favoured by higher temperatures [7]. The different SRT employed in experiments with as-received feedstock did not produce noticeable visual differences between phases.

After collection and finishing each experiment, the liquid products were stored in glass flasks in a fridge at ≈ 4 °C. The aqueous phase from each liquid product was decanted and transferred to a different flask and stored separately from the organic phase. Figure D.1 shows flasks with pyrolysis liquids produced from as-received wheat straw at different pyrolysis temperatures (6 minutes SRT). The top flasks contain aqueous phases, while the bottom flasks contain organic phases. The two flasks on the left correspond to experiments using pyrolysis temperature of 500 °C, while the two flasks on the right have pyrolysis liquids produced at 600 °C.

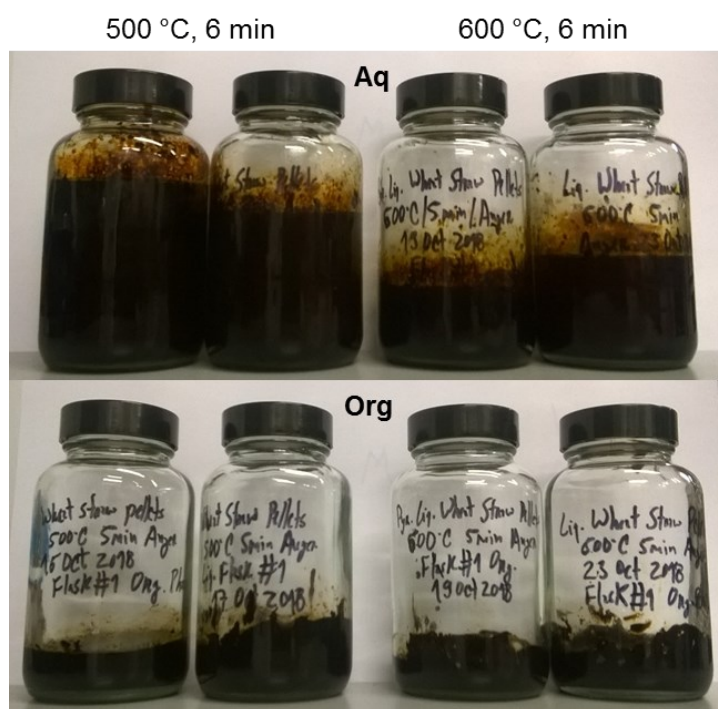


Figure D.1: Pyrolysis liquids produced from wheat straw at temperatures of 500 and 600 °C and 6 minutes SRT (top: aqueous phases; bottom: organic phases).

The greater proportion of produced aqueous phase compared to organic phase can be verified, as well as the dark colour that was characteristic from the pyrolysis liquids in the experiments with varying temperature and SRT. The aqueous phases were originally lighter, however, due to contact with part of the organic phase (separation not 100% effective) and aging, the colour became darker with time.

From experiments with varying feedstock moisture content, changes were verified in the pyrolysis liquids. The aqueous phase was produced in even greater proportion in the experiments with feedstock with elevated M, due to condensation of

most of the evolved moisture. Likely for the same reason, the colour of the aqueous phase was lighter when the feedstock had elevated moisture content, with a yellow/orange tone. Separation between aqueous and organic phases was more efficient, however, the colour of the aqueous phase also became significantly darker with time. Examples of pyrolysis liquids from wheat straw with elevated moisture content are displayed in Figure D.2.

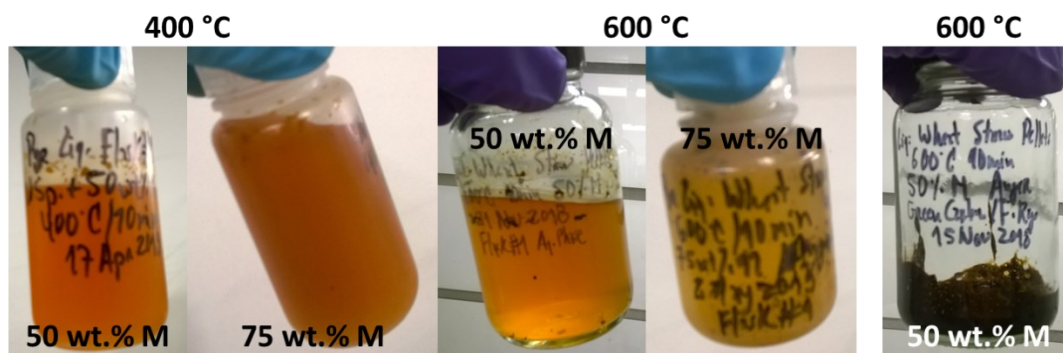


Figure D.2: Aqueous phases of pyrolysis liquids produced from wheat straw (400-600 °C and 10 min SRT); picture on the far right is an organic phase.

The aqueous phases became lighter with pyrolysis temperatures, as occurred for the experiments with varying temperature. Only one example of organic phase is shown because no visible differences were observed between organic phases from varying moisture content.

D.1.2. Water content and reaction water

Aqueous phases of liquid products from slow pyrolysis experiments with varying temperature (400, 500 and 600 °C, 3 minutes SRT) were analysed with Karl Fisher titration to determine water content. The results are indicated in Table D.1.

Table D.1: Water contents of aqueous phases of pyrolysis liquids produced from wheat straw slow pyrolysis.

T (°C)	Water content (wt.%)
400	69.5 ± 5.1
500	82.5 ± 2.0
600	85.8 ± 2.5

If it is assumed that the organic phase has negligible water content, the water content in the pyrolysis liquids (using the yields of aqueous phase in Table 4.11 in Chapter 4, subsection 4.3.1) is: 53.3, 66.5, and 65.0 wt.%, for 400, 500 and 600 °C,

respectively (3 minutes SRT). Other research indicates a maximum water content in pyrolysis liquid products of ≈ 50 wt.% [6], depending on feedstock, pyrolysis conditions and liquid collection method. One study, with rice straw (high inorganic content), water contents in pyrolysis liquid of ≈ 60 wt.% [8]. The relatively high water contents in the produced liquid products may be due to aging during storage, which is known to be increase water content, especially if there are solids and/or inorganics present [4][5]. The higher water content detected in the liquids produced at higher pyrolysis temperatures correlated with the lighter colour of the liquids produced at a higher temperature. The presence of water can reduce viscosity, which can be useful for pumping and transfer, despite reducing heating value, which is not advantageous if the liquid is to be used as fuel [6].

The water present in the liquid products from pyrolysis originates from the moisture in the feedstock and from water that is created in the process, called reaction water. On a dry feedstock basis, the reaction water was found to be 23.0, 31.2, and 28.6 wt.%, respectively, for pyrolysis temperatures of 400, 500, and 600 °C (3 minutes SRT). A study of pyrolysis of olive mill wastes (0.25 to 2.0 mm particles) in a bubbling fluidised bed reactor at EBRI obtained between 21 and 24 wt.% (dry feedstock basis) of reaction water, for temperatures between 450 and 550 °C [9]. The higher reaction water values obtained in the screw reactor for wheat straw can be explained by the different conditions applied: screw reactor, larger particle sizes and broken pellet form, longer (solid and vapour) residence times, absence of heat carrier (sand in fluidised bed) and absence of carrier gas, etc. These factors contribute to the favouring of secondary reactions which can form water, along with char and gas product [7][10].

D.1.3. pH of the liquid products

The aqueous phases produced at 400, 500 and 600 °C and 3 minutes SRT were analysed for pH value. The results are indicated in Table D.2. The organic phases were not analysed due to their considerably higher viscosity, compared to the aqueous phases.

Table D.2: pH value of the aqueous phase of the pyrolysis liquids produced from wheat straw.

T (°C)	pH (at 20 °C)
400	3.3 ± 0.1
500	3.6 ± 0.1
600	4.1 ± 0.1

Examples from other research indicate pH values between 2 and 4 for pyrolysis liquids (from woody feedstocks) [4]. A study of rice straw pyrolysis (550 °C) comparing different reactors found that the pH of the pyrolysis liquid was higher when produced in a screw reactor (5.3 pH) compared to fixed bed (3.1) or fluidised bed reactors (2.6) [11]. The pH of the liquid product is dependent on various process variables such as temperature and vapour residence time, and on post-conversion aspects such as liquid collection method.

The increase in pH to less acidic values with pyrolysis temperature is related to the chemical contents of the liquids, which have a decreased oxygen and hydrogen content when pyrolysis is performed at higher temperatures. The increase of pyrolysis temperature leads to an increased cracking of compounds with oxygen and hydrogen, decreasing carboxyl groups and deprotonating acidic chemical groups [12]. The change of chemical compounds in the pyrolysis liquid with increasing pyrolysis temperatures can be assessed using elemental analysis and GC-MS. The pH value is a very important factor that influences post-processing: higher pH values (less acidic) are preferred, due to a lowering of the potential for corrosion of equipment and pipes. To use the pyrolytic liquids for energy production, they would need to undergo an upgrading process, for example to reduce their oxygen content and acidity, and decrease their viscosity [6].

D.1.4. Elemental analyses and heating values

The organic phases of the pyrolysis liquids produced at 400, 500 and 600 °C and 3 minutes SRT were analysed externally for ultimate analysis. The averaged results are presented in Table D.3, with averages and standard deviations based on two replicates.

Table D.3: Ultimate analyses of the organic phases of the liquids produced from wheat straw pyrolysis.

T (°C)	C (wt.%)	H (wt.%)	N (wt.%)	S (wt.%)	O (+ Ash) (wt.%, by difference)
400	56.4 ± 0.3	7.6 ± 0.1	1.3 ± 0.1	≤0.1	34.8 ± 0.2
500	61.3 ± 0.1	7.6 ± 0.1	1.6 ± 0.0	0.9 ± 0.1	28.6 ± 0.1
600	62.5 ± 0.1	7.8 ± 0.1	1.6 ± 0.0	0.9 ± 0.2	27.3 ± 0.0

As pyrolysis temperature increased, the carbon, hydrogen and nitrogen fractions increased, and the oxygen fraction decreased. This was connected to favoured fragmentation, depolymerisation, cracking, and other reactions as temperature increased [7]. These reactions formed more gas product at the expense of solid and liquid products.

The pyrolysis liquids produced at 400, 500 and 600 °C and 3 minutes SRT were tested for HHV in a bomb calorimeter. The experimental HHV values for the organic phases are indicated in Table D.4, along with calculated HHV based on elemental distribution and using the Channiwala and Parikh correlation (Equation 3.3 in Chapter 3; ash content assumed as negligible) [13]. The aqueous phases did not achieve combustion within the bomb calorimeter (partially or completely), which was attributed to the considerable water content, and therefore the heating value was considered negligible.

Table D.4: Experimental and calculated HHV of the organic phases produced from wheat straw pyrolysis.

T (°C)	HHV _{exp} (MJ/kg)	HHV _{calc} (MJ/kg)
400	21.5 ± 0.7	25.0 ± 0.0
500	25.9 ± 0.2	27.5 ± 0.1
600	25.8 ± 0.1	28.3 ± 0.2

Overall, the HHVs increased with pyrolysis temperature, which was due to the changing elemental composition (increase in carbon and hydrogen, decrease in oxygen). In terms of experimental HHV, it increased significantly when pyrolysis temperature increased from 400 to 500 °C. However, the experimental HHV for the organic phase produced at 600 °C was approximately the same as the one from 500 °C. This was related to the similar elemental composition of the liquid products from those two temperatures. The HHVs of the organic phases were ≈33-40% lower than liquid fuels such as gasoline and diesel, which have typically 42-47 MJ/kg [14].

In terms of energy yields, the organic phases analysed here represented 7-18% of the feedstock energy. The energy yield from the organic phases is by extension the energy yield from the liquid products since the aqueous phases had negligible energy content. The energy yield from the liquid products increased with pyrolysis temperature, both due to the increase in quality of the organic phase (less oxygen content, higher carbon and hydrogen contents) and in organic phase mass yield. Comparing to the results obtained by Park *et al.* from slow pyrolysis of rice straw, which were ≈40% [15], the energy yields obtained in this work were significantly smaller, due to lower product quality. The aqueous phases from the work of Park *et al.* had ≈4 MJ/kg, and the organic phases had ≈29-31 MJ/kg [15].

D.1.5. GC-MS

The chemical compounds present in the pyrolysis liquids were assessed using GC-MS as described in Chapter 3. The GC chromatograms obtained for the tested aqueous and organic phases (400, 500, and 600 °C, 3 minutes SRT) are presented in Figure D.3 (400 °C), Figure D.4 (500 °C), and Figure D.5 (600 °C). For the aqueous phase from 400 °C, however, there was an error with the analysis and the results could not be obtained.

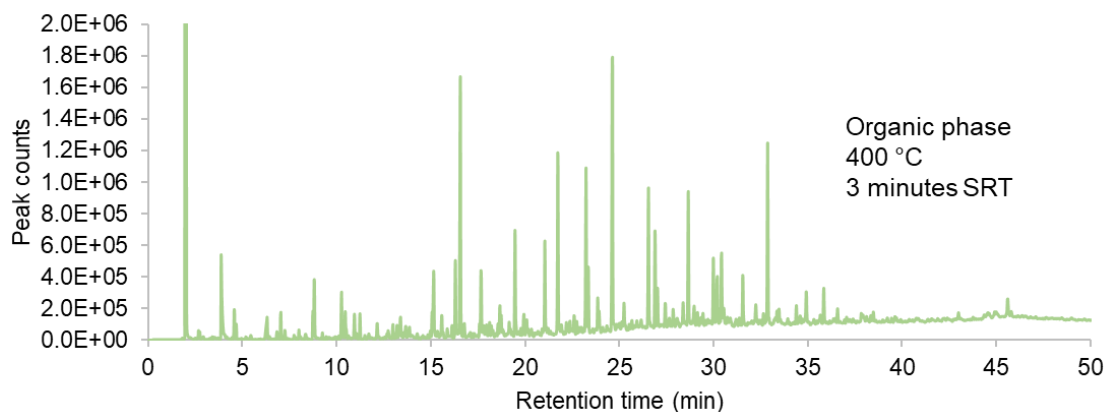


Figure D.3: GC-MS chromatogram for the aqueous phase produced at 400 °C and 3 minutes SRT.

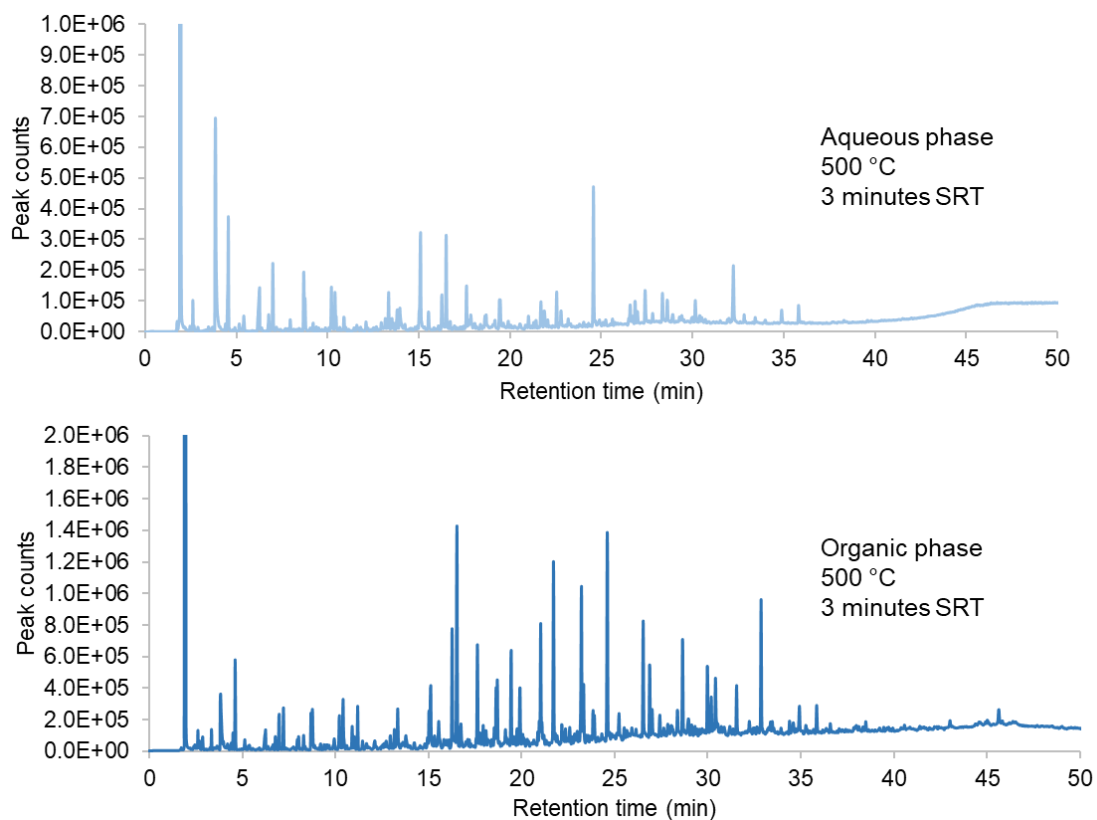


Figure D.4: GC-MS chromatograms for the aqueous (top) and organic (bottom) phases produced at 500 °C and 3 minutes SRT.

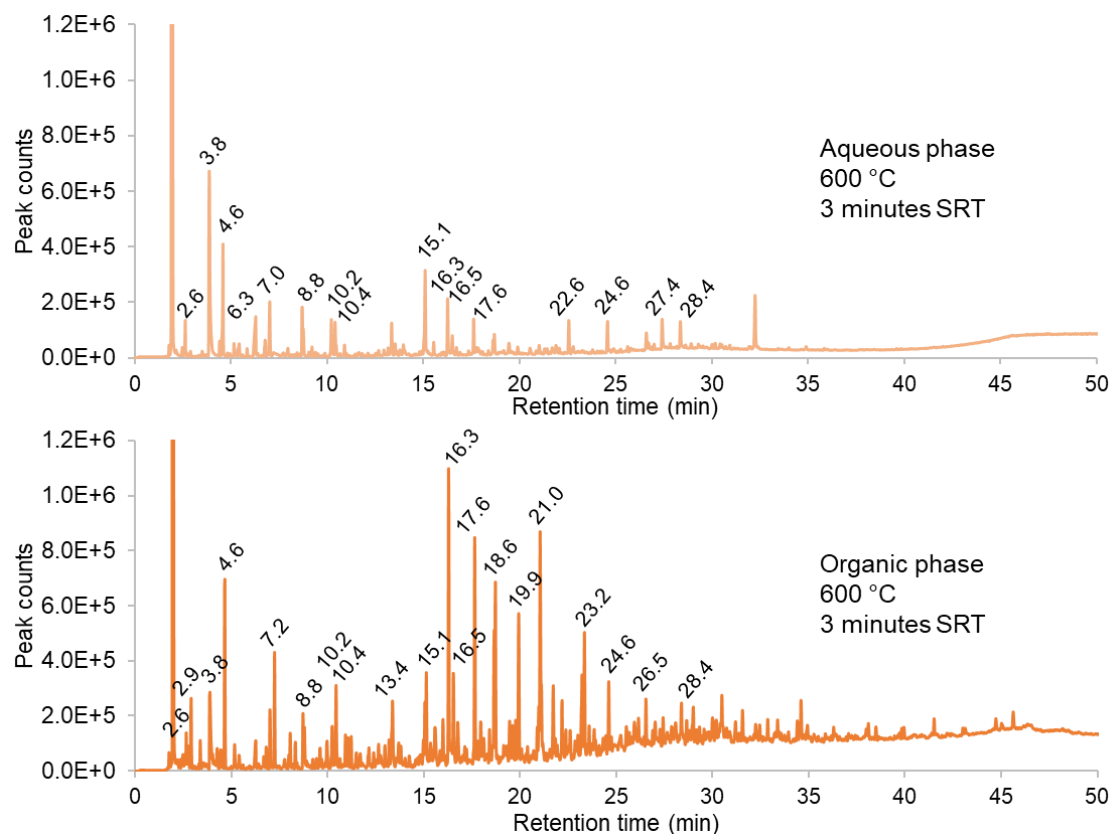


Figure D.5: GC-MS chromatograms for the aqueous (top) and organic (bottom) phases produced at 600 °C and 3 minutes SRT.

Identification of the present compounds (and presented here) was only performed for GC-MS peaks with over 100,000 counts. The first peak with very high peak counts corresponds to the solvent used for sample preparation (acetone). Table D.5 indicates the most common compounds found in the liquid products from the GC-MS analysis. The chromatograms for the liquids from 600 °C (Figure D.5) have retention times on peaks with relatively high counts in order to correspond to identified compounds in Table D.5.

Table D.5: Most common compounds (ordered by retention time) found from GC-MS of the liquids produced from wheat straw pyrolysis at 400-600 °C and 3 minutes SRT.

Chemical compound	Ret. time (min)	Aqueous phase			Organic phase		
		400 °C	500 °C	600 °C	400 °C	500 °C	600 °C
Methylguanidine	2.6		✓	✓		✓	✓
Benzene	2.9						✓
Glycerin	3.8	✓	✓	✓	✓	✓	
Propanoic acid	6.3	✓	✓	✓	✓	✓	✓
2,2,4,4-tetramethylpentane	7.0	✓	✓	✓			
p-xylene	7.2					✓	✓
3-methylfuran	8.7				✓	✓	✓
Cyclopentenone	8.7	✓	✓	✓			
Furfural	8.8	✓	✓	✓	✓	✓	✓
m-ethyltoluene	9.9						✓
Furfuryl alcohol	10.2	✓	✓	✓	✓	✓	✓
2-methylcyclopentenone	10.4	✓	✓	✓	✓	✓	✓
Acetylfuran	10.9				✓	✓	✓
1,2,4-trimethylbenzene	11.0						✓
Limonene	11.2				✓	✓	✓
3-methylcyclopentenone	13.4				✓	✓	✓
Dimethylcyclopentenone	15.0				✓	✓	✓
Methylcyclopentanedione	15.1	✓	✓	✓	✓	✓	✓
Phenol	16.3	✓	✓	✓	✓	✓	✓
Guaiacol	16.5	✓	✓	✓	✓	✓	✓
Cresol	17.6				✓	✓	✓
p-cresol	18.6				✓	✓	✓
Xylenol	19.9				✓	✓	✓
4-ethylphenol	21.0				✓	✓	✓
p-ethylguaiacol	21.7				✓	✓	✓
Levogluconan	22.6	✓	✓	✓			
p-vinylguaiacol	23.2	✓			✓	✓	✓
Syringol (or dimethoxyphenol)	24.6				✓	✓	✓
Isoeugenol	26.5				✓	✓	✓
4-methoxy-3-(methoxymethyl)-phenol	26.9				✓	✓	
Isovanillin	27.0				✓	✓	
Hydroquinone	27.4	✓	✓	✓	✓	✓	
Methylbenzenediol	28.4	✓	✓	✓	✓	✓	✓
Trimethoxymethylbenzene	28.6				✓	✓	
Guaiacylacetone	30.2				✓	✓	
Methoxyeugenol	31.5				✓	✓	

The number of compounds identified in the organic phases was considerably higher than the one found in the aqueous phases. This indicates a higher complexity of the organic phase compared to the aqueous phase, which is mainly composed of water

and water-soluble compounds such as sugars derived from carbohydrates (i.e., cellulose and hemicellulose) [4]. The organic phase is known to contain more lignin-derived organic compounds [4].

The most prominent examples of compounds found in both phases overall were phenol and its derivatives (e.g., syringol, guaiacol, eugenol, hydroquinone), propanoic acid, cyclopentenones, furfural, furfuryl alcohol, etc.

The organic phases were found to have significantly more phenol derivatives than the aqueous phases, due to the relatively low water solubility of phenol (water is the main compound in the aqueous phases). Furthermore, the organic phases produced at the lowest pyrolysis temperatures of 400 and 500 °C have more phenol-based compounds than the organic phase produced at 600 °C. This effect is due to the further breakdown of compounds with higher pyrolysis temperature.

Levoglucosan, an anhydrosugar derived from cellulose [16], was only identified in the aqueous phases, which is due to these types of degradation products being water soluble. Levoglucosan can suffer rearrangement into furfural [17], which was detected in both the aqueous and organic phases.

Benzene and its derivatives were only identified in the organic phase produced at the highest pyrolysis temperature (600 °C). Examples of peaks corresponding to benzene and benzene-derivatives were found at retention times of 2.9, 9.9, and 11.0 minutes. Other phenolic compounds were only identified for the highest pyrolysis temperature or were found to increase (in counts) with that process variable: p-xylene only appeared in the 500 and 600 °C organic phases; xylenol, cresol, and 4-ethylphenol increased with pyrolysis temperature. Another likely derivative from lignin is methylguanidine, which was not identified in both the aqueous and the organic phase produced at 400 °C. On the other hand, some phenol-derived compounds were found to decrease with pyrolysis temperature instead, such as creosol, p-ethylguaiacol, p-vinylguaiacol, syringol, isoeugenol, and methoxyeugenol. Lignin, being comprised of different types of phenolic-based compounds, contributes to the liquid products mainly with phenol and its derivatives [18]. As pyrolysis temperature increases, more proportion of lignin gets degraded, releasing more phenolic-based compounds, and, at the same time, the vaporised compounds get broken down into gaseous products. This can lead to contrasting effects for different phenolic compounds identified with GC-MS.

Some of the detected compounds (e.g., levoglucosan, furfural, etc.) have added value and if extracted from the liquid product and commercialised could serve as a revenue stream and improve the process economics [19]. The pyrolysis liquids could

also be upgraded and used for heat and power generation through combustion in a boiler or engine, or as precursors for second-generation transportation biofuels [6].

D.2. Liquid products from varying injected gas during slow pyrolysis (CO₂, N₂, and none)

Laboratory analyses were not performed on the liquid products from the slow pyrolysis experiments with CO₂ or N₂ as injected gas. However, in this subsection, comments on collection, colour, homogeneity, and other physical features of the liquid products are made, along with pictures, whenever relevant.

Injecting gas into the reactor during slow pyrolysis had the consequence of increasing the flow of product vapours in the cooling/condensing system, especially at the highest temperature of 600 °C. At this temperature, the vapours filled the condensing system to a point where its efficiency decreased (contact time was not sufficient for heat transfer), consequently leading to liquid being collected even in the last piece of glassware (cotton filter, pictured in Figure D.6). This can ultimately lead to vapours passing the cotton and going into the gas meter, which can harm the equipment. The cooling system could potentially be modified to improve heat transfer and maximise liquid condensation and collection, e.g., by using an electrostatic precipitator.



Figure D.6: First section of the cotton filter with accumulated condensate at the end of an experiment using gas injection during slow pyrolysis.

Regarding the collected liquid products from all experiments in this experimental set (different injected gas and temperatures), no visible differences were found between them.

As was observed for other slow pyrolysis liquid products produced in this work, the aqueous phases produced at lower temperature were darker than the other ones. The colour of the aqueous phases also became darker with time (for both temperatures

tested), from contact with organic phases and aging. Examples of pyrolysis liquids produced from using CO₂ are shown in Figure D.7.

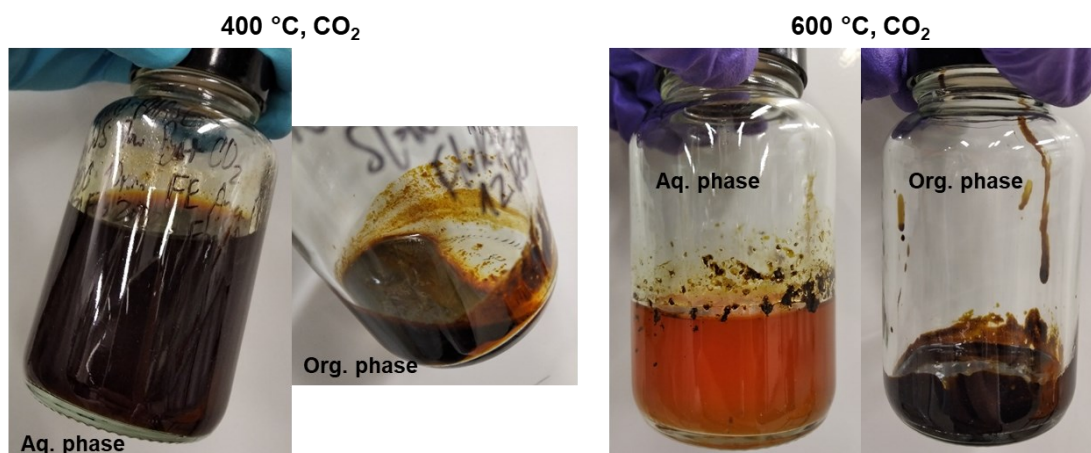


Figure D.7: Pyrolysis liquids produced with CO₂ as injected gas at 400 °C (two left-hand side pictures) and 600 °C (two right-hand side pictures) (10 min SRT).

The aqueous phase produced at 400 °C is darker on the picture than when it was produced, due to aging and contact with some organic phase that is left on the flask due to separation not being 100% efficient.

It was verified that the organic liquid phases produced from the experiments using CO₂ were relatively mobile (especially from 400 °C), which suggests they have lower viscosity than the ones from experiments without injected gas, which were significantly less mobile. Due to this, efficient separation of phases was more challenging for experiments using injected gas. Lower viscosity in pyrolysis liquid is however useful for transportation purposes and for post-treatment and use as fuel.

D.3. Liquid products from varying KOH solution concentration (0.1 and 1 M KOH)

Figure D.8 shows pyrolysis liquids from experiments with KOH-impregnated feedstock at 400 °C, and Figure D.9 the same, at 600 °C.

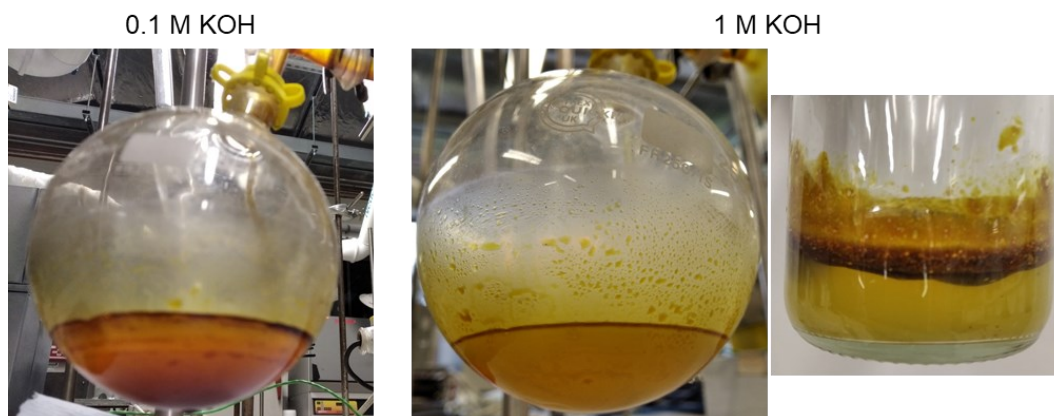


Figure D.8: Examples of produced pyrolysis liquids with KOH-impregnated feedstock at 400 °C slow pyrolysis temperature.

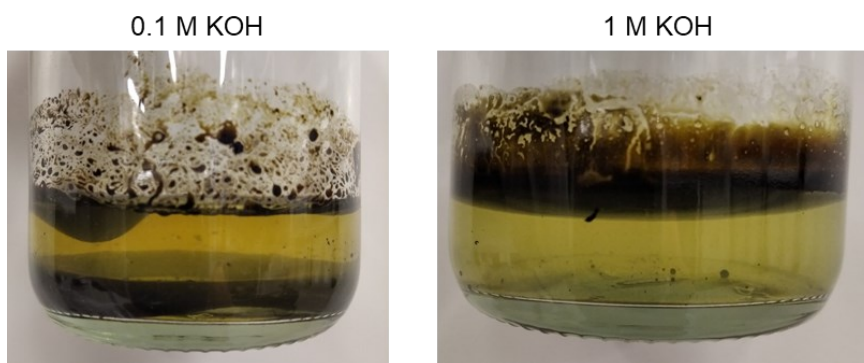


Figure D.9: Examples of produced pyrolysis liquids with KOH-impregnated feedstock at 600 °C slow pyrolysis temperature.

The aqueous phases produced at 600 °C were overall lighter in colour compared to 400 °C ones, which has been linked to increased water content produced from reactions favoured by higher temperatures such as fragmentation and dehydration [7]. The aqueous phases produced at 400 °C and 0.1 M KOH had the darkest colour of all, with the one from 1 M KOH having colour more similar to the 600 °C aqueous phases. This suggests the greater KOH presence may have favoured H₂O-forming reactions. The organic phases were on the other hand slightly darker for the 600 °C experiments.

The organic phase from KOH experiments had changes in density depending on KOH concentration. The ones from 1 M KOH were on top of the aqueous phase, while for 0.1 M KOH some of the organic phase was found on the bottom of the flask, as well as on top. This suggests a greater KOH proportion during slow pyrolysis favours cracking of compounds into ones with lower molecular weight and density. These secondary reactions usually result in higher char and gas yields, however, gas yields were only significantly increased for 600 °C with 1 M KOH, and char yield did not increase very

significantly. This could be due to a greater tar (high molecular weight compounds) formation for 600 °C, and a favouring of cracking reactions for higher temperatures as well.

Comparing to experiments without KOH, one noticeable visual difference was that the organic phase had overall greater mobility (less viscosity) when KOH was used, which brought difficulties during phase separation. Nevertheless, phase separation benefited from the fact that the phases did not mix between themselves as much as in experiments without KOH, especially for higher KOH concentration and temperature. Some clumps (spheres) of organic phase spread in the aqueous phase were also seen for liquids from 1 M KOH, which was due to property differences between the two phases, such as density and hydrophobicity.

Appendix E - Characterisation of commercial activated carbon

E.1 – FTIR analysis

Figure E.1 presents the FTIR spectrum of the commercial activated carbon compared to the product chars in this work. As it was commented in Chapter 7, the IR manifestation of chemical bonds was significantly lower compared to the char products, in line with the highly carbonaceous nature and more ordered structure of the activated carbon.

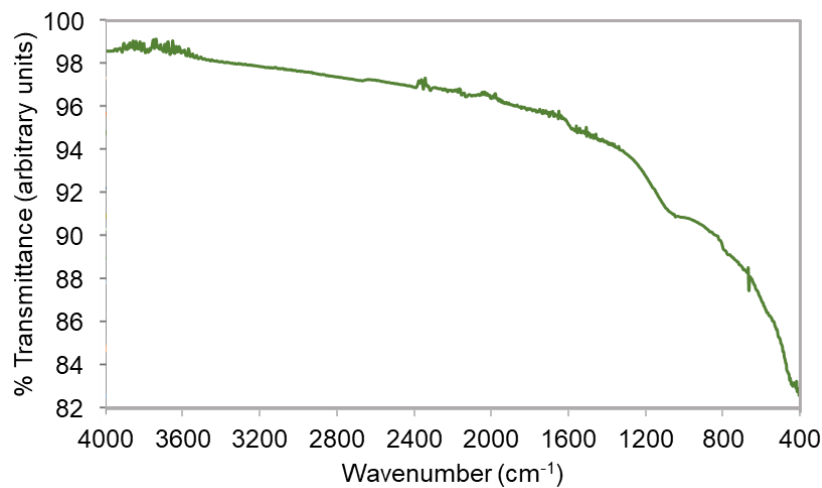


Figure E.1: FTIR spectrum for the commercial activated carbon tested in this work.

E.2 – N₂ physisorption (77 K)

Figure E.2 presents the isotherm and pore size distribution from N₂ physisorption (at 77 K) for the commercial activated carbon tested in this work. The model QS-DFT was used.

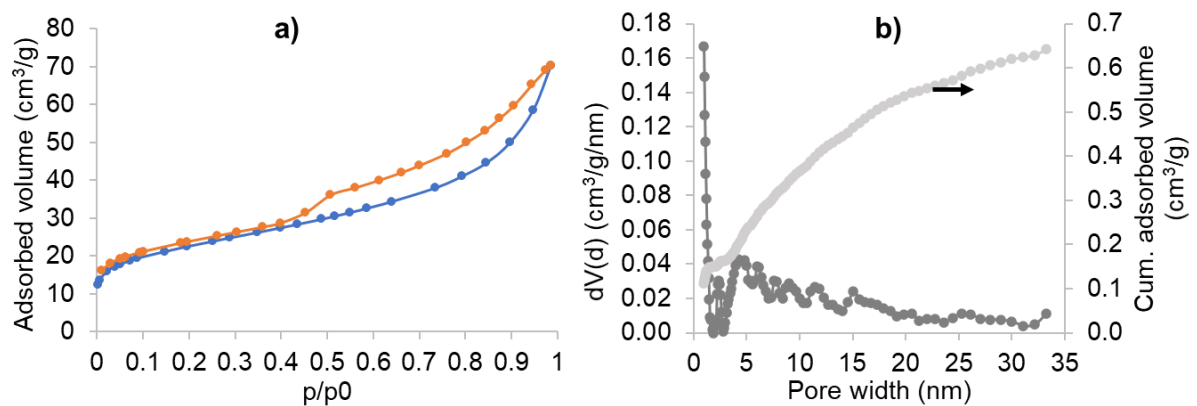


Figure E.2: N₂ adsorption-desorption isotherm (a) and pore size distribution (QS-DFT applied on adsorption branch) (b) for the commercial activated carbon.

Appendix F – Correlations between maximum MB dye removal and char properties

Figure F.1 presents the linear correlations between maximum removal of MB from solution and char properties, for chars produced from slow pyrolysis experiments with varying temperature (400, 500 and 600 °C) and solid residence time (3, 6 and 10 minutes).

Figure F.2 presents the linear correlations between maximum removal of MB from solution and char properties, for chars produced from slow pyrolysis experiments with varying feedstock moisture content (0.1, 50, and 75 wt.%, wet basis).

Figure F.3 presents the linear correlations between maximum removal of MB from solution and char properties, for chars produced from slow pyrolysis experiments with different carrier gases (N₂ and CO₂) and using no carrier gas.

Figure F.4 presents the linear correlations between maximum removal of MB from solution and char properties, for chars produced from slow pyrolysis experiments with KOH-impregnated feedstock, using solutions with 0, 0.1, or 1.0 M KOH concentration.

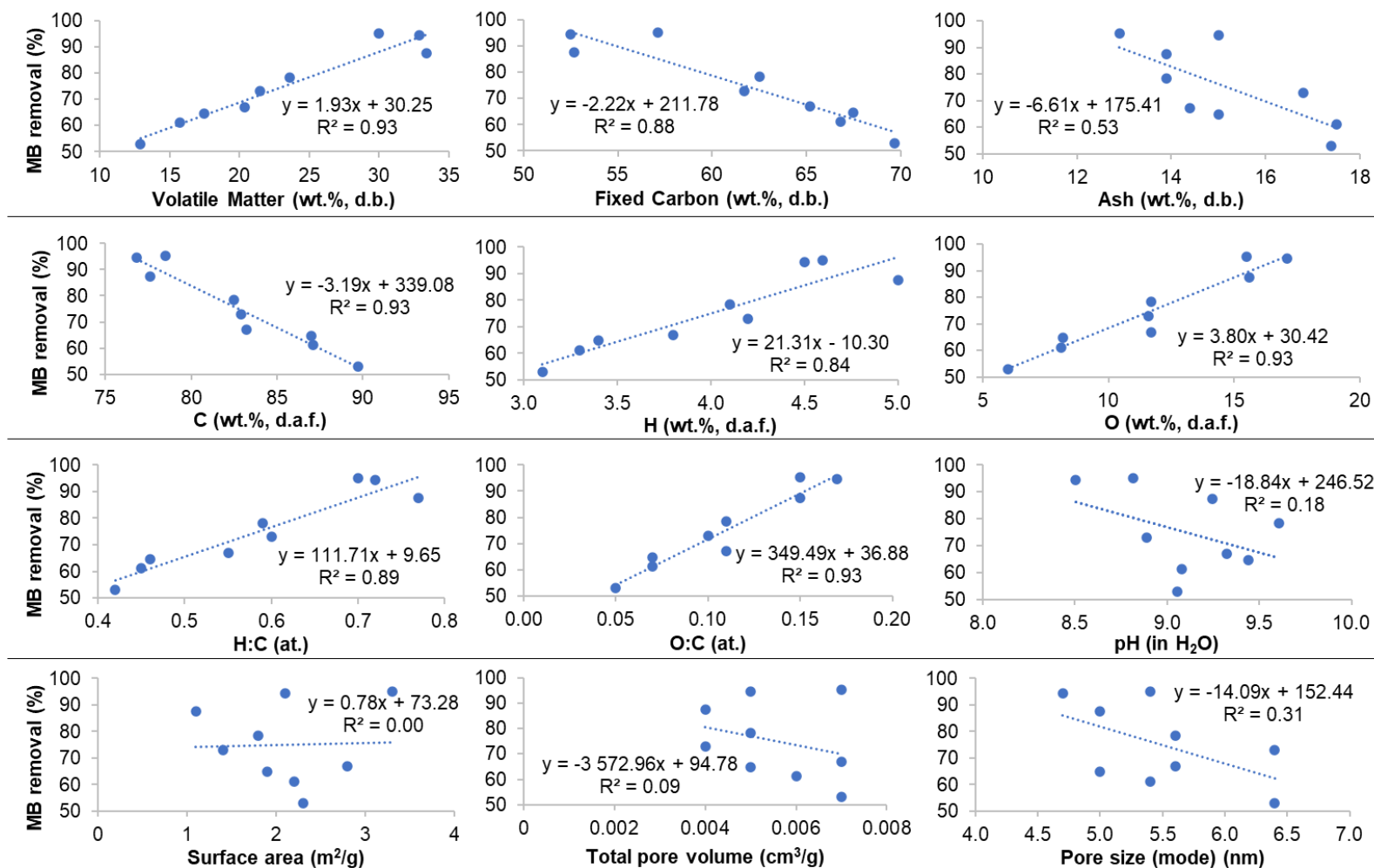


Figure F.1: Correlations between MB removal from solution (% at equilibrium; vertical axis) and char properties (horizontal axis), for the chars produced with varying slow pyrolysis temperature and solid residence time.

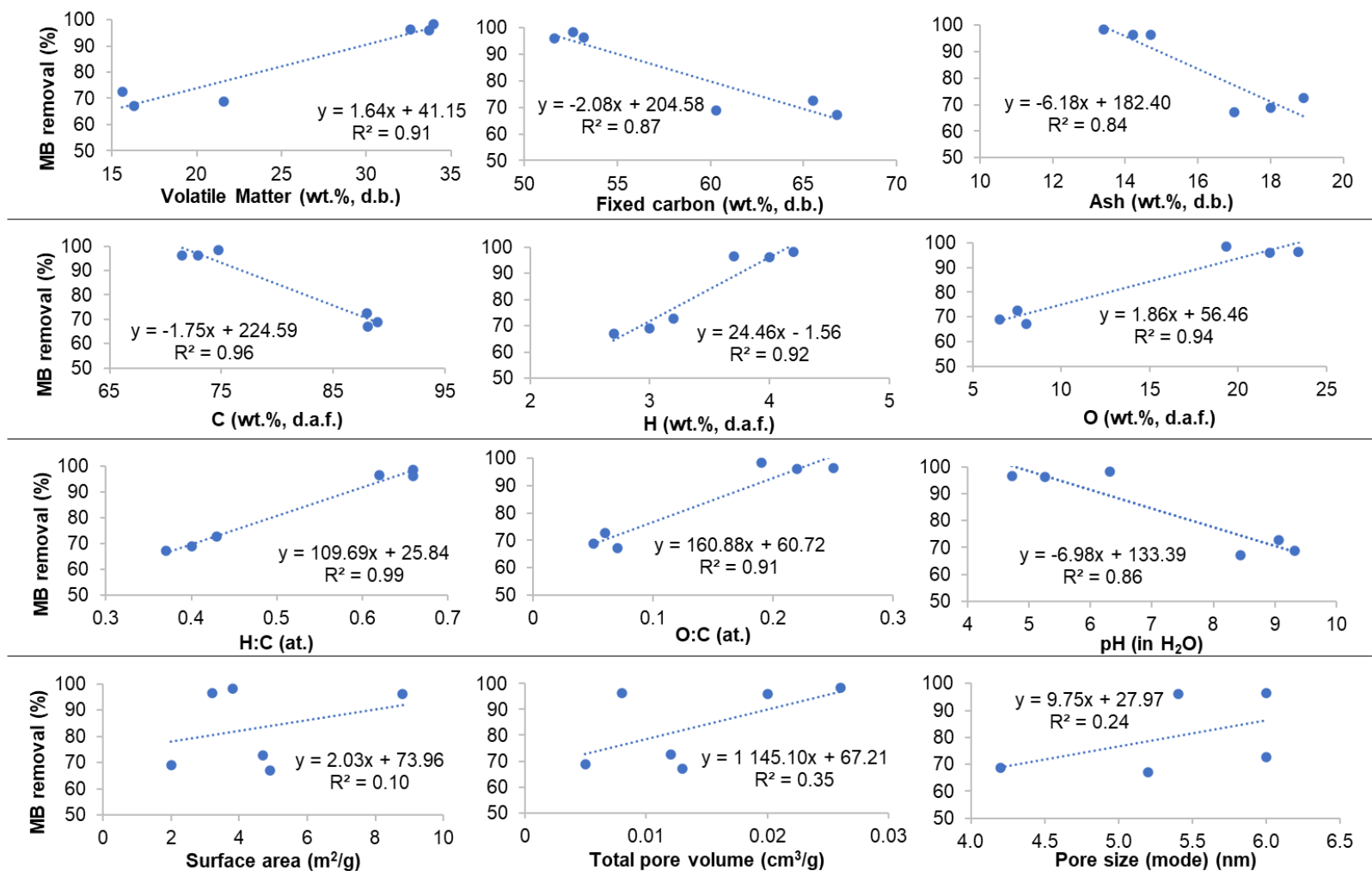


Figure F.2: Correlations between MB removal from solution (% at equilibrium; vertical axis) and char properties (horizontal axis), for the chars produced with varying feedstock moisture content.

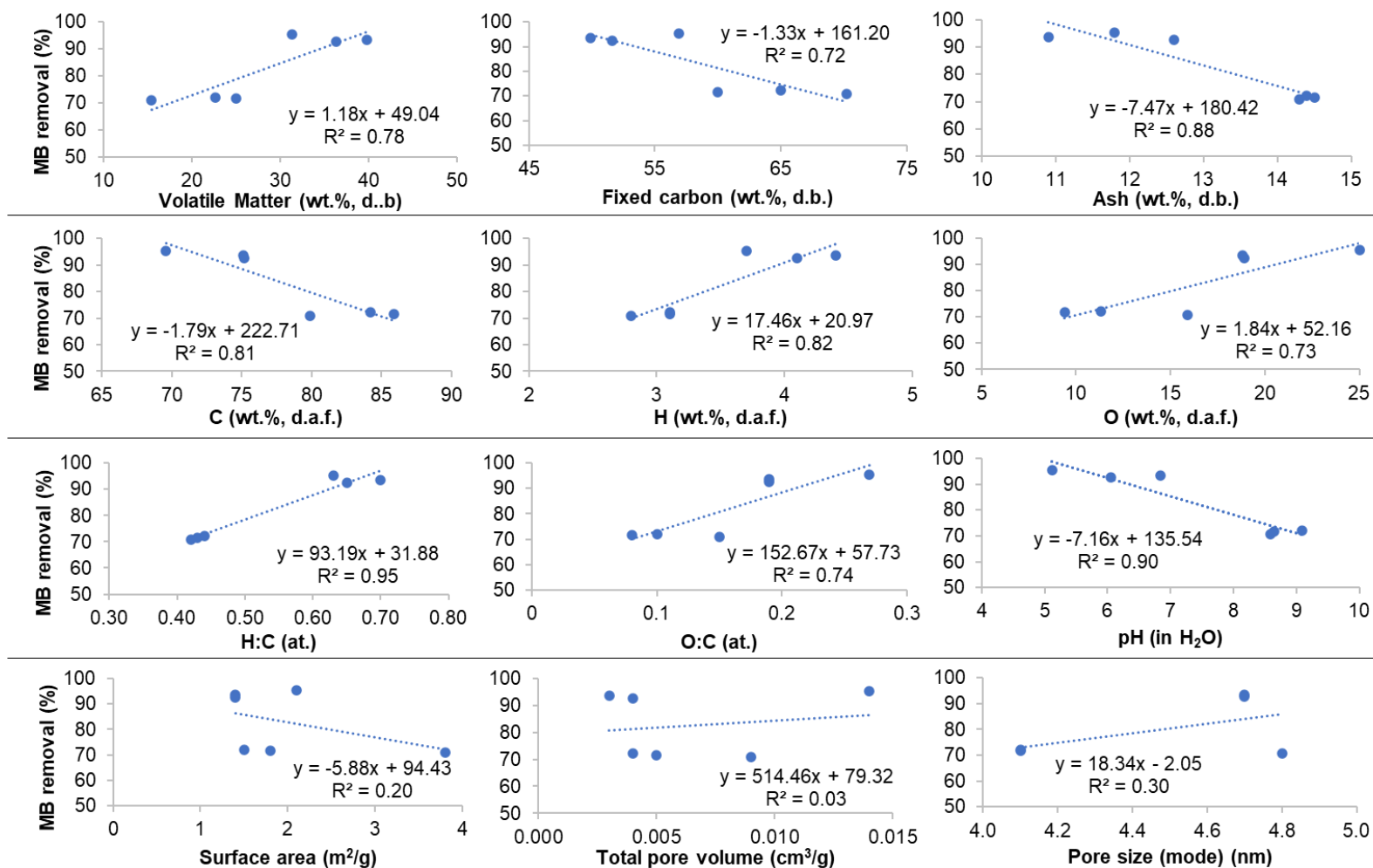


Figure F.3: Correlations between MB removal from solution (% at equilibrium; vertical axis) and char properties (horizontal axis), for the chars produced with varying carrier gas.

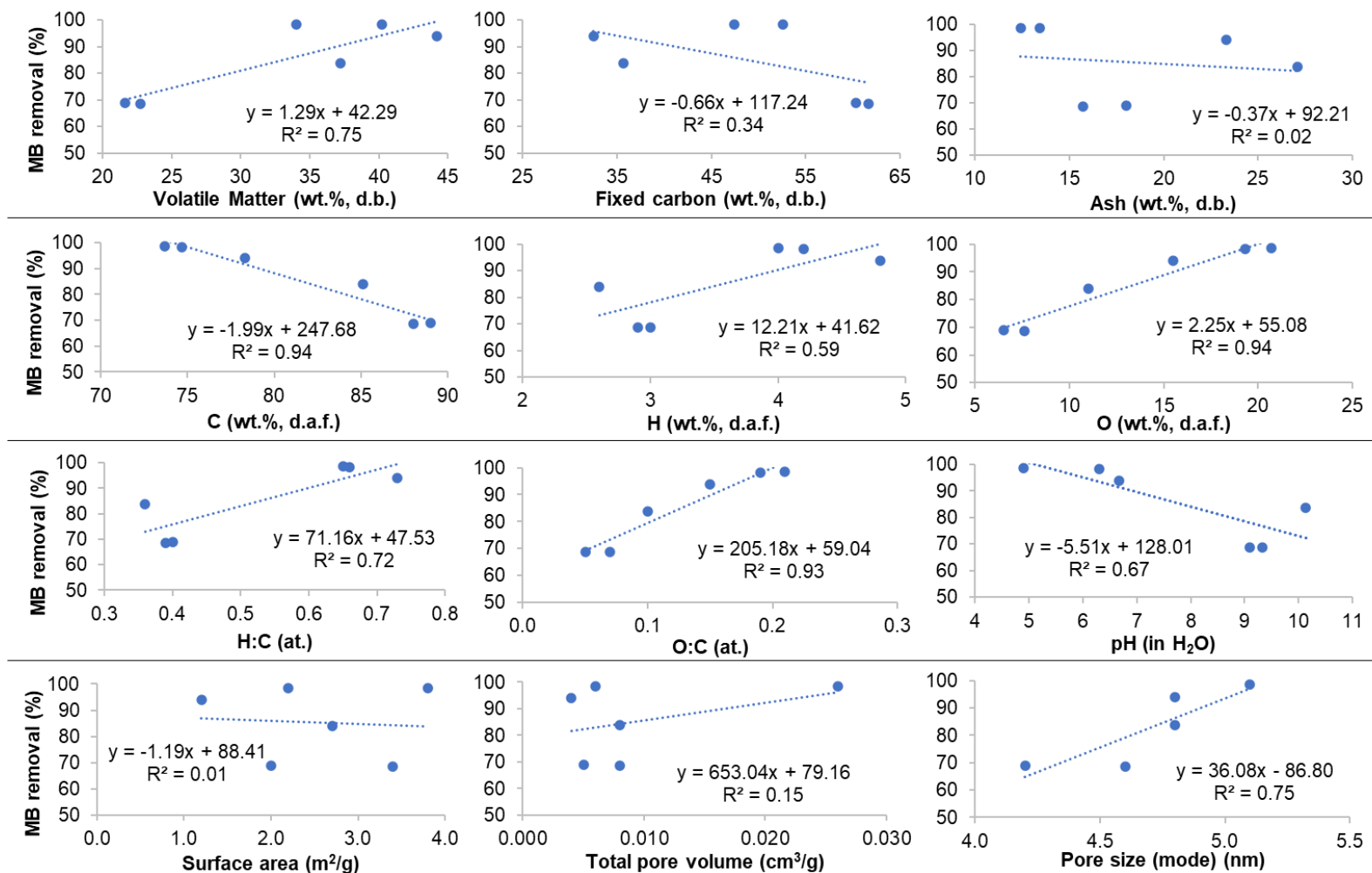


Figure F.4: Correlations between MB removal from solution (% at equilibrium; vertical axis) and char properties (horizontal axis), for the chars produced with KOH-impregnated feedstock.

Appendix G– Kinetics study of adsorption of methylene blue from water using the chars

Figure G.1 presents the adsorption of methylene blue (MB) dye from aqueous solution from 0-180 minutes, for the tested chars and a commercial activated carbon.

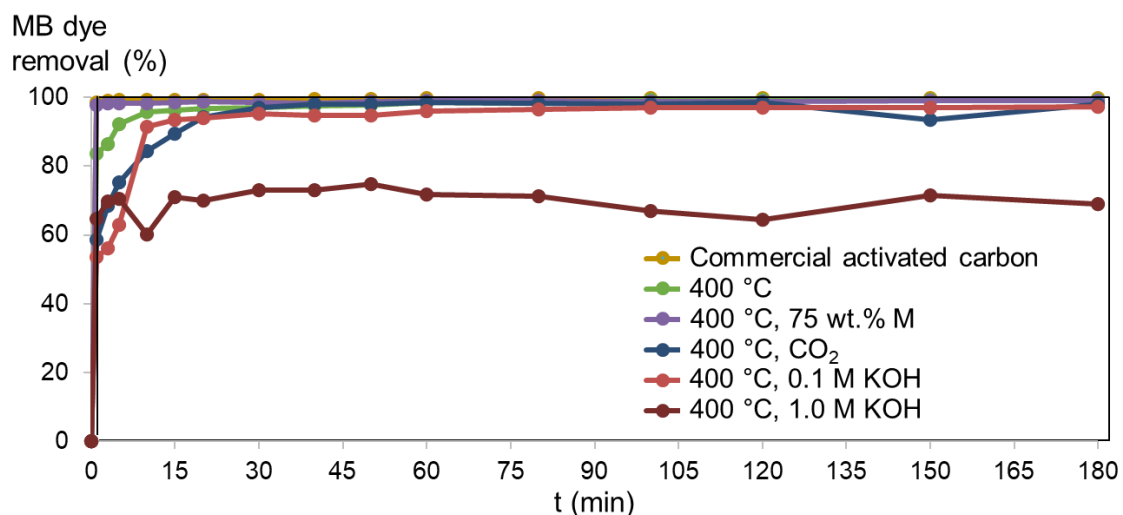


Figure G.1: Adsorption of methylene blue dye from aqueous solution using selected chars and commercial activated carbon (0-180 minutes).

The following graphs present the linear fittings of the MB adsorption to pseudo first and pseudo-second order kinetics models, for the commercial activated carbon and the 400 °C char (from as-received feedstock) (Figure G.2), the char produced with 75 wt.% feedstock moisture content and the char produced using CO₂ as injected gas (Figure G.3 both), and the chars produced with KOH-impregnated feedstock (0.1 and 1 M KOH solutions) (Figure G.4 both).

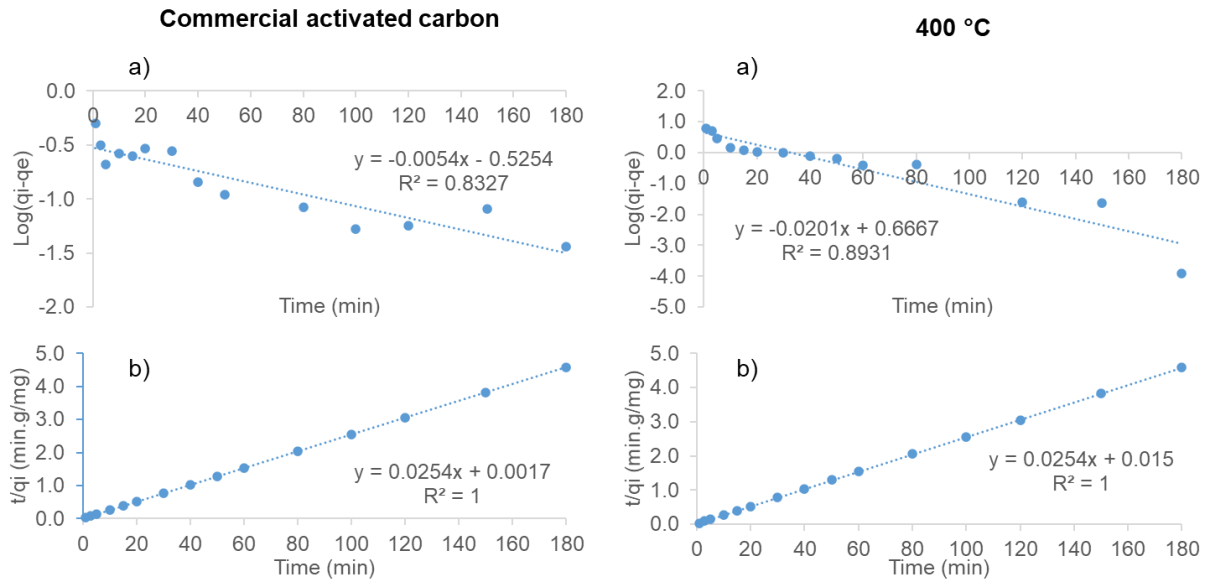


Figure G.2: Linear fittings of MB adsorption to pseudo-first (a) and pseudo-second order (b) kinetics models, for a commercial activated carbon and char produced at 400 °C from as-received feedstock.

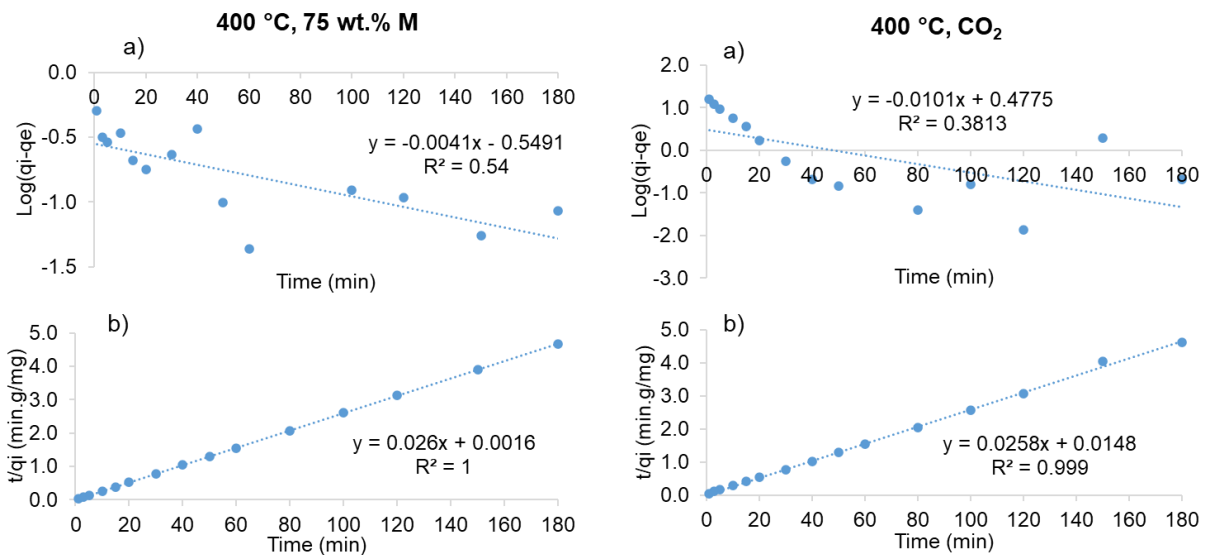


Figure G.3: Linear fittings of MB adsorption to pseudo-first (a) and pseudo-second order (b) kinetics models, for char produced from feedstock with 75 wt.% moisture content, and char from using CO₂ as injected gas.

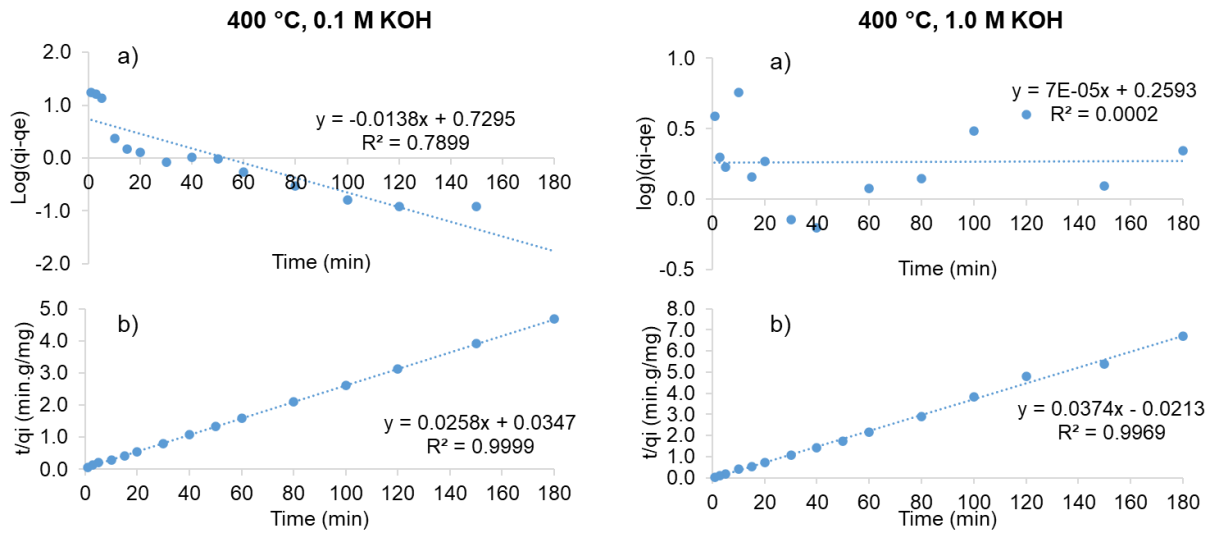


Figure G.4: Linear fittings of MB adsorption to pseudo-first (a) and pseudo-second order (b) kinetics models, for chars produced from feedstock impregnated with 0.1 M (left-hand side) and 1 M KOH solutions (right-hand side).

Appendix H – Dissemination, outputs, and list of publications

The work for this thesis has been presented in conferences, webinars, and other events, for dissemination purposes:

Posters:

- Intermediate pyrolysis of biomass in a pilot scale continuous screw reactor, at Innovate 17 (8 November 2017, NEC, Birmingham, UK),
- Pyrolysis of wheat straw pellets in a bench-scale auger reactor for producing char with enhanced adsorption capabilities, at the 12th ECCRIA - The European Conference on Fuel and Energy Research and its Applications (5-7 September 2018, Cardiff University, UK).

Oral presentations:

- Char - the jack of all trades, at the ERA Vision Conference (26 November 2018, EMCC, Nottingham, UK),
- Development of an integrated and continuous slow pyrolysis and activation process for the production of activated carbon from waste biomass, at the 27th European Biomass Conference & Exhibition, EUBCE 2019 (27-30 May 2019, Lisbon Congress Centre (CCL), Lisbon, Portugal). Included publication in the Proceedings of the 27th European Biomass Conference (EUBCE) / ETA-Florence Renewable Energies).

A first publication regarding the work in this thesis is in the final stages of preparation, entitled “Investigation of the role of feedstock properties and process conditions on the slow pyrolysis of biomass in a continuous auger reactor”, having been accepted for publication in the Journal of Analytical and Applied Pyrolysis (<https://doi.org/10.1016/j.jaap.2021.105378>). Other subsequent publications are planned.

The GreenCarbon project published a book entitled “Advanced Carbon Materials from Biomass: An Overview”, with each chapter corresponding roughly to the work of each ESR, and two chapters being done in collaboration between ESRs. The book was edited by the project coordinator Joan J. Manyà, published in May 2019, and is publicly available on Zenodo (DOI: 10.5281/zenodo.3233733).

I also had the chance to collaborate with other fellow researchers in the project, performing product analyses and/or supplying char products for their work. This resulted in the following co-authored papers:

- Effects of slow-pyrolysis conditions on the products yields and properties and on exergy efficiency: A comprehensive assessment for wheat straw, G. Greco, C. Di Stasi, F. Rego, B. González, Joan J. Manyà, Applied Energy, 279 (2020) 115842 (<https://doi.org/10.1016/j.apenergy.2020.115842>),

- Chemical stabilization of Cd-contaminated soil using fresh and aged wheat straw biochar, D. Rathnayake, F. Rego, R. Van Poucke, A. V. Bridgwater, O. Masek, E. Meers, J. Wang, Y. Yang, F. Ronsse, Environmental Science and Pollution Research (2020) (<https://doi.org/10.1007/s11356-020-11574-6>).

Furthermore, I had the possibility to assist visitors at EBRI with their research (e.g., feedstock and product analyses, slow pyrolysis experiments), which resulted in the following publication (others in preparation/awaiting revisions):

- Converting coffee silverskin to value-added products by a slow pyrolysis-based biorefinery process, C. del Pozo, F. Rego, Y. Yang, N. Puy, J. Bartrolí, E. Fàbregas, A. V. Bridgwater, Fuel Processing Technology 214 (2021) 106708 (<https://doi.org/10.1016/j.fuproc.2020.106708>).

References for Appendices

- [1] Ragland K, Bryden K. Combustion Engineering. 2nd Ed. CRC Press; 2011.
- [2] Yang H, Yan R, Chen H, Lee DH, Zheng C. Characteristics of hemicellulose, cellulose and lignin pyrolysis. *Fuel* 2007;86:1781–8. <https://doi.org/10.1016/j.fuel.2006.12.013>.
- [3] Bridgwater A V. Renewable fuels and chemicals by thermal processing of biomass. *Chem Eng J* 2003;91:87–102. [https://doi.org/10.1016/S1385-8947\(02\)00142-0](https://doi.org/10.1016/S1385-8947(02)00142-0).
- [4] Oasmaa A, Czernik S. Fuel oil quality of biomass pyrolysis oils - state of the art for the end users. *Energy and Fuels* 1999;13:914–21. <https://doi.org/10.1021/ef980272b>.
- [5] Diebold JP. A Review of the Chemical and Physical Mechanisms of the Storage Stability of Fast Pyrolysis Bio-Oils. 2000. <https://doi.org/NREL/SR-570-27613>.
- [6] Bridgwater A V. Review of fast pyrolysis of biomass and product upgrading. *Biomass and Bioenergy* 2012;38:68–94. <https://doi.org/10.1016/j.biombioe.2011.01.048>.
- [7] Anca-Couce A. Reaction mechanisms and multi-scale modelling of lignocellulosic biomass pyrolysis. *Prog Energy Combust Sci* 2016;53:41–79. <https://doi.org/10.1016/j.pecs.2015.10.002>.
- [8] Jung S-H, Kang B-S, Kim J-S. Production of bio-oil from rice straw and bamboo sawdust under various reaction conditions in a fast pyrolysis plant equipped with a fluidized bed and a char separation system. *J Anal Appl Pyrolysis* 2008;82:240–7. <https://doi.org/https://doi.org/10.1016/j.jaap.2008.04.001>.
- [9] Christoforou EA, Fokaides PA, Banks SW, Nowakowski D, Bridgwater A V., Stefanidis S, et al. Comparative Study on Catalytic and Non-Catalytic Pyrolysis of Olive Mill Solid Wastes. *Waste and Biomass Valorization* 2018;9:301–13. <https://doi.org/10.1007/s12649-016-9809-5>.
- [10] Bridgwater A V., Meier D, Radlein D. An overview of fast pyrolysis of biomass. *Org Geochem* 1999:1479–93.
- [11] Nam H, Capareda SC, Ashwath N, Kongkasawan J. Experimental investigation of pyrolysis of rice straw using bench-scale auger, batch and fluidized bed reactors. *Energy* 2015;93:2384–94. <https://doi.org/10.1016/j.energy.2015.10.028>.
- [12] Ronsse F, van Hecke S, Dickinson D, Prins W. Production and characterization of slow pyrolysis biochar: Influence of feedstock type and pyrolysis conditions. *GCB Bioenergy* 2013;5:104–15. <https://doi.org/10.1111/gcbb.12018>.
- [13] Channiwala SA, Parikh PP. A unified correlation for estimating HHV of solid, liquid and gaseous fuels. *Fuel* 2002;81:1051–63. [https://doi.org/10.1016/S0016-2361\(01\)00131-4](https://doi.org/10.1016/S0016-2361(01)00131-4).
- [14] World Nuclear Association. Heat Values of Various Fuels 2021. <https://www.world-nuclear.org/information-library/facts-and-figures/heat-values-of-various-fuels.aspx>

- (accessed March 30, 2021).
- [15] Park J, Lee Y, Ryu C, Park YK. Slow pyrolysis of rice straw: Analysis of products properties, carbon and energy yields. *Bioresour Technol* 2014;155:63–70. <https://doi.org/10.1016/j.biortech.2013.12.084>.
- [16] Lu Q, Yang X, Dong C, Zhang Z, Zhang X, Zhu X. Influence of pyrolysis temperature and time on the cellulose fast pyrolysis products: Analytical Py-GC/MS study. *J Anal Appl Pyrolysis* 2011;92:430–8. <https://doi.org/https://doi.org/10.1016/j.jaap.2011.08.006>.
- [17] Shen DK, Gu S. The mechanism for thermal decomposition of cellulose and its main products. *Bioresour Technol* 2009;100:6496–504. <https://doi.org/https://doi.org/10.1016/j.biortech.2009.06.095>.
- [18] Collard FX, Blin J. A review on pyrolysis of biomass constituents: Mechanisms and composition of the products obtained from the conversion of cellulose, hemicelluloses and lignin. *Renew Sustain Energy Rev* 2014;38:594–608. <https://doi.org/10.1016/j.rser.2014.06.013>.
- [19] Czernik S, Bridgwater A V. Overview of applications of biomass fast pyrolysis oil. *Energy and Fuels* 2004;18:590–8. <https://doi.org/10.1021/ef034067u>.